

THREE-DIMENSIONAL RIDDLES OF THE RADIAL WRIST: DERIVED CARPAL
AND CARPOMETACARPAL JOINT MORPHOLOGY IN THE GENUS *HOMO*
AND THE IMPLICATIONS FOR UNDERSTANDING THE EVOLUTION OF
STONE TOOL-RELATED BEHAVIORS IN HOMININS

by

Matthew Wayne Tocheri

A Dissertation Presented in Partial Fulfillment
of the Requirements for the Degree
Doctor of Philosophy

ARIZONA STATE UNIVERSITY

May 2007

©2007 Matthew Wayne Tocheri
All Rights Reserved

THREE-DIMENSIONAL RIDDLES OF THE RADIAL WRIST: DERIVED CARPAL
AND CARPOMETACARPAL JOINT MORPHOLOGY IN THE GENUS *HOMO*
AND THE IMPLICATIONS FOR UNDERSTANDING THE EVOLUTION OF
STONE TOOL-RELATED BEHAVIORS IN HOMININS

by

Matthew Wayne Tocheri

has been approved

April 2007

Graduate Supervisory Committee:

Mary W. Marzke, Co-Chair
Robert C. Williams, Co-Chair
Kaye E. Reed
Anshuman Razdan
David R. Begun

ACCEPTED BY THE DIVISION OF GRADUATE STUDIES

ABSTRACT

This dissertation tests a hypothesis of morphological adaptation to manipulative behaviors related to the use and manufacture of tools within the hominin lineage. The basic question, or ‘riddle of the wrist’, is as follows: do hominins show morphological commitment in the radial carpometacarpal and carpal region of the hand to tool behaviors such that a) the ancestral morphology is sacrificed, and b) the derived morphology has performance advantages for the behavior (i.e., it is better than the primitive structure with respect to the novel behavior)? If so, when, in which hominins, and in which behavioral contexts did this event most likely occur?

The three-dimensional quantitative evidence presented indicates that this ‘riddle of the wrist’ is solvable. The solution may be found in the trapezoid and the bones with which it articulates. In certain species of *Homo* (i.e., *H. sapiens*, *H. neanderthalensis*, and *H. antecessor*), the radio-ulnar expansion of the palmar aspect of the trapezoid results in supination of the trapezium such that the distal carpals are more aligned with one another. This re-alignment of the wrist occurs along with a complete re-configuration of the joint morphology in the radial carpal and carpometacarpal region. This complex of derived features shows biomechanical advantages for withstanding large forces that are directed radio-ulnarly across the palmar aspect of the wrist during strong contraction of the thenar musculature.

The morphological specialization of the radial wrist is a hallmark of *H. sapiens*, *H. neanderthalensis*, and their most recent common ancestor. The evidence presented indicates that the distinct morphology of the complex is derived in comparison with extant hominids as well as *Australopithecus afarensis*, *Australopithecus africanus*, and

Homo habilis. Given that OH7 (*H. habilis*) is associated with direct evidence of stone tools, it is tentatively concluded that at 1.75 Ma, the complex of derived features had yet to evolve in hominins. However, the evidence is clear that by 800,000 years ago the complex of derived features had evolved within at least one hominin lineage represented by *H. antecessor*. Therefore, the present evidence suggests that this important evolutionary event occurred during a temporal span characterized by Acheulian technology.

To the original “handy man,”
whichever hominin species he (or she) belonged

ACKNOWLEDGMENTS

I want to express my sincere gratitude to all of the members of my dissertation committee: Mary Marzke (co-chair), Robert Williams (co-chair), Kaye Reed, Anshuman Razdan, and David Begun. Without their encouragement and support, I never would have reached the finish line. I am forever indebted to each of them for guiding and inspiring me along every stage of the research and writing process. Special thanks also to Robert Marzke for participating as a committee member at my defense.

For access to comparative and fossil specimens, I would like to thank David Hunt, Linda Gordon, Bruce Latimer, Lyman Jellema, Emmanuel Gilissen, Wim Wendelen, David Begun, Bill Kimbel, Don Johanson, Erik Trinkaus, Mike Rose, and Rick Potts.

I want to thank everyone at PRISM, past and present, for access to the hardware and software that made my dissertation research possible. In particular, I'd like to thank John Femiani, Scott Van Note, and Anshuman Razdan for their 3D expertise. I also want to thank the faculty, staff, and graduate students in the School of Human Evolution and Social Change for creating a stimulating and intellectually challenging environment in which to pursue my research and higher education. In particular, thanks to Caley Orr, Amy Rector, Jeremiah Scott, Wilson Sweitzer, Luke Delezene, Kristi Lewton, Marc Jacofsky, Scott Burnett, and Mark Spencer.

At the National Museum of Natural History, I thank Rick Potts, Dave Hunt, Richard Thorington, Don Ortner, Jenny Clark, Christian Tryon, Chris Campisano, Briana Pobiner, Fire Kovarovic, and Rebecca Snyder, for making my Smithsonian Predoctoral Fellowship so rewarding.

For general discussions related to this research and physical anthropology in general, I thank Mariam Nargowalla, Tracy Kivell, Brian Richmond, Carol Ward, David Green, Tosha Dupras, and El Molto. Lastly, I thank my parents, Wayne and Earlene Tocheri, for all of their constant love and support through the years.

This dissertation research was funded, in part, by NSF # IIS-998016, a Smithsonian Institution Predoctoral Fellowship, and a SSHRC Doctoral Fellowship (Canada).

TABLE OF CONTENTS

	Page
LIST OF TABLES	xii
LIST OF FIGURES	xxvi
CHAPTER	
1 INTRODUCTION	1
Adaptation	3
To be precise or powerful? A question of grip	14
Capability vs. commitment	22
The search for the earliest tool-maker	26
Statement of the problem	31
2 THE BASIC BIOMECHANICAL PREDICTIONS	36
3 THE FIRST CARPOMETACARPAL JOINT	45
Results of shape analyses	45
The trapezium joint surface	46
The first metacarpal joint surface	56
Multivariate analyses	63
Summary of shape characteristics	72
Discussion	76
4 THE TRAPEZIUM	85
Results of shape analyses	85
Angles of the trapezium	87
Relative areas of the trapezium	93

CHAPTER	Page
Multivariate analyses.....	98
Summary of shape characteristics	103
Discussion.....	109
5 THE TRAPEZOID	117
Results of shape analyses	117
Angles of the trapezoid.....	119
Relative areas of the trapezoid	129
Multivariate analyses.....	135
Summary of shape characteristics	144
Discussion.....	150
6 THE SCAPHOID	158
Results of shape analyses	158
Angles of the scaphoid	159
Relative areas of the scaphoid	164
Multivariate analyses.....	169
Summary of shape characteristics	175
Discussion.....	178
7 THE SECOND METACARPAL BASE	185
Results of shape analyses	185
Angles of the second metacarpal base.....	187
Relative areas of the second metacarpal base.....	195
Multivariate analyses.....	200

CHAPTER	Page
Summary of shape characteristics	204
Discussion.....	208
8 EVOLUTIONARY HISTORY AND ADAPTIVE SIGNIFICANCE.....	214
Results of shape analyses on fossil hominins.....	214
Upper Paleolithic <i>Homo sapiens</i> and <i>Homo neanderthalensis</i>	215
<i>Homo habilis</i> (OH7).....	231
<i>Australopithecus afarensis</i>	243
Other hominin fossils	252
Summary discussion.....	263
Evidence from extant catarrhines	267
Evidence from Upper Paleolithic <i>Homo sapiens</i> and Upper and Middle Paleolithic Neandertals.....	267
Evidence from <i>Australopithecus</i>	272
Evidence from <i>Homo habilis</i>	278
Evidence from Swartkrans	279
Evidence from development.....	281
Conclusions	286
Implications for further work	290
9 MATERIALS AND METHODS	292
Materials.....	292
Methods	295
Three-dimensional data acquisition.....	295

CHAPTER	Page
Relative surface area.....	296
Angles between joint surfaces	297
Measures of curvedness.....	301
Statistical analyses.....	304
LITERATURE CITED.....	308

LIST OF TABLES

Table		Page
3.1	Pairwise comparisons of genus means for relative area of the trapezium joint surface	47
3.2	Pairwise comparisons of genus means for dorso-palmar curvedness of the trapezium joint surface	50
3.3	Pairwise comparisons of genus means for radio-ulnar curvedness of the trapezium joint surface	51
3.4	Pairwise comparisons of genus means for absolute curvature of the trapezium joint surface	52
3.5	Pairwise comparisons of genus means for RMS curvature of the trapezium joint surface	53
3.6	Pairwise comparisons of genus means for mean curvature of the trapezium joint surface	54
3.7	Pairwise comparisons of genus means for Gaussian curvature of the trapezium joint surface	55
3.8	Pairwise comparisons of genus means for relative area of the 1 st metacarpal joint surface.....	56
3.9	Pairwise comparisons of genus means for dorso-palmar curvedness of the 1 st metacarpal joint surface.....	57
3.10	Pairwise comparisons of genus means for radio-ulnar curvedness of the 1 st metacarpal joint surface.....	58

Table	Page
3.11 Pairwise comparisons of genus means for absolute curvature of the 1 st metacarpal joint surface.....	59
3.12 Pairwise comparisons of genus means for RMS curvature of the 1 st metacarpal joint surface.....	60
3.13 Pairwise comparisons of genus means for mean curvature of the 1 st metacarpal joint surface.....	61
3.14 Pairwise comparisons of genus means for Gaussian curvature of the 1 st metacarpal joint surface.....	62
3.15 Correlations between each variable and canonical axis (bolded values indicate the variables that best explain the observed variation along each axis).....	65
3.16 Cross-validated posterior probabilities of genus membership using relative area and curvedness measures of the trapezium joint surface.....	65
3.17 Correlations between each variable and canonical axis (bolded values indicate the variables that best explain the observed variation along each axis).....	67
3.18 Cross-validated posterior probabilities of genus membership using relative area and curvedness measures of the 1 st metacarpal joint surface.....	68

Table	Page
3.19 Correlations between each variable and canonical axis (bolded values indicate the variables that best explain the observed variation along each axis).....	71
3.20 Cross-validated posterior probabilities of genus membership using relative area and curvedness measures of the 1 st metacarpal and trapezium joint surfaces.....	72
3.21 Summary of mean 1 st carpometacarpal joint features (distinctive features in bold).....	72
4.1 Pairwise comparisons of genus means for the angle between the 1 st and 2 nd metacarpal joint surfaces.....	87
4.2 Pairwise comparisons of genus means for the angle between the 1 st metacarpal and scaphoid joint surfaces	88
4.3 Pairwise comparisons of genus means for the angle between the 1 st metacarpal and trapezoid joint surfaces	89
4.4 Pairwise comparisons of genus means for the angle between the 2 nd metacarpal and scaphoid joint surfaces	90
4.5 Pairwise comparisons of genus means for the angle between the 2 nd metacarpal and trapezoid joint surfaces	91
4.6 Pairwise comparisons of genus means for the angle between the scaphoid and trapezoid joint surfaces.....	92
4.7 Pairwise comparisons of genus means for relative area of the 1 st metacarpal joint surface.....	93

Table	Page	
4.8	Pairwise comparisons of genus means for relative area of the 2 nd metacarpal joint surface.....	94
4.9	Pairwise comparisons of genus means for relative area of the scaphoid (centrale included) joint surface.....	95
4.10	Pairwise comparisons of genus means for relative area of the trapezoid joint surface	96
4.11	Pairwise comparisons of genus means for relative area of the non-articular surface	97
4.12	Correlations between each variable and canonical axis (bolded values indicate the variables that best explain the observed variation along each axis).....	100
4.13	Cross-validated posterior probabilities of genus membership using the trapezium carpal and carpometacarpal joint and non-articular relative surface area and angle measures.....	102
4.14	Summary of mean trapezium carpal and carpometacarpal joint and non-articular features (distinctive features in bold).....	103
5.1	Pairwise comparisons of genus means for the angle between the lateral and medial 2 nd metacarpal joint surfaces.....	119
5.2	Pairwise comparisons of genus means for the angle between the lateral 2 nd metacarpal and scaphoid joint surfaces.....	120
5.3	Pairwise comparisons of genus means for the angle between the lateral 2 nd metacarpal and trapezium joint surfaces.....	121

Table	Page
5.4 Pairwise comparisons of genus means for the angle between the medial 2 nd metacarpal and scaphoid joint surfaces.....	122
5.5 Pairwise comparisons of genus means for the angle between the medial 2 nd metacarpal and trapezium joint surfaces.....	123
5.6 Pairwise comparisons of genus means for the angle between the scaphoid and trapezium joint surfaces.....	124
5.7 Pairwise comparisons of genus means for the angle between the capitate and lateral 2 nd metacarpal joint surfaces	125
5.8 Pairwise comparisons of genus means for the angle between the capitate and medial 2 nd metacarpal joint surfaces	126
5.9 Pairwise comparisons of genus means for the angle between the capitate and scaphoid joint surfaces	127
5.10 Pairwise comparisons of genus means for the angle between the capitate and trapezium joint surfaces	128
5.11 Pairwise comparisons of genus means for relative area of the lateral 2 nd metacarpal joint surface	129
5.12 Pairwise comparisons of genus means for relative area of the medial 2 nd metacarpal joint surface	130
5.13 Pairwise comparisons of genus means for relative area of the scaphoid joint surface	131
5.14 Pairwise comparisons of genus means for relative area of the trapezium joint surface	132

Table	Page
5.15 Pairwise comparisons of genus means for relative area of the capitata joint surface.....	133
5.16 Pairwise comparisons of genus means for relative area of the non-articular surface	134
5.17 Correlations between each variable and canonical axis (bolded values indicate the variables that best explain the observed variation along each axis).....	137
5.18 Cross-validated posterior probabilities of genus membership using the trapezoid carpal and carpometacarpal joint and non-articular relative surface area and angle measures.....	140
5.19 Correlations between each variable and canonical axis (bolded values indicate the variables that best explain the observed variation along each axis).....	142
5.20 Cross-validated posterior probabilities of genus membership using the trapezoid carpal and carpometacarpal joint and non-articular relative surface area and angle measures.....	143
5.21 Summary of mean trapezoid carpal joint and non-articular features (distinctive features in bold).....	144
5.22 The ratio of total 2 nd metacarpal to scaphoid relative areas	145
6.1 Pairwise comparisons of genus means for the angle between the capitata and lunate joint surfaces.....	159

Table	Page
6.2 Pairwise comparisons of genus means for the angle between the capitata and radius joint surfaces.....	160
6.3 Pairwise comparisons of genus means for the angle between the capitata and trapezium-trapezoid joint surfaces	161
6.4 Pairwise comparisons of genus means for the angle between the lunate and radius joint surfaces	162
6.5 Pairwise comparisons of genus means for the angle between the lunate and trapezium-trapezoid joint surfaces.....	163
6.6 Pairwise comparisons of genus means for the angle between the radius and trapezium-trapezoid joint surfaces.....	163
6.7 Pairwise comparisons of genus means for relative area of the capitata joint surface.....	164
6.8 Pairwise comparisons of genus means for relative area of the lunate joint surface	165
6.9 Pairwise comparisons of genus means for relative area of the radius joint surface	166
6.10 Pairwise comparisons of genus means for relative area of the trapezium-trapezoid joint surface	167
6.11 Pairwise comparisons of genus means for relative area of the non-articular surface	168

Table	Page
6.12 Correlations between each variable and canonical axis (bolded values indicate the variables that best explain the observed variation along each axis).....	171
6.13 Cross-validated posterior probabilities of genus membership using six relative areas and angles of the scaphoid articular surfaces	172
6.14 Correlations between each variable and canonical axis (bolded values indicate the variables that best explain the observed variation along each axis).....	174
6.15 Cross-validated posterior probabilities of genus membership using ten relative areas and angles of the scaphoid articular surfaces	174
6.16 Summary of mean scaphoid carpal joint and non-articular features (distinctive features shown in bold)	175
7.1 Pairwise comparisons of genus means for the angle between the capitate and 3 rd metacarpal joint surfaces.....	187
7.2 Pairwise comparisons of genus means for the angle between the capitate and medial trapezoid surfaces	188
7.3 Pairwise comparisons of genus means for the angle between the capitate and lateral trapezoid surfaces.....	189
7.4 Pairwise comparisons of genus means for the angle between the capitate and trapezium joint surfaces	190
7.5 Pairwise comparisons of genus means for the angle between the lateral trapezoid and trapezium joint surfaces	191

Table	Page
7.6 Pairwise comparisons of genus means for the angle between the lateral and medial trapezoid joint surfaces	192
7.7 Pairwise comparisons of genus means for the angle between the medial trapezoid and trapezium joint surfaces	193
7.8 Pairwise comparisons of genus means for the angle between the 3 rd metacarpal and trapezium joint surfaces	194
7.9 Pairwise comparisons of genus means for relative area of the 3 rd metacarpal joint surface.....	195
7.10 Pairwise comparisons of genus means for relative area of the capitate joint surface.....	196
7.11 Pairwise comparisons of genus means for relative area of the medial trapezoid joint surface	197
7.12 Pairwise comparisons of genus means for relative area of the lateral trapezoid joint surface	198
7.13 Pairwise comparisons of genus means for relative area of the trapezium joint surface	199
7.14 Correlations between each variable and canonical axis (bolded values indicate the variables that best explain the observed variation along each axis).....	202
7.15 Cross-validated posterior probabilities of genus membership using the relative areas and angles of the articular surfaces of the 2 nd metacarpal base	203

Table	Page
7.16 Summary of mean 2 nd metacarpal joint features (distinctive features in bold).....	204
8.1 Correlations between each variable and canonical axis (bolded values indicate the variables that best explain the observed variation along each axis).....	218
8.2 Cross-validated posterior probabilities of genus membership using relative area and curvedness measures of the 1 st carpometacarpal joint surfaces.....	218
8.3 Posterior probabilities of genus membership using relative area and curvedness measures of the of the 1 st carpometacarpal joint surfaces	218
8.4 Correlations between each variable and canonical axis (bolded values indicate the variables that best explain the observed variation along each axis).....	221
8.5 Cross-validated posterior probabilities of genus membership using relative areas and angles of the trapezium articular surfaces	222
8.6 Posterior probabilities of genus membership using relative areas and angles of the trapezium articular surfaces	222
8.7 Correlations between each variable and canonical axis (bolded values indicate the variables that best explain the observed variation along each axis).....	225

Table	Page
8.8 Cross-validated posterior probabilities of genus membership using relative areas and angles of the trapezoid articular surfaces	225
8.9 Posterior probabilities of genus membership using relative areas and angles of the trapezoid articular surfaces.....	225
8.10 Correlations between each variable and canonical axis (bolded values indicate the variables that best explain the observed variation along each axis).....	227
8.11 Cross-validated posterior probabilities of genus membership using relative areas and angles of the scaphoid articular surfaces	228
8.12 Posterior probabilities of genus membership using relative areas and angles of the scaphoid articular surfaces	228
8.13 Correlations between each variable and canonical axis (bolded values indicate the variables that best explain the observed variation along each axis).....	230
8.14 Cross-validated posterior probabilities of genus membership using relative areas and angles of the second metacarpal base articular surfaces	231
8.15 Posterior probabilities of genus membership using relative areas and angles of the second metacarpal base articular surfaces.....	231
8.16 Correlations between each variable and canonical axis (bolded values indicate the variables that best explain the observed variation along each axis).....	237

Table	Page
8.17 Cross-validated posterior probabilities of genus membership using the relative areas, angles, and curvedness measures of the trapezium articular surfaces.....	237
8.18 Posterior probabilities of genus membership using the relative areas, angles, and curvedness measures of the trapezium articular surfaces	238
8.19 Correlations between each variable and canonical axis (bolded values indicate the variables that best explain the observed variation along each axis).....	242
8.20 Cross-validated posterior probabilities of genus membership using three relative areas and angles of the scaphoid articular surfaces	243
8.21 Posterior probabilities of genus membership using three relative areas and angles of the scaphoid articular surfaces	243
8.22 Correlations between each variable and canonical axis (bolded values indicate the variables that best explain the observed variation along each axis).....	245
8.23 Cross-validated posterior probabilities of genus membership using relative curvedness of the proximal 1 st metacarpal articular surface.....	246
8.24 Posterior probabilities of genus membership using relative curvedness of the proximal 1 st metacarpal articular surface	246

Table	Page
8.25 Correlations between each variable and canonical axis (bolded values indicate the variables that best explain the observed variation along each axis).....	248
8.26 Cross-validated posterior probabilities of genus membership using relative areas and angles of the trapezium articular surfaces	249
8.27 Posterior probabilities of genus membership using relative areas and angles of the trapezium articular surfaces	249
8.28 Correlations between each variable and canonical axis (bolded values indicate the variables that best explain the observed variation along each axis).....	251
8.29 Cross-validated posterior probabilities of genus membership using relative areas and angles of the second metacarpal base articular surfaces	251
8.30 Posterior probabilities of genus membership using relative areas and angles of the second metacarpal base articular surfaces.....	251
8.31 Summary of the trapezium surface curvedness measures of the 1 st metacarpal in the fossil specimens	254
8.32 Summary of the angles, relative areas, and curvedness measures of the trapezium in the fossil specimens	255
8.33 Summary of the angles and relative areas of the trapezoid in the fossil specimens.....	257

Table	Page
8.34 Summary of the angles and relative areas of the scaphoid in the fossil specimens.....	259
8.35 Summary of the angles and relative areas of the 2 nd metacarpal base in the fossil specimens.....	261
9.1 Sample breakdown by genus and bone for the extant taxa used in this study.....	292
9.2 Sample breakdown of the fossil specimens used in this study.....	293

LIST OF FIGURES

Figure	Page
<p>2.1 The radial halves of the right wrists and 1st and 2nd metacarpals of modern <i>Homo sapiens</i> (pictured at left) and <i>Pan troglodytes</i> (pictured at right). Non-human primates are predicted to show carpal and carpometacarpal bone and joint morphology in the region of the index finger that is more stable radio-ulnarly (R-U) and more effective in distributing forces directed proximally and distally (P-D).....</p>	42
<p>2.2 In human and non-human primates, the first carpometacarpal joint (A) is oriented roughly perpendicular to the other carpometacarpal joints (B and C). The radial halves of the right wrists of modern <i>Homo sapiens</i> (pictured at left) and <i>Pan troglodytes</i> (pictured at right) are shown in a distal view (top) and a rotated palmar view (bottom).</p>	43
<p>2.3 The radial halves of the right wrists and 1st and 2nd metacarpals of modern <i>Homo sapiens</i> (pictured at left) and <i>Pan troglodytes</i> (pictured at right). Modern humans are predicted to show carpal and carpometacarpal bone and joint morphology that is more stable proximo-distally (P-D) and more effective in distributing forces directed radially and ulnarly (R-U) through the thumb and wrist.....</p>	44

Figure	Page
3.1 Visual comparison of the trapezium articular surface on the right 1 st metacarpal in five extant primate genera (radio-ulnar curvedness = top row; proximal view = middle row; dorso-palmar curvedness = bottom row). All bones scaled to approximately the same length.....	48
3.2 Visual comparison of the 1 st metacarpal articular surface on the right trapezium in five extant primate genera (radio-ulnar curvedness = top row; distal view = middle row; dorso-palmar curvedness = bottom row). All bones scaled to approximately the same size.....	49
3.3 Plot of the canonical variables (CAN1, CAN2) generated from analysis of trapezium joint surface area and curvedness measures (<i>Homo</i> = open squares, <i>Pan</i> = closed triangles, <i>Gorilla</i> = open diamonds, <i>Pongo</i> = closed circles, <i>Papio</i> = Xs).....	64
3.4 Plot of the canonical variables (CAN1, CAN2) generated from analysis of 1 st metacarpal joint surface area and curvedness measures (<i>Homo</i> = open squares, <i>Pan</i> = closed triangles, <i>Gorilla</i> = open diamonds, <i>Pongo</i> = closed circles, <i>Papio</i> = Xs).....	67
3.5 Plot of the canonical variables (CAN1, CAN2) generated from analysis of 1 st metacarpal and trapezium joint surface areas and curvedness measures (<i>Homo</i> = open squares, <i>Pan</i> = closed	

Figure	Page
<p>triangles, <i>Gorilla</i> = open diamonds, <i>Pongo</i> = closed circles, <i>Papio</i> = Xs).....</p>	69
<p>3.6 Plot of the canonical variables (CAN2, CAN3) generated from analysis of 1st metacarpal and trapezium joint surface areas and curvedness measures (<i>Homo</i> = open squares, <i>Pan</i> = closed triangles, <i>Gorilla</i> = open diamonds, <i>Pongo</i> = closed circles, <i>Papio</i> = Xs).....</p>	70
<p>3.7 The right 1st carpometacarpal joint axes of motion after (A) Napier (1961) and after (B) Buford et al. (1990) and Hollister et al. (1992). Note the flexion-extension and abduction-adduction axes in (A) are perpendicular to one another and occur in the same plane whereas in (B) they do not; also (A) requires a third joint axis to explain rotation whereas (B) does not.</p>	84
<p>4.1 Visual comparison of trapezium shape in five primate genera (<i>Papio</i>, far left; <i>Pongo</i>, 2nd from left; <i>Gorilla</i>, middle; <i>Pan</i>, 2nd from right; <i>Homo</i>, far right). Key: top row, palmar view; middle row, distal view; bottom row, proximo-medial view; light blue, 1st metacarpal joint; dark blue, 2nd metacarpal joint; teal, trapezoid joint; light green, scaphoid joint; dark green, central joint (<i>Papio</i> only); pink, non-articular area. Bones are from the right side.....</p>	86

Figure	Page
4.2 Plot of the canonical variables (CAN1, CAN2) generated from analysis of relative areas and angles of the trapezium articular surfaces (<i>Homo</i> = open squares, <i>Pan</i> = closed triangles, <i>Gorilla</i> = open diamonds, <i>Pongo</i> = closed circles, <i>Papio</i> = Xs).....	99
4.3 Plot of the canonical variables (CAN2, CAN3) generated from analysis of relative areas and angles of the trapezium articular surfaces (<i>Homo</i> = open squares, <i>Pan</i> = closed triangles, <i>Gorilla</i> = open diamonds, <i>Pongo</i> = closed circles, <i>Papio</i> = Xs).....	101
4.4 Plot of the canonical variables (CAN1, CAN4) generated from analysis of relative areas and angles of the trapezium articular surfaces (<i>Homo</i> = open squares, <i>Pan</i> = closed triangles, <i>Gorilla</i> = open diamonds, <i>Pongo</i> = closed circles, <i>Papio</i> = Xs).....	102
4.5 Differences in trapezium carpal joint morphology observed in <i>Homo</i> (at left) in comparison to other primates (<i>Pan</i> is shown at right) that reflect differences in ability to reduce compressive and shear stresses during strong contraction of the thenar musculature. Note the relative areas and orientations of the scaphoid joint surface (dotted arrows) and the palmar non-articular area (solid arrows). Both <i>Homo</i> and <i>Pan</i> are scaled relative to actual size. Bones are from the right side.....	115
4.6 When force is applied to the 1 st carpometacarpal joint when the thumb is in an abducted posture (downward arrows), the ulnar	

Figure	Page
<p>portion of the trapezium tends to move disto-radially (upward arrows). The circles highlight the different orientation of the trapezium-2nd metacarpal joint in <i>Homo</i> (at left), which stabilizes the ulnar aspect of the trapezium against disto-radial subluxation, in contrast to non-human primates (<i>Pan</i> is shown at right). Bones are from the right side.....</p>	116
<p>5.1 Visual comparison of trapezoid shape in five primate genera (<i>Papio</i>, far left; <i>Pongo</i>, 2nd from left; <i>Gorilla</i>, middle; <i>Pan</i>, 2nd from right; <i>Homo</i>, far right). Key: top row, palmar view; middle row, medial view; bottom row, proximal view; pink, medial 2nd metacarpal joint; dark blue, lateral 2nd metacarpal joint; light blue, trapezium joint; medium blue, scaphoid joint; light green, capitate joint; dark green, non-articular area. Bones are from the right side.</p>	118
<p>5.2 Plot of the canonical variables (CAN1, CAN2) generated from analysis of relative areas and angles of the trapezoid articular surfaces (<i>Homo</i> = open squares, <i>Pan</i> = closed triangles, <i>Gorilla</i> = open diamonds, <i>Pongo</i> = closed circles, <i>Papio</i> = Xs).....</p>	136
<p>5.3 Plot of the canonical variables (CAN2, CAN3) generated from analysis of relative areas and angles of the trapezoid articular surfaces (<i>Homo</i> = open squares, <i>Pan</i> = closed triangles, <i>Gorilla</i> = open diamonds, <i>Pongo</i> = closed circles, <i>Papio</i> = Xs).....</p>	137

Figure	Page
5.4	Plot of the canonical variables (CAN1, CAN4) generated from analysis of relative areas and angles of the trapezoid articular surfaces (<i>Homo</i> = open squares, <i>Pan</i> = closed triangles, <i>Gorilla</i> = open diamonds, <i>Pongo</i> = closed circles, <i>Papio</i> = Xs)..... 138
5.5	Plot of the canonical variables (CAN1, CAN2) generated from analysis of relative areas and angles of the trapezoid articular surfaces (<i>Homo</i> = open squares, <i>Pan</i> = closed triangles, <i>Pongo</i> = closed circles, <i>Papio</i> = Xs)..... 142
5.6	Plot of the canonical variables (CAN2, CAN3) generated from analysis of relative areas and angles of the trapezoid articular surfaces (<i>Homo</i> = open squares, <i>Pan</i> = closed triangles, <i>Pongo</i> = closed circles, <i>Papio</i> = Xs)..... 143
5.7	Visual comparison of the differences between modern human and non-human primates in trapezoid morphology (<i>Homo</i> , shown at left; <i>Pan</i> , shown at right). In humans, the palmar portion of the trapezoid is expanded radio-ulnarly as well as proximo-distally such that the palmar nonarticular surface is more rectangular in shape rather than the pinched-tip wedge shape seen in non-human primates. Also, note the more parallel relationship in non-human primates between the radial articulation of the scaphoid (dotted-line) and the medial trapezoid-2 nd metacarpal joint, as

Figure	Page
well as the radio-ulnar stability provided by the capitate-second metacarpal joint. Bones are from the right side.....	156
5.8 Summary of differences in carpal joint morphology discussed in relation to the shape change of the trapezoid and the biomechanical predictions (<i>Homo</i> , shown at left; <i>Pan</i> , shown at right). The labeled features are derived in <i>Homo</i> relative to other primates; Key: A, larger 1 st carpometacarpal joint; B, larger trapezium-scaphoid joint; C, narrower palmar trapezium non-articular area; D, broader palmar trapezoid non-articular area; E, larger, more medio-palmarly-placed trapezoid-capitate joint; F, medial 2 nd carpometacarpal joint oriented more parallel to trapezoid-scaphoid joint; and G, smaller, rectangular shaped trapezoid-scaphoid joint. Bones are from the right side.....	157
6.1 Plot of the canonical variables (CAN1, CAN2) generated from analysis of six relative areas and angles of the scaphoid articular surfaces (<i>Homo</i> = open squares, <i>Pan</i> = closed triangles, <i>Gorilla</i> = open diamonds, <i>Pongo</i> = closed circles, <i>Papio</i> = Xs).....	171
6.2 Plot of the canonical variables (CAN1, CAN2) generated from analysis of ten relative areas and angles of the scaphoid articular surfaces (<i>Homo</i> = open squares, <i>Pan</i> = closed triangles, <i>Gorilla</i> = open diamonds, <i>Pongo</i> = closed circles, <i>Papio</i> = Xs).....	173

Figure	Page
<p>6.3 Visual comparison of the different scaphoid joint morphology observed in <i>Homo</i> (at left) in comparison to other primates (<i>Pan</i> is shown at right). Key: top row, difference in distal portion of capitate joint; middle row, difference in relative area of lunate joint; bottom row, differences in shape and orientation of trapezium-trapezoid joint. Bones are from the right side.</p>	181
<p>6.4 Visual comparison of the differences between modern human and non-human primates in scaphoid morphology (<i>Homo</i>, shown at left; <i>Pan</i>, shown at right). The labeled features are derived in <i>Homo</i> relative to other primates; Key: A, larger scaphoid-trapezium joint; B, distally more open scaphoid-capitate joint. Bones are from the right side.</p>	182
<p>6.5 Key differences, viewed medially, in scaphoid carpal joint morphology discussed in relation to the biomechanical predictions of Chapter 2 (<i>Homo</i>, shown at left; <i>Pan</i>, shown at right). The arrows denote the direction of applied net force at the first carpometacarpal joint during strong contraction of the thumb musculature. Note the larger ulnar joint area (circles) for the capitate created by the combination of trapezoid and scaphoid joint surfaces in <i>Homo</i>. Bones are from the right side.</p>	183
<p>6.6 The capitate-trapezoid and capitate-scaphoid joints are oriented relative to the 1st carpometacarpal joint (dotted lines) such that</p>	

Figure	Page
<p>shear stress is minimized regardless of the direction in which the thumb is compressed into the trapezium (arrows). Bones are from the right side.</p>	184
<p>7.1 Visual comparison of 2nd metacarpal base shape in five primate genera (<i>Papio</i>, far left; <i>Pongo</i>, 2nd from left; <i>Gorilla</i>, middle; <i>Pan</i>, 2nd from right; <i>Homo</i>, far right). Key: top row, palmar view; middle row, proximal view; bottom row, medial view; pink, 3rd metacarpal joint; light blue, capitate joint; dark blue, medial trapezoid joint; dark green, lateral trapezoid joint; medium blue, trapezium joint; light green, non-articular area. Bones are from the left side.....</p>	186
<p>7.2 Plot of the canonical variables (CAN1, CAN2) generated from analysis of the relative articular areas and angles of the 2nd metacarpal base (<i>Homo</i> = open squares, <i>Pan</i> = closed triangles, <i>Gorilla</i> = open diamonds, <i>Pongo</i> = closed circles, <i>Papio</i> = Xs).....</p>	202
<p>7.3 Plot of the canonical variables (CAN2, CAN3) generated from analysis of the relative articular areas and angles of the 2nd metacarpal base (<i>Homo</i> = open squares, <i>Pan</i> = closed triangles, <i>Gorilla</i> = open diamonds, <i>Pongo</i> = closed circles, <i>Papio</i> = Xs).....</p>	203
<p>7.4 In <i>Homo</i>, the 2nd metacarpal base acts to prevent the trapezium, trapezoid, and capitate from sliding distally with more proximo-distally oriented joints. This ensures that maximum joint surface</p>	

Figure	Page
<p>area contact is maintained at the trapezium-trapezoid and capitate-trapezoid joints (circled portion). Bones are from the right side.</p>	211
<p>7.5 Visual palmar comparison of the differences between modern human and non-human primates in 2nd carpometacarpal joint morphology (<i>Homo</i>, shown at left; <i>Pan</i>, shown at right). The arrows point to the more proximo-distally oriented joints in <i>Homo</i> versus the more radio-ulnarly oriented joints in the other genera. The derived features in <i>Homo</i> stabilize the inter-carpal joints of the trapezium, trapezoid, and capitate such that they maintain maximum contact with one another during radio-ulnar compression (circled area). Bones are from the right side.</p>	212
<p>7.6 Visual dorsal comparison of the differences between modern human and non-human primates in 2nd carpometacarpal joint morphology (<i>Homo</i>, shown at left; <i>Pan</i>, shown at right). The arrows point as in Figure 7.5. Bones are from the right side.</p>	213
<p>8.1 Plot of the canonical variables (CAN1, CAN2) generated from analysis of the 1st carpometacarpal joint relative areas and curvedness measures (<i>Homo sapiens</i> = open squares, <i>Pan</i> = closed triangles, <i>Gorilla</i> = open diamonds, Qafzeh 9 = grey square, Neandertal = closed squares).</p>	217

Figure	Page
8.2 Plot of the canonical variables (CAN1, CAN2) generated from analysis of relative areas and angles of the trapezium articular surfaces (<i>Homo sapiens</i> = open squares, <i>Pan</i> = closed triangles, <i>Gorilla</i> = open diamonds, Qafzeh 9 = grey square, Neandertal = closed squares).....	221
8.3 Plot of the canonical variables (CAN1, CAN2) generated from analysis of relative areas and angles of the trapezoid articular surfaces (<i>Homo sapiens</i> = open squares, <i>Pan</i> = closed triangles, <i>Gorilla</i> = open diamonds, Upper Paleolithic <i>H. sapiens</i> = grey squares, Neandertal = closed squares).....	224
8.4 Plot of the canonical variables (CAN1, CAN2) generated from analysis of relative areas and angles of the scaphoid articular surfaces (<i>Homo sapiens</i> = open squares, <i>Pan</i> = closed triangles, <i>Gorilla</i> = open diamonds, Upper Paleolithic <i>H. sapiens</i> = grey squares, Neandertal = closed squares).....	227
8.5 Plot of the canonical variables (CAN1, CAN2) generated from analysis of relative areas and angles of the second carpometacarpal joint surfaces (<i>Homo sapiens</i> = open squares, <i>Pan</i> = closed triangles, <i>Gorilla</i> = open diamonds, Neandertal = closed squares).....	230
8.6 Plot of the canonical variables (CAN1, CAN2) generated from analysis of trapezium relative areas, angles, and curvedness	

Figure	Page
measures of the articular surfaces (<i>Homo</i> = open squares, <i>Pan</i> = closed triangles, <i>Gorilla</i> = open diamonds, <i>Pongo</i> = closed circles, <i>Papio</i> = Xs, <i>Theropithecus</i> = grey +s, <i>Nasalis</i> = grey stars, <i>A. afarensis</i> = grey triangle, <i>H. habilis</i> = closed diamond).....	235
8.7 Plot of the canonical variables (CAN2, CAN3) generated from analysis of trapezium relative areas, angles, and curvedness measures of the articular surfaces (<i>Homo</i> = open squares, <i>Pan</i> = closed triangles, <i>Gorilla</i> = open diamonds, <i>Pongo</i> = closed circles, <i>Papio</i> = Xs, <i>Theropithecus</i> = grey +s, <i>Nasalis</i> = grey stars, <i>A. afarensis</i> = grey triangle, <i>H. habilis</i> = closed diamond).....	236
8.8 Plot of the canonical variables (CAN1, CAN2) generated from analysis of trapezium relative areas, angles, and curvedness measures, excluding those involving the second metacarpal surface (<i>Homo</i> = open squares, <i>Pan</i> = closed triangles, <i>Gorilla</i> = open diamonds, <i>Pongo</i> = closed circles, <i>Papio</i> = Xs, <i>Theropithecus</i> = grey +s, <i>Erythrocebus</i> = grey Xs <i>Nasalis</i> = grey stars, <i>A. afarensis</i> = grey triangle, <i>H. habilis</i> = closed diamond).....	238
8.9 Plot of the canonical variables (CAN2, CAN3) generated from analysis of trapezium relative areas, angles, and curvedness measures, excluding those involving the second metacarpal surface (<i>Homo</i> = open squares, <i>Pan</i> = closed triangles, <i>Gorilla</i> = open diamonds, <i>Pongo</i> = closed circles, <i>Papio</i> = Xs,	

Figure	Page
<p><i>Theropithecus</i> = grey +s, <i>Erythrocebus</i> = grey Xs <i>Nasalis</i> = grey stars, <i>A. afarensis</i> = grey triangle, <i>H. habilis</i> = black diamond).</p>	239
<p>8.10 Plot of the canonical variables (CAN1, CAN2) generated from analysis of three scaphoid joint surface measures (<i>Homo</i> = open squares, <i>Pan</i> = closed triangles, <i>Gorilla</i> = open diamonds, <i>Pongo</i> = closed circles, <i>Papio</i> = Xs, Qafzeh 9 = grey square, Neandertals = closed squares, <i>H. habilis</i> = grey circle).</p>	242
<p>8.11 Plot of the canonical variables (CAN1, CAN2) generated from analysis of relative curvedness of the proximal articular surface of the 1st metacarpal (<i>Homo sapiens</i> = open squares, <i>Pan</i> = closed triangles, <i>Gorilla</i> = open diamonds, <i>A. afarensis</i> = grey triangles).</p>	245
<p>8.12 Plot of the canonical variables (CAN1, CAN2) generated from analysis of relative areas and angles of the trapezium articular surfaces (<i>Homo sapiens</i> = open squares, <i>Pan</i> = closed triangles, <i>Gorilla</i> = open diamonds, <i>A. afarensis</i> = grey triangle).</p>	248
<p>8.13 Plot of the canonical variables (CAN1, CAN2) generated from analysis of relative areas and angles of the second carpometacarpal joint surfaces (<i>Homo sapiens</i> = open squares, <i>Pan</i> = closed triangles, <i>Gorilla</i> = open diamonds, <i>A. afarensis</i> = grey triangles).</p>	250

Figure	Page
<p>8.14 Plot of the canonical variables (CAN1, CAN2) generated from analysis of relative curvedness of the proximal articular surface of the first metacarpal (<i>Homo sapiens</i> = open squares, <i>Pan</i> = closed triangles, <i>Gorilla</i> = open diamonds, SK84 = open circle, SKX5020 = grey circle).....</p>	253
<p>8.15 Visual comparison of trapezium shape in extant hominines with fossil specimens (<i>Gorilla</i>, far left; <i>Pan</i>, 2nd from left; AL333-80, 3rd from left; OH7, 3rd from right; Shanidar 3, 2nd from right; modern <i>Homo sapiens</i>, far right). Key: top row, palmar view; middle row, distal view; bottom row, proximo-medial view; medium blue, 1st metacarpal joint; dark blue, 2nd metacarpal joint; light blue, trapezoid joint; light green, scaphoid joint; pink, non-articular area. Bones are from the right side.</p>	256
<p>8.16 Visual comparison of trapezoid shape in extant hominines with fossil specimens (<i>Gorilla</i>, far left; <i>Pan</i>, 2nd from left; Kebara 2, middle; Qafzeh 9, 2nd from right; modern <i>Homo sapiens</i>, far right). Key: top row, palmar view; middle row, medial view; bottom row, proximal view; pink, medial 2nd metacarpal joint; dark blue, lateral 2nd metacarpal joint; light blue, trapezium joint; medium blue, scaphoid joint; light green, capitate joint; dark green, non-articular area. Bones are from the right side (images of Kebara 2 and Qafzeh 9 are mirrored).....</p>	258

- 8.17 Visual comparison of scaphoid shape in extant hominines with fossil specimens (*Gorilla*, far left; *Pan*, 2nd from left; OH7 (partial), 3rd from left; Regourdou 1, 3rd from right; Qafzeh 9, 2nd from right; modern *Homo sapiens*, far right). Key: top row, radial view; middle row, distal view; bottom row, ulnar view; medium blue, capitate joint; dark blue, radius joint; light blue, trapezium-trapezoid joint; light green, lunate joint; pink, non-articular area. Bones are from the right side (image of Regourdou 1 is mirrored).260
- 8.18 Visual comparison of 2nd metacarpal base shape in extant hominines with fossil specimens (*Gorilla*, far left; *Pan*, 2nd from left; AL333-15, 3rd from left; AL333-48, 4th from left; AL333w-23, 4th from right; Regourdou 2, 3rd from right; La Chapelle-aux-Saints 1, 2nd from right; modern *Homo sapiens*, far right). Key: top row, palmar view; middle row, proximal view; bottom row, medial view; dark green, 3rd metacarpal joint; pink, capitate joint; dark blue, medial trapezoid joint; light blue, lateral trapezoid joint; light green, trapezium joint; medium blue, non-articular area. Bones are from the left side (images of AL333w-23, Regourdou 2, and La Chapelle-aux-Saints 1 are mirrored).....262
- 8.19 Summary of key features of radial carpal and carpometacarpal joint morphology that are derived in *Homo sapiens* in

comparison to non-human primates: a, larger 1st carpometacarpal joint; b, more proximo-distal orientation of trapezium-2nd metacarpal joint; c, larger trapezium-scaphoid joint that extends palmar-radially onto scaphoid tubercle; d, narrower palmar trapezium non-articular area; e, broader palmar trapezoid non-articular area; f, larger, more palmarly-placed trapezoid-capitate joint; g, smaller, rectangular shaped trapezoid-scaphoid joint; h, more proximo-distal orientation of capitate-2nd metacarpal joint; i, more distally-open capitate-scaphoid joint; j, medial 2nd carpometacarpal joint oriented more parallel to trapezoid-scaphoid joint. Bones are from the right side. 265

8.20 Summary of key features of radial carpal and carpometacarpal joint morphology that are primitive in non-human primates (*Pan troglodytes* is shown): a, smaller 1st carpometacarpal joint; b, more radio-ulnar orientation of trapezium-2nd metacarpal joint; c, smaller trapezium-scaphoid joint that extends palmarly in front of trapezoid; d, wider palmar trapezium non-articular area; e, narrower palmar trapezoid non-articular area; f, smaller, more dorsally-placed trapezoid-capitate joint; g, larger, triangular shaped trapezoid-scaphoid joint; h, more radio-ulnar orientation of capitate-2nd metacarpal joint; i, more distally-closed capitate-

Figure	Page
scaphoid joint; j, medial 2 nd carpometacarpal joint oriented more parallel to scaphoid-radius joint. Bones are from the right side.....	266
8.21 Cladogram based on the comparative analyses presented in the previous chapters. Together, the evidence indicates that the complex of derived features observed in <i>H. sapiens</i> (horizontal line) evolved sometime after the <i>Pan-Homo</i> split.....	267
8.22 The principle of parsimony suggests that the complex of derived features evolved either prior to the Neandertal-modern <i>H. sapiens</i> divergence (dotted line) or after (solid line) depending on whether the complex is present or absent in Neandertals.....	268
8.23 The principle of parsimony suggests that complex of derived morphological features evolved either prior to the first appearance of intensified stone tool-related manipulative behaviors (dotted line) or after (solid line) depending on whether the complex is present or absent in <i>A. afarensis</i>	273
8.24 Plot of the canonical variables (CAN1, CAN2) generated from analysis of relative areas, angles, and curvedness measures of the trapezium, 1 st metacarpal, and 2 nd metacarpal joint surfaces (<i>Homo sapiens</i> = open squares, <i>Pan</i> = closed triangles, <i>Gorilla</i> = open diamonds, <i>A. afarensis</i> = grey triangles).	276
8.25 A parallel section through the palm of the left wrist in a human embryo (crown-rump length, 16mm; approximately 45 days old).	

Figure	Page
<p>Note the radioulnar expansion of the trapezoid (A, black arrows) and the broadening of the capitate head (B, black arrows); the former corresponds to a more supinated trapezium and the latter corresponds to a distally-open scaphoid-capitate joint. The scaphoid is still separate from the centrale (white arrows) (adapted from Čihák, 1972).....</p>	284
<p>8.26 A parallel section through the palm of the right wrist in a human embryo (crown-rump length, 25mm; approximately 54 days old). Note the radioulnar expansion of the trapezoid (A, black arrows) and the broadening of the capitate head (B, black arrows); the former corresponds to a more supinated trapezium and the latter corresponds to a distally-open scaphoid-capitate joint (adapted from Čihák, 1972).</p>	285
<p>8.27 A transverse section through the distal carpal row in a human embryo (crown-rump length, 50mm; approximately 10-12 weeks old). Note the radioulnar expansion of the trapezoid (A), the palmar articulation (white circle) between the trapezoid and capitate (B), and the more supinated position of the trapezium (C) (adapted from Čihák, 1972).</p>	285
<p>9.1 Visual example of the process of fitting least-square planes to the articular areas of a left trapezium (<i>Gorilla</i> is shown).....</p>	300

9.2	Visual demonstration of the family of simple surfaces that exist within Quadric Shape Space (left). All quadric surfaces that are equidistant from the origin have the same amount of ‘curved-ness’ (middle), which increases as one moves further from the origin (right).	307
-----	---	-----

Chapter 1: Introduction

This dissertation is about adaptation; specifically, it is about testing a hypothesis of morphological adaptation to manipulative behaviors related to the use and manufacture of tools within the hominin lineage. The basic question is straightforward: what is the evolutionary history and adaptive significance of the modern human wrist in relation to the evolution of tool behavior in hominins? Indeed, this is the riddle of the wrist that I attempt to solve. Despite the current paucity of fossil hominin hand remains, I argue that the available evidence is sufficient to reasonably answer this interesting and important evolutionary question. In order to answer this question, however, I also argue that a slightly modified theoretical approach to the problem is necessary.

Typically, studies of the functional morphology and evolution of the hominin hand involve the demonstration of morphological correlates to either precision or power grasping (Leakey et al., 1964; Marzke et al., 1992; Marzke, 1997; Napier, 1962; Susman, 1988, 1991, 1994, 1998; Tocheri et al., 2003, 2005). Marzke (1997, 2005, and Marzke and Marzke, 2000) challenges this approach to asking questions about the evolution of the hominin hand and its relationship to tool behaviors. She raises an important point, “Have we been asking the right questions regarding the hand?” (2005: 252). She argues that the general approach is overly focused on functional interpretations of isolated bones and joints, which are likely not accurate in predicting the true function of the total anatomical interactions involved in manipulative behavior. She also questions the common assumption that unique features in the human hand are causally related to unique tool behaviors, and calls for more adequate testing of such assumptions (Marzke, 2005). These criticisms are constructive in that they highlight the

overemphasis on identifying the earliest tool-making hominins while underscoring the need for broader “consideration of the full range of manipulative and locomotor activities that might explain patterns of hand morphology in the fossil hominin species” (Marzke, 2005: 253).

This dissertation research attempts to address these concerns by adopting a strict approach that is firmly rooted in evolutionary theory and historical concepts of adaptation. To begin, I provide a brief overview of the theoretical and methodological approaches to studying adaptation and I discuss how these approaches apply to studying the human fossil record and, in particular, this dissertation research. Second, I conduct 3D morphological analyses of the radial wrist and carpometacarpal region of the hand to quantitatively establish how modern humans differ from extant great apes and baboons; this also involves determination of the polarity (i.e., primitive vs. derived) of various morphological characters in this hand region. The results are interpreted within a teleonomic framework (i.e. argument from design) that attempts to explain the functional significance of the observed differences in morphology. Third, I examine select groups of extinct hominins to determine when derived characters observed in modern humans appear in the fossil record and within what kind of behavioral context (e.g., prior to the first appearance of stone tools in the fossil record, in association with Oldowan technology, in association with Acheulian technology, etc.). Finally, based on the results of this dissertation research, I discuss the evolutionary history and adaptive significance of the modern human hand in relation to the evolution of stone tool behavior in hominins, while also providing suggestions for future research.

ADAPTATION

Adaptation is a central concept of any theory of evolution. Darwin's (1859) monumental work, *The Origin of Species*, introduced the concept of natural selection, which is at its very core an explanation of adaptation. But what exactly 'is' adaptation, 'an' adaptation, or adaptedness? Darwin proposed that distinct groups of organisms, or species, are in a constant struggle for existence. The result of this on-going struggle is that only certain individuals of any given group survive and produce offspring. These offspring have a higher probability of exhibiting the characteristics that enabled their parents to survive than do other non-related individuals of the same group; hence, characteristics that consistently improve fitness over generations end up being more common in the descending lineage of the ancestral group. Such characteristics are adaptations, organisms that possess them are adapted to their conditions of life, and the process of acquiring such characteristics is adaptation through natural selection.

Adaptation, whether conceived of as a process, state, or thing, is always a comparison between two or more things. The process of adaptation is the result of directed change (natural selection) rather than random change (gene drift). A species that is adapted to its habitat displays characteristics that improve its fitness within its habitat in comparison to other characteristics it could reasonably display but does not. Finally, an adaptation is a particular characteristic that is better than an alternate characteristic within some given context. As a state or thing, adaptation is always about the better of two or more possibilities; it need not be, and rarely is, the perfect solution to a particular problem (Amundson, 1996; Simpson, 1947; Williams, 1997). Therefore, it is also

important to study the deficiencies of adaptations in order to get a balanced perspective of the strengths and weaknesses of the evolutionary processes that led to the observed condition (Williams, 1997).

The scientific literature of the 20th century is filled with attempts to further define, describe, and analyze 'adaptation' as an evolutionary concept (e.g., Bock, 1981; Bock and von Wahlert, 1965; Brandon, 1978; Burian, 1983; Dobzhansky, 1956, 1968; Lewontin, 1978, 1979; Muller, 1949; Munson, 1971; Reeve and Sherman, 1993; Sober, 1984; Stern, 1970; Williams, 1966; Wright, 1949). Many well-formulated criticisms and revisions of the various theoretical and methodological approaches to studying adaptation have also been presented (Amundson, 1996; Baum and Larson, 1991; Bock and von Wahlert, 1965; Cartmill, 2000a, b; Gans, 1988; Gould and Lewontin, 1979; Gould and Vrba, 1982; Harvey and Pagel, 1991; Harvey and Purvis, 1991; Kay and Cartmill, 1977; Larson and Losos, 1996; Lauder, 1981, 1982, 1995, 1996; Lewontin, 1978, 1979; Mayr, 1983, 1988; Reeve and Sherman, 1993; Rose and Lauder, 1996; Ross, 1999; Ross et al., 2002; Rudwick, 1964; Sober, 1984). These approaches to studying adaptation are generally classified as using either a non-historical or historical concept of adaptation (Amundson, 1996).

The primary distinction between these two concepts of adaptation involves the relationship between adaptation and natural selection. The historical concept is intimately tied to the process of natural selection whereas the non-historical concept is not. The historical concept of adaptation attempts to explain both the origin and subsequent maintenance of characters as the result of natural selection (Amundson,

1996; Baum and Larson, 1991; Brandon, 1978, 1990; Coddington, 1988, 1990, 1994; Gould and Vrba, 1982; Harvey and Pagel, 1991; Lauder, 1995, 1996; Lauder et al., 1993, 1995; Leroi et al., 1994). Alternatively, the non-historical concept attempts to explain only the maintenance, or current-fitness, of characters (Reeve and Sherman, 1993; Ross et al., 2002). Historical approaches maintain an explicit relationship with the process of natural selection but may often become impractical when studying many extant and fossil forms; non-historical approaches say nothing about the process of natural selection but are practical in that they assess the current utility of a given character. This relationship to evolutionary theory determines the types of questions of interest: the non-historical concept is typically used to study adaptation at the level of the organism (e.g., reconstructing behavior and life-history of an individual) whereas the historical concept is typically used to reconstruct the processes responsible for the observed divergence of characteristics (e.g., behavioral, morphological, etc.) between distantly and closely related species.

Since the focus of this dissertation research is on reconstructing the evolutionary history and adaptive significance of the modern human hand, I utilize the historical concept of adaptation. In other words, the focus is on demonstrating how closely related extant and extinct groups of the family Hominidae differ from one another in particular aspects of their hand and wrist morphology, while reconstructing when and why such changes occurred within the tribe Hominini.

The historical concept of adaptation is rigorous in its definition (Amundson, 1996; Baum and Larson, 1992; Brandon, 1990; Coddington, 1988; Gould and Vrba, 1982;

Harvey and Pagel, 1991; Lauder et al., 1993, 1995; Lauder, 1996; Leroi et al., 1994).

An adaptation originates in a population as a random character, which is subsequently maintained in the population by the process of natural selection. Most importantly, the adaptation is present in the lineage descending from the original population and still serves the same utility as it did when it initially arose. Indeed, this was how Darwin (1859) defined adaptation.

Using the historical concept of adaptation, traits that confer an ‘adaptive’ advantage but arose due to selection for another reason (e.g., allometry, pleiotropy, etc.) are not adaptations. Darwin (1859) recognized many such traits as correlations of growth. To facilitate interpretation of various nuances of the adaptive process, the historical concept is subdivided into several explicit categories. These include: aptation, adaptation, exaptation, nonadaptation, and disaptation (Gould and Vrba, 1982; Larson and Losos, 1996). Each category describes the pattern of adaptive function (e.g., useful or detrimental) and the process of how the pattern arose (e.g., was there initial selection for the adaptive function or was a previous adaptive function co-opted for some other function?). The explicit definitions of each category of adaptation presented below are summarized from the paper in which they were first introduced (Gould and Vrba, 1982).

An aptation defines any particular phenotype that improves the fitness of the organism. The current utility of the character is the primary importance and there is no concern whether natural selection was involved in its phylogenetic origin. Aptations are therefore similar to “adaptations” defined in a non-historical sense.

An adaptation serves current utility for the organism and arose and evolved for that utility. In other words, it has always performed the same function in the organism, it was initially selected for that purpose, and selection has maintained its presence in the lineage.

An exaptation has subsequently become adaptive for some purpose other than the one for which it initially evolved. In other words, it represents a certain preadaptive capacity, but only in an *a posteriori* sense. This is a necessary condition of the theory of descent with modification. With lineages undergoing constant modifications over time, features adaptive at one given time may become adapted, or exapted, for some other purpose during the process of modification.

A nonadaptation serves no current utility for the organism and its origin cannot be explained by the process of natural selection. Nonadaptations may also represent a previous adaptation that has now lost its initial ability and serves no other purpose for the organism. It differs from a disadaptation, which results in the organism being selected against, or otherwise decreases the organism's fitness relative to others in its population without the disadapted character.

The various definitions of 'adaptations' are critical components of the historical concept of adaptation. It is important to recognize that the delineations between each definition are always interpreted in a historical context. In other words, it is the context in which a particular character evolves that determines which type of adaptation it represents. It is not uncommon for this aspect of the historical concept to be misunderstood. For instance, one might incorrectly infer that all morphologically adaptive characters of an

extant species, such as *Homo sapiens*, are exaptations since they are all ultimately derived from the anatomy of a primitive tetrapod. If the context of character evolution is considered, however, the result is a nested hierarchy of a series of adaptations and exaptations. Consider, for example, morphological anatomy relating to bipedality, the locomotor behavior characteristic of the genus *Homo*. Characteristics initially co-opted from the ancestral locomotor strategy of the *Pan-Homo* last common ancestor represent exaptations for bipedality. Any derived characteristics that arose in a context in which bipedal behavior was adaptive, however, constitute morphological adaptations for this form of locomotion.

The above example underscores several important concepts that are required to make reasonable probabilistic inferences or statements regarding adaptation. First, we must recognize the importance of behavior in adaptation, which is by definition a hierarchical process. Behavioral adaptation must always precede morphological adaptation because it is a statement of conditional probability (Coddington, 1988). It is divergence in behavioral characteristics that leads to the possibility of selection for certain behaviors over others within a given ecological context. If selection of certain behaviors over others occurs, a new behavioral context is created in which divergence of morphological characteristics leads to the possibility of selection of certain morphologies over others. In this case, the behavioral modifications represent adaptations to the habitat or ecosystem while the morphological modifications represent adaptations to the behavior. If, on the other hand, morphological modifications precede the acquisition of useful behavioral characteristics, then the conditional probability

statement does not hold, and the morphological modifications are equivalent to exaptations. That is, the morphology arose in a context other than that which it is now of use to the organism.

The determination of the context is obviously dependent on the completeness of the fossil record and the known or assumed phylogenetic relationships of the taxonomic groups under study. Incorporating phylogenetic evidence into studies of adaptation has become a critical component of the response to criticisms of the adaptationist program (Baum and Larson, 1991; Brooks and McLennan, 1991, 2002; Cartmill, 2002a, b; Coddington, 1994; Felsenstein, 1985; Harvey and Pagel, 1991; Harvey and Purvis, 1991; Larson and Losos, 1996; Maddison and Maddison, 1992; Swofford and Maddison, 1992; Witmer, 1995). In many respects, this response returns to the more pluralistic Darwinian concept that it is a combination of genealogical and environmental processes that results in the evolution of biological diversity (Brooks and McLennan, 1991, 2002; Gould and Lewontin, 1979).

Phylogenetic reconstructions are important for studying evolutionary events such as adaptation because they aid in the identification of independent events and independence is a critical assumption of almost all statistical tests of hypotheses relating to the tempo and mode of evolution (Harvey and Pagel, 1991). Phylogenies help to determine if an evolutionary event has occurred only once as opposed to several different times. In other words, it is necessary to investigate whether a particular character seen in two or more taxa represents a similar adaptation or is simply the result of descent from a common ancestor. For example, it has long been held that

pentadactyly is the primitive condition in all terrestrial vertebrates because the first tetrapods to survive on land had five digits on each appendage before they became land-dwelling. In this case, the retention of pentadactyly in living species indicates shared descent and therefore the occurrence of only one evolutionary event. Recent evidence, however, suggests that pentadactyly is not the primitive condition in tetrapods, as some have six, seven, and even eight digits (Coates and Clack, 1990; Galis et al., 2001a, b; Hinchliffe, 1989). Pentadactyly may therefore represent several independent evolutionary events as different lineages have converged on the same character of five digits (Gould, 1993). While pentadactyly may still have an adaptive basis in both cases, it is important to distinguish whether it has been selectively maintained in the descendant lineages or selection forces have been responsible for its repeated origin (Harvey and Pagel, 1991).

One of the most useful contributions that phylogenetic information gives to the study of adaptation is the ability to bracket a form-function relationship in its historical context. This contribution is known as the phylogenetic method for inferring function and behavior from morphology (Brooks and McLennan, 1991; Larson and Losos, 1996; Witmer, 1995). This method typically involves two steps: 1) related extant taxa are compared to establish the form-function relationship in particular groups, and 2) fossil taxa that are closely related to the extant sample are considered to share the form-function relationship with their extant relatives if they share the homologous structures associated with a particular function. For instance, consider three closely related extant taxa (A, B, and C). All three share a structure (S1) but taxa A and B share an additional

structure (S2) to the exclusion of taxon C. If S2 can be shown to have a strong relationship with a function (F2), then any fossil taxa considered more closely related to taxa A and B than taxon C that exhibit S2, may be inferred to also have F2 (however, see Lauder [1995] for alternative).

There are two predictions made by the hypothesis that a particular character evolved as an adaptation through the process of natural selection (Baum and Larson, 1991; Coddington, 1988, 1990; Greene, 1986; Larson and Losos, 1996). These predictions state that 1) the evolution of the character occurred within the context of a particular selective regime, and 2) the descendant forms display the character which is more advantageous in that context than is the character of the ancestral form.

Various approaches for testing these predictions have been proposed (Baum and Larson, 1991; Coddington, 1988, 1990; Greene, 1986; Larson and Losos, 1996). There are many common goals inherent to these approaches despite the fact that each approach differs in certain details. These commonalities serve as the basis of the protocol for testing hypotheses of adaptation initially proposed by Baum and Larson (1991) and subsequently revised by Larson and Losos (1996). This phylogenetic approach is rigorous and includes the formulation of adaptive hypotheses, phylogeny reconstruction, scoring and phylogenetic partitioning of characters and selective regimes, assessment of biological role or utility, and classification of traits into categories of utility and historical genesis (Larson and Losos, 1996). Unfortunately, this approach is most often impractical for studying fossils given the difficulties involved in 1) acquiring phylogenetic data that are accurate and dense, 2) assuming that

homologous functions, behaviors, and selective regimes are readily identifiable, and 3) having relevant extant taxa to serve as reasonable models to study character origins (Ross et al., 2002).

In general, the historical concept of adaptation strictly follows evolutionary theory and natural selection at the expense of practical methodology. Advocates of the non-historical approach often cite the focus of the historical approach on explaining adaptive origins opposed to current utility as too extreme to allow for reasonable hypothesis testing of adaptation, particularly when fossils are included in the analysis (e.g., Mayr, 1988; Reeve and Sherman, 1993; Ross et al., 2002; Williams, 1997). In almost all fossil records of vertebrates, one must continually infer behavior indirectly from morphology. In such cases, it is next to impossible to identify behavioral adaptations in the absence of evidence of morphological adaptations to such behaviors. Therefore, the non-historical approach is often the only option available.

The human fossil record, however, is different than all other vertebrate fossil records in one very important feature: there is over 2.5 million years of direct evidence of tool behavior (i.e., in the form of stone tools). In many instances, stone tools are present in the record yet they are unaccompanied by any biological evidence of which hominin made them. However, the stone tools are direct evidence of hominin manipulative behaviors related to tools. Therefore, the human fossil record provides the raw material necessary for testing whether morphological adaptation to manipulative behaviors related to the use and manufacture of tools has occurred within the hominin lineage.

This assumes that tool behavior, in the general sense, is adaptive in comparison to its behavioral alternatives, which do not include tools, within certain ecological contexts.

There is no guarantee that morphological modifications that improve aspects of an already present adaptive behavior will occur, although this is a common assumption. However, the longer a particular behavior remains adaptively successful within an evolving lineage, the higher is the likelihood that descendants of that lineage will show morphological adaptations to the behavior. Again, it is a statement of probability. It is also a statement of morphological commitment to an adaptive behavior (a historical concept), rather than a statement of morphological capability or capacity to perform a behavior (a non-historical concept).

Nature is full of examples of species that exhibit unexpected behaviors given their current morphological state. As Darwin (1859) noted: “We have seen that a species may under new conditions of life change its habits, or have diversified habits, with some habits very unlike those of its nearest congeners. Hence we can understand, bearing in mind that each organic being is trying to live wherever it can live, how it has arisen that there are upland geese with webbed feet, ground woodpeckers, diving thrushes, and petrels with the habits of auks” (1859: 204).

The specific question, “who made the Oldowan tools?” has been the focus of many studies (e.g., Napier, 1962; Susman, 1988, 1989, 1991, 1994, 1998); however, this is a question of morphological capability to perform a behavior and is, by definition, a non-historical approach. Behavior is inferred from the morphology, which is already assumed to be adapted to the behavior through a specific hand function, the precision

grasp or grip (Susman, 1998). Alternatively, other studies have focused on a broader approach that attempts to discern adaptive changes to hand morphology across different stages in the evolution of tool behavior (i.e., stone and non-stone related) in hominids, with an emphasis on the importance of both the precision and power grips (Marzke, 1997, 2005; Marzke et al., 1992, 1996; Marzke and Marzke, 1987, 2000).

TO BE PRECISE OR POWERFUL? A QUESTION OF GRIP

Prior to the discovery of OH7 (*Homo habilis*), Napier (1956) defined the terms precision grip and power grip in an effort to classify all of the prehensile movements of the human hand. In essence, he synthesized previous efforts of grip classifications (Griffiths, 1943; McBride, 1942; Slocum and Pratt, 1946) into a simpler scheme and provided an anatomical and functional basis of each basic grip in humans. Prehensile movements involve movements that include the grasping of an object, either wholly or in part, with one hand, whereas non-prehensile movements include using the hand to manipulate an object without grasping it (e.g., lifting or pushing the object) (Napier, 1956). Napier found that the seemingly infinite number of prehensile movements that the human hand can perform is explained, both anatomically and functionally, by two basic types of grips. He defined the power grip as when an “object is held as in a clamp between the flexed fingers and the palm, counter pressure being applied by the thumb lying more or less in the plane of the palm” (Napier, 1956: 913). Alternatively, the precision grip is defined as when an “object is pinched between the flexor aspects of the fingers and that of the opposing thumb” (Napier, 1956: 913).

These two basic grips are not necessarily mutually exclusive, and Napier discusses how precision is applied to the power grip and vice versa. In the power grip, he suggests that the position of the thumb determines the amount of precision applied to the grip. If the thumb is in an adducted position, power is sacrificed for the sake of precision. In this instance, the thumb is often in line with the forearm and runs along the long axis of the object being grasped. Alternatively, as the thumb assumes a more abducted posture, precision is sacrificed for more power and buttressing capability, until the point at which the thumb is no longer in direct contact with the object and acts solely to reinforce the dorsal surface of the fingers (e.g., as in a closed fist). In the precision grip, the thumb is abducted and flexed such that it is in opposition to the fingers. The opposed thumb and fingers grasp the object without the aid of the palm.

According to Napier (1956), each of these grips has essential anatomical features associated with it. It is important to remember that his proposed form-function associations are based solely on observations of the human hand; no comparative analysis with nonhuman primates was performed. He proposed that the associated features of the power grip in humans are: 1) a thumb capable of providing stability in positions of adduction and abduction; 2) fingers capable of inclining toward the ulnar side of the hand through the combined motion of flexion and lateral rotation; 3) a muscular cushion provided by a hypothenar elevation in opposition to the thenar eminence; 4) a wrist capable of ulnar deviation when held in the neutral position between full flexion and full extension, such that the long axis of the thumb lines up with the long axis of the forearm (Napier, 1956). In contrast, he proposed that the

associated features of the precision grip in humans are: 1) a thumb capable of opposition, which he defines as a combination of abduction and medial rotation at both the carpometacarpal and metacarpophalangeal joints; 2) fingers capable of flexing and abducting at the metacarpophalangeal joints, producing a degree of axial rotation at the digits while also increasing hand span; 3) a wrist capable of marked extension when held midway between ulnar and radial deviation (Napier, 1956).

At the time of this initial publication on the precision and power grips, the associated anatomical features were not meant to have any particular relevance to human evolution. In fact, Napier (1956) even stressed that these features are likely shared by most other primates.

“While the perfection and completeness of its accomplishments are not in doubt, the implicit idea that such an organ is a specialization of man is open to criticism. In many respects the human hand is a remarkably primitive structure, the pitfalls of extreme specialization shown, for example, by the gibbon, the potto and the baboon having been avoided in its phylogenetic history. In its pentadactyl form, the relative lengths of its digits, the arrangement of its musculature and in the generalised nature of its movements, man’s hand shows an ancient simplicity of structure and function. The human hand is little better endowed, in a purely material sense, than that of any generalized primate in whom the thumb is present and specialized. In this connection Wood Jones (1941) wrote: “We shall look in vain if we seek for movements that man can do and a monkey cannot, but we shall find much if we seek for purposive actions that man can do and a monkey cannot.” The heart of the matter lies in the term “purposive actions,” for it is in the elaboration of the central nervous system and not in the specialization of the hand that we find the basis of human skill” (Napier, 1956: 912-913).

The evolutionary significance of Napier’s original morphological correlates to the precision and power grips takes on a new meaning in his subsequent publications that examined the functional anatomy of other primate hands. Often, there are inconsistencies in Napier’s evolutionary arguments that reflect a combination of the

general theoretical approach of his time to studying human evolution and the lack of stricter methodological approaches to studying adaptation that are more accepted today.

Napier's first published account of his examination of the hands of living apes appears four years after his seminal paper on precision and power grips in humans (Napier, 1956, 1960). In his study, he examines two chimpanzees and one orangutan, all of which are from the Zoological Gardens in London and each is around two years of age. His study is divided into analyses of passive and active movements, and the results are discussed relative to his classification of human precision and power grips.

The main conclusion that Napier draws from his observations is that apes also use precision and power grips but these differ substantially from those used by humans (Napier, 1960). In particular, he suggests that it is the disproportionate length of the ape thumb in comparison to the fingers that contributes to the fundamental differences between apes and humans in precision and power grips. As such, he added relative thumb length to his list of morphological correlates for both the human-like precision and power grips (Napier, 1960, 1962). This particular feature has since received considerable discussion in the primate hand functional morphology literature. Although some researchers reject the applicability of this feature to the fossil record because of the rarity of finding complete hands (Marzke, 1997; Susman, 1998), others have used randomization procedures to reasonably estimate this feature, even when bones from a single individual are lacking, in order to make inferences about human-like precision and power grasping (Alba et al., 2003). Others have even gone as far as using this feature, along with other features, to infer that human-like precision grasping was

within the capabilities of the Miocene hominoid genus, *Oreopithecus* (Moya Sola et al., 1999).

However, closer examination of Napier's study reveals that the proposed link between relative thumb length and human-like precision and power grips is not supported by his own observations. With respect to this feature in the three juvenile apes he examined, Napier initially states, "In spite of a discrepancy in length between the index finger and thumb, the two digits in both genera could be placed in opposition by acutely flexing the index finger at its interphalangeal joints and widely abducting the thumb. The movement of opposition as it is understood in Man, however, is never performed actively by either genus and therefore the flexibility that permits it is a measure of mobility of the hand rather than a pointer to function" (Napier, 1960: 650). Clearly, the shorter relative length of the thumb in *Pan* and *Pongo* does not morphologically constrain the ability to form a human-like precision grip. Rather, it results in a 'change of preference' on how the apes instinctively form their precision grip. As Napier's (1960) original study and many others have since noted, *Pan* displays a number of precision grips, most of which involve manipulating objects between the thumb and various aspects of the side of the index finger (Christel, 1993; Christel et al., 1998; Marzke, 1997; Marzke and Wullstein, 1996; Marzke et al., 1992; Shrewsbury and Sonek, 1986). Moreover, many nonhuman primates have relative thumb and finger proportions that are similar to humans.

A direct comparison between Napier's (1956) original anatomical correlates of the human power grip and the hand morphology of the great apes, as understood at present,

reveals the following conclusions. Napier (1955) considered that stability at the first carpometacarpal joint is related to the incongruence of the saddle-shaped articular surfaces of the human trapezium and first metacarpal. When the metacarpal is adducted or abducted, the mutually articulating surfaces become congruent over a portion of the joint and this results in stability of the joint (Napier, 1955). Therefore, all great apes display a thumb capable of providing stability in positions of adduction and abduction, their shorter relative thumb lengths notwithstanding. Napier commented on “the extensive range found at the metacarpo-phalangeal joints of the chimpanzee and orang” and clearly the fingers of great apes are capable of inclining toward the ulnar side of the hand through the combined motion of flexion and lateral rotation (Napier, 1960: 652 and see 656, figure 12). Although Napier reported that *Pan* and *Pongo* show a smaller range of ulnar deviation of the wrist than in humans (Napier, 1956), his figures (12 and 15 in particular) as well as data that have become available since his initial study clearly indicate that great ape wrists are capable of ulnar deviation when held in the neutral position between flexion and extension (Richmond, 2006; Rose, 1988; Tuttle, 1967, 1969). Therefore, only one of Napier’s original anatomical correlates with the human power grip is not observed in the great apes—a muscular cushion provided by a hypothenar elevation in opposition to the thenar eminence. However, the observation that great apes can, at times, produce “a remarkably human power grip posture” (Napier, 1960: 656, figure 12) seriously undermines the relevance of this feature to the power grip. In total, Napier’s statements are more about morphological capability (exaptation) rather than morphological commitment (adaptation).

Similar inconsistencies are observed when reexamining Napier's (1956) original anatomical correlates of the human precision grip. Great ape thumbs are capable of a combination of flexion and abduction at both the carpometacarpal and metacarpo-phalangeal joints, which together contribute to the ability to oppose the thumb to the remaining digits. It is important to note that Napier (1961) considered true opposability to involve medial rotation of the first metacarpal, a movement that has since been demonstrated, both anatomically and kinematically, to occur only as a combined movement along the two non-perpendicular axes of the two-axis first carpometacarpal joint (Buford et al., 1990; Hollister et al., 1992). As discussed above, the fingers of great apes are capable of flexion and abduction at the metacarpo-phalangeal joints, and can therefore axially rotate while also increasing hand span. Finally, while the African apes display limited extension ability at the wrist, *Pongo* does not and so the third original correlate of the precision grip is also questionable (Richmond et al., 2001; Richmond, 2006; Rose, 1988; Tuttle, 1967, 1969).

The main conclusions that I draw from Napier's initial studies are that humans and great apes are capable of precision and power grips, and that there are differences in the preference of which types of precision and power grips are used most frequently and in their effectiveness in accomplishing certain tasks. These conclusions have been amply demonstrated by subsequent analyses of grip types and grip preferences in human and nonhuman primates (Christel, 1993; Christel and Fragaszy, 2000; Christel et al., 1998; Marzke, 1997; Marzke and Shackley, 1986; Marzke and Wullstein, 1996; Marzke et al., 1992, 1994; Shrewsbury and Sonek, 1986). Susman (1998) argues that it is unlikely

that the form-function relationship between more subtle types of precision and power grips and the musculo-skeletal hand anatomy can be reliably established, such that it can be used to infer function and behavior from fossil hands. However, this reasoning should not lead to a reliance solely on the “application of Napier’s morphological criteria to the study of fossil hand bones and a few additional observations more recently by others” to test questions surrounding the evolution of stone tool behaviors in hominins (*contra* Susman, 1998: 44). Rather, Napier’s morphological criteria are clearly insufficient in resolving the presence of human-like precision and power grips in fossils as is demonstrated by recent debates of these issues (Hamrick and Innouye, 1995; Marzke, 1997; Marzke and Shrewsbury, 2006; Moya Sola et al., 1999; Ohman et al., 1995; Susman, 1994, 1998, 2004, 2005).

Experiments involving the manufacture of prehistoric stone tools by modern humans further underscore the problems inherent to the precision versus power grip dichotomy (Marzke and Shackley, 1986; Marzke and Wullstein, 1996). Such work demonstrates that the grips necessary for manufacturing such tools combine aspects of both grips (Marzke and Wullstein, 1996; Marzke, 1997). This combination of grip features is referred to as ‘forceful precision grips’ by Marzke and Wullstein (1996), and include both ‘firm precision pinching’ (Marzke, 1997) and ‘precision handling’ (Landsmeer, 1962; Marke, 1997). It is clear that modern humans differ from nonhuman primates in the ‘quality’ of their precision and power grips and that there are morphological correlates that appear linked to this quality (Marzke, 1997). The question is whether this quality has been achieved via morphological adaptation to stone tool behavior or

through a combination of exaptations that evolved initially in other behavioral contexts (e.g., direct food-processing manipulative behaviors).

CAPABILITY VS. COMMITMENT

Whether a particular fossil hominid possessed anatomical features that enabled it to perform precision or power grips is a question of morphological *capability*. While this is an important question for improving the understanding of how morphology functions and how exaptation may occur, it is not a direct question of whether morphology represents an adaptation to the behavior. Precision and power grips represent a functional interface between morphology and behavior. This functional interface is similar to the concept of the faculty, as defined by Bock and von Wahlert (1965). According to Bock and von Wahlert (1965), how an organism utilizes a faculty in its behavioral repertoire during its lifetime defines the biological role of the form-function complex.

An inherent assumption of ‘capability’ arguments is that morphological adaptation to behavior has already occurred. Yet a wide range of organisms consistently perform behaviors that are novel and unexpected given the morphology inherited from their ancestors (Darwin, 1859; Jones, 1999), seriously undermining this assumption. All extant hominids perform their own distinct versions of precision and power grips because they each possess the basic morphological prerequisites, or exaptations, for such grips: a prehensile hand that has a palm, fingers, and thumb, all of which are primitive characteristics of the family Hominidae (Groves, 2001).

The observed or inferred differences in the functional capabilities between extant hominids likely represent differences in the biological role of the hand within the various behavioral adaptations that each group possesses. In other words, chimpanzees have yet to be observed making Oldowan-like stone tools not because they lack the basic morphology necessary, but because behavior that includes the use of stone tools is not adaptive within the context of their entire behavioral repertoire. The hand morphology that chimpanzees have inherited from their ancestors has not been exapted to a behavioral adaptation that includes the use and manufacture of stone tools. West African chimpanzees commonly use stones to crack open nuts otherwise unavailable to them (Matsuzawa, 1994; McGrew, 1994). This novel behavior may play an important role in the current diet of these populations; however, whether such behavioral innovation provides an adaptive advantage has yet to be determined. Even if this interesting behavior confers an adaptive advantage within this population, it does not yet appear that any members of this population have undergone any morphological specialization toward improving this behavior in comparison to chimpanzees that do not use stone to crack nuts.

From the perspective of studying adaptation in the historical sense, the question of who made the earliest stone tools is more a question about behavioral adaptation within an ecological context. For example, what are the ecological variables that may have triggered the divergence in behavioral characteristics (Potts, 1991; Reed, 1997, 2002)? Again it is only when the behavior is firmly established as a legitimate factor in increasing reproductive success that we can expect an increase in the likelihood of

observing morphological adaptations to the behavior in the descendants of the lineage.

Otherwise, the observed morphology represents an exaptation to the behavior.

A behavioral adaptation, by definition, represents a *commitment* to a particular adaptive behavior over others. Therefore, morphological adaptation represents a structural commitment to a behavior, which given particular ecological circumstances, is adaptive. Modern whales are derived in their limb morphology in comparison to their terrestrial ancestors (Thewissen and Bajpai, 2001). Ecological circumstances, and not morphological changes, resulted in an alteration of their ancestors' terrestrial behaviors to include a partly terrestrial and partly marine lifestyle. It was only when the marine component of their behavior became increasingly adaptive (in comparison to the terrestrial component) in response to ecological circumstances, that their behavior became increasingly adapted to a more marine lifestyle. Only with behavioral commitment are morphological modifications expected to show the greatest likelihood of being maintained or increased in the population, if the fortunate occasion that they appear should arise. If useful morphological modifications arise within the context of an already present adaptive behavior, then the likelihood is greater that the population's descendants will be morphologically committed to the novel behavior. If this former statement of conditional probability holds true, then morphological commitments to previously adaptive ancestral behaviors risk being lost.

If we were to look for the 'precision or power grasp' analogue in the evolutionary history of modern whales we would fail to find the morphology because their ancestors that took the first steps on that evolutionary journey had only the morphology of their

own ancestors (Thewissen and Bajpai, 2001). It was the initial and continued adaptedness of the derived behavior using exapted morphology that began their journey. In modern whales, we see only the clear result of the process of morphological adaptation to behavior that has unfolded over time along with the sacrifice of older morphological specializations, be they adaptations or exaptations, to ancestral behaviors (Thewissen and Bajpai, 2001). It is reasonable to expect the same to be true in the evolution of hominins (e.g., Foley, 1987a, b; Foley and Lahr, 2003).

Susman (1994) is likely correct in his conclusion that, by 2 Ma, all fossil hominin species had the capability of making and using stone tools. But his line of reasoning for arriving at this conclusion, based on inferences of functional morphology, is suspect. The technological stage in human evolution referred to as the Oldowan or Mode I (2.6 – 1.5 Ma) is most likely not evidence of the origin of stone tool behaviors in hominins, it is more appropriately interpreted as the first direct evidence of the intensification of stone tool behaviors in hominins (Clark, 1971; Isaac, 1984; Panger et al., 2002; Potts, 1991; Schick, 1987; Toth, 1985, 1987; Toth and Schick, 1986; Wynn and McGrew, 1989). Whether such behavior was tool-assisted or tool-dependent is still open to question (Binford, 1985; Potts, 1991). There is no reason to expect that the hominins dating to this time period should show morphological adaptations to such behaviors. Rather, questions should be directed at uncovering the ecological circumstances surrounding such a curious yet clear advent of divergence of behavioral characteristics (Reed, 1997). Evolutionary arguments based on morphological capability are weak in this context because we already have direct evidence of the behavior. No matter what

morphological features are found in the different hominins that exist during the Oldowan we are always forced to accept the possibility that they each practiced some degree of stone tool behavior because the tools are present. A brief review of the history of the discoveries of stone tools in the fossil record helps clarify my argument.

THE SEARCH FOR THE EARLIEST TOOL-MAKER

During the first half of the 20th century, the general idea of human evolution involved gradual changes through an anagenetic lineage such that only one species ancestral to modern humans existed at any one given time (see Reader, 1981 for historical overview). In this model, stone tool behavior originated with one species and was subsequently retained by each successive species. As each successive species became more and more like modern humans physically, their tools also became more sophisticated and similar to those used in the present. Using this evolutionary model, the goal of paleoanthropology was simple. Find the fossil hominin that is associated with the earliest stone tools and you have found the first ‘tool-maker’.

The discovery of OH5, *Paranthropus* (*Zinjanthropus*) *boisei*, by Mary and Louis Leakey in 1959 represented the first evidence of a hominin fossil clearly associated with some of the earliest known stone tools (Leakey, 1959). Despite Louis Leakey’s previous reluctance to accept australopithecine fossils as directly ancestral to *Homo sapiens*, the direct association of the fossil skull with the stone tools of the FLK living floor in Bed I was strong enough evidence to make Leakey at least partly change his mind. He declared that OH5 was responsible for making and using the stone tools; since man was defined as the tool-maker, then this fossil skull was therefore the oldest

known tool-maker and was a direct human ancestor (Leahey, 1959). Unable to reconcile his views about the evolutionary relationships between australopithecines and modern humans, he chose to place OH5 into a new genus, “Zinjanthropus”, rather than recognize the clear morphological affinities to the known genera of *Australopithecus* and *Paranthropus* (Leahey, 1959; Robinson, 1960).

At the time of the discovery of OH5, Bed I at Olduvai Gorge was relatively dated at around 600,000 years old. However, less than two years after the discovery, a new technique at that time known as potassium-argon dating was used to date the surrounding sediments, and it was revealed that the absolute age of the FLK living floor was 1.75 million years old (Leahey et al., 1961). While the majority of paleoanthropologists disagreed with Leahey’s naming of a new genus and his reluctance to view australopithecines as ancestral to man, they unanimously accepted the evidence that OH5 represented the oldest known tool-maker (Washburn, 1960).

P. boisei’s reign as the oldest known stone tool-maker was short-lived. One year after the discovery of OH5, a new set of hominin remains was discovered only a few hundred meters away from the FLK living floor (Leahey, 1971; Leahey et al., 1964). The new site, FLK NN, was also part of Bed I, and several hominin fossils were recovered from it. These fossils included one mandible, left and right parietals, and twenty-one hand bones (OH7), one clavicle and twelve foot bones (OH8), as well as other cranial and postcranial fragments (Leahey et al., 1964). Further hominin fossil discoveries around this same time included a tibia and fibula from Bed I at FLK as well

as a distal phalanx (OH10), a femoral neck (OH20), and an ulna (OH36) from the boundary zone between Bed I and II (Day, 1976; Leakey, 1971).

The living floor of FLK NN also dated to approximately 1.75 million years ago, and as such, the new fossils were not necessarily any older than OH5 (Leakey, 1971; Leakey et al., 1964). However, the morphological evidence indicated that this hominin was very different from *P. boisei*. A series of papers by several different authors was published between 1960 and 1964 describing the various parts of the anatomy that were preserved in this new set of fossils. First, the discoveries of the hand and foot bones followed by the mandible and parietal bones were announced (Leakey, 1960, 1961). These initial reports were followed by descriptions of the bones of the hand (Napier, 1962), foot (Day and Napier, 1964), lower leg (Davis, 1964), and reconstructed skull (Tobias, 1964). Together, these descriptions formed the basis for the naming of a new fossil taxon, *Homo habilis* (Leakey et al., 1964).

The so-called ‘handy man’ was described as having a larger cranial capacity and thinner cranial bones than *Australopithecus*, *Paranthropus*, or OH5 (Tobias, 1964; Leakey et al., 1964). The dentition consisted of small premolars and molars and large incisors and canines in comparison to the small front and large cheek teeth of the other known hominin taxa (Leakey et al., 1964). The tibia, fibula, and foot suggested the new taxon was a biped (Day and Napier, 1964; Davis, 1964), while the hand bones were interpreted as having the capability to form the basic grips necessary to fashion the stone tools found on the living floor (Napier, 1962). Together, the mandible, parietals,

and hand bones were presented as the holotype of *Homo habilis*, while the remaining fossils were given as paratypes.

The interpretation that the OH7 fossils were part of a hand capable of making and using the stone tools at Olduvai is a critical component of Leakey et al.'s (1964) taxonomic argument. In the original description of the fossil hand anatomy of OH7, Napier concludes that, "Morphologically, the Olduvai hand bones cannot be closely matched with any known hominoid species living today" (1962: 409). He lists seven morphological features that differ from the hand in modern humans, "1) robustness; 2) dorsal curvature of the shafts of the phalanges; 3) distal insertion of the flexor digitorum superficialis; 4) strength of fibro-tendinous markings; 5) 'set' of the trapezium; 6) the form of the scaphoid; 7) the depth of the carpal tunnel" (1962: 410), and three features that resemble the modern human hand, "1) presence of broad, stout terminal phalanges on fingers and thumb; 2) form of the distal articular surface of the capitate; 3) ellipsoidal form of metacarpo-phalangeal joint surfaces" (1962:410). Napier (1962, and Leakey et al., 1964) was faced with the uncompromising position that, given this hand was found in association with stone tools, this odd combination of morphological characters must have been sufficient for this hominin to make and use the tools. It is clear that in this instance the direct evidence of behavior, the stone tools themselves, resulted in the acceptance that the morphology exhibited the capability to perform the necessary behavior.

As the old adage says, hindsight is 20/20, and overt criticism of Napier is not my intention. In retrospect, his descriptions of the morphology are directly on the mark. It

is the evolutionary and adaptive inferences made from the combination of the morphological and behavioral evidence with which I take issue. Napier's astute observations that the overall general structure of the human hand was already present in the very first primates led him to suggest "that the evolution of the primate hand has been principally one of evolving *function* rather than the evolution of any new structure" (Napier, 1965: 552, emphasis in original). Napier had some interesting ideas about how there were successive evolutionary stages in which the primate hand gradually acquired more and more functional capability such that it could form first a power grip, later on a precision grip, and finally to the 'advanced form' of precision grip in humans (Napier, 1965).

I recognize that his evolutionary ideas are reasonable within the context of when they were formulated and presented. At that time, the stone tools found in association with OH7 were thought to be the oldest stone tools ever. There is now direct evidence of Oldowan stone tools at 2.6 Ma (Semaw et al., 1997) and several other Pliocene dates (Harris et al., 1987; Kimbel et al., 1996; Plummer et al., 1999; Roche et al., 1999), as well as direct evidence of the processing of animal bone using stone tools at 2.5 Ma (de Heinzelin et al., 1999). Therefore it is reasonable to ask why, almost 1 Ma years after the first appearance of stone tools in the fossil record, the hand of the so-called 'handy man' shows a combination of morphological features that suggests it is more likely to represent a hominin that is experimenting with a relatively novel behavior in comparison to its ancestors, using its inherited primitive morphology, rather than a

hominin that has morphologically committed, or adapted, to a behavior which has already secured its adaptive dominance within its behavioral repertoire?

Marzke (1997, 2005, and Marzke and Marzke, 2000) has continually advocated hypotheses of morphological adaptation, or commitment, to the habitual stresses of stone tool behaviors within fossil hominin species. These hypotheses have received critical responses from arguments based solely on morphological capability (Susman, 1998). In this dissertation research, I extend Marzke's approach within an explicit framework of the historical concept of adaptation that focuses on evidence of morphological commitment to behavior rather than capability per se. As I stated at the beginning of this introductory chapter, this dissertation is about adaptation. More specifically, it is about testing hypotheses of morphological adaptation to manipulative behaviors within the hominin lineage as evinced by stone tools—this represents the riddle of the wrist.

STATEMENT OF THE PROBLEM

The molecular evidence indicates that the hypothetical most recent common ancestor (MRCA) of the *Pan-Homo* clade existed between 4 and 8 Ma while the MRCA of the *Gorilla-Pan/Homo* clade existed between 6 and 10 Ma (Eizirik et al., 2004; Kumar et al., 2005; Steiper and Young, 2006). This evidence has important consequences for interpreting the evolutionary history and adaptive significance of the hand within the hominin lineage. First, it solidifies the hypothesis that the hand of the *Pan-Homo* MRCA most likely resembled the hand of *Pan* because parsimony suggests that many of the shared hand characteristics among the extant great apes are symplesiomorphic

(i.e., shared, primitive traits). Second, it provides a much needed context for interpreting the adaptive significance of subsequently derived changes to the hand that are observed within the hominin clade. For example, by 3 Ma, the *Australopithecus afarensis* hand had achieved thumb-finger proportions similar to modern *Homo* (Alba et al., 2003), suggesting that this derived feature evolved prior to the intensification of stone tool-related manipulative behaviors characteristic of the Oldowan. Therefore, the derived thumb-finger proportions of *A. afarensis* may represent either an adaptation for tool-related behaviors that are as yet unrecognizable in the fossil record or an exaptation to stone tool-related manipulative behaviors that are recognizable in the fossil record.

The primary research goal of this dissertation is to test whether there are derived morphological features present in the radial carpal and carpometacarpal region of the modern human wrist that represent one or more adaptive events within the evolution of hominins. More specifically, do some hominin species exhibit derived morphology in comparison to other species of hominin that are reasonably interpretable as morphological adaptations to manipulative behaviors related to tool use and manufacture (i.e., commitment rather than capability)? Reasonable interpretation includes an argument from design (Rudwick, 1964; West-Eberhard, 1992; Williams, 1992). That is, biomechanical analysis should suggest that any observed derived morphology has a functional advantage during tool behaviors over the ancestral morphology.

Using both a derived trait definition of adaptation and a teleonomic definition of adaptation is generally too strict an approach for testing hypotheses of adaptation. In

fact, the strictness of these historical approaches is what prompted a revised definition of a non-historical concept of adaptation (Reeve and Sherman, 1993). As I have argued in this introduction, however, the human fossil record has some unique attributes that allow such a strict approach to be undertaken. Most important among these attributes is the direct evidence of behavior in the form of stone tool technology. The presence of stone tools in the fossil record is evidence that tool behaviors in hominins first became intensified during the Pliocene (de Heinzelin et al., 1999; Harris et al., 1987; Kimbel et al., 1996; Plummer et al., 1999; Roche et al., 1999; Semaw et al., 1997), and such behaviors have continued in particular hominin lineages through to the present (Foley, 1987b; Foley and Lahr, 2003).

In this dissertation, I attempt to answer the following basic question: do hominins show morphological commitment to tool behaviors such that a) the ancestral morphology is sacrificed, and b) the derived morphology has performance advantages for the behavior (i.e., it is better than the primitive structure with respect to the novel behavior)? If so, when, in which hominins, and in which behavioral contexts did this event most likely occur?

In my attempt to answer these questions, I make the following assumption: the first hominins to make and use stone tools most likely did so with a hand that is otherwise indistinguishable from its most recent non-stone-tool-behaving ancestor (e.g., *Australopithecus afarensis*) (Beck, 1980; Goodall, 1964, 1986, Jordan, 1982; Lethmate, 1982; Sumita et al., 1985; Toth et al., 1993; Wright, 1972; Wynn and McGrew, 1989). I make this assumption based on a simple inference from the theory of evolution; that is,

divergence of behavioral characteristics often precedes divergence of morphological characteristics within an evolving lineage (Darwin, 1859). Moreover, it may even be reasonable to assume that the stone tools of the Oldowan, and perhaps even much of the Acheulian, were produced by hominins who were adapting behaviorally to their habitat, and not necessarily morphologically to their behavior.

To answer my research questions, I proceed as follows:

- 1) I introduce some basic biomechanical predictions, which are used to compare and contrast the basic functional design of the morphological characteristics of the primate genera sampled (Chapter 2);
 - a. these predictions are also used to evaluate the presented comparative evidence within the context of a hypothesis of morphological adaptation to tool-related manipulative behaviors (Chapters 3-8);
- 2) I present the results of the quantitative shape analyses performed on the radial carpal and carpometacarpal region in five extant primate genera (Chapters 3-7);
 - a. these results establish the polarity of the morphological features (i.e., primitive vs derived) within the family Hominidae, enabling the primitive characteristics of the hypothetical most recent common ancestor of the subtribe Homini to be reasonably inferred (i.e., humans and all extinct hominins more closely related to one another than any are to *Pan*);

- 3) I present the results of the quantitative shape analyses performed on the radial carpal and carpometacarpal region in extinct hominins (Chapter 8);
 - a. these results establish the polarity of the morphological features (i.e., primitive vs derived) within hominins and provide insights into when certain characteristics evolved and in which behavioral contexts;
- 4) I discuss the conclusions regarding the evolutionary history and adaptive significance of this region of the wrist along with the implications for future research (Chapter 8);
- 5) I describe the materials and methods used in the analyses (Chapter 9).

Chapter 2: The Basic Biomechanical Predictions

In an attempt to make my dissertation more readable, I include a discussion section at the end of each chapter using an overarching theme. The chosen theme takes the form of some basic biomechanical predictions, which are used to compare and contrast the morphology of the primate genera sampled. These predictions are also used to evaluate the presented comparative evidence within the context of a hypothesis of morphological adaptation to stone tool-related manipulative behaviors (i.e., an argument from design, or a teleonomic definition of adaptation).

As I discussed in my introductory chapter, any animal that possesses a prehensile hand that consists of a palm, convergent fingers, and a thumb has a ‘preadaptive’ capability of forming precision and power grips (Napier, 1961). This raises the question, what is it about modern humans that results in their duality of grips being so distinct from what we see in other primates? One aspect of this interesting question has already been answered effectively—it has been shown that modern humans, in comparison to non-human primates, perform both types of grips with greater amounts of force (Marzke, 1997; Marzke et al., 1992; Marzke and Wullstein, 1996).

During power grips, modern humans forcefully manipulate objects as extensions of the forearm as in hammering or clubbing (Marzke et al., 1992). During precision grips, modern humans apply large amounts of force to an object using their thumb and fingers, often referred to as precision-pinching (Marzke, 1997). Therefore, morphology that improved the effectiveness of the ability to manipulate objects with greater amounts of force would likely simultaneously improve the function of a wide variety of human-like precision and power grips. For example, during a pad-to-side thumb/index finger

precision grip used to turn a key inside a lock, the hand and wrist must withstand and distribute the reaction loads and torques from the locking mechanism. Similarly, the hand and wrist must withstand and distribute the loads and torques that arise from striking an object with a hammer using a typical power grip.

As I stated in Chapter 1, the goal of this research is not to predict whether a given species or specimen is capable of performing modern human-like precision or power grips based on the morphological features that it possesses. Rather, the goal is to determine if hominins show a morphological commitment to tool-related manipulative behaviors. Such commitment implies that there are derived changes in the wrist that, in comparison to the observed or inferred ancestral state, show clear biomechanical advantages for regularly performing modern human-like precision and power grips. Moreover, the derived changes must have evolved within a context that tool-related manipulative behaviors were adaptive.

Assuming that the morphology of a generalized prehensile hand of a hominid was exapted for use within the novel context of intensified manipulative behaviors involving stone tools, what derived modifications might we expect would represent improvements over the ancestral condition? Non-human primates regularly use their hands during locomotor behaviors. Quadrupedal locomotor behaviors result in compressive loads across the carpal and carpometacarpal joints to the second through fifth metacarpals due to ground reaction forces directed proximally. Therefore, in quadrupedal primates we should expect a pattern of morphological features that helps the carpal and

carpometacarpal joints to a) minimize compressive stress¹ by maximizing mutual joint surface area contact to distribute and withstand the joint reaction forces acting proximo-distally through the wrist, b) minimize shear² stress by lining up the joint surfaces such that they are more orthogonal to the joint reaction force, and c) minimize compressive and shear stresses by remaining stable from moving or sliding radio-ulnarly when experiencing joint reaction forces directed proximo-distally through the wrist.

In other words, non-human primates should typically benefit from a carpus that is more stable radio-ulnarly and more effective in distributing forces directed proximally and distally (Fig. 2.1). More specifically, non-human primates are predicted to show the following primitive pattern of morphological features:

- 1) articular surfaces that are oriented roughly orthogonal to the proximo-distal axis should have proportionately larger surface areas to minimize compressive stress;
- 2) the proximal and distal joint surfaces of each carpal bone should be oriented roughly orthogonal to the proximo-distal axis to minimize shear stress;

¹ By convention, a force (F) acting on an area (A) is defined as stress (S); mathematically, this is expressed as $S = F / A$. Therefore, given a particular amount of force, larger areas result in less stress.

² By convention, if a force acting on a surface is not perpendicular to the area, then the stress is subdivided into normal and shear components. The normal stress is the component perpendicular to the area while the shear stress is the component parallel to the area. The normal stress component increases and the shear stress component decreases as the acting force assumes a direction that is more perpendicular to the area.

- 3) the carpal and carpometacarpal joints should limit mobility radio-ulnarly, particularly when compressed proximo-distally (i.e., close-packed during locomotor behaviors).

Alternatively, modern humans generate and withstand greater amounts of force during precision and power grips that involve the thumb in comparison to non-human primates (Marzke, 1997; Marzke et al., 1992). These forceful grips consistently involve strong contraction of the thenar musculature and result in compression of the first metacarpal base into the trapezium. In human and non-human primates, the first carpometacarpal joint is oriented roughly perpendicular to the other carpometacarpal joints (Fig. 2.2). As a consequence, compression of the first metacarpal base into the trapezium results in loads directed transversely, or radio-ulnarly, across the wrist. Therefore, in modern humans we should expect a pattern of morphological features that helps the carpal and carpometacarpal joints in the region of the thumb to a) minimize compressive stress by maximizing mutual joint surface area contact to distribute and withstand the joint reaction forces acting radio-ulnarly across the wrist during strong contraction of the thenar musculature, b) minimize shear stress by lining up the joint surfaces such that they are orthogonal to the joint reaction force, and c) minimize compressive and shear stresses by remaining stable from moving or sliding proximo-distally when experiencing joint reaction forces directed radio-ulnarly across the wrist.

In other words, modern humans should typically benefit from a carpus that is more stable proximo-distally and more effective in distributing forces directed radially and

ulnarly (Fig. 2.3). More specifically, modern humans are predicted to show the following derived pattern of morphological features:

- 1) articular surfaces that are oriented roughly orthogonal to the radio-ulnar axis should have proportionately larger surface areas to minimize compressive stress;
- 2) the radial and ulnar joint surfaces of each carpal bone should be oriented roughly orthogonal to the radio-ulnar axis to minimize shear stress;
- 3) the carpal and carpometacarpal joints should limit mobility proximodistally, particularly when compressed radio-ulnarly (i.e., close-packed during forceful manipulative behaviors).

I use these basic biomechanical predictions as the general theme for presenting and discussing the results of my dissertation research in the chapters that follow. Since the goal of this research is to test a hypothesis of morphological adaptation to manipulative behaviors related to the use and manufacture of tools within the hominin lineage, the discussion sections focus on the predictions for the derived, adapted morphology expected in modern humans. Therefore, the results of the quantitative comparison for each morphological feature are presented in an order that begins with compressive load being applied to the trapezium via the first metacarpal base—the presentation begins with the analytical results of the quantitative comparisons of the first carpometacarpal joint morphology (Chapter 3), followed by comparisons of the carpal and carpometacarpal joints and non-articular area of the trapezium (Chapter 4), trapezoid

(Chapter 5), and scaphoid (Chapter 6), and the joints of the second metacarpal base (Chapter 7). Finally, the results, discussion, and conclusions regarding the evolutionary history and adaptive significance of this region of the hominin wrist are presented in Chapter 8. A complete description of the materials and methods is found in Chapter 9.

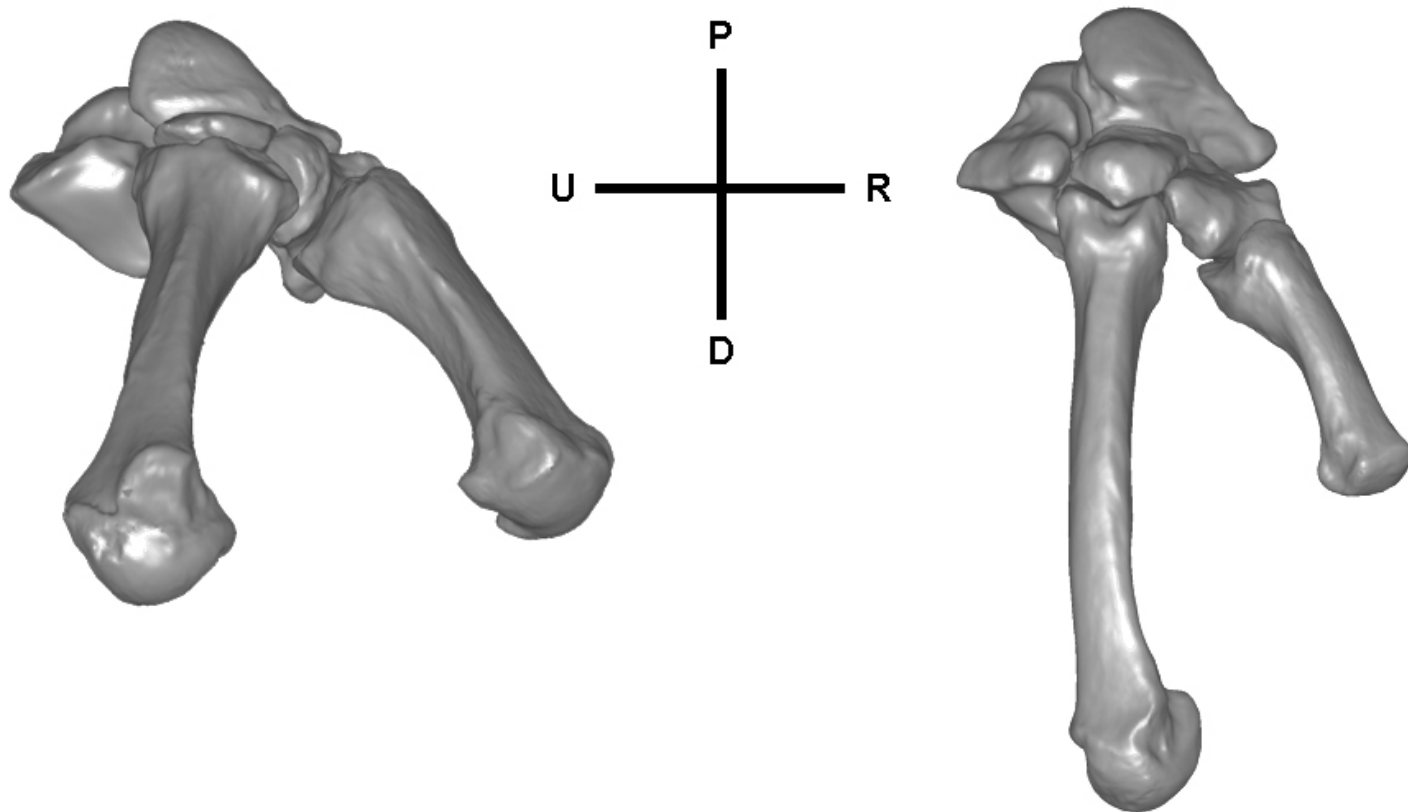


Fig. 2.1 The radial halves of the right wrists and 1st and 2nd metacarpals of modern *Homo sapiens* (pictured at left) and *Pan troglodytes* (pictured at right). Non-human primates are predicted to show carpal and carpometacarpal bone and joint morphology in the region of the index finger that is more stable radio-ulnarly (R-U) and more effective in distributing forces directed proximally and distally (P-D).

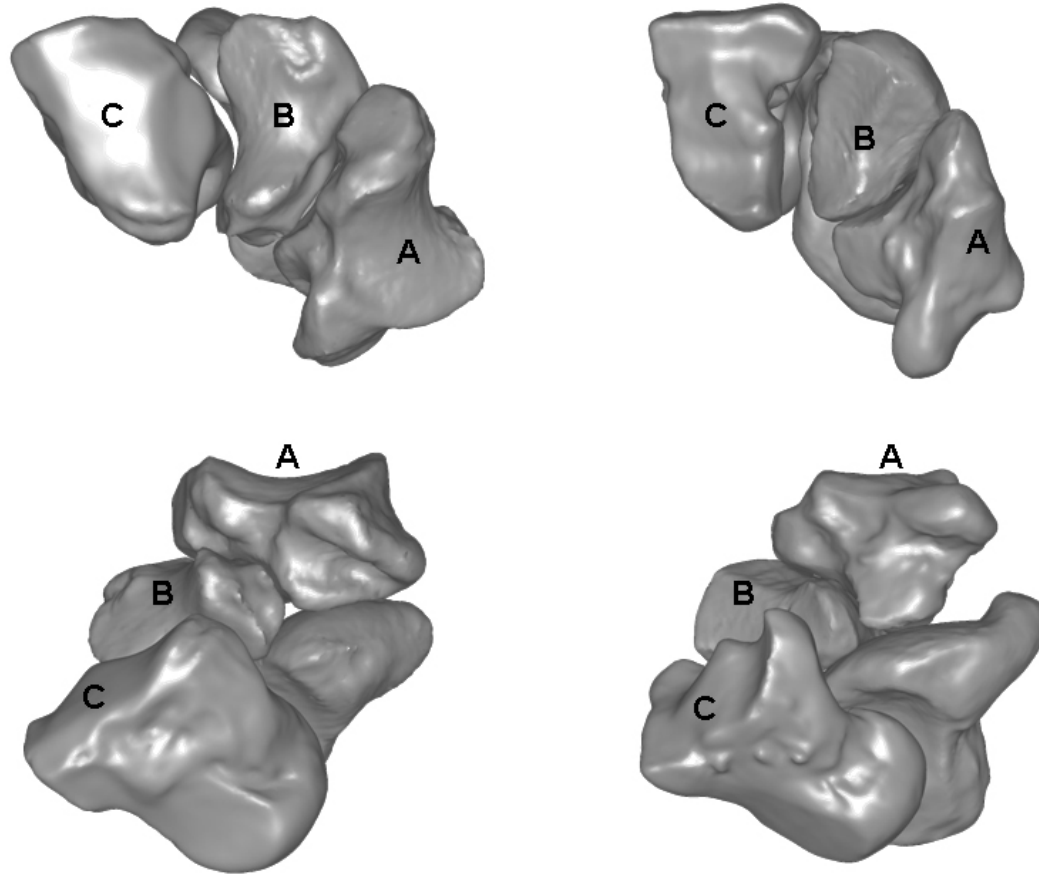


Fig. 2.2 In human and non-human primates, the first carpometacarpal joint (**A**) is oriented roughly perpendicular to the other carpometacarpal joints (**B** and **C**). The radial halves of the right wrists of modern *Homo sapiens* (pictured at left) and *Pan troglodytes* (pictured at right) are shown in a distal view (top) and a rotated palmar view (bottom).

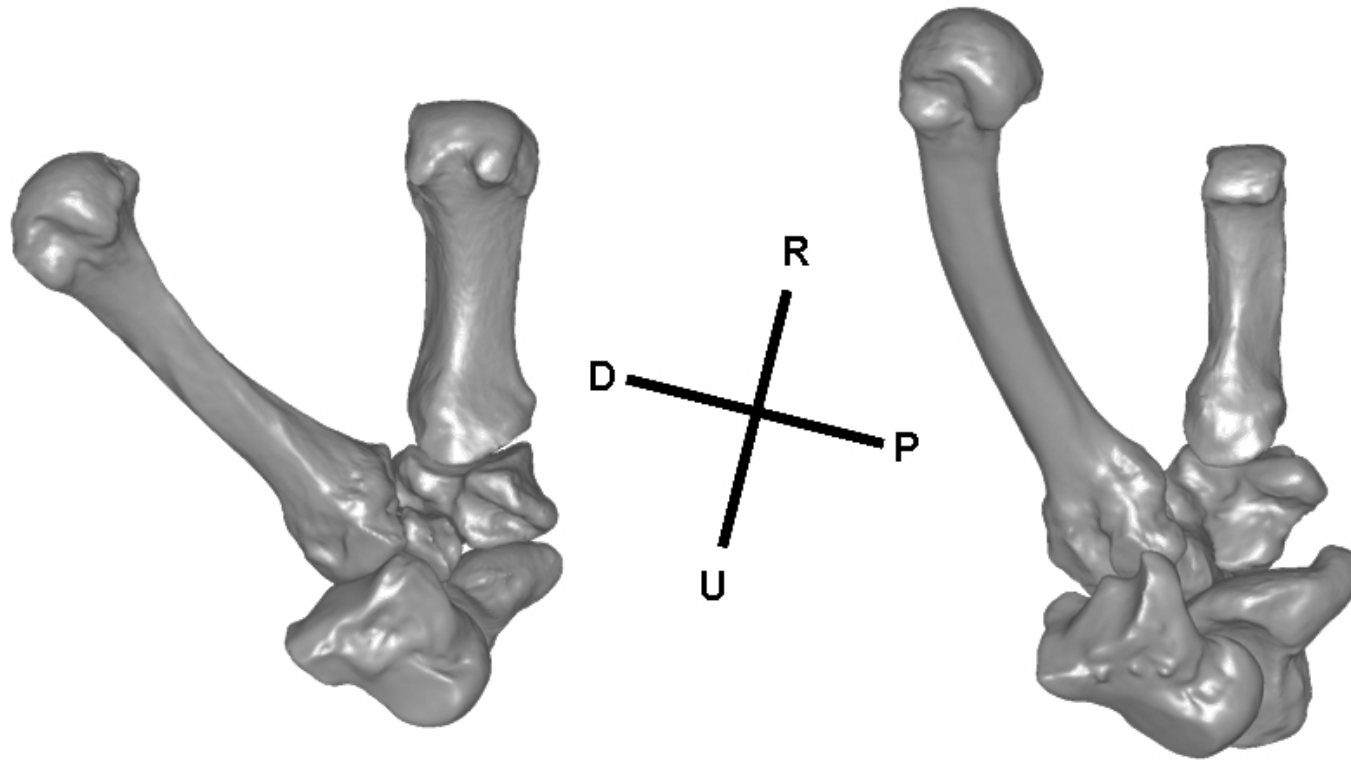


Fig. 2.3 The radial halves of the right wrists and 1st and 2nd metacarpals of modern *Homo sapiens* (pictured at left) and *Pan troglodytes* (pictured at right). Modern humans are predicted to show carpal and carpometacarpal bone and joint morphology that is more stable proximo-distally (P-D) and more effective in distributing forces directed radially and ulnarly (R-U) through the thumb and wrist.

Chapter 3: The First Carpometacarpal Joint

RESULTS OF SHAPE ANALYSES

In the following five chapters (3 to 7), I present the results of the shape analyses performed on the features and bones of the radial carpal and carpometacarpal region of the wrist. All analyses utilize taxonomic classifications using the genus as the unit of comparison. Five extant catarrhine genera are examined: *Homo*, *Pan*, *Gorilla*, *Pongo*, and *Papio*. The genus *Homo* is represented by a world-wide sample of *H. sapiens* including individuals of recent African, European, Australian, Asian, and Native American descent. The genus *Pan* is represented by a sample of *P. troglodytes* while the genus *Gorilla* is represented by a combined sample of *G. gorilla* and *G. beringei*. The genus *Pongo* is represented by a combined sample of *P. pygmaeus* and *P. abelii* while the genus *Papio* is represented by a combined sample of *P. anubis*, *P. cynocephalus*, *P. hamadryas*, and *P. ursinus*.

For the scaphoid, trapezium, trapezoid, and second metacarpal, the variables analyzed include the angles between articular surfaces and the relative areas of articular and non-articular surfaces (Tocheri et al., 2003; Tocheri et al., 2005). Various measures of curvedness are the focus of the analysis of the first carpometacarpal joint surfaces (Tocheri et al., 2006; Tocheri and Femiani, in press). A bootstrap procedure is used to analyze differences between the means of each measured variable. The bootstrap is a distribution-free statistic ideally suited to examine differences between means of groups with varying sample sizes that are small relative to the population they represent (Efron and Tibshirani, 1993; Manly, 1997). Numbers appearing in parentheses indicate genus means, which are also summarized along with the *p*-values of each pairwise comparison

in the accompanying tables. Canonical and discriminant analyses are used to evaluate the efficacy of different variable combinations in correctly classifying individual bones belonging to the extant genera (Johnson and Wichern, 2002). A complete description of the materials and methods is given in Chapter 9.

In this section, I present the results of the shape analyses performed on the first carpometacarpal joint. The variables measured include the relative areas and curvedness measures of the mutually articulating surfaces. The results of the comparative shape analyses for each variable are presented separately, followed by multivariate analyses of all the variables for each joint surface (Partial Models I and II), as well as both joint surfaces together (Full Model). Following the presentation of the statistical results, a summary of the shape characteristics of each genus is given. Finally, the results are discussed in relation to previous studies as well as the biomechanical predictions introduced in Chapter 2. For clarification purposes, the articular surface on the first metacarpal is referred to as the trapezium joint surface (Fig. 3.1), whereas the articular surface on the trapezium is referred to as the first metacarpal joint surface (Fig. 3.2).

The Trapezium Joint Surface

Relative area. The area of the trapezium joint surface is measured relative to the first metacarpal joint surface, rather than relative to the non-articular area of the first metacarpal, given the differences in first metacarpal bone length and robusticity among these extant genera. Proportions greater than 100% indicate that the articular area of the trapezium joint is larger than its counterpart and vice versa. Significant differences in

relative area are observed in four of the ten pairwise comparisons between genus means (Table 3.1). This ratio of mutual surface areas is significantly larger in *Papio* (123.6%) than in the hominine genera, while in *Pan* (100.8%) it is significantly smaller than in *Gorilla* (111.4%). *Pongo* (111.4%) shows no significant differences with any genera in terms of this relative area.

TABLE 3.1 Pairwise comparisons of genus means for relative area of the trapezium joint surface¹

Genus A	Genus B	Mean _A	Mean _B	N _A	N _B	θ	p
<i>Homo</i>	<i>Pan</i>	105.9	100.8	108	44	5.1	0.071
<i>Homo</i>	<i>Gorilla</i>	105.9	111.4	108	42	5.5	0.013
<i>Homo</i>	<i>Pongo</i>	105.9	111.4	108	16	5.5	0.154
<i>Homo</i>	<i>Papio</i>	105.9	123.6	108	17	17.6	<.001
<i>Pan</i>	<i>Gorilla</i>	100.8	111.4	44	42	10.6	0.002
<i>Pan</i>	<i>Pongo</i>	100.8	111.4	44	16	10.6	0.024
<i>Pan</i>	<i>Papio</i>	100.8	123.6	44	17	22.8	<.001
<i>Gorilla</i>	<i>Pongo</i>	111.4	111.4	42	16	0.0	0.997
<i>Gorilla</i>	<i>Papio</i>	111.4	123.6	42	17	12.1	0.002
<i>Pongo</i>	<i>Papio</i>	111.4	123.6	16	17	12.1	0.016

¹ Mean_A, mean of Genus A; N_A, sample size of Genus A; Mean_B, mean of Genus B; N_B, sample size of Genus B; | θ |, absolute value of difference between observed sample means; p, probability that a difference between the bootstrapped means equaled or exceeded | θ |. Numbers in bold indicate statistical significance at alpha = .01.

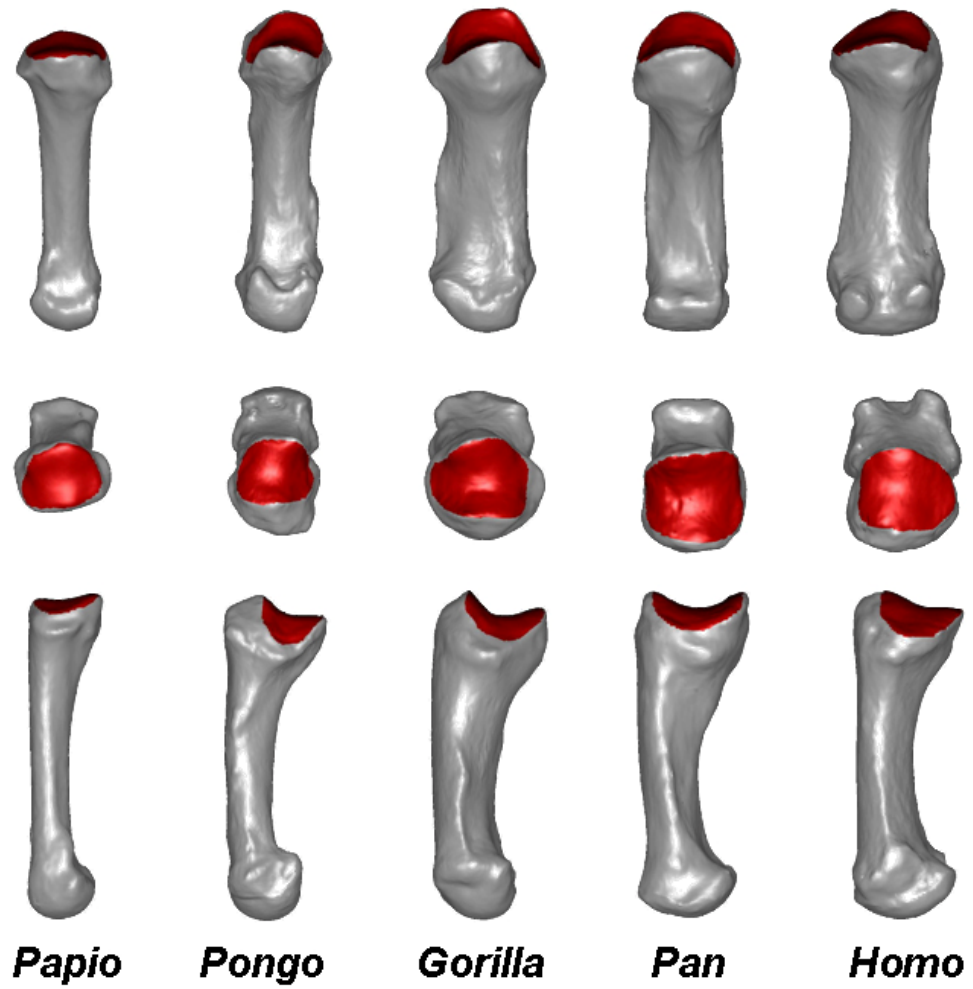


Fig. 3.1 Visual comparison of the trapezium articular surface on the right 1st metacarpal in five extant primate genera (radio-ulnar curvedness = top row; proximal view = middle row; dorso-palmar curvedness = bottom row). All bones scaled to approximately the same length.

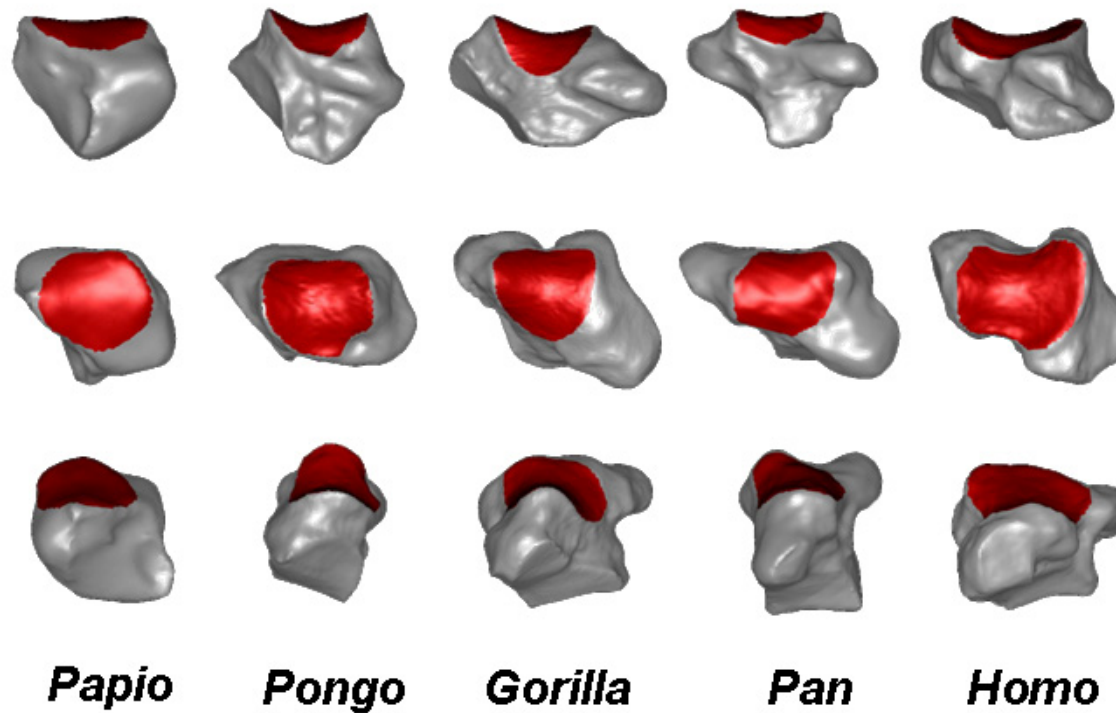


Fig. 3.2 Visual comparison of the 1st metacarpal articular surface on the right trapezium in five extant primate genera (radio-ulnar curvedness = top row; distal view = middle row; dorso-palmar curvedness = bottom row). All bones scaled to approximately the same size.

Dorso-palmar curvedness. This measure approximates the surface curvedness in the direction of the flexion-extension axis (Fig. 3.1, bottom row), and is significantly different in eight of the ten pairwise comparisons between genus means (Table 3.2). *Gorilla* (0.94) is significantly more curved dorso-palmarly than the other genera, whereas *Papio* (0.22) is significantly less curved than the rest. The remaining significant difference occurs between *Homo* (0.39) and *Pan* (0.52), the former being less curved than the latter. *Pongo* (0.45) shows no significant differences in comparison to either *Pan* or *Homo* in terms of dorso-palmar curvedness.

TABLE 3.2 Pairwise comparisons of genus means for dorso-palmar curvedness of the trapezium joint surface¹

Genus A	Genus B	Mean _A	Mean _B	N _A	N _B	θ	p
<i>Homo</i>	<i>Pan</i>	0.39	0.52	121	46	0.12	<.001
<i>Homo</i>	<i>Gorilla</i>	0.39	0.94	121	47	0.54	<.001
<i>Homo</i>	<i>Pongo</i>	0.39	0.45	121	19	0.05	0.443
<i>Homo</i>	<i>Papio</i>	0.39	0.22	121	19	0.17	<.001
<i>Pan</i>	<i>Gorilla</i>	0.52	0.94	46	47	0.42	<.001
<i>Pan</i>	<i>Pongo</i>	0.52	0.45	46	19	0.07	0.379
<i>Pan</i>	<i>Papio</i>	0.52	0.22	46	19	0.30	<.001
<i>Gorilla</i>	<i>Pongo</i>	0.94	0.45	47	19	0.49	<.001
<i>Gorilla</i>	<i>Papio</i>	0.94	0.22	47	19	0.71	<.001
<i>Pongo</i>	<i>Papio</i>	0.45	0.22	19	19	0.23	0.002

¹ Mean_A, mean of Genus A; N_A, sample size of Genus A; Mean_B, mean of Genus B; N_B, sample size of Genus B; | θ |, absolute value of difference between observed sample means; p, probability that a difference between the bootstrapped means equaled or exceeded | θ |. Numbers in bold indicate statistical significance at $\alpha = .01$.

Radio-ulnar curvedness. This measure approximates the surface curvedness in the direction of the abduction-adduction axis (Fig. 3.1, top row), and is significantly different in seven of the ten pairwise comparisons between genus means (Table 3.3). *Papio* (-0.64) is significantly less curved radio-ulnarly than the other genera while *Homo* (-0.82) is also significantly less curved than the great apes. No significant differences in radio-ulnar curvedness are observed between the great ape genera (*Pan*, -1.14; *Gorilla*, -1.11; *Pongo*, -1.15).

TABLE 3.3 Pairwise comparisons of genus means for radio-ulnar curvedness of the trapezium joint surface¹

Genus A	Genus B	Mean _A	Mean _B	N _A	N _B	θ	p
<i>Homo</i>	<i>Pan</i>	-0.82	-1.14	121	46	0.32	<.001
<i>Homo</i>	<i>Gorilla</i>	-0.82	-1.11	121	47	0.29	<.001
<i>Homo</i>	<i>Pongo</i>	-0.82	-1.15	121	19	0.33	<.001
<i>Homo</i>	<i>Papio</i>	-0.82	-0.64	121	19	0.18	<.001
<i>Pan</i>	<i>Gorilla</i>	-1.14	-1.11	46	47	0.03	0.476
<i>Pan</i>	<i>Pongo</i>	-1.14	-1.15	46	19	0.01	0.882
<i>Pan</i>	<i>Papio</i>	-1.14	-0.64	46	19	0.51	<.001
<i>Gorilla</i>	<i>Pongo</i>	-1.11	-1.15	47	19	0.04	0.431
<i>Gorilla</i>	<i>Papio</i>	-1.11	-0.64	47	19	0.48	<.001
<i>Pongo</i>	<i>Papio</i>	-1.15	-0.64	19	19	0.51	<.001

¹ Mean_A, mean of Genus A; N_A, sample size of Genus A; Mean_B, mean of Genus B; N_B, sample size of Genus B; | θ |, absolute value of difference between observed sample means; p, probability that a difference between the bootstrapped means equaled or exceeded | θ |. Numbers in bold indicate statistical significance at alpha = .01.

Absolute curvature. This measure maximizes the overall surface curvature by summing the absolute values of dorso-palmar and radio-ulnar curvedness (e.g., Farin, 1996; Farin and Hansford, 2000; and see Chapter 9 for details). Nine of the ten pairwise comparisons between genus means are significantly different (Table 3.4). The trapezium joint surface in *Papio* (0.86) is significantly less curved than the other genera, whereas *Gorilla* (2.05) has a significantly more curved surface than the rest. *Homo* (1.22) also shows a significantly less curved surface than does either *Pan* (1.69) or *Pongo* (1.61).

TABLE 3.4 Pairwise comparisons of genus means for absolute curvature of the trapezium joint surface¹

Genus A	Genus B	Mean _A	Mean _B	N _A	N _B	θ	p
<i>Homo</i>	<i>Pan</i>	1.22	1.69	121	46	0.47	<.001
<i>Homo</i>	<i>Gorilla</i>	1.22	2.05	121	47	0.83	<.001
<i>Homo</i>	<i>Pongo</i>	1.22	1.61	121	19	0.40	<.001
<i>Homo</i>	<i>Papio</i>	1.22	0.86	121	19	0.36	<.001
<i>Pan</i>	<i>Gorilla</i>	1.69	2.05	46	47	0.36	<.001
<i>Pan</i>	<i>Pongo</i>	1.69	1.61	46	19	0.08	0.312
<i>Pan</i>	<i>Papio</i>	1.69	0.86	46	19	0.83	<.001
<i>Gorilla</i>	<i>Pongo</i>	2.05	1.61	47	19	0.44	<.001
<i>Gorilla</i>	<i>Papio</i>	2.05	0.86	47	19	1.19	<.001
<i>Pongo</i>	<i>Papio</i>	1.61	0.86	19	19	0.75	<.001

¹ Mean_A, mean of Genus A; N_A, sample size of Genus A; Mean_B, mean of Genus B; N_B, sample size of Genus B; | θ |, absolute value of difference between observed sample means; p, probability that a difference between the bootstrapped means equaled or exceeded | θ |. Numbers in bold indicate statistical significance at $\alpha = .01$.

RMS curvature. This measure minimizes the overall surface curvature by taking the root mean square values of dorso-palmar and radio-ulnar curvedness (e.g., Farin, 1996; Farin and Hansford, 2000; and see Chapter 9 for details). Nine of the ten pairwise comparisons between genus means are significantly different (Table 3.5). The trapezium joint surface in *Papio* (0.68) is significantly less curved than the other genera, whereas *Gorilla* (1.47) has a significantly more curved surface than the rest. *Homo* (0.93) also shows a significantly less curved surface than does either *Pan* (1.286) or *Pongo* (1.26).

TABLE 3.5 Pairwise comparisons of genus means for RMS curvature of the trapezium joint surface¹

Genus A	Genus B	Mean _A	Mean _B	N _A	N _B	θ	p
<i>Homo</i>	<i>Pan</i>	0.93	1.29	121	46	0.36	<.001
<i>Homo</i>	<i>Gorilla</i>	0.93	1.47	121	47	0.55	<.001
<i>Homo</i>	<i>Pongo</i>	0.93	1.26	121	19	0.34	<.001
<i>Homo</i>	<i>Papio</i>	0.93	0.68	121	19	0.24	<.001
<i>Pan</i>	<i>Gorilla</i>	1.29	1.47	46	47	0.19	<.001
<i>Pan</i>	<i>Pongo</i>	1.29	1.26	46	19	0.02	0.602
<i>Pan</i>	<i>Papio</i>	1.29	0.68	46	19	0.60	<.001
<i>Gorilla</i>	<i>Pongo</i>	1.47	1.26	47	19	0.21	<.001
<i>Gorilla</i>	<i>Papio</i>	1.47	0.68	47	19	0.79	<.001
<i>Pongo</i>	<i>Papio</i>	1.26	0.68	19	19	0.58	<.001

¹ Mean_A, mean of Genus A; N_A, sample size of Genus A; Mean_B, mean of Genus B; N_B, sample size of Genus B; | θ |, absolute value of difference between observed sample means; p, probability that a difference between the bootstrapped means equaled or exceeded | θ |. Numbers in bold indicate statistical significance at $\alpha = .01$.

Mean curvature. This measure assesses how evenly a saddle surface is curved in alternate directions (e.g., Farin, 1996; Farin and Hansford, 2000; and see Chapter 9 for details). Eight of the ten pairwise comparisons between genus means are significantly different (Table 3.6). *Gorilla* (-0.09) has a significantly more evenly curved surface than do the other genera. Significantly more evenly curved surfaces are also observed in *Homo* (-0.21) and *Papio* (-0.21) in comparison to *Pongo* (-0.35) and *Pan* (-0.31).

TABLE 3.6 Pairwise comparisons of genus means for mean curvature of the trapezium joint surface¹

Genus A	Genus B	Mean _A	Mean _B	N _A	N _B	θ	p
<i>Homo</i>	<i>Pan</i>	-0.21	-0.31	121	46	0.10	<.001
<i>Homo</i>	<i>Gorilla</i>	-0.21	-0.09	121	47	0.12	<.001
<i>Homo</i>	<i>Pongo</i>	-0.21	-0.35	121	19	0.14	<.001
<i>Homo</i>	<i>Papio</i>	-0.21	-0.21	121	19	0.00	0.835
<i>Pan</i>	<i>Gorilla</i>	-0.31	-0.09	46	47	0.22	<.001
<i>Pan</i>	<i>Pongo</i>	-0.31	-0.35	46	19	0.04	0.369
<i>Pan</i>	<i>Papio</i>	-0.31	-0.21	46	19	0.10	<.001
<i>Gorilla</i>	<i>Pongo</i>	-0.09	-0.35	47	19	0.26	<.001
<i>Gorilla</i>	<i>Papio</i>	-0.09	-0.21	47	19	0.12	<.001
<i>Pongo</i>	<i>Papio</i>	-0.35	-0.21	19	19	0.14	<.001

¹ Mean_A, mean of Genus A; N_A, sample size of Genus A; Mean_B, mean of Genus B; N_B, sample size of Genus B; | θ |, absolute value of difference between observed sample means; p, probability that a difference between the bootstrapped means equaled or exceeded | θ |. Numbers in bold indicate statistical significance at alpha = .01.

Gaussian curvature. This measure is an assessment of the shape of the surface curvedness (i.e., elliptical, cylindrical, or saddle-shaped) (e.g., Farin, 1996; Farin and Hansford, 2000; and see Chapter 9 for details). The mean Gaussian curvature in each genus is negative indicating that the trapezium joint surface is reasonably saddle-shaped in all of these genera. Eight of the ten pairwise comparisons between genus means are significantly different (Table 3.7). The Gaussian curvature of *Gorilla* (-1.04) is significantly greater (in absolute value) than in the other genera, whereas in *Papio* (-0.14) it is significantly less than the rest. *Homo* (-0.31) also shows significantly less Gaussian curvature than does *Pan* (-0.58). *Pongo* (-0.52) shows no significant difference from either *Pan* or *Homo* in Gaussian curvature.

TABLE 3.7 Pairwise comparisons of genus means for Gaussian curvature of the trapezium joint surface¹

Genus A	Genus B	Mean _A	Mean _B	N _A	N _B	θ	p
<i>Homo</i>	<i>Pan</i>	-0.31	-0.58	121	46	0.26	<.001
<i>Homo</i>	<i>Gorilla</i>	-0.31	-1.04	121	47	0.73	<.001
<i>Homo</i>	<i>Pongo</i>	-0.31	-0.52	121	19	0.21	0.019
<i>Homo</i>	<i>Papio</i>	-0.31	-0.14	121	19	0.17	<.001
<i>Pan</i>	<i>Gorilla</i>	-0.58	-1.04	46	47	0.46	<.001
<i>Pan</i>	<i>Pongo</i>	-0.58	-0.52	46	19	0.06	0.541
<i>Pan</i>	<i>Papio</i>	-0.58	-0.14	46	19	0.44	<.001
<i>Gorilla</i>	<i>Pongo</i>	-1.04	-0.52	47	19	0.52	<.001
<i>Gorilla</i>	<i>Papio</i>	-1.04	-0.14	47	19	0.90	<.001
<i>Pongo</i>	<i>Papio</i>	-0.52	-0.14	19	19	0.38	<.001

¹ Mean_A, mean of Genus A; N_A, sample size of Genus A; Mean_B, mean of Genus B; N_B, sample size of Genus B; | θ |, absolute value of difference between observed sample means; p, probability that a difference between the bootstrapped means equaled or exceeded | θ |. Numbers in bold indicate statistical significance at alpha = .01.

The First Metacarpal Joint Surface

Relative area. The area of the first metacarpal joint surface is measured relative to the surface area of the entire trapezium; hence, the relative area of the first metacarpal joint surface equals how much area this surface contributes to the total surface area of the trapezium. The relative area of the first metacarpal joint surface is significantly different in seven of the ten pairwise comparisons between genus means (Table 3.8). The relative area is significantly larger in *Homo* (16.5%) than in all the other genera, whereas in *Gorilla* (12.3%) it is significantly smaller than in all the others. Non-significant differences in this mean occur between *Pan* (13.7%), *Pongo* (13.5%), and *Papio* (14.6%).

TABLE 3.8 Pairwise comparisons of genus means for relative area of the 1st metacarpal joint surface¹

Genus A	Genus B	Mean _A	Mean _B	N _A	N _B	θ	p
<i>Homo</i>	<i>Pan</i>	16.5	13.7	113	47	2.9	<.001
<i>Homo</i>	<i>Gorilla</i>	16.5	12.3	113	44	4.3	<.001
<i>Homo</i>	<i>Pongo</i>	16.5	13.5	113	21	3.0	<.001
<i>Homo</i>	<i>Papio</i>	16.5	14.6	113	20	2.0	<.001
<i>Pan</i>	<i>Gorilla</i>	13.7	12.3	47	44	1.4	0.002
<i>Pan</i>	<i>Pongo</i>	13.7	13.5	47	21	0.1	0.723
<i>Pan</i>	<i>Papio</i>	13.7	14.6	47	20	0.9	0.021
<i>Gorilla</i>	<i>Pongo</i>	12.3	13.5	44	21	1.3	<.001
<i>Gorilla</i>	<i>Papio</i>	12.3	14.6	44	20	2.3	<.001
<i>Pongo</i>	<i>Papio</i>	13.5	14.6	21	20	1.0	0.011

¹ Mean_A, mean of Genus A; N_A, sample size of Genus A; Mean_B, mean of Genus B; N_B, sample size of Genus B; | θ |, absolute value of difference between observed sample means; p, probability that a difference between the bootstrapped means equaled or exceeded | θ |. Numbers in bold indicate statistical significance at alpha = .01.

Dorso-palmar curvedness. This measure approximates the surface curvedness in the direction of the flexion-extension axis (Fig. 3.2, bottom row), and is significantly different in eight of the ten pairwise comparisons between genus means (Table 3.9). *Gorilla* (-1.37) and *Pan* (-1.32) are significantly more curved dorso-palmarly than the other genera, whereas *Homo* (-0.83) and *Papio* (-0.78) are significantly less curved than *Pongo* (-0.98). Neither *Gorilla* and *Pan* nor *Homo* and *Papio* are significantly different in terms of dorso-palmar curvedness.

TABLE 3.9 Pairwise comparisons of genus means for dorso-palmar curvedness of the 1st metacarpal joint surface¹

Genus A	Genus B	Mean _A	Mean _B	N _A	N _B	θ	p
<i>Homo</i>	<i>Pan</i>	-0.83	-1.32	113	47	0.49	<.001
<i>Homo</i>	<i>Gorilla</i>	-0.83	-1.37	113	44	0.53	<.001
<i>Homo</i>	<i>Pongo</i>	-0.83	-0.98	113	21	0.14	0.01
<i>Homo</i>	<i>Papio</i>	-0.83	-0.78	113	20	0.05	0.2
<i>Pan</i>	<i>Gorilla</i>	-1.32	-1.37	47	44	0.04	0.519
<i>Pan</i>	<i>Pongo</i>	-1.32	-0.98	47	21	0.35	<.001
<i>Pan</i>	<i>Papio</i>	-1.32	-0.78	47	20	0.54	<.001
<i>Gorilla</i>	<i>Pongo</i>	-1.37	-0.98	44	21	0.39	<.001
<i>Gorilla</i>	<i>Papio</i>	-1.37	-0.78	44	20	0.59	<.001
<i>Pongo</i>	<i>Papio</i>	-0.98	-0.78	21	20	0.20	0.001

¹ Mean_A, mean of Genus A; N_A, sample size of Genus A; Mean_B, mean of Genus B; N_B, sample size of Genus B; | θ |, absolute value of difference between observed sample means; p, probability that a difference between the bootstrapped means equaled or exceeded | θ |. Numbers in bold indicate statistical significance at alpha = .01.

Radio-ulnar curvedness. This measure approximates the surface curvedness in the direction of the abduction-adduction axis (Fig. 3.2, top row), and is significantly different in four of the ten pairwise comparisons between genus means (Table 3.10). *Papio* (0.10) is significantly less curved radio-ulnarly than the other genera. No significant differences in radio-ulnar curvedness are observed between the hominid genera (*Homo*, 0.43; *Pan*, 0.41; *Gorilla*, 0.41; *Pongo*, 0.44).

TABLE 3.10 Pairwise comparisons of genus means for radio-ulnar curvedness of the 1st metacarpal joint surface¹

Genus A	Genus B	Mean _A	Mean _B	N _A	N _B	θ	p
<i>Homo</i>	<i>Pan</i>	0.43	0.41	113	47	0.03	0.443
<i>Homo</i>	<i>Gorilla</i>	0.43	0.41	113	44	0.03	0.447
<i>Homo</i>	<i>Pongo</i>	0.43	0.44	113	21	0.01	0.911
<i>Homo</i>	<i>Papio</i>	0.43	0.10	113	20	0.33	<.001
<i>Pan</i>	<i>Gorilla</i>	0.41	0.41	47	44	0.00	0.977
<i>Pan</i>	<i>Pongo</i>	0.41	0.44	47	21	0.03	0.613
<i>Pan</i>	<i>Papio</i>	0.41	0.10	47	20	0.30	<.001
<i>Gorilla</i>	<i>Pongo</i>	0.41	0.44	44	21	0.03	0.618
<i>Gorilla</i>	<i>Papio</i>	0.41	0.10	44	20	0.31	<.001
<i>Pongo</i>	<i>Papio</i>	0.44	0.10	21	20	0.34	<.001

¹ Mean_A, mean of Genus A; N_A, sample size of Genus A; Mean_B, mean of Genus B; N_B, sample size of Genus B; | θ |, absolute value of difference between observed sample means; p, probability that a difference between the bootstrapped means equaled or exceeded | θ |. Numbers in bold indicate statistical significance at alpha = .01.

Absolute curvature. This measure maximizes the overall surface curvature by summing the absolute values of dorso-palmar and radio-ulnar curvedness. Nine of the ten pairwise comparisons between genus means are significantly different (Table 3.11). The first metacarpal surface in *Papio* (0.90) is significantly less curved than the other genera whereas *Gorilla* (1.79) and *Pan* (1.75) have a significantly more curved surface than does *Pongo* (1.42) and *Homo* (1.27). Finally, *Pongo* also shows a significantly more curved surface than does *Homo*.

TABLE 3.11 Pairwise comparisons of genus means for absolute curvature of the 1st metacarpal joint surface¹

Genus A	Genus B	Mean _A	Mean _B	N _A	N _B	θ	p
<i>Homo</i>	<i>Pan</i>	1.27	1.75	113	47	0.48	<.001
<i>Homo</i>	<i>Gorilla</i>	1.27	1.79	113	44	0.52	<.001
<i>Homo</i>	<i>Pongo</i>	1.27	1.42	113	21	0.15	0.005
<i>Homo</i>	<i>Papio</i>	1.27	0.90	113	20	0.37	<.001
<i>Pan</i>	<i>Gorilla</i>	1.75	1.79	47	44	0.04	0.593
<i>Pan</i>	<i>Pongo</i>	1.75	1.42	47	21	0.33	<.001
<i>Pan</i>	<i>Papio</i>	1.75	0.90	47	20	0.84	<.001
<i>Gorilla</i>	<i>Pongo</i>	1.79	1.42	44	21	0.37	<.001
<i>Gorilla</i>	<i>Papio</i>	1.79	0.90	44	20	0.88	<.001
<i>Pongo</i>	<i>Papio</i>	1.42	0.90	21	20	0.51	<.001

¹ Mean_A, mean of Genus A; N_A, sample size of Genus A; Mean_B, mean of Genus B; N_B, sample size of Genus B; | θ |, absolute value of difference between observed sample means; p, probability that a difference between the bootstrapped means equaled or exceeded | θ |. Numbers in bold indicate statistical significance at alpha = .01.

RMS curvature. This measure minimizes the overall surface curvature by taking the root mean square values of dorso-palmar and radio-ulnar curvedness. Nine of the ten pairwise comparisons between genus means are significantly different (Table 3.12). *Gorilla* (1.45) and *Pan* (1.41) have a significantly more curved surface than the other genera, whereas *Papio* (0.80) has a significantly less curved surface than does either *Homo* (0.96) or *Pongo* (1.11). Finally, *Pongo* also shows a significantly more curved surface in comparison to *Homo*.

TABLE 3.12 Pairwise comparisons of genus means for RMS curvature of the 1st metacarpal joint surface¹

Genus A	Genus B	Mean _A	Mean _B	N _A	N _B	θ	p
<i>Homo</i>	<i>Pan</i>	0.96	1.41	113	47	0.45	<.001
<i>Homo</i>	<i>Gorilla</i>	0.96	1.45	113	44	0.49	<.001
<i>Homo</i>	<i>Pongo</i>	0.96	1.11	113	21	0.15	<.001
<i>Homo</i>	<i>Papio</i>	0.96	0.80	113	20	0.16	<.001
<i>Pan</i>	<i>Gorilla</i>	1.41	1.45	47	44	0.04	0.517
<i>Pan</i>	<i>Pongo</i>	1.41	1.11	47	21	0.30	<.001
<i>Pan</i>	<i>Papio</i>	1.41	0.80	47	20	0.61	<.001
<i>Gorilla</i>	<i>Pongo</i>	1.45	1.11	44	21	0.34	<.001
<i>Gorilla</i>	<i>Papio</i>	1.45	0.80	44	20	0.65	<.001
<i>Pongo</i>	<i>Papio</i>	1.11	0.80	21	20	0.31	<.001

¹ Mean_A, mean of Genus A; N_A, sample size of Genus A; Mean_B, mean of Genus B; N_B, sample size of Genus B; | θ |, absolute value of difference between observed sample means; p, probability that a difference between the bootstrapped means equaled or exceeded | θ |. Numbers in bold indicate statistical significance at alpha = .01.

Mean curvature. This measure is an assessment of how evenly a saddle surface is curved in alternate directions. Seven of the ten pairwise comparisons between genus means are significantly different (Table 3.13). *Homo* (-0.20) has a significantly more evenly curved surface than does *Pan* (-0.46), *Gorilla* (-0.48), and *Papio* (-0.34). Significantly more evenly curved surfaces are also observed in *Pongo* (-0.27) and *Papio* in comparison to the African apes.

TABLE 3.13 Pairwise comparisons of genus means for mean curvature of the 1st metacarpal joint surface¹

Genus A	Genus B	Mean _A	Mean _B	N _A	N _B	θ	p
<i>Homo</i>	<i>Pan</i>	-0.20	-0.46	113	47	0.26	<.001
<i>Homo</i>	<i>Gorilla</i>	-0.20	-0.48	113	44	0.28	<.001
<i>Homo</i>	<i>Pongo</i>	-0.20	-0.27	113	21	0.07	0.148
<i>Homo</i>	<i>Papio</i>	-0.20	-0.34	113	20	0.14	<.001
<i>Pan</i>	<i>Gorilla</i>	-0.46	-0.48	47	44	0.02	0.63
<i>Pan</i>	<i>Pongo</i>	-0.46	-0.27	47	21	0.19	<.001
<i>Pan</i>	<i>Papio</i>	-0.46	-0.34	47	20	0.12	0.006
<i>Gorilla</i>	<i>Pongo</i>	-0.48	-0.27	44	21	0.21	<.001
<i>Gorilla</i>	<i>Papio</i>	-0.48	-0.34	44	20	0.14	<.001
<i>Pongo</i>	<i>Papio</i>	-0.27	-0.34	21	20	0.07	0.165

¹ Mean_A, mean of Genus A; N_A, sample size of Genus A; Mean_B, mean of Genus B; N_B, sample size of Genus B; | θ |, absolute value of difference between observed sample means; p, probability that a difference between the bootstrapped means equaled or exceeded | θ |. Numbers in bold indicate statistical significance at alpha = .01.

Gaussian curvature. This measure is an assessment of the shape of the surface curvedness (i.e., elliptical, cylindrical, or saddle-shaped). Six of the ten pairwise comparisons between genus means are significantly different (Table 3.14). The mean Gaussian curvature in each genus is negative indicating that, on average, the first metacarpal surface is saddle-shaped. However, the mean Gaussian curvature of *Papio* (-.07) closely approaches a zero value indicating its surface is almost cylindrical in shape and is significantly less saddle-shaped than in all the other genera. *Homo* (-.35) is also significantly different than *Pan* (-.52) and *Gorilla* (-5.56) in terms of Gaussian curvature.

TABLE 3.14 Pairwise comparisons of genus means for Gaussian curvature of the 1st metacarpal joint surface¹

Genus A	Genus B	Mean _A	Mean _B	N _A	N _B	θ	p
<i>Homo</i>	<i>Pan</i>	-0.35	-0.52	113	47	0.17	<.001
<i>Homo</i>	<i>Gorilla</i>	-0.35	-0.56	113	44	0.21	<.001
<i>Homo</i>	<i>Pongo</i>	-0.35	-0.40	113	21	0.05	0.297
<i>Homo</i>	<i>Papio</i>	-0.35	-0.07	113	20	0.28	<.001
<i>Pan</i>	<i>Gorilla</i>	-0.52	-0.56	47	44	0.04	0.538
<i>Pan</i>	<i>Pongo</i>	-0.52	-0.40	47	21	0.11	0.076
<i>Pan</i>	<i>Papio</i>	-0.52	-0.07	47	20	0.45	<.001
<i>Gorilla</i>	<i>Pongo</i>	-0.56	-0.40	44	21	0.15	0.021
<i>Gorilla</i>	<i>Papio</i>	-0.56	-0.07	44	20	0.49	<.001
<i>Pongo</i>	<i>Papio</i>	-0.40	-0.07	21	20	0.33	<.001

¹ Mean_A, mean of Genus A; N_A, sample size of Genus A; Mean_B, mean of Genus B; N_B, sample size of Genus B; | θ |, absolute value of difference between observed sample means; p, probability that a difference between the bootstrapped means equaled or exceeded | θ |. Numbers in bold indicate statistical significance at alpha = .01.

Multivariate Analyses

In this section, the results of the canonical and discriminant function analyses using three combinations of the first carpometacarpal joint variables are presented. The first two combinations, or Partial Model I and II, each utilize five measures of either the trapezium or first metacarpal joint surface as predictor variables. These measures include the relative area of the joint surface, and four measures of surface curvedness. Absolute and RMS curvatures represent the overall magnitude of surface curvedness while mean and Gaussian curvatures represent overall surface shape. Each of these curvatures is a function of the dorso-palmar and radio-ulnar curvedness measures of each joint surface. The third combination, or Full Model, utilizes all of the carpometacarpal joint variables used in Partial Model I and II as predictor variables. These variables include the relative areas and curvedness measures for both the first metacarpal and trapezium joint surfaces.

Partial Model I: Trapezium joint surface measures only. The first canonical axis (CAN1) accounts for 83% of the variation while the second (CAN2) accounts for 12%. Along CAN1, *Papio* clusters toward the far left followed by *Homo* in the middle left, while *Gorilla* clusters more toward the far right followed by *Pan* and *Pongo* in the middle right (Fig. 3.3). The correlations with CAN1 (Table 3.15) indicate that this axis is a comparison of the absolute and RMS curvatures with the Gaussian curvature (i.e., curvedness magnitude vs. shape). Along CAN2, no clear genus clusters are observed (Fig. 3.3).

Along CAN1, four general clusters are observed (Fig. 3.3). *Papio* clusters in the far left area reflecting a more cylindrical-shaped surface that is relatively flat both dorso-palmarly and radio-ulnarly. *Homo* clusters in the middle left area reflecting a more saddle-shaped surface than in *Papio*, but less curved than in the great apes. In the middle right area, *Pongo*, *Pan*, and about half of the *Gorilla* sample form a cluster reflecting a saddle-shaped surface that is more curved than in *Homo*. Finally, the remaining half of the *Gorilla* sample forms a cluster in the far right reflecting highly curved saddle-shaped surfaces.

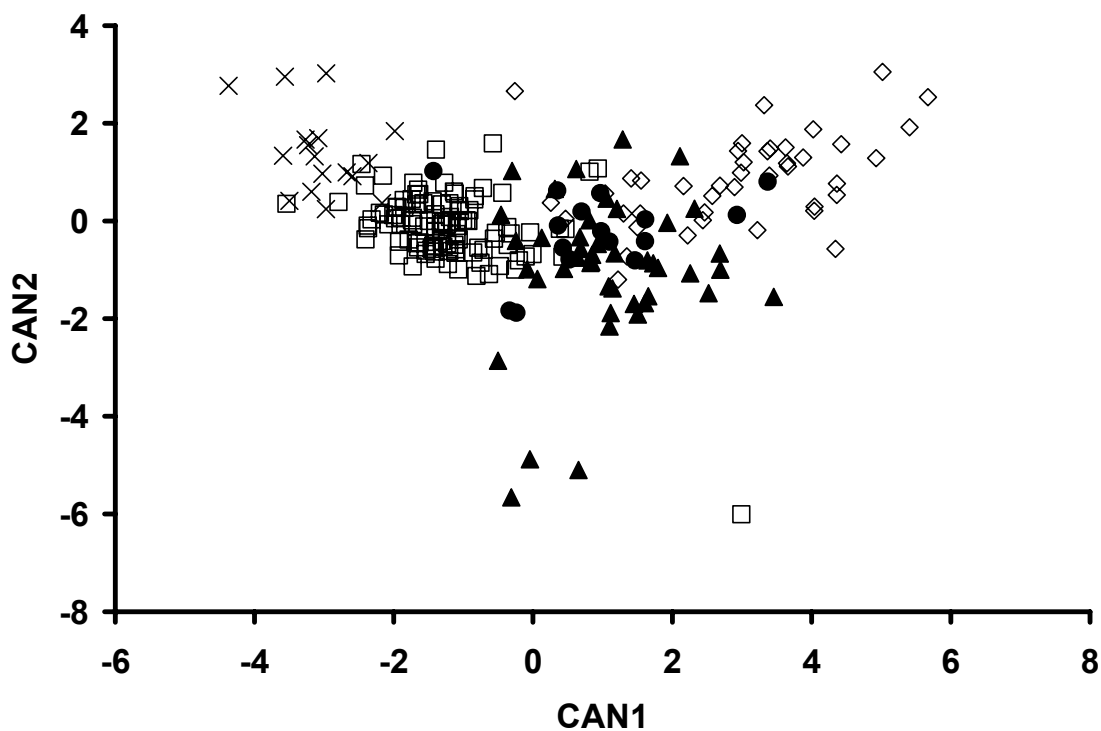


Fig. 3.3 Plot of the canonical variables (CAN1, CAN2) generated from analysis of trapezium joint surface area and curvedness measures (*Homo* = open squares, *Pan* = closed triangles, *Gorilla* = open diamonds, *Pongo* = closed circles, *Papio* = Xs).

TABLE 3.15. Correlations between each variable and canonical axis (bolded values indicate the variables that best explain the observed variation along each axis)

Pooled-within canonical structure		
Variable	CAN1	CAN2
Relative Area	-0.04	0.56
RMS	0.90	-0.16
Absolute	0.91	-0.02
Gaussian	-0.67	-0.41
Mean	0.07	0.57

The cross-validation procedure results in the correct classification of 90 *Homo* (83.3%), 29 *Pan* (65.9%), 32 *Gorilla* (76.2%), 7 *Pongo* (43.8%), and 16 *Papio* (94.1%; Table 3.16). The majority of misclassifications occur among the great apes (29). Overall, the results suggest that these five measures of the trapezium carpometacarpal joint surface discriminate *Papio* from all hominids as well as *Homo* from the great apes.

TABLE 3.16 Cross-validated posterior probabilities of genus membership using relative area and curvedness measures of the trapezium joint surface

	<i>Homo</i>	<i>Pan</i>	<i>Gorilla</i>	<i>Pongo</i>	<i>Papio</i>
<i>Homo</i>	90	5	2	4	7
%	83.3	4.6	1.9	3.7	6.5
<i>Pan</i>	3	29	3	9	0
%	6.8	65.9	6.8	20.5	0.0
<i>Gorilla</i>	1	8	32	1	0
%	2.4	19.1	76.2	2.4	0.0
<i>Pongo</i>	0	6	2	7	1
%	0.0	37.5	12.5	43.8	6.3
<i>Papio</i>	1	0	0	0	16
%	5.9	0.0	0.0	0.0	94.1

Partial Model II: First metacarpal joint surface measures only. This model utilizes five measures of the first metacarpal joint surface as predictor variables. These measures include the area of the first metacarpal surface relative to the entire area of the trapezium, and four measures of surface curvedness. Absolute and RMS curvatures

represent the overall magnitude of surface curvedness while mean and Gaussian curvatures represent overall surface shape. Each of these curvatures is a function of the dorso-palmar and radio-ulnar curvedness measures of the first metacarpal joint surface.

The first canonical axis (CAN1) accounts for 80% of the variation while the second (CAN2) accounts for 19%. Along CAN1, *Homo* and *Papio* cluster more toward the right while the great apes cluster more toward the left (Fig. 3.4). The correlations with CAN1 (Table 3.17) indicate that this axis is a comparison of the absolute and RMS curvatures (i.e., curvedness magnitude) with the relative area of the joint surface. Along CAN2, *Papio* clusters more toward the bottom while the hominid genera cluster more toward the top, with the exception of a few specimens from each genus (Fig. 3.4). The correlations with CAN2 (Table 3.17) indicate that this axis represents a comparison between the absolute and Gaussian curvatures (i.e., curvedness magnitude vs. shape).

Together, CAN1 and CAN2 result in three general clusters (Fig. 3.4). *Papio* clusters in the lower right area reflecting a more cylindrical surface that is very flat radio-ulnarly. *Homo* clusters in the upper right area reflecting a large relative joint area that is more saddle-shaped than in *Papio*, but less curved than in the great apes. Finally, the great apes mostly cluster in the upper left area reflecting a smaller relative joint area that is more saddle-shaped than in *Papio*, but more curved than in *Homo*.

The cross-validation procedure results in the correct classification of 91 *Homo* (80.5%), 17 *Pan* (36.2%), 28 *Gorilla* (63.6%), 10 *Pongo* (47.6%), and 19 *Papio* (95%; Table 3.18). The majority of misclassifications occur among the great apes (48). Overall, the results suggest that these five measures of the first metacarpal

carpometacarpal joint surface discriminate *Papio* from all hominids as well as *Homo* from the great apes.

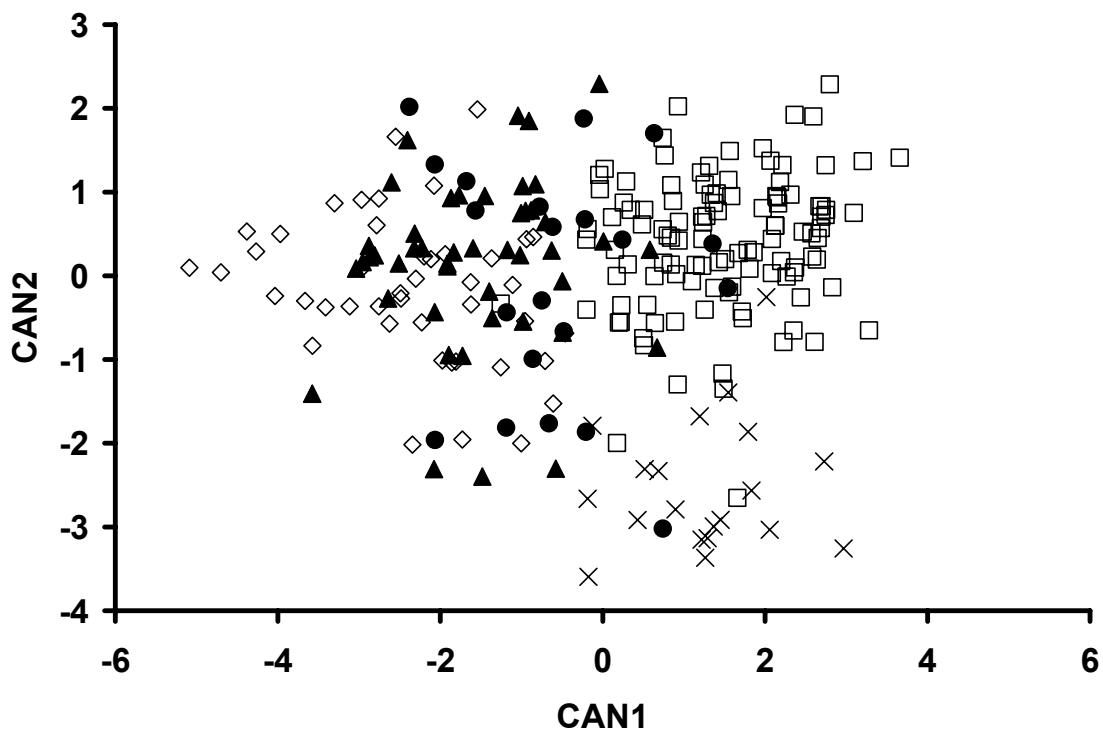


Fig. 3.4 Plot of the canonical variables (CAN1, CAN2) generated from analysis of 1st metacarpal joint surface area and curvedness measures (*Homo* = open squares, *Pan* = closed triangles, *Gorilla* = open diamonds, *Pongo* = closed circles, *Papio* = Xs).

TABLE 3.17 Correlations between each variable and canonical axis (bolded values indicate the variables that best explain the observed variation along each axis)

Pooled-within canonical structure		
Variable	CAN1	CAN2
Relative Area	0.62	0.39
RMS	-0.60	0.31
Absolute	-0.57	0.52
Gaussian	0.29	-0.45
Mean	0.39	0.20

TABLE 3.18 Cross-validated posterior probabilities of genus membership using relative area and curvedness measures of the 1st metacarpal joint surface

	<i>Homo</i>	<i>Pan</i>	<i>Gorilla</i>	<i>Pongo</i>	<i>Papio</i>
<i>Homo</i>	91	4	0	13	5
%	80.5	3.5	0.0	11.5	4.4
<i>Pan</i>	3	17	19	7	1
%	6.4	36.2	40.4	14.9	2.1
<i>Gorilla</i>	0	7	28	9	0
%	0.0	15.9	63.6	20.5	0.0
<i>Pongo</i>	3	3	3	10	2
%	14.3	14.3	14.3	47.6	9.5
<i>Papio</i>	1	0	0	0	19
%	5.0	0.0	0.0	0.0	95.0

Full Model: First metacarpal and trapezium joint surface measures. The first canonical axis (CAN1) accounts for 75% of the variation, the second (CAN2) accounts for 14%, and the third (CAN3) 10%. Along CAN1, *Homo* and *Papio* cluster more toward the left while the great apes cluster more toward the right (Fig. 3.5). The correlations with CAN1 (Table 3.19) indicate that this axis is a comparison of the absolute and RMS curvatures of both joint surfaces with the relative area of the first metacarpal joint surface and the Gaussian curvature of the trapezium joint surface. Along CAN2, *Papio* and *Pan* cluster more negatively and *Homo* and *Gorilla* cluster more positively, while no clear cluster is observed for *Pongo* (Figs. 3.5 and 3.6). The correlations with CAN2 (Table 3.19) indicate that this axis represents a trapezium joint surface comparison between the absolute and mean curvatures with the Gaussian curvature.

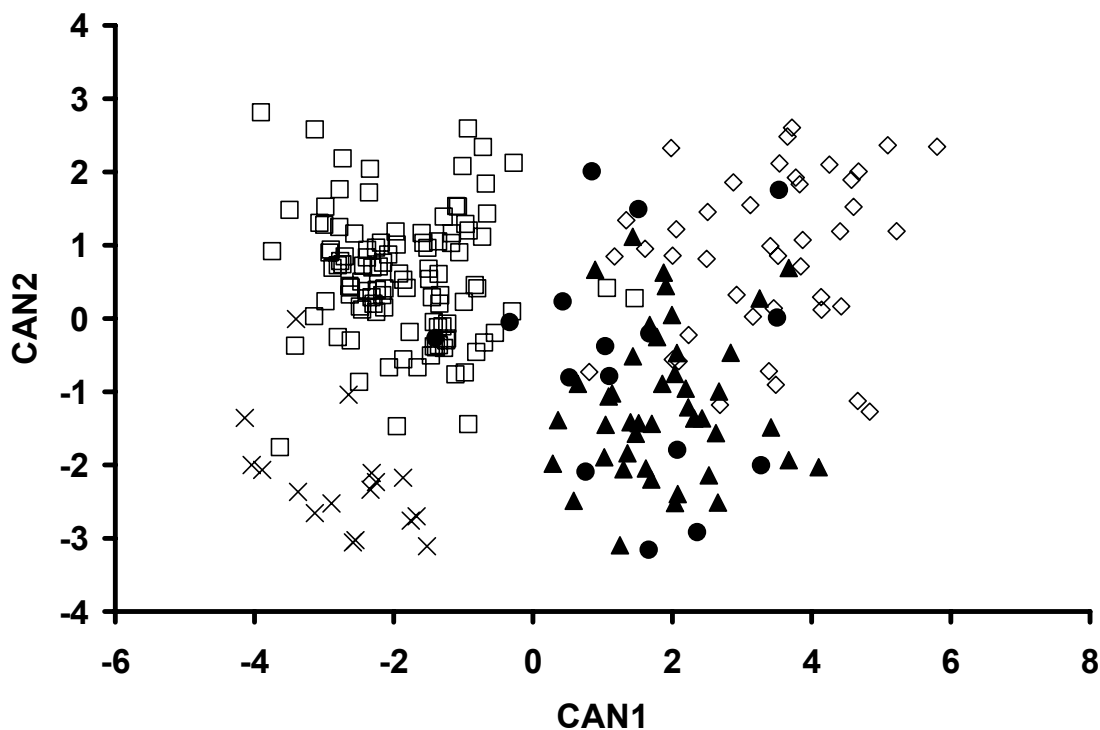


Fig. 3.5 Plot of the canonical variables (CAN1, CAN2) generated from analysis of 1st metacarpal and trapezium joint surface areas and curvedness measures (*Homo* = open squares, *Pan* = closed triangles, *Gorilla* = open diamonds, *Pongo* = closed circles, *Papio* = Xs).

Together, CAN1 and CAN2 result in four general clusters (Fig. 3.5). *Papio* clusters in the lower left area reflecting a larger relative first metacarpal joint area and flatter joint surfaces that almost appear cylindrical rather than saddle-shaped, because the saddles are very shallow. *Homo* clusters in the upper left area reflecting a large relative first metacarpal joint area that is more saddle-shaped than in *Papio*, but less curved than in the great apes. *Gorilla* clusters in the upper right area reflecting a smaller relative first metacarpal joint area and highly curved joint surfaces that produce a deep, even saddle-shape. *Pan* clusters in the lower right area reflecting a smaller relative first metacarpal joint area and highly curved joint surfaces that are less evenly curved than in

Gorilla, resulting in a deep, but uneven saddle-shape. Finally, *Pongo* is scattered among the African ape cluster showing a mixture of the joint morphologies observed in *Pan* and *Gorilla*.

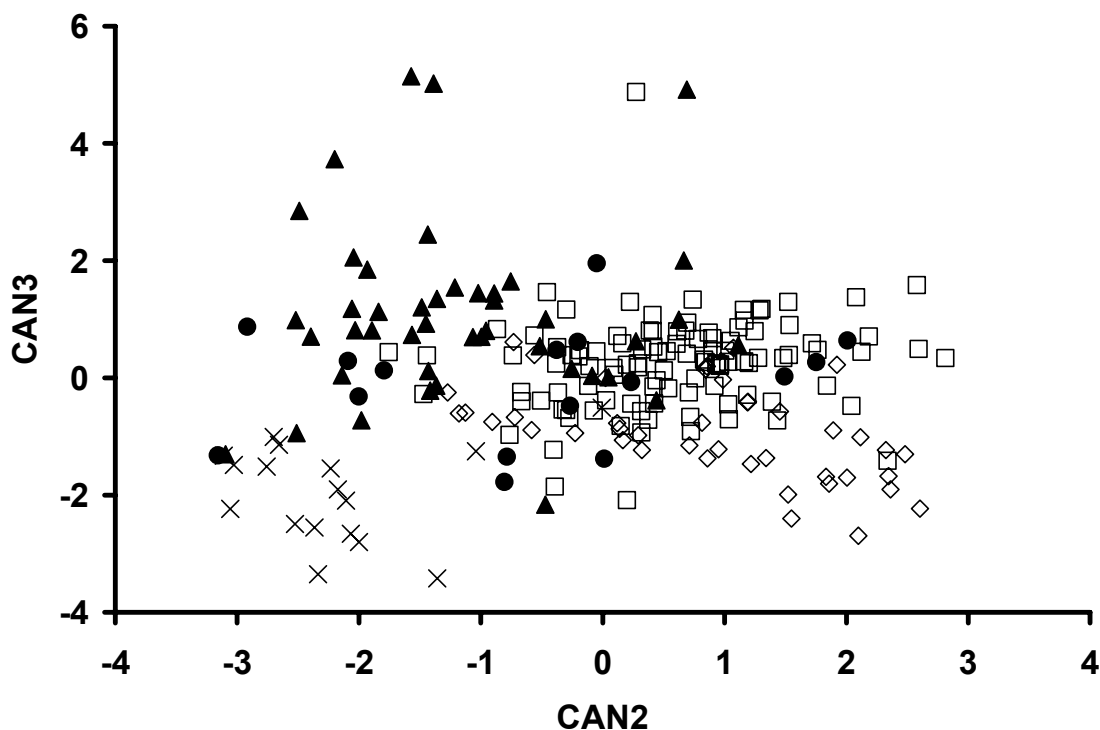


Fig. 3.6 Plot of the canonical variables (CAN2, CAN3) generated from analysis of 1st metacarpal and trapezium joint surface areas and curvedness measures (*Homo* = open squares, *Pan* = closed triangles, *Gorilla* = open diamonds, *Pongo* = closed circles, *Papio* = Xs).

Two general clusters result from the combination of CAN2 and CAN3 (Fig. 3.6). *Papio* again clusters in the lower left area for similar reasons as in Figure 3.5; however, the large relative area of the trapezium joint surface also plays an important role in driving *Papio* negatively along CAN3. The hominids tend to cluster away from the lower left reflecting the more curved saddle-shaped surfaces and more equivalent first

metacarpal and trapezium joint areas. A partial cluster of *Pan* is also discernable in the upper left area, reflecting similar morphology as described above along CAN2.

TABLE 3.19 Correlations between each variable and canonical axis (bolded values indicate the variables that best explain the observed variation along each axis)

<u>Pooled-within canonical structure</u>			
<u>Variable</u>	CAN1	CAN2	CAN3
<u>Proximal</u>			
RMS	0.43	-0.02	0.25
Absolute	0.41	0.10	0.35
Gaussian	-0.21	-0.18	-0.25
Mean	0.27	0.24	0.06
Relative Area	-0.43	0.26	0.39
<u>Distal</u>			
RMS	0.72	0.22	0.14
Absolute	0.71	0.33	0.05
Gaussian	-0.52	-0.36	0.29
Mean	0.03	0.34	-0.39
Relative Area	-0.02	-0.09	-0.49

The cross-validation procedure results in the correct classification of 101 *Homo* (93.5%), 29 *Pan* (65.9%), 35 *Gorilla* (83.3%), 9 *Pongo* (56.3%), and 16 *Papio* (94.1%; Table 3.20). The majority of misclassifications occur among the great apes (28). Overall, the results suggest that these ten measures of the first metacarpal and trapezium carpometacarpal joint surfaces discriminate *Papio* from all hominids, *Homo* from the great apes, as well as *Gorilla* from *Pan* and *Pongo*.

TABLE 3.20 Cross-validated posterior probabilities of genus membership using relative area and curvedness measures of the 1st metacarpal and trapezium joint surfaces

	<i>Homo</i>	<i>Pan</i>	<i>Gorilla</i>	<i>Pongo</i>	<i>Papio</i>
<i>Homo</i>	101	2	0	2	3
%	93.5	1.9	0.0	1.9	2.8
<i>Pan</i>	0	29	5	10	0
%	0.0	65.9	11.4	22.7	0.0
<i>Gorilla</i>	0	3	35	4	0
%	0.0	7.1	83.3	9.5	0.0
<i>Pongo</i>	1	3	3	9	0
%	6.3	18.8	18.8	56.3	0.0
<i>Papio</i>	1	0	0	0	16
%	5.9	0.0	0.0	0.0	94.1

Summary of Shape Characteristics

TABLE 3.21 Summary of mean 1st carpometacarpal joint features (distinctive features in bold)

<u>Variable</u>	<u>Genus</u>				
	<i>Homo</i>	<i>Pan</i>	<i>Gorilla</i>	<i>Pongo</i>	<i>Papio</i>
<u>Proximal</u>					
Dorsopalmar	-0.83	-1.32	-1.37	-0.98	-0.78
Radioulnar	0.43	0.41	0.41	0.44	0.10
RMS	0.96	1.41	1.45	1.11	0.80
Absolute	1.27	1.75	1.79	1.42	0.90
Gaussian	-0.35	-0.52	-0.56	-0.40	-0.07
Mean	-0.20	-0.46	-0.48	-0.27	-0.34
Relative Area	16.5	13.7	12.3	13.5	14.6
<u>Distal</u>					
Dorsopalmar	0.39	0.52	0.94	0.45	0.22
Radioulnar	-0.82	-1.14	-1.11	-1.15	-0.64
RMS	0.93	1.29	1.47	1.26	0.68
Absolute	1.22	1.69	2.05	1.61	0.86
Gaussian	-0.31	-0.58	-1.04	-0.52	-0.14
Mean	-0.21	-0.31	-0.09	-0.35	-0.21
Relative Area	105.9	100.8	111.4	111.4	123.6

Papio. The lowest probability of correctly classifying a first carpometacarpal joint as belonging to *Papio* was 94%, which used either the trapezium surface only (Partial Model I; Table 3.16), or both first metacarpal and trapezium surfaces (Full Model; Table 3.20). The first carpometacarpal joint in *Papio* is distinguished by relatively flat first metacarpal and trapezium joint surfaces that, although saddle-shaped, are so shallow that they approach being cylindrical—this is particularly the case for the first metacarpal joint surface (Table 3.21). Moreover, the trapezium joint surface area is, on average, 20-25% larger than its counterpart (Table 3.21).

The first carpometacarpal joint in hominids is more likely to show shape similarities to the *Papio* joint when only one of the surfaces is examined. Eight hominid joint surfaces are misclassified as belonging to *Papio* in each model that includes a single surface compared to only three misclassifications when both surfaces are included in the model. For example, the first metacarpal and trapezium joint surfaces in *Homo* show a 4.4% and 6.5% probability of misclassification as *Papio* respectively; however, when both surfaces are examined together the probability drops to 2.8%.

Pongo. The lowest probability of correctly classifying a first carpometacarpal joint as belonging to *Pongo* was 44%, which used the trapezium surface only (Partial Model I; Table 3.16), and only 56% classification was achieved using both surfaces (Full Model; Table 3.20). The poor classification results for *Pongo* are the result of this taxon always overlapping with one or more of the other genera in the ranges of variation for each measured variable (Table 3.21). However, in the majority of cases, the *Pongo* joint is misclassified as belonging to another hominid genus rather than as belonging to *Papio*.

In general, the *Pongo* first carpometacarpal joint has well-developed saddle-shaped surfaces. The first metacarpal surface tends to be more curved dorso-palmarly than radio-ulnarly while the reverse is true for the trapezium surface. Finally, the trapezium surface is, on average, around 10% larger than the first metacarpal (Table 3.21).

Gorilla. The lowest probability of correctly classifying a first carpometacarpal joint as belonging to *Gorilla* was 64%, which used the first metacarpal surface only (Partial Model II; Table 3.16), whereas 83% classification was achieved using both first metacarpal and trapezium surfaces (Full Model; Table 3.20). *Gorilla* is distinguished by having a first metacarpal surface that is strongly curved dorso-palmarly and a trapezium surface that is strongly curved in both directions. Moreover, the trapezium surface tends to be equally curved dorso-palmarly and radio-ulnarly, as evidenced by near-zero mean curvature value (-0.09; Table 3.21). Another distinctive feature in *Gorilla* is the small relative area of the first metacarpal joint surface, while the trapezium surface, like in *Pongo*, is approximately 10% larger than the first metacarpal (Table 3.21).

Because of the strong curvedness of both surfaces, the *Gorilla* first carpometacarpal joint is never misclassified as belonging to *Papio* and only once as *Homo*. Instead, the misclassifications occur almost always with *Pan* and *Pongo*, since both of these taxa also tend to show well-developed, highly-curved, saddle-shaped surfaces.

Pan. The lowest probability of correctly classifying a first carpometacarpal joint as belonging to *Pan* was 36%, which used the first metacarpal surface only (Partial Model II; Table 3.16), whereas 66% classification was achieved using either the trapezium

surface only or both first metacarpal and trapezium surfaces (Full Model; Table 3.20). The poor classification results for *Pan* are the result of this genus sharing most of its distinctive features with the other great apes (Table 3.21). Generally, *Pan* shows a first metacarpal surface that is most similar to *Gorilla* and a trapezium surface more like in *Pongo* (Tables 3.16 and 3.18). The first metacarpal joint surface is more curved dorso-palmarly and radio-ulnarly, whereas the opposite is true for the trapezium surface (Table 3.21). Finally, in *Pan* both joint surfaces tend to be similar in size to one another (Table 3.21).

Homo. The lowest probability of correctly classifying a first carpometacarpal joint as belonging to *Homo* was 81%, which used the first metacarpal surface only (Partial Model II; Table 3.18), whereas 94% classification was achieved using both first metacarpal and trapezium surfaces (Full Model; Table 3.20). The first carpometacarpal joint in *Homo* is distinguished by well-developed, saddle-shaped surfaces, as seen in the great apes. However, the primary difference between *Homo* and the great apes in terms of joint curvedness is that the first metacarpal surface in *Homo* is less curved dorso-palmarly while the trapezium surface is less curved radio-ulnarly. In other words, in these two aspects *Homo* tends to fall in between the more flattened joint observed in *Papio* and the more curved joint observed in the great apes. Finally, the *Homo* first carpometacarpal joint is also distinguished by having the largest relative area for the first metacarpal surface as well as a relative trapezium joint area that is, on average, slightly larger than its counterpart (Table 3.21).

DISCUSSION

The first carpometacarpal joint is the most discussed joint of the hand and wrist. Therefore, I present a brief review of the main functional and phylogenetic points of discussion that have arisen over the past several decades. Subsequent to this review, the results of this chapter are discussed in relation to previous studies as well as the biomechanical predictions introduced in Chapter 2.

The opposable thumb is an important feature of many, but not all, primate hands. Napier (1961) defined opposition as “a compound movement of abduction, flexion and medial rotation occurring at the carpometacarpal articulation of the pollex” (1961:119). He distinguished the capability to converge the thumb toward the remaining digits, characteristic of platyrrhines, from the ability to truly oppose the thumb as defined above, characteristic of catarrhines. A curved carpal arch allows the fingers of the hand to converge during flexion, thus providing an initial degree of prehensility. Many mammals, such as otters, mongooses, and raccoons, display convergent, prehensile hands (Haines, 1958; Napier, 1961). As the carpal arch becomes more curved, the trapezium becomes more in-turned relative to the other carpals, subsequently enabling pseudo-opposability of the thumb during combined movements of flexion and abduction (Napier, 1961). According to Napier (1961), platyrrhines have deep carpal arches that allow passage of the important wrist and finger flexor tendons but the first carpometacarpal joint is more cylindrical in shape and thus does not allow rotation; hence, New World monkeys have pseudo-opposable thumbs. The ability to rotate the thumb in addition to flexion and abduction arises from possessing a more saddle-shaped

joint resulting in “the more specialized hand of Old World monkeys, apes and man” (Napier, 1961:128).

Rotation of the thumb at the carpometacarpal joint became the centerpiece of a debate over whether *Proconsul africanus* had an opposable thumb. Napier and Davis (1959) considered the carpometacarpal joint in *Proconsul africanus* to be more cylindrical, ergo the thumb could not rotate, ergo the thumb was not opposable. Lewis (1977) argued that the joint was saddle-shaped and hence opposable. Subsequent discoveries of *P. africanus* confirmed Lewis’ observations that the joint is indeed saddle-shaped (Beard et al., 1986). Finally, a reassessment of the functional morphology and kinematics of this joint in living anthropoids, *Proconsul spp.*, and *Afropithecus turkanensis* concluded that both living and fossil hominoids have considerably more abduction-adduction and rotatory mobility at this joint than do other anthropoids (Rose, 1992). This functional conclusion was based on the observed differences between hominoid and non-hominoid primates in radio-ulnar curvedness and general incongruity of the mutual surfaces, which as Napier (1956) had argued played an important role in rotation.

Recently, it has been demonstrated anatomically and kinematically that the first carpometacarpal joint in modern humans is only a two-axis joint (Brand and Hollister, 1999; Buford et al., 1990; Hollister et al., 1992). The flexion-extension axis runs through the trapezium in a dorso-palmar direction while the abduction-adduction axis runs through the first metacarpal in a radio-ulnar direction (Fig. 3.7). Because the axes are not perpendicular to one another and do not cross, rotation occurs at this joint as a

combined movement of flexion and abduction. This revision regarding the basic mechanics of this joint is not surprising, given that neither Napier (1956) nor anyone else was able to successfully and unequivocally demonstrate which muscles were actually responsible for independent rotation of the first metacarpal. However, this presents a slight problem because Napier's (1961) basic dichotomy of opposability was based on the notion that a pseudo-opposable metacarpal could only flex and abduct whereas an opposable thumb could flex, abduct, and rotate.

Since the mechanics of the joint are reasonably established at least in modern humans (Brand and Hollister, 1999; Buford et al., 1990; Hollister et al., 1992), some reinterpretations of the joint mechanics in other anthropoids as described by Napier (1961), Lewis (1977), and Rose (1992) are necessary. It is the combined ability to flex-extend and abduct-adduct simultaneously along non-orthogonal joint axes, which together impart an effect that the metacarpal is rotating, that enables true opposition as originally described by Napier (1956, 1961). Clearly, saddle-shaped carpometacarpal joints have an advantage over cylinder-shaped joints for opposition because they allow movement along both axes whereas the others allow movement along only one axis.

In a broad evaluation of anthropoid first carpometacarpal joint kinematics, Rose (1992) concludes that, "the strongest hypothesis remains that the morphology and kinematics of the trapezium-first metacarpal joint in *Proconsul*, *Afropithecus*, and large living hominoids represents a shared derived complex" (1992: 264). This conclusion is primarily based on the large differences in abduction-adduction ability that he observed between hominoid and non-hominoid primates.

The results of this chapter build upon Rose's (1992) conclusions by quantitatively demonstrating the fundamental differences between the first metacarpal joint in *Papio* and the hominids (Figs. 3.1, 3.2, 3.5, and 3.6). Baboons, in general, have considerable manipulative skill (Guthrie, 1991; Jolly, 1970; Rose, 1977). Baboons are capable of forming a variety of precision grips; these include pad-to-side, pad tip-to-pad tip, and pad-to-pad hold (Guthrie, 1991; Jolly, 1970; Rose, 1977). However, they utilize these grips primarily for retrieving and holding food or other objects when there is only a mild amount of resistance to overcome (Guthrie, 1991; Jude, 1993; Marzke, 1997). When it is necessary to form a stronger grasp to counter stronger amounts of resistance, baboons recruit both hands rather than just one (Guthrie, 1991; Marzke, 1997). The results presented here concur with the available behavioral evidence by indicating that the first carpometacarpal joint in *Papio* simply does not have the necessary morphology required to efficiently handle joint loads generated from strong grasps that involve the thumb.

In *Papio*, the mutual surfaces of this joint are extremely flat, particularly radio-ulnarly, producing a slight cylinder-like shape overall. The overall flatness of the surfaces suggests that maximum compression of the mutual surfaces occurs only when the thumb assumes a relatively neutral posture along the flexion-extension axis (i.e., neither abducted nor adducted). Alternatively, hominid first carpometacarpal joint surfaces are strongly saddle-shaped. Therefore, maximum compression of the reciprocal joint surfaces occurs when the first metacarpal assumes either an adducted or abducted posture along the flexion-extension axis (Napier, 1956).

In general, the great apes share more similarities in first carpometacarpal shape with one another than they do with *Homo* (Table 3.20). Great apes tend to display more strongly curved joint surfaces in both directions of movement. Mutual joint surfaces that are tightly curved maintain a degree of stability throughout the joint range of motion. In this sense, the first carpometacarpal joint morphology observed in great apes indicates an ability to oppose the thumb while also providing the required stability to apply load to the trapezium from a variety of thumb postures. In other words, as the great ape thumb moves through its range of motion along the highly curved mutual joint surfaces, there are many instances where load can be applied by compressing the trapezium surface into the first metacarpal surface while the opposite curves of the surfaces offer joint stability. There does not appear to be any indication that the joint by itself, as it is shaped in great apes, is not capable of accommodating considerable load to the trapezium.

In *Homo*, several key differences from the great ape condition are observed. First, joint stability is decreased as evidenced by a first metacarpal surface that is less curved dorso-palmarly and a trapezium surface that is less curved radio-ulnarly. However, these relatively flatter surfaces in comparison to the great apes should not be confused with the absolutely flatter surfaces seen in *Papio*; there is nothing overtly *Papio*-like about the joint in *Homo*. In other words, *Homo* tends to fall in between the more flattened joint observed in *Papio* and the more curved joint observed in the great apes.

This distinctive joint morphology in *Homo* likely reflects a compromise between joint stability and mobility (Marzke, 1992). For instance, the first metacarpal joint surface is

relatively large and this increase in surface area occurs across the whole joint but, in particular, along the radial border (Fig. 3.2, middle row). A radio-ulnarly flatter trapezium surface in combination with an enlarged area along the radial border of the first metacarpal surface suggests more joint mobility along the adduction-abduction axis, yet the area of the trapezium surface relative to the first metacarpal surface in *Homo* is not significantly different than in the great apes (Table 3.1). However, the first carpometacarpal joint morphology in *Homo* is better understood by considering the basic anatomy of the carpal arch in non-human primates.

In non-human primates, the trapezium contributes to the curvedness of the carpal arch by sitting in front of the trapezoid (palmar) rather than beside it (lateral). This more palmar placement of the trapezium is directly affected by the shape of the palmar aspect of the trapezoid, which is considerably narrower than it is in *Homo* (Lewis, 1989). The non-human primate thumb, therefore, is already in a position to oppose to the fingers by simply flexing the fingers and thumb simultaneously. It follows that a more curved first carpometacarpal joint likely provides more joint stability without seriously compromising joint mobility.

In humans, however, the trapezoid is broader palmarly and this results in the trapezium acquiring a more supinated position relative to the rest of the carpus (these important particulars of the morphology in *Homo* are discussed in more detail in subsequent chapters). In essence, the human thumb is less opposed in its neutral position than the non-human primate thumb because of the differences in the curvedness of the carpal arch. Therefore, in order to maintain the ability to oppose the

thumb to the fingers, the first carpometacarpal joint has had to sacrifice joint stability through relatively flatter mutual joint surfaces. The result is the observed compromise of morphology, “that allows full opposition to the fingers, but which retains enough mutual curvature of the trapezium and metacarpal base to stabilize thumb/index finger pinch grips” (Marzke and Marzke, 2000: 123; Marzke, 1992).

Indeed, visual inspection clearly shows the relative radial expansion of both joint surfaces in *Homo* (Figs. 3.1 and 3.2). This radial expansion of joint surface area likely reduces compressive stress at the joint when the metacarpal is abducted and the thumb musculature is strongly contracted. It is known that modern humans apply considerable load at this joint (Cooney and Chao, 1977; Eaton and Littler, 1969; Linscheid, 1982), and the joint morphology of *Homo* appears well-suited to handle and distribute the resulting compressive stress.

Although previous research suggests that the joint surface areas of the humeral and femoral heads relate more to joint mobility than to joint loading (Rafferty and Ruff, 1994), it is not clear whether this also applies to the first carpometacarpal joint. Experimental results of long bone articular area responses to mechanical loading suggest that joint surface area is constrained ontogenetically and represents a species-level relationship to locomotor behavior rather than an individual-level relationship to activity (Leiberman et al., 2001). The first carpometacarpal joint morphology in *Homo*, when considered in context of the shape of the carpal arch and in comparison to non-human primates, shows the most efficient compromise for distributing the compressive stress that results from strong contraction of the thumb musculature. At present, it

appears reasonable to conclude that the first carpometacarpal joint surface morphology in humans likely represents a species-level relationship to manipulative behaviors involving the thumb, which are accomplished through a combination of thumb mobility, stability, and ability to distribute large compressive loads.

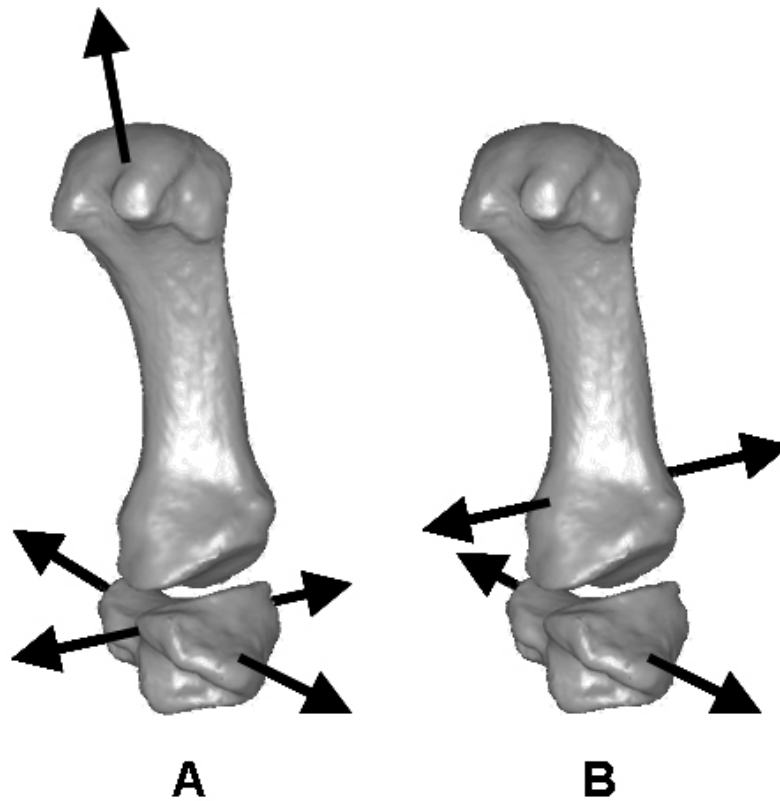


Fig. 3.7 The right 1st carpometacarpal joint axes of motion after (A) Napier (1961) and after (B) Buford et al. (1990) and Hollister et al. (1992). Note the flexion-extension and abduction-adduction axes in (A) are perpendicular to one another and occur in the same plane whereas in (B) they do not; also (A) requires a third joint axis to explain rotation whereas (B) does not.

Chapter 4: The Trapezium

RESULTS OF SHAPE ANALYSES

In this chapter, I present the results of the shape analyses performed on the carpal and carpometacarpal joints and non-articular area of the trapezium. Since all of the features examined in this chapter belong to the trapezium, the name of the articulating bone is used to describe each joint surface. For example, the area on the trapezium for articulation with the trapezoid is referred to as the trapezoid joint surface (Fig. 4.1). The trapezium variables measured include all the relative areas and angles of the carpal and carpometacarpal joints as well as the relative non-articular area. The results of the comparative shape analyses for each variable are presented separately, followed by multivariate analyses of all the variables (Full Model). Following the presentation of the statistical results, a summary of the shape characteristics of each genus is given. Finally, the results are discussed in relation to previous studies as well as the biomechanical predictions introduced in Chapter 2.

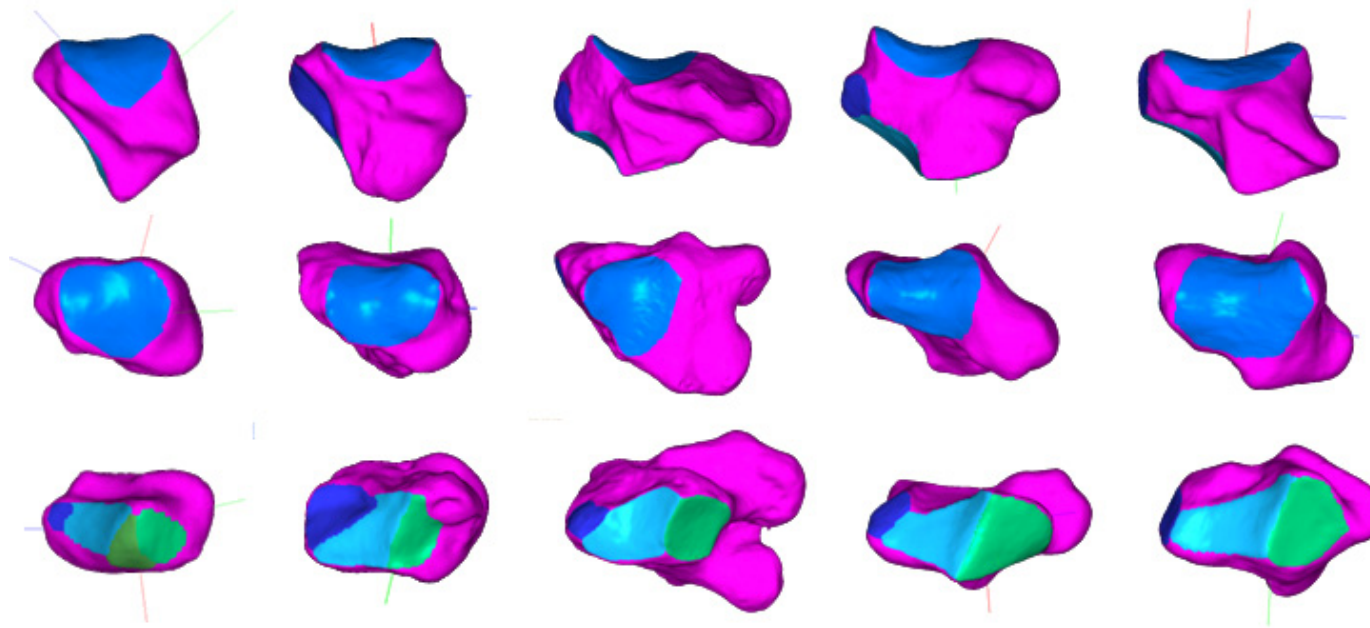


Fig. 4.1 Visual comparison of trapezium shape in five primate genera (*Papio*, far left; *Pongo*, 2nd from left; *Gorilla*, middle; *Pan*, 2nd from right; *Homo*, far right). Key: top row, palmar view; middle row, distal view; bottom row, proximo-medial view; medium blue, 1st metacarpal joint; dark blue, 2nd metacarpal joint; light blue, trapezoid joint; light green, scaphoid joint; dark green, centrale joint (*Papio* only); pink, non-articular area. Bones are from the right side.

Angles of the trapezium

The first and second metacarpal articulations. The angle between these two joint surfaces is significantly different in six of the ten pairwise comparisons between genus means (Table 4.1). This angle is significantly wider in *Homo* (93°) than in all the other genera except *Papio* (85°). Both *Pan* (68°) and *Gorilla* (73°) show significantly narrower angles than does *Papio* (85°), while *Pan* has a significantly narrower angle than does *Pongo* (80°).

TABLE 4.1 Pairwise comparisons of genus means for the angle between the 1st and 2nd metacarpal joint surfaces¹

Genus A	Genus B	Mean _A	Mean _B	N _A	N _B	θ	p
<i>Homo</i>	<i>Pan</i>	93	68	112	47	25	<.001
<i>Homo</i>	<i>Gorilla</i>	93	73	112	43	20	<.001
<i>Homo</i>	<i>Pongo</i>	93	80	112	21	13	<.001
<i>Homo</i>	<i>Papio</i>	93	85	112	13	8	0.011
<i>Pan</i>	<i>Gorilla</i>	68	73	47	43	5	0.032
<i>Pan</i>	<i>Pongo</i>	68	80	47	21	12	<.001
<i>Pan</i>	<i>Papio</i>	68	85	47	13	17	<.001
<i>Gorilla</i>	<i>Pongo</i>	73	80	43	21	7	0.013
<i>Gorilla</i>	<i>Papio</i>	73	85	43	13	12	0.002
<i>Pongo</i>	<i>Papio</i>	80	85	21	13	5	0.217

¹ Mean_A, mean of Genus A; N_A, sample size of Genus A; Mean_B, mean of Genus B; N_B, sample size of Genus B; | θ |, absolute value of difference between observed sample means; p, probability that a difference between the bootstrapped means equaled or exceeded | θ |. Numbers in bold indicate statistical significance at alpha = .01.

The first metacarpal and scaphoid articulations. The angle between these two joint surfaces is significantly different in eight of the ten pairwise comparisons between genus means (Table 4.2). This angle is significantly narrower in *Homo* (10°) than in the other genera. This angle is not significantly different between *Pan* (19°) and *Gorilla* (18°) or between *Pongo* (36°) and *Papio* (44°); however, the former two genera show significantly narrower angles than do the latter two.

TABLE 4.2 Pairwise comparisons of genus means for the angle between the 1st metacarpal and scaphoid joint surfaces¹

Genus A	Genus B	Mean _A	Mean _B	N _A	N _B	θ	p
<i>Homo</i>	<i>Pan</i>	10	19	113	47	10	<.001
<i>Homo</i>	<i>Gorilla</i>	10	18	113	44	9	<.001
<i>Homo</i>	<i>Pongo</i>	10	36	113	21	27	<.001
<i>Homo</i>	<i>Papio</i>	10	44	113	20	35	<.001
<i>Pan</i>	<i>Gorilla</i>	19	18	47	44	1	0.606
<i>Pan</i>	<i>Pongo</i>	19	36	47	21	17	<.001
<i>Pan</i>	<i>Papio</i>	19	44	47	20	25	<.001
<i>Gorilla</i>	<i>Pongo</i>	18	36	44	21	18	<.001
<i>Gorilla</i>	<i>Papio</i>	18	44	44	20	26	<.001
<i>Pongo</i>	<i>Papio</i>	36	44	21	20	8	0.03

¹ Mean_A, mean of Genus A; N_A, sample size of Genus A; Mean_B, mean of Genus B; N_B, sample size of Genus B; | θ |, absolute value of difference between observed sample means; p, probability that a difference between the bootstrapped means equaled or exceeded | θ |. Numbers in bold indicate statistical significance at alpha = .01.

The first metacarpal and trapezoid articulations. The angle between these two joint surfaces is significantly different in eight of the ten pairwise comparisons between genus means (Table 4.3). This angle is significantly wider in *Papio* (78°) than in the other genera. *Homo* (49°), *Pongo* (47°), and *Gorilla* (45°) have significantly wider angles than does *Pan* (38°). The angle in *Pongo* is not significantly different than in *Homo* or *Gorilla*; however, in *Homo* it is significantly wider than in *Gorilla*.

TABLE 4.3 Pairwise comparisons of genus means for the angle between the 1st metacarpal and trapezoid joint surfaces¹

Genus A	Genus B	Mean _A	Mean _B	N _A	N _B	θ	p
<i>Homo</i>	<i>Pan</i>	49	38	113	47	11	<.001
<i>Homo</i>	<i>Gorilla</i>	49	45	113	44	4	0.005
<i>Homo</i>	<i>Pongo</i>	49	47	113	21	2	0.07
<i>Homo</i>	<i>Papio</i>	49	78	113	20	28	<.001
<i>Pan</i>	<i>Gorilla</i>	38	45	47	44	7	<.001
<i>Pan</i>	<i>Pongo</i>	38	47	47	21	9	<.001
<i>Pan</i>	<i>Papio</i>	38	78	47	20	40	<.001
<i>Gorilla</i>	<i>Pongo</i>	45	47	44	21	2	0.25
<i>Gorilla</i>	<i>Papio</i>	45	78	44	20	33	<.001
<i>Pongo</i>	<i>Papio</i>	47	78	21	20	31	<.001

¹ Mean_A, mean of Genus A; N_A, sample size of Genus A; Mean_B, mean of Genus B; N_B, sample size of Genus B; | θ |, absolute value of difference between observed sample means; p, probability that a difference between the bootstrapped means equaled or exceeded | θ |. Numbers in bold indicate statistical significance at alpha = .01.

The second metacarpal and scaphoid articulations. The angle between these two joint surfaces is significantly different in eight of the ten pairwise comparisons between genus means (Table 4.4). This angle is significantly narrower in *Pongo* (66°) and *Papio* (70°) than in the other genera, among which *Homo* (81°) also has a significantly narrower angle than *Pan* (97°) and *Gorilla* (101°).

TABLE 4.4 Pairwise comparisons of genus means for the angle between the 2nd metacarpal and scaphoid joint surfaces¹

Genus A	Genus B	Mean _A	Mean _B	N _A	N _B	θ	p
<i>Homo</i>	<i>Pan</i>	81	97	112	47	16	<.001
<i>Homo</i>	<i>Gorilla</i>	81	101	112	43	19	<.001
<i>Homo</i>	<i>Pongo</i>	81	66	112	21	16	<.001
<i>Homo</i>	<i>Papio</i>	81	70	112	13	11	0.003
<i>Pan</i>	<i>Gorilla</i>	97	101	47	43	4	0.076
<i>Pan</i>	<i>Pongo</i>	97	66	47	21	31	<.001
<i>Pan</i>	<i>Papio</i>	97	70	47	13	27	<.001
<i>Gorilla</i>	<i>Pongo</i>	101	66	43	21	35	<.001
<i>Gorilla</i>	<i>Papio</i>	101	70	43	13	31	<.001
<i>Pongo</i>	<i>Papio</i>	66	70	21	13	4	0.347

¹ Mean_A, mean of Genus A; N_A, sample size of Genus A; Mean_B, mean of Genus B; N_B, sample size of Genus B; | θ |, absolute value of difference between observed sample means; p, probability that a difference between the bootstrapped means equaled or exceeded | θ |. Numbers in bold indicate statistical significance at alpha = .01.

The second metacarpal and trapezoid articulations. The angle between these two joint surfaces is significantly different in nine of the ten pairwise comparisons between genus means (Table 4.5). Only *Homo* (131°) and *Pongo* (134°) show no significant difference in this mean angle, and both of these genera have angles that are significantly narrower than in the other genera. *Papio* (161°) has the largest mean angle, followed by *Gorilla* (151°), and then *Pan* (146°); all of which are significantly different from one another.

TABLE 4.5 Pairwise comparisons of genus means for the angle between the 2nd metacarpal and trapezoid joint surfaces¹

Genus A	Genus B	Mean _A	Mean _B	N _A	N _B	θ	p
<i>Homo</i>	<i>Pan</i>	131	146	112	47	15	<.001
<i>Homo</i>	<i>Gorilla</i>	131	151	112	43	20	<.001
<i>Homo</i>	<i>Pongo</i>	131	134	112	21	3	0.188
<i>Homo</i>	<i>Papio</i>	131	161	112	13	30	<.001
<i>Pan</i>	<i>Gorilla</i>	146	151	47	43	5	0.008
<i>Pan</i>	<i>Pongo</i>	146	134	47	21	12	<.001
<i>Pan</i>	<i>Papio</i>	146	161	47	13	15	<.001
<i>Gorilla</i>	<i>Pongo</i>	151	134	43	21	17	<.001
<i>Gorilla</i>	<i>Papio</i>	151	161	43	13	10	<.001
<i>Pongo</i>	<i>Papio</i>	134	161	21	13	27	<.001

¹ Mean_A, mean of Genus A; N_A, sample size of Genus A; Mean_B, mean of Genus B; N_B, sample size of Genus B; | θ |, absolute value of difference between observed sample means; p, probability that a difference between the bootstrapped means equaled or exceeded | θ |. Numbers in bold indicate statistical significance at alpha = .01.

The scaphoid and trapezoid articulations. The angle between these two joint surfaces is significantly different in seven of the ten pairwise comparisons between genus means (Table 4.6). This angle is significantly narrower in *Papio* (73°) than in *Pongo* (101°), and both of these genera have a significantly narrower angle than do any of the hominines; it is not significantly different among *Pan* (126°), *Gorilla* (126°), and *Homo* (127°).

TABLE 4.6 Pairwise comparisons of genus means for the angle between the scaphoid and trapezoid joint surfaces¹

Genus A	Genus B	Mean _A	Mean _B	N _A	N _B	θ	p
<i>Homo</i>	<i>Pan</i>	127	126	113	47	1	0.213
<i>Homo</i>	<i>Gorilla</i>	127	126	113	44	1	0.525
<i>Homo</i>	<i>Pongo</i>	127	101	113	21	26	<.001
<i>Homo</i>	<i>Papio</i>	127	73	113	20	54	<.001
<i>Pan</i>	<i>Gorilla</i>	126	126	47	44	1	0.623
<i>Pan</i>	<i>Pongo</i>	126	101	47	21	24	<.001
<i>Pan</i>	<i>Papio</i>	126	73	47	20	53	<.001
<i>Gorilla</i>	<i>Pongo</i>	126	101	44	21	25	<.001
<i>Gorilla</i>	<i>Papio</i>	126	73	44	20	54	<.001
<i>Pongo</i>	<i>Papio</i>	101	73	21	20	28	<.001

¹ Mean_A, mean of Genus A; N_A, sample size of Genus A; Mean_B, mean of Genus B; N_B, sample size of Genus B; | θ |, absolute value of difference between observed sample means; p, probability that a difference between the bootstrapped means equaled or exceeded | θ |. Numbers in bold indicate statistical significance at alpha = .01.

Relative areas of the trapezium

First metacarpal articulation. The relative area of the first metacarpal joint surface is significantly different in seven of the ten pairwise comparisons between genus means (Table 4.7). The relative area is significantly larger in *Homo* (16.5%) than in all the other genera, whereas in *Gorilla* (12.3%) it is significantly smaller than in all the others. Non-significant differences in the means occur between *Pan* (13.7%), *Pongo* (13.5%), and *Papio* (14.6%).

TABLE 4.7 Pairwise comparisons of genus means for relative area of the 1st metacarpal joint surface¹

Genus A	Genus B	Mean _A	Mean _B	N _A	N _B	θ	p
<i>Homo</i>	<i>Pan</i>	16.5	13.7	113	47	2.9	<.001
<i>Homo</i>	<i>Gorilla</i>	16.5	12.3	113	44	4.3	<.001
<i>Homo</i>	<i>Pongo</i>	16.5	13.5	113	21	3.0	<.001
<i>Homo</i>	<i>Papio</i>	16.5	14.6	113	20	2.0	<.001
<i>Pan</i>	<i>Gorilla</i>	13.7	12.3	47	44	1.4	0.002
<i>Pan</i>	<i>Pongo</i>	13.7	13.5	47	21	0.1	0.723
<i>Pan</i>	<i>Papio</i>	13.7	14.6	47	20	0.9	0.021
<i>Gorilla</i>	<i>Pongo</i>	12.3	13.5	44	21	1.3	<.001
<i>Gorilla</i>	<i>Papio</i>	12.3	14.6	44	20	2.3	<.001
<i>Pongo</i>	<i>Papio</i>	13.5	14.6	21	20	1.0	0.011

¹ Mean_A, mean of Genus A; N_A, sample size of Genus A; Mean_B, mean of Genus B; N_B, sample size of Genus B; | θ |, absolute value of difference between observed sample means; p, probability that a difference between the bootstrapped means equaled or exceeded | θ |. Numbers in bold indicate statistical significance at alpha = .01.

Second metacarpal articulation. The relative area of the second metacarpal joint surface is significantly different in seven of the ten pairwise comparisons between genus means (Table 4.8). The relative area is significantly larger in *Pongo* (5.4%) than in the other genera, whereas in *Papio* (1.3%) it is significantly smaller than in all the others (note that this is true even though all *Papio* individuals that lack a second metacarpal facet are excluded from the analysis). No significant differences occur between *Gorilla* (2.7%), *Pan* (2.5%), or *Homo* (2.7%).

TABLE 4.8 Pairwise comparisons of genus means for relative area of the 2nd metacarpal joint surface¹

Genus A	Genus B	Mean _A	Mean _B	N _A	N _B	θ	p
<i>Homo</i>	<i>Pan</i>	2.7	2.5	112	47	0.1	0.337
<i>Homo</i>	<i>Gorilla</i>	2.7	2.7	112	43	0.1	0.624
<i>Homo</i>	<i>Pongo</i>	2.7	5.4	112	21	2.7	<.001
<i>Homo</i>	<i>Papio</i>	2.7	1.3	112	13	1.4	<.001
<i>Pan</i>	<i>Gorilla</i>	2.5	2.7	47	43	0.2	0.217
<i>Pan</i>	<i>Pongo</i>	2.5	5.4	47	21	2.8	<.001
<i>Pan</i>	<i>Papio</i>	2.5	1.3	47	13	1.3	<.001
<i>Gorilla</i>	<i>Pongo</i>	2.7	5.4	43	21	2.6	<.001
<i>Gorilla</i>	<i>Papio</i>	2.7	1.3	43	13	1.5	<.001
<i>Pongo</i>	<i>Papio</i>	5.4	1.3	21	13	4.1	<.001

¹ Mean_A, mean of Genus A; N_A, sample size of Genus A; Mean_B, mean of Genus B; N_B, sample size of Genus B; | θ |, absolute value of difference between observed sample means; p, probability that a difference between the bootstrapped means equaled or exceeded | θ |. Numbers in bold indicate statistical significance at alpha = .01.

Scaphoid (centrale included) articulation. For *Papio* and *Pongo*, the areas of the scaphoid and centrale joint surfaces are combined to calculate the total joint relative area, given that the combination is structurally homologous with the scaphoid joint surfaces in *Gorilla*, *Pan*, and *Homo*. The relative area of the scaphoid (centrale included) joint surface is significantly different in seven of the ten pairwise comparisons between genus means (Table 4.9). The relative area is significantly larger in *Homo* (8.1%) than in the great apes, while *Papio* (7.6%) also has a significantly larger relative area than does either *Pan* (6.3%) or *Gorilla* (5.6%). Finally, the relative area is also significantly smaller in *Gorilla* than in either *Pongo* (6.9%) or *Pan*.

TABLE 4.9 Pairwise comparisons of genus means for relative area of the scaphoid (centrale included) joint surface¹

Genus A	Genus B	Mean _A	Mean _B	N _A	N _B	θ	p
<i>Homo</i>	<i>Pan</i>	8.1	6.3	113	47	1.8	<.001
<i>Homo</i>	<i>Gorilla</i>	8.1	5.6	113	44	2.5	<.001
<i>Homo</i>	<i>Pongo</i>	8.1	6.9	113	21	1.2	<.001
<i>Homo</i>	<i>Papio</i>	8.1	7.6	113	20	0.5	0.216
<i>Pan</i>	<i>Gorilla</i>	6.3	5.6	47	44	0.7	0.006
<i>Pan</i>	<i>Pongo</i>	6.3	6.9	47	21	0.6	0.107
<i>Pan</i>	<i>Papio</i>	6.3	7.6	47	20	1.2	0.007
<i>Gorilla</i>	<i>Pongo</i>	5.6	6.9	44	21	1.3	<.001
<i>Gorilla</i>	<i>Papio</i>	5.6	7.6	44	20	2.0	<.001
<i>Pongo</i>	<i>Papio</i>	6.9	7.6	21	20	0.6	0.247

¹ Mean_A, mean of Genus A; N_A, sample size of Genus A; Mean_B, mean of Genus B; N_B, sample size of Genus B; | θ |, absolute value of difference between observed sample means; p, probability that a difference between the bootstrapped means equaled or exceeded | θ |. Numbers in bold indicate statistical significance at alpha = .01.

Trapezoid articulation. The relative area of the trapezoid joint surface is significantly different in seven of the ten pairwise comparisons between genus means (Table 4.10). The relative area is significantly smaller in *Gorilla* (6.8%) than in all the other genera, while in *Pongo* (7.6%) it is also significantly smaller than in *Papio* (9.3%), *Pan* (9%), and *Homo* (9.2%). No significant differences occur between the latter three taxa.

TABLE 4.10 Pairwise comparisons of genus means for relative area of the trapezoid joint surface¹

Genus A	Genus B	Mean _A	Mean _B	N _A	N _B	θ	p
<i>Homo</i>	<i>Pan</i>	9.2	9.0	113	47	0.2	0.371
<i>Homo</i>	<i>Gorilla</i>	9.2	6.8	113	44	2.3	<.001
<i>Homo</i>	<i>Pongo</i>	9.2	7.6	113	21	1.5	<.001
<i>Homo</i>	<i>Papio</i>	9.2	9.3	113	20	0.2	0.532
<i>Pan</i>	<i>Gorilla</i>	9.0	6.8	47	44	2.2	<.001
<i>Pan</i>	<i>Pongo</i>	9.0	7.6	47	21	1.3	<.001
<i>Pan</i>	<i>Papio</i>	9.0	9.3	47	20	0.3	0.281
<i>Gorilla</i>	<i>Pongo</i>	6.8	7.6	44	21	0.8	0.002
<i>Gorilla</i>	<i>Papio</i>	6.8	9.3	44	20	2.5	<.001
<i>Pongo</i>	<i>Papio</i>	7.6	9.3	21	20	1.7	<.001

¹ Mean_A, mean of Genus A; N_A, sample size of Genus A; Mean_B, mean of Genus B; N_B, sample size of Genus B; | θ |, absolute value of difference between observed sample means; p, probability that a difference between the bootstrapped means equaled or exceeded | θ |. Numbers in bold indicate statistical significance at alpha = .01.

Non-articular surface. The relative non-articular area is significantly different in eight of the ten pairwise comparisons between genus means (Table 4.11). In *Gorilla* (72.7%), this area is significantly larger than in the other genera while in *Homo* (63.6%), it is significantly smaller. Also, *Pan* (68.5%) shows a significantly larger area than does *Pongo* (66.5%). Non-significant differences occur between *Papio* (67.7%) and *Pan*, and between *Papio* and *Pongo*.

TABLE 4.11 Pairwise comparisons of genus means for relative area of the non-articular surface¹

Genus A	Genus B	Mean _A	Mean _B	N _A	N _B	θ	p
<i>Homo</i>	<i>Pan</i>	63.6	68.5	113	47	4.9	<.001
<i>Homo</i>	<i>Gorilla</i>	63.6	72.7	113	44	9.1	<.001
<i>Homo</i>	<i>Pongo</i>	63.6	66.5	113	21	2.9	<.001
<i>Homo</i>	<i>Papio</i>	63.6	67.7	113	20	4.2	<.001
<i>Pan</i>	<i>Gorilla</i>	68.5	72.7	47	44	4.1	<.001
<i>Pan</i>	<i>Pongo</i>	68.5	66.5	47	21	2.0	0.008
<i>Pan</i>	<i>Papio</i>	68.5	67.7	47	20	0.8	0.25
<i>Gorilla</i>	<i>Pongo</i>	72.7	66.5	44	21	6.1	<.001
<i>Gorilla</i>	<i>Papio</i>	72.7	67.7	44	20	4.9	<.001
<i>Pongo</i>	<i>Papio</i>	66.5	67.7	21	20	1.2	0.147

¹ Mean_A, mean of Genus A; N_A, sample size of Genus A; Mean_B, mean of Genus B; N_B, sample size of Genus B; | θ |, absolute value of difference between observed sample means; p, probability that a difference between the bootstrapped means equaled or exceeded | θ |. Numbers in bold indicate statistical significance at alpha = .01.

Multivariate analyses

In this section, the results of the canonical and discriminant function analyses using one combination of trapezium carpal and carpometacarpal joint and non-articular variables is presented. In this Full Model, all six angles between articular surfaces are used as predictor variables along with four of the relative areas (relative non-articular area is excluded). Using all five relative areas results in a singular covariance matrix because all six sum to 1; this is an unacceptable violation for multivariate analyses. It should be noted, however, that the results are statistically identical no matter which four relative areas are selected because the fifth is always implied by the others.

Full Model. The first canonical axis (CAN1) accounts for 44% of the variation, the second (CAN2) accounts for 31%, the third (CAN3) 18%, and the fourth (CAN4) 7%. Along CAN1, *Homo* is clustered on the left, with the African apes in the middle, and *Pongo* and *Papio* on the right (Fig. 4.2). The correlations with CAN1 indicate that this axis represents the first metacarpal-scaphoid angle and the second metacarpal-trapezoid angle in comparison with the first metacarpal-second metacarpal angle, the scaphoid-trapezoid angle, and the relative area of the first metacarpal surface (Table 4.12). Along CAN2, *Gorilla* and *Pan* cluster more negatively, *Papio* and *Pongo* cluster more positively, while *Homo* clusters more in the middle (Figs. 4.2 and 4.3). The correlations with CAN2 indicate that this axis represents the first metacarpal-second metacarpal angle and the first metacarpal-trapezoid angle in comparison with the second metacarpal-scaphoid angle and the scaphoid-trapezoid angle (Table 4.12).

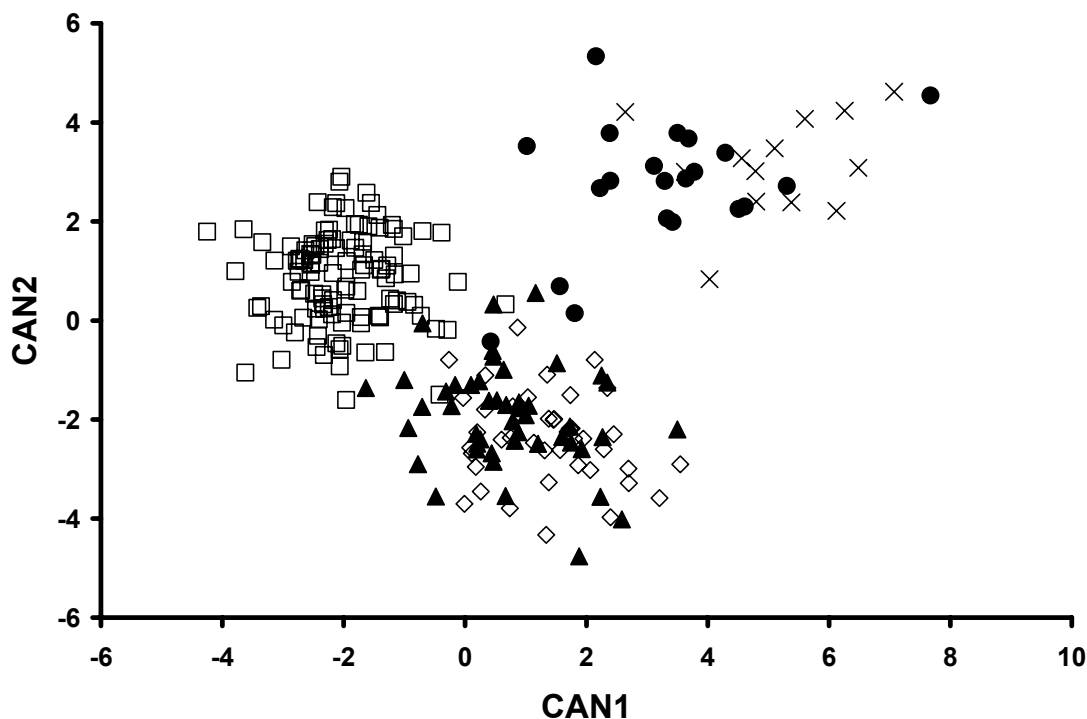


Fig. 4.2 Plot of the canonical variables (CAN1, CAN2) generated from analysis of relative areas and angles of the trapezium articular surfaces (*Homo* = open squares, *Pan* = closed triangles, *Gorilla* = open diamonds, *Pongo* = closed circles, *Papio* = Xs).

The correlations with CAN3 indicate that this axis is a comparison between the first metacarpal-trapezoid angle and the relative area of the second metacarpal surface (Table 4.12). Along CAN3, *Pongo* clusters more negatively, *Papio* clusters more positively, while the hominines cluster in the middle (Fig. 4.3). The correlations with CAN4 indicate that this axis is a comparison between the first metacarpal-trapezoid angle and the relative area of the trapezoid surface (Table 4.12).

Together, the four canonical variables result in distinct clusters for each genus (Figs. 4.2-4.4). The first two axes clearly distinguish *Papio* and *Pongo* from the hominines (Fig. 4.2) because both *Papio* and *Pongo* have the smallest scaphoid-trapezoid angle

(Table 4.6) and the largest first metacarpal-scaphoid angle (Table 4.2); together, these angles drive *Papio* and *Pongo* positively along both axes (Table 4.12). Along CAN3, *Papio* and *Pongo* cluster apart from one another (Fig. 4.3). The separation along this axis results primarily from *Pongo* having significantly larger relative second metacarpal area than does *Papio* (Table 4.8).

The first two axes also clearly distinguish *Homo* from the African apes (Fig. 4.2) because of the significant differences between these genera in angles involving the second metacarpal joint surface (Tables 4.1, 4.4, and 4.5) as well as the relative first metacarpal area (Table 4.7). *Pan* and *Gorilla* cluster together on the first three axes (Figs. 4.2 and 4.3) but they separate from one another along CAN4 (Fig. 4.4). *Pan* is driven negatively along CAN4 because of a narrow first metacarpal-trapezoid angle (Table 4.3) and a large relative trapezoid area (Table 4.10) in comparison with *Gorilla*, which loads positively along this axis.

TABLE 4.12 Correlations between each variable and canonical axis (bolded values indicate the variables that best explain the observed variation along each axis)

Variable		Pooled-within canonical structure			
Angle between		CAN1	CAN2	CAN3	CAN4
1st metacarpal	2nd metacarpal	-0.35	0.46	0.14	0.33
1st metacarpal	scaphoid	0.64	0.22	-0.01	-0.15
1st metacarpal	trapezoid	0.14	0.43	0.52	0.38
2nd metacarpal	scaphoid	-0.02	-0.65	0.10	0.04
2nd metacarpal	trapezoid	0.40	-0.29	0.34	0.05
scaphoid	trapezoid	-0.65	-0.58	-0.31	0.09
<u>Relative surface area</u>					
	1st metacarpal	-0.36	0.35	0.16	-0.18
	2nd metacarpal	0.10	0.16	-0.69	0.13
	scaphoid-centrale	-0.22	0.34	0.11	-0.11
	trapezoid	-0.22	0.19	0.19	-0.67

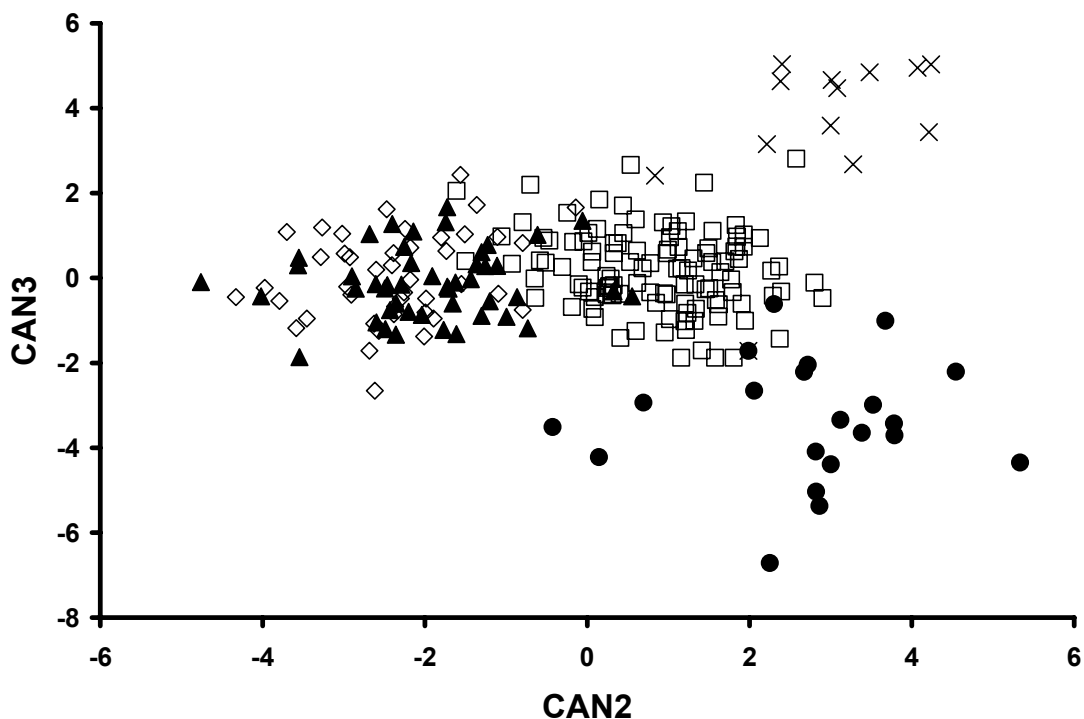


Fig. 4.3 Plot of the canonical variables (CAN2, CAN3) generated from analysis of relative areas and angles of the trapezium articular surfaces (*Homo* = open squares, *Pan* = closed triangles, *Gorilla* = open diamonds, *Pongo* = closed circles, *Papio* = Xs).

The cross-validation procedure of the discriminant function analysis resulted in the correct classification of 110 *Homo* (98.2%), 43 *Pan* (91.5%), 40 *Gorilla* (93%), 20 *Pongo* (95.2%), and 13 *Papio* (100%; Table 4.13). The majority of misclassifications occur among the hominines (9/10). Overall, the results indicate that the relative areas and angles of the carpal and carpometacarpal joints and the relative non-articular area of the trapezium are an effective combination for discriminating all of these genera from each other.

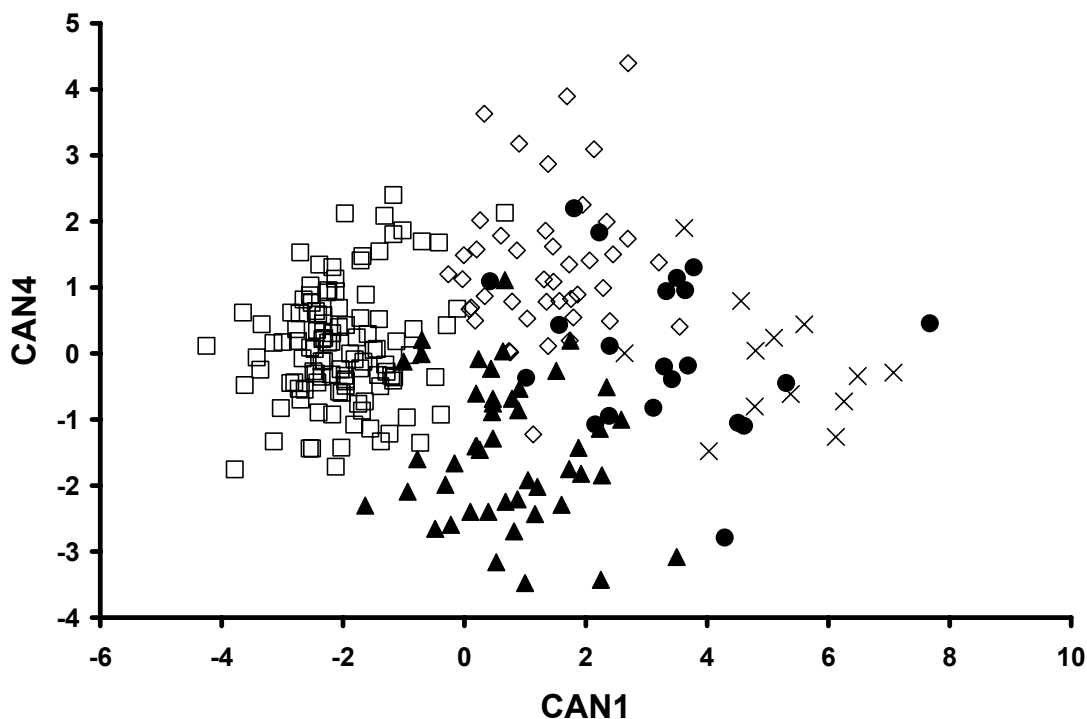


Fig. 4.4 Plot of the canonical variables (CAN1, CAN4) generated from analysis of relative areas and angles of the trapezium articular surfaces (*Homo* = open squares, *Pan* = closed triangles, *Gorilla* = open diamonds, *Pongo* = closed circles, *Papio* = Xs).

TABLE 4.13 Cross-validated posterior probabilities of genus membership using the trapezium carpal and carpometacarpal joint and non-articular relative surface area and angle measures

	<i>Homo</i>	<i>Pan</i>	<i>Gorilla</i>	<i>Pongo</i>	<i>Papio</i>
<i>Homo</i>	110	0	2	0	0
%	98.2	0.0	1.8	0.0	0.0
<i>Pan</i>	2	43	2	0	0
%	4.3	91.5	4.3	0.0	0.0
<i>Gorilla</i>	1	2	40	0	0
%	2.3	4.7	93.0	0.0	0.0
<i>Pongo</i>	0	0	1	20	0
%	0.0	0.0	4.8	95.2	0.0
<i>Papio</i>	0	0	0	0	13
%	0.0	0.0	0.0	0.0	100.0

Summary of shape characteristics

TABLE 4.14 Summary of mean trapezium carpal and carpometacarpal joint and non-articular features (distinctive features in bold)

Variable		Genus				
Angle between		<i>Homo</i>	<i>Pan</i>	<i>Gorilla</i>	<i>Pongo</i>	<i>Papio</i>
1st metacarpal	2nd metacarpal	93	68	73	80	85
1st metacarpal	scaphoid	10	19	18	36	44
1st metacarpal	trapezoid	49	38	45	47	78
2nd metacarpal	scaphoid	81	97	101	66	70
2nd metacarpal	trapezoid	131	146	151	134	161
scaphoid	trapezoid	127	126	126	101	73
<u>Relative surface area</u>						
	1st metacarpal	16.5	13.7	12.3	13.5	14.6
	2nd metacarpal	2.7	2.5	2.7	5.4	1.3
	scaphoid-centrale	8.1	6.3	5.6	6.9	7.6
	trapezoid	9.2	9.0	6.8	7.6	9.3
	non-articular	63.6	68.5	72.7	66.5	67.7

Papio. The probability of correctly classifying *Papio* based on features of the trapezium carpal and carpometacarpal joints and non-articular area was 100% (Table 4.13). The trapezium features that best characterize *Papio* are the first metacarpal-scaphoid angle, the first metacarpal-trapezoid angle, the second metacarpal-trapezoid angle, the first scaphoid-trapezoid angle, and the relative second metacarpal joint area (Table 4.14).

The relative angles between articular surfaces indicate that the relationships between the first metacarpal, scaphoid, and trapezoid joint surfaces are particularly characteristic of *Papio*. All three of these angles are significantly different from all of the hominids, except for the first metacarpal-scaphoid angle, which is significantly different from the hominines only (Table 4.14). The angle between the first metacarpal and trapezoid joint surfaces is almost twice as wide in *Papio* resulting in a trapezium that is relatively longer proximo-distally; a narrower angle results in the more flattened shape, which is

more characteristic of hominids (Fig. 4.1). This shape difference is further delineated by the angle between the scaphoid and trapezoid joint surfaces. This angle is narrower in *Papio* creating a more triangular overall shape to the trapezium. Alternatively, in hominines the angle is much wider generating a more rectangular form. Note that *Pongo* tends to fall in between these two extremes reflecting a somewhat more flattened, yet still triangular trapezium shape; this result is discussed in more detail in the following section on *Pongo*. This difference in overall form causes the first metacarpal and scaphoid joint surfaces to be more parallel with one another in the hominines (i.e., angle values approaching 0°) whereas in *Papio*, and also in *Pongo*, they are offset approximately 45° from one another. Again, it is this overall shape difference that drives the separation of these genera along the first two axes of the canonical analysis (Fig. 4.2).

Papio is also different than the hominids in the second metacarpal-trapezoid angle. The mean angle in *Papio* (161°) indicates that these two surfaces are almost in the same plane as one another. The African apes appear most similar to *Papio* in this regard, but their angle is still significantly more offset than in *Papio*.

Finally, the relative area of the second metacarpal joint surface is significantly smaller in *Papio* than in all of the hominids. This difference is true regardless of whether *Papio* specimens that completely lack diarthroidial contact between the trapezium and second metacarpal are included in the analysis. In other words, when the joint is present in *Papio*, the mutual surfaces are still significantly smaller than in

hominids. Alternatively, when the joint is absent in *Papio*, the connection between the trapezium and the second metacarpal is typically ligamentous instead.

***Pongo*.** The probability of correctly classifying *Pongo* based on features of the trapezium carpal and carpometacarpal joints and non-articular area was 95% (Table 4.13). Only one *Pongo* specimen (5%) was misclassified as *Gorilla*, but no hominine specimens were misclassified as *Pongo*. The trapezium features that best characterize *Pongo* are the relative second metacarpal area and all of the angles involving the scaphoid and trapezoid joint surfaces (Table 4.14).

As mentioned briefly above, the three relative angles in *Pongo* between the first metacarpal, scaphoid, and trapezoid joint surfaces result in an overall trapezium shape that is intermediate between the more triangular and rectangular forms observed in *Papio* and hominines respectively (Fig. 4.1). Basically, the angle between the first metacarpal and trapezoid joint surfaces contributes to a more hominine-like shape whereas the angle between the first metacarpal and scaphoid joint surfaces contributes to more *Papio*-like shape. The angle between the scaphoid and trapezoid surfaces, however, is significantly wider than in *Papio* but also significantly narrower than in the hominines and thus, contributes to the characteristic intermediate shape of the *Pongo* trapezium.

The large relative area of the second metacarpal joint surface clearly distinguishes *Pongo* from the hominines and *Papio*. In *Pongo*, this relative joint area is twice as large as in any of the other genera. Moreover, this joint surface typically extends palmarly across the entire medial side of the trapezium. In other words, the trapezium-second

metacarpal joint in *Pongo* lies almost parallel to the flexion-extension axis of the first carpometacarpal joint whereas in hominines it is approximately more parallel to the abduction-adduction axis (note that each joint axis is perpendicular to the direction of movement).

This modification in the relative position of the second metacarpal articular surface is not necessarily reflected by any one angle involving this surface, but rather when all of the angles are examined as a shape complex. In other words, each second metacarpal angle is always indistinguishable from at least one of the other taxa, but at least one of the angles is always significantly different from each other genus. For instance, in *Pongo* the angle between the second metacarpal and trapezoid joint surfaces is significantly different than in all genera except *Homo*, but both other angles involving the second metacarpal joint surface are significantly different than in *Homo*. In comparison to *Papio*, the *Pongo* second metacarpal joint surface angles with the first metacarpal and scaphoid joint surfaces are not significantly different; however, the angle with the trapezoid joint surface is significantly different.

Both *Pongo* and *Papio* typically have an articulation between the centrale and the trapezium. The reason that the relative area of the scaphoid joint surface in these two taxa was calculated by adding the centrale and scaphoid articular areas together is because the scaphoid and centrale bones are congenitally coalesced in the hominines. As such, it is unclear exactly how much the hominine scaphoid surface articulates with the coalesced centrale portion of the scaphoid. It must be remembered, however, that in both *Pongo* and *Papio* the centrale articular surface is most often markedly offset from

the scaphoid surface as evidenced by the angles between these two surfaces (data not shown). Therefore, while these two articular surfaces are structurally homologous with the single articulation in the hominines, they likely differ with respect to function at this inter-carpal joint.

One final morphological attribute of the *Pongo* trapezium worth discussing includes a relatively small trapezoid joint surface area (Table 4.10). While the difference between *Pongo* and *Gorilla* in relative trapezoid joint surface area is significant ($p = .002$; more relative area observed in *Pongo*), the relative area in both of these taxa is also significantly smaller than in *Papio*, *Pan*, and *Homo* (Table 4.10).

Gorilla. The probability of correctly classifying *Gorilla* based on features of the trapezium carpal and carpometacarpal joints and non-articular area was 93% (Table 4.13); two *Gorilla* specimens (5%) were misclassified as *Pan* and one as *Homo* (2%). The trapezium features that best characterize *Gorilla* are the relative areas of the first metacarpal, scaphoid, trapezoid, and non-articular surfaces, as well as the second metacarpal-scaphoid angle (Table 4.14).

The major distinctiveness of the *Gorilla* trapezium results from its significantly larger relative nonarticular area (Table 4.11). Consequently, the relative areas of the first metacarpal, scaphoid, and trapezoid joint surfaces are also significantly smaller in *Gorilla* than in the other taxa (Tables 4.7, 4.9, and 4.10).

Pan. The probability of correctly classifying *Pan* based on features of the trapezium carpal and carpometacarpal joints and non-articular area was 92% (Table 4.13); two specimens of *Pan* (4%) were each misclassified as either *Gorilla* or *Homo*. The

trapezium features that best characterize *Pan* are the first metacarpal-trapezoid angle, and the first metacarpal-second metacarpal angle (Table 4.14).

As was noted earlier, the hominine trapezium is characterized by a narrow angle between the first metacarpal and trapezoid joint surfaces and wide angles between these two surfaces and the scaphoid surface. The *Pan* trapezium is modified even further along these lines, displaying the narrowest first metacarpal-trapezoid angle observed among the hominines (Table 4.3). Because of this narrower angle, the *Pan* trapezium visually appears relatively longer medio-laterally and relatively thinner proximo-distally on the more medial aspect of the bone. Of all six relative angles of the trapezium, this is the only significant difference between *Pan* and *Gorilla*, who otherwise appear identical in terms of relative angles.

***Homo*.** The probability of correctly classifying *Homo* based on features of the trapezium carpal and carpometacarpal joints and non-articular area was 98% (Table 4.13); two *Homo* specimens (2%) were misclassified as *Gorilla*. The trapezium features that best characterize *Homo* are the first metacarpal-second metacarpal angle, the first metacarpal-scaphoid angle, and the second metacarpal-trapezoid angle, as well as the relative areas of the first metacarpal, scaphoid, and non-articular surfaces (Table 4.14).

The distinct angles involving the second metacarpal surface in *Homo* reflect the more proximo-distal orientation of the trapezium-second metacarpal joint as opposed to the more radio-ulnar orientation observed in the other genera (Tables 4.1, 4.4, and 4.5). This difference in orientation of this joint in *Homo* is indicated by the larger first metacarpal-second metacarpal angle and the smaller second metacarpal-scaphoid and

second metacarpal-trapezoid angles (this last angle is not significantly different than *Pongo* for reasons discussed above).

The angle between the first metacarpal and scaphoid joint surfaces in *Homo* more closely approaches 0° indicating these two surfaces are more parallel to one another (Table 4.2). Finally, the relative areas of the first metacarpal and scaphoid joint surfaces in *Homo* are significantly larger than in the other genera (Tables 4.7 and 4.9) whereas the relative non-articular area is significantly smaller (Table 4.11).

DISCUSSION

In Chapter 2, modern humans were predicted to show the following derived pattern of morphological features: 1) articular surfaces that are oriented roughly orthogonal to the radio-ulnar axis should have proportionately larger surface areas to minimize compressive stress; 2) the radial and ulnar joint surfaces of each carpal bone should be oriented roughly orthogonal to the radio-ulnar axis to minimize shear stress; and 3) the carpal and carpometacarpal joints should limit mobility proximo-distally, particularly when compressed radio-ulnarly (i.e., close-packed during forceful manipulative behaviors).

The results of this chapter demonstrate several derived features of the trapezium in *Homo* that satisfy these three predictions. The relative areas of the first metacarpal and scaphoid surfaces are significantly larger in *Homo* than in the non-human genera (Tables 4.7 and 4.9). Moreover, these two joint surfaces are significantly more parallel to one another in *Homo* (Table 4.2). Together, these features satisfy the first two predictions and contribute to a morphological configuration that is more efficiently

designed to reduce compressive and shear stresses that result from compression of the first metacarpal into the trapezium.

Although the significantly smaller relative non-articular area in *Homo* is due, in part, to the enlargements of the first metacarpal and scaphoid joint surfaces, the non-articular area directly between the first metacarpal and trapezoid joint surfaces is also reduced in comparison to the other genera (Fig. 4.5). This reduction in palmar non-articular area is a concomitant of the derived trapezoid shape in *Homo* (see Chapter 5). The trapezoid in *Homo* is expanded palmarly and the trapezium accommodates this expansion by reducing its palmar non-articular area (Fig. 4.5). However, the trapezoid expands palmarly more than the trapezium contracts. This interdependent relationship between the trapezium and trapezoid contributes to the trapezium in *Homo* obtaining a more supinated position relative to the carpal arch (see also Chapter 3).

The supinated position of the trapezium aligns the entire distal carpal row creating a narrower carpal arch. In non-human primates, the trapezium is positioned more in front of the trapezoid generating a deeper carpal arch (Napier, 1961). This more pronated position of the non-human primate trapezium is less effective for distributing radio-ulnarly directed forces because the trapezium, trapezoid, and capitate form an L-shape rather than the straight-line configuration observed in *Homo*.

The third predictions for both human and non-human primates are satisfied by the observed differences in second metacarpal joint surface orientation. When the thenar musculature is strongly contracted, the first carpometacarpal joint experiences compressive stress, and the trapezium tends to move in the direction of the applied

force. If the force is applied when the first metacarpal is in an abducted posture, then the trapezium tends to rotate around an axis that is perpendicular to the palm. This tendency to rotate sends the more ulnar portion of the trapezium in the direction opposite to the applied force (Fig. 4.6).

In the great apes and *Papio*, the radio-ulnar orientation of the trapezium-second metacarpal joint is not conducive to resisting the tendency for the ulnar portion of the trapezium to displace disto-radially. Therefore, force applied to the radial portion of the first metacarpal surface on the trapezium would cause the ulnar aspect of the trapezium to experience a disto-radially directed force equal in magnitude to the applied force (Fig. 4.6). Much of the latter force is likely accommodated in part by surrounding ligaments; however, repeated use of grips involving strong pinch or power grips may put undue pressure on the ligaments, and eventually lead to ligament failure and joint subluxation. Similar detrimental results are expected from repeated use of an object such as a hammer to strike other objects. In order to keep hold of the hammer, the hand must generate a force equal to the strike's reaction force, which typically is much greater than any internal force generated by thenar musculature contraction. Again, the continuous strain on the ligaments would likely lead to eventual joint subluxation.

It is clear that the trapezium-second metacarpal joint in these non-human primate genera is not designed to efficiently counter the effect of strong forces applied to the radial portions of the first metacarpal surface on the trapezium. The more radio-ulnar orientation of the joint in non-human primates, however, is better designed to help stabilize the base of the second metacarpal from sliding or slipping radially when it

experiences proximo-distally directed joint reaction forces during locomotor behaviors (Marzke, 1983, 1997; Tocheri et al., 2003).

In *Homo*, however, the ulnar aspect of the trapezium is stabilized from displacing disto-radially because of the more proximo-distal orientation of the trapezium-second metacarpal joint (Fig. 4.6). The stability of the ulnar aspect of the trapezium is likely further facilitated during recruitment of the flexor carpi radialis (FCR) and the first dorsal interosseous muscles (DI-1). FCR, which primarily inserts into the palmar base of the second metacarpal (Bowden and Bowden, 2005; Lewis, 1989; Olson, 1996), and DI-1, which originates on the dorsal shafts of the first and second metacarpals and inserts into the base of the proximal second phalanx (Jacofsky, 2002), both help pull the second metacarpal base proximally when force is applied to the first carpometacarpal joint during neutral or abducted thumb postures.

Because of this resistance to distal displacement of the ulnar portion of the trapezium, the applied force to the radial portion of the first metacarpal articular surface is translated into a bending moment—the distal portion of the trapezium experiences tension while the proximal portion experiences compression. Recently, a cantilever model was used to infer which ligaments help resist the bending stresses experienced by the trapezium during strong pinches and grasps (Bettinger et al., 1999, 2000; Bettinger and Berger, 2001). When force is applied to the first carpometacarpal joint during muscle contraction (e.g., Cooney and Chao, 1977; Eaton and Littler, 1969; Linscheid, 1982), the ligaments that connect the trapezium to the trapezoid, capitate, and second

and third metacarpals appear to accommodate the resulting bending stresses (Bettinger et al., 1999, 2000; Bettinger and Berger, 2001).

Stabilizing the ulnar aspect of the trapezium from moving distally with a more proximo-distally oriented trapezium-second metacarpal joint simultaneously enables pronation of the base of the second metacarpal when this morphology is accompanied by a more proximo-distal orientation of the capitate-second metacarpal joint (Marzke, 1983, 1997; Tocheri et al., 2003). This illustrates the reciprocal relationship between joint stability in one direction and joint mobility in the other. In *Homo*, stabilizing the ulnar aspect of the trapezium from moving distally has the reciprocal effect of making the base of the second metacarpal less stable (more mobile) radio-ulnarly. In non-human primates, stabilizing the base of the second metacarpal from moving radio-ulnarly has the reciprocal effect of making the ulnar aspect of the trapezium less stable (more mobile) proximo-distally.

Clearly, the morphological pattern of the trapezium observed in *Homo* is in stark contrast to that observed in the other genera. In summary, note in *Homo* the relatively larger and radially expanded first metacarpal surface, the distally-oriented second metacarpal surface, the more parallel orientation of the first metacarpal and scaphoid joints, and the larger relative area of the scaphoid joint. Together, these features function as a complex to more efficiently withstand and distribute radio-ulnarly directed forces across the wrist. Such forces result during strong contraction of the thenar musculature, which compresses the base of the first metacarpal into the trapezium. As

force is applied to the first carpometacarpal joint, all of these features work to reduce the compressive and shear stresses as well as to stabilize the trapezium from dislocating.

Alternatively, the non-human primate trapezium simply does not appear designed to function efficiently in this manner. There is an increased likelihood of subluxation of the ulnar aspect of the trapezium when force is applied to the radial aspect of the first carpometacarpal joint (e.g., during grips involving an abducted thumb). Moreover, the placement of the trapezium in front of the trapezoid, rather than in line with the trapezoid and capitate, is not conducive to distributing the resulting compressive and shear stresses (Fig. 4.5). Instead, the trapezium functions to stabilize the base of the second metacarpal from sliding radio-ulnarly when the wrist is compressed proximodistally during locomotor behaviors.

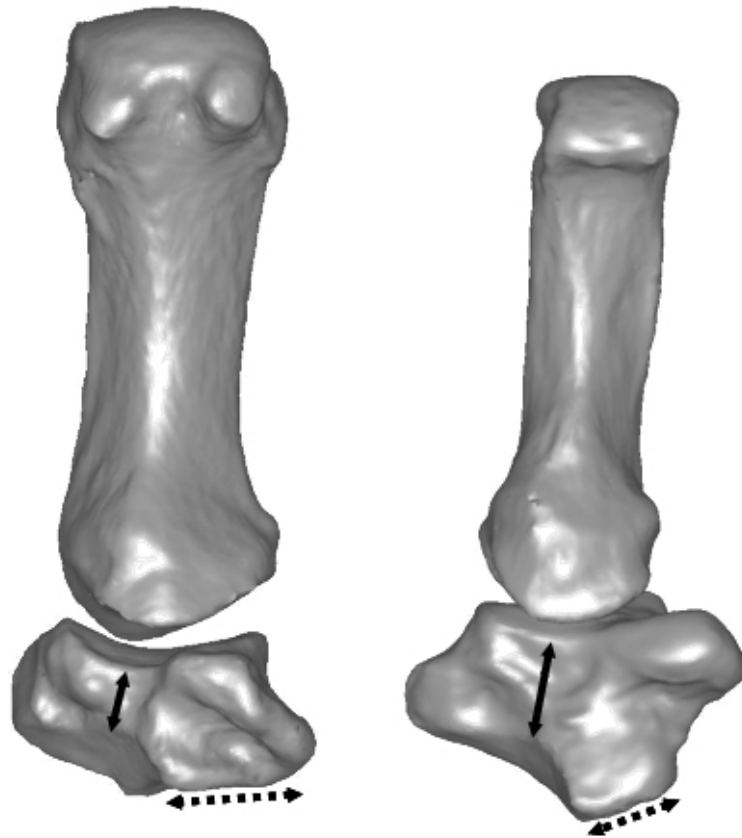


Fig. 4.5 Differences in trapezium carpal joint morphology observed in *Homo* (at left) in comparison to other primates (*Pan* is shown at right) that reflect differences in ability to reduce compressive and shear stresses during strong contraction of the thenar musculature. Note the relative areas and orientations of the scaphoid joint surface (dotted arrows) and the palmar non-articular area (solid arrows). Both *Homo* and *Pan* are scaled relative to actual size. Bones are from the right side.

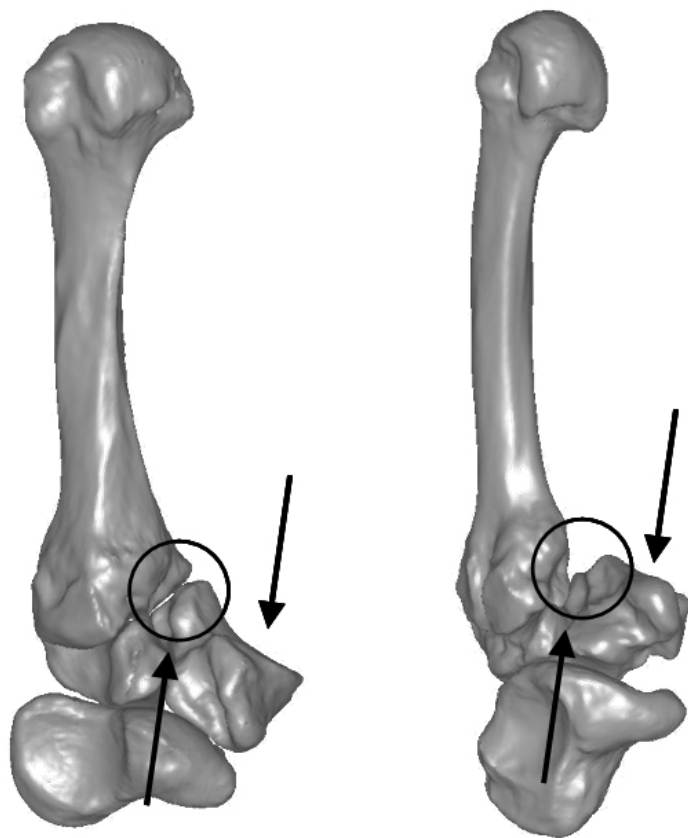


Fig. 4.6 When force is applied to the 1st carpometacarpal joint when the thumb is in an abducted posture (downward arrows), the ulnar portion of the trapezium tends to move disto-radially (upward arrows). The circles highlight the different orientation of the trapezium-2nd metacarpal joint in *Homo* (at left), which stabilizes the ulnar aspect of the trapezium against disto-radial subluxation, in contrast to non-human primates (*Pan* is shown at right). Bones are from the right side.

Chapter 5: The Trapezoid

RESULTS OF SHAPE ANALYSES

In this chapter, I present the results of the shape analyses performed on the carpal and carpometacarpal joints and non-articular area of the trapezoid. Since all of the features examined in this chapter belong to the trapezoid, the name of the articulating bone is used to describe each joint surface. For example, the area on the trapezoid for articulation with the scaphoid is referred to as the scaphoid joint surface (Fig. 5.1). The second carpometacarpal joint is divided into lateral and medial surfaces because in primates this joint is typically Λ -shaped. The trapezoid variables measured include all the relative areas and angles of the carpal and carpometacarpal joints as well as the relative non-articular area. The results of the comparative shape analyses for each variable are presented separately, followed by multivariate analyses using two combinations of the variables (Full Model's I and II). Following the presentation of the statistical results, a summary of the trapezoid shape characteristics of each genus is given. Finally, the results are discussed in relation to previous studies as well as to the biomechanical predictions introduced in Chapter 2.

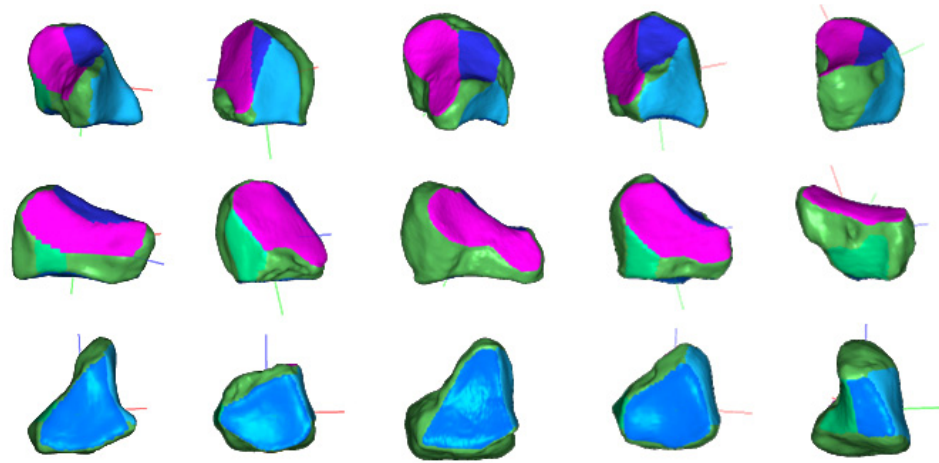


Fig. 5.1 Visual comparison of trapezoid shape in five primate genera (*Papio*, far left; *Pongo*, 2nd from left; *Gorilla*, middle; *Pan*, 2nd from right; *Homo*, far right). Key: top row, palmar view; middle row, medial view; bottom row, proximal view; pink, medial 2nd metacarpal joint; dark blue, lateral 2nd metacarpal joint; light blue, trapezium joint; medium blue, scaphoid joint; light green, capitate joint; dark green, non-articular area. Bones are from the right side.

Angles of the trapezoid

The lateral and medial second metacarpal articulations. The angle between these two surfaces is significantly different in five of the ten pairwise comparisons between genus means (Table 5.1). This angle is significantly wider in *Pongo* (134°) than in the other genera except *Gorilla* (127°), whereas *Pan* (119°) has a significantly narrower angle than in all the other genera except *Papio* (124°). *Homo* (125°), *Gorilla*, and *Papio* show no significant differences for this angle.

TABLE 5.1 Pairwise comparisons of genus means for the angle between the lateral and medial 2nd metacarpal joint surfaces¹

Genus A	Genus B	Mean _A	Mean _B	N _A	N _B	θ	p
<i>Homo</i>	<i>Pan</i>	125	119	111	47	6	<.001
<i>Homo</i>	<i>Gorilla</i>	125	127	111	44	2	0.245
<i>Homo</i>	<i>Pongo</i>	125	134	111	20	9	0.003
<i>Homo</i>	<i>Papio</i>	125	124	111	19	1	0.478
<i>Pan</i>	<i>Gorilla</i>	119	127	47	44	8	<.001
<i>Pan</i>	<i>Pongo</i>	119	134	47	20	15	<.001
<i>Pan</i>	<i>Papio</i>	119	124	47	19	5	0.034
<i>Gorilla</i>	<i>Pongo</i>	127	134	44	20	7	0.031
<i>Gorilla</i>	<i>Papio</i>	127	124	44	19	3	0.152
<i>Pongo</i>	<i>Papio</i>	134	124	20	19	10	0.005

¹ Mean_A, mean of Genus A; N_A, sample size of Genus A; Mean_B, mean of Genus B; N_B, sample size of Genus B; | θ |, absolute value of difference between observed sample means; p, probability that a difference between the bootstrapped means equaled or exceeded | θ |. Numbers in bold indicate statistical significance at alpha = .01.

The lateral second metacarpal and scaphoid articulations. The angle between these two surfaces is significantly different in seven of the ten pairwise comparisons between genus means (Table 5.2). This angle is significantly wider in *Pongo* (43°) than in all the other genera except *Gorilla* (38°), whereas both *Homo* (24°) and *Papio* (28°) show significantly narrower angles than do the African apes. Between *Pan* (37°) and *Gorilla*, this angle is not significantly different.

TABLE 5.2 Pairwise comparisons of genus means for the angle between the lateral 2nd metacarpal and scaphoid joint surfaces¹

Genus A	Genus B	Mean _A	Mean _B	N _A	N _B	θ	p
<i>Homo</i>	<i>Pan</i>	24	37	111	47	12	<.001
<i>Homo</i>	<i>Gorilla</i>	24	38	111	44	13	<.001
<i>Homo</i>	<i>Pongo</i>	24	43	111	20	19	<.001
<i>Homo</i>	<i>Papio</i>	24	28	111	19	3	0.043
<i>Pan</i>	<i>Gorilla</i>	37	38	47	44	1	0.523
<i>Pan</i>	<i>Pongo</i>	37	43	47	20	6	0.009
<i>Pan</i>	<i>Papio</i>	37	28	47	19	9	<.001
<i>Gorilla</i>	<i>Pongo</i>	38	43	44	20	5	0.028
<i>Gorilla</i>	<i>Papio</i>	38	28	44	19	10	<.001
<i>Pongo</i>	<i>Papio</i>	43	28	20	19	15	<.001

¹ Mean_A, mean of Genus A; N_A, sample size of Genus A; Mean_B, mean of Genus B; N_B, sample size of Genus B; | θ |, absolute value of difference between observed sample means; p, probability that a difference between the bootstrapped means equaled or exceeded | θ |. Numbers in bold indicate statistical significance at alpha = .01.

The lateral second metacarpal and trapezium articulations. The angle between these two surfaces is significantly different in eight of the ten pairwise comparisons between genus means (Table 5.3). This angle is significantly narrower in *Papio* (106°) than in the other genera. Both *Homo* (117°) and *Gorilla* (120°) also show significantly narrower angles than do *Pan* (128°) and *Pongo* (126°).

TABLE 5.3 Pairwise comparisons of genus means for the angle between the lateral 2nd metacarpal and trapezium joint surfaces¹

Genus A	Genus B	Mean _A	Mean _B	N _A	N _B	θ	p
<i>Homo</i>	<i>Pan</i>	117	128	111	47	12	<.001
<i>Homo</i>	<i>Gorilla</i>	117	120	111	44	3	0.053
<i>Homo</i>	<i>Pongo</i>	117	126	111	20	9	<.001
<i>Homo</i>	<i>Papio</i>	117	106	111	19	11	<.001
<i>Pan</i>	<i>Gorilla</i>	128	120	47	44	8	<.001
<i>Pan</i>	<i>Pongo</i>	128	126	47	20	3	0.246
<i>Pan</i>	<i>Papio</i>	128	106	47	19	22	<.001
<i>Gorilla</i>	<i>Pongo</i>	120	126	44	20	6	0.012
<i>Gorilla</i>	<i>Papio</i>	120	106	44	19	14	<.001
<i>Pongo</i>	<i>Papio</i>	126	106	20	19	20	<.001

¹ Mean_A, mean of Genus A; N_A, sample size of Genus A; Mean_B, mean of Genus B; N_B, sample size of Genus B; | θ |, absolute value of difference between observed sample means; p, probability that a difference between the bootstrapped means equaled or exceeded | θ |. Numbers in bold indicate statistical significance at alpha = .01.

The medial second metacarpal and scaphoid articulations. The angle between these two surfaces is significantly different in eight of the ten pairwise comparisons between genus means (Table 5.4). This angle is significantly narrower in *Homo* (38°) than in the other genera. Both *Pan* (69°) and *Papio* (72°) show significantly wider angles than do *Gorilla* (61°) and *Pongo* (63°).

TABLE 5.4 Pairwise comparisons of genus means for the angle between the medial 2nd metacarpal and scaphoid joint surfaces¹

Genus A	Genus B	Mean _A	Mean _B	N _A	N _B	θ	p
<i>Homo</i>	<i>Pan</i>	38	69	111	47	32	<.001
<i>Homo</i>	<i>Gorilla</i>	38	61	111	45	23	<.001
<i>Homo</i>	<i>Pongo</i>	38	63	111	20	25	<.001
<i>Homo</i>	<i>Papio</i>	38	72	111	19	35	<.001
<i>Pan</i>	<i>Gorilla</i>	69	61	47	45	8	<.001
<i>Pan</i>	<i>Pongo</i>	69	63	47	20	6	<.001
<i>Pan</i>	<i>Papio</i>	69	72	47	19	3	0.094
<i>Gorilla</i>	<i>Pongo</i>	61	63	45	20	2	0.275
<i>Gorilla</i>	<i>Papio</i>	61	72	45	19	11	<.001
<i>Pongo</i>	<i>Papio</i>	63	72	20	19	9	<.001

¹ Mean_A, mean of Genus A; N_A, sample size of Genus A; Mean_B, mean of Genus B; N_B, sample size of Genus B; | θ |, absolute value of difference between observed sample means; p, probability that a difference between the bootstrapped means equaled or exceeded | θ |. Numbers in bold indicate statistical significance at alpha = .01.

The medial second metacarpal and trapezium articulations. The angle between these two surfaces is significantly different in nine of the ten pairwise comparisons between genus means (Table 5.5). Only between *Pan* (74°) and *Gorilla* (74°) is this angle not significantly different. This angle is significantly narrower in *Papio* (60°) than in the other genera, whereas *Pongo* (86°) shows a significantly wider angle than do the rest. Finally, *Homo* (67°) has a significantly narrower angle than does either *Pan* or *Gorilla*.

TABLE 5.5 Pairwise comparisons of genus means for the angle between the medial 2nd metacarpal and trapezium joint surfaces¹

Genus A	Genus B	Mean _A	Mean _B	N _A	N _B	θ	p
<i>Homo</i>	<i>Pan</i>	67	74	111	47	6	<.001
<i>Homo</i>	<i>Gorilla</i>	67	74	111	45	6	<.001
<i>Homo</i>	<i>Pongo</i>	67	86	111	20	19	<.001
<i>Homo</i>	<i>Papio</i>	67	60	111	19	7	<.001
<i>Pan</i>	<i>Gorilla</i>	74	74	47	45	0	0.917
<i>Pan</i>	<i>Pongo</i>	74	86	47	20	12	<.001
<i>Pan</i>	<i>Papio</i>	74	60	47	19	14	<.001
<i>Gorilla</i>	<i>Pongo</i>	74	86	45	20	13	<.001
<i>Gorilla</i>	<i>Papio</i>	74	60	45	19	14	<.001
<i>Pongo</i>	<i>Papio</i>	86	60	20	19	26	<.001

¹ Mean_A, mean of Genus A; N_A, sample size of Genus A; Mean_B, mean of Genus B; N_B, sample size of Genus B; | θ |, absolute value of difference between observed sample means; p, probability that a difference between the bootstrapped means equaled or exceeded | θ |. Numbers in bold indicate statistical significance at alpha = .01.

The scaphoid and trapezium articulations. The angle between these two surfaces is significantly different in seven of the ten pairwise comparisons between genus means (Table 5.6). This angle is significantly narrower in *Pan* (72°) than in the other genera, whereas *Homo* (86°) has a significantly wider angle than either *Pongo* (78°) or *Papio* (78°). Finally, *Gorilla* (83°) is also significantly wider than *Pongo* in terms of this angle.

TABLE 5.6 Pairwise comparisons of genus means for the angle between the scaphoid and trapezium joint surfaces¹

Genus A	Genus B	Mean _A	Mean _B	N _A	N _B	θ	p
<i>Homo</i>	<i>Pan</i>	86	72	111	47	14	<.001
<i>Homo</i>	<i>Gorilla</i>	86	83	111	45	4	0.022
<i>Homo</i>	<i>Pongo</i>	86	78	111	20	8	<.001
<i>Homo</i>	<i>Papio</i>	86	78	111	19	8	<.001
<i>Pan</i>	<i>Gorilla</i>	72	83	47	45	10	<.001
<i>Pan</i>	<i>Pongo</i>	72	78	47	20	6	0.001
<i>Pan</i>	<i>Papio</i>	72	78	47	19	6	<.001
<i>Gorilla</i>	<i>Pongo</i>	83	78	45	20	5	0.01
<i>Gorilla</i>	<i>Papio</i>	83	78	45	19	4	0.014
<i>Pongo</i>	<i>Papio</i>	78	78	20	19	0	0.89

¹ Mean_A, mean of Genus A; N_A, sample size of Genus A; Mean_B, mean of Genus B; N_B, sample size of Genus B; | θ |, absolute value of difference between observed sample means; p, probability that a difference between the bootstrapped means equaled or exceeded | θ |. Numbers in bold indicate statistical significance at alpha = .01.

The capitate and lateral second metacarpal articulations. The angle between these two surfaces is significantly different in eight of the ten pairwise comparisons between genus means (Table 5.7). This angle is significantly narrower in *Homo* (54°) than in the other genera, and *Pan* (59°) also has a significantly narrower angle than does either *Pongo* (80°), *Papio* (91°), or *Gorilla* (94°). The remaining significant difference in this angle occurs between *Pongo* and *Papio*. It is important to note that *Gorilla* typically has no articulation between the trapezoid and capitate; only eight of the *Gorilla* specimens sampled display an articulation, and five of these only display a small articular area that extends from the palmar portion of the medial second metacarpal facet.

TABLE 5.7 Pairwise comparisons of genus means for the angle between the capitate and lateral 2nd metacarpal joint surfaces¹

Genus A	Genus B	Mean _A	Mean _B	N _A	N _B	θ	p
<i>Homo</i>	<i>Pan</i>	54	59	111	47	5	0.002
<i>Homo</i>	<i>Gorilla</i>	54	94	111	7	40	<.001
<i>Homo</i>	<i>Pongo</i>	54	80	111	20	26	<.001
<i>Homo</i>	<i>Papio</i>	54	91	111	19	37	<.001
<i>Pan</i>	<i>Gorilla</i>	59	94	47	7	35	<.001
<i>Pan</i>	<i>Pongo</i>	59	80	47	20	21	<.001
<i>Pan</i>	<i>Papio</i>	59	91	47	19	32	<.001
<i>Gorilla</i>	<i>Pongo</i>	94	80	7	20	15	0.119
<i>Gorilla</i>	<i>Papio</i>	94	91	7	19	3	0.718
<i>Pongo</i>	<i>Papio</i>	80	91	20	19	11	<.001

¹ Mean_A, mean of Genus A; N_A, sample size of Genus A; Mean_B, mean of Genus B; N_B, sample size of Genus B; | θ |, absolute value of difference between observed sample means; p, probability that a difference between the bootstrapped means equaled or exceeded | θ |. Numbers in bold indicate statistical significance at alpha = .01.

The capitate and medial second metacarpal articulations. The angle between these two surfaces is significantly different in eight of the ten pairwise comparisons between genus means (Table 5.8). This angle is significantly narrower in *Homo* (108°) than in all the other genera, and significantly wider in *Papio* (146°) than in all other genera except *Gorilla* (141°). *Pan* (119°) also shows a significantly narrower angle than does either *Pongo* (125°) or *Gorilla*.

TABLE 5.8 Pairwise comparisons of genus means for the angle between the capitate and medial 2nd metacarpal joint surfaces¹

Genus A	Genus B	Mean _A	Mean _B	N _A	N _B	θ	p
<i>Homo</i>	<i>Pan</i>	108	119	111	47	11	<.001
<i>Homo</i>	<i>Gorilla</i>	108	141	111	8	33	<.001
<i>Homo</i>	<i>Pongo</i>	108	125	111	20	17	<.001
<i>Homo</i>	<i>Papio</i>	108	146	111	19	38	<.001
<i>Pan</i>	<i>Gorilla</i>	119	141	47	8	22	0.001
<i>Pan</i>	<i>Pongo</i>	119	125	47	20	6	0.003
<i>Pan</i>	<i>Papio</i>	119	146	47	19	27	<.001
<i>Gorilla</i>	<i>Pongo</i>	141	125	8	20	16	0.04
<i>Gorilla</i>	<i>Papio</i>	141	146	8	19	5	0.571
<i>Pongo</i>	<i>Papio</i>	125	146	20	19	21	<.001

¹ Mean_A, mean of Genus A; N_A, sample size of Genus A; Mean_B, mean of Genus B; N_B, sample size of Genus B; | θ |, absolute value of difference between observed sample means; p, probability that a difference between the bootstrapped means equaled or exceeded | θ |. Numbers in bold indicate statistical significance at alpha = .01.

The capitata and scaphoid articulations. The angle between these two surfaces is significantly different in four of the ten pairwise comparisons between genus means (Table 5.9). This angle is significantly wider in *Pan* (113°) than in all the other genera; no significant differences in this angle occur between *Homo* (105°), *Gorilla* (99°), *Pongo* (100°), and *Papio* (105°).

TABLE 5.9 Pairwise comparisons of genus means for the angle between the capitata and scaphoid joint surfaces¹

Genus A	Genus B	Mean _A	Mean _B	N _A	N _B	θ	p
<i>Homo</i>	<i>Pan</i>	105	113	111	47	9	<.001
<i>Homo</i>	<i>Gorilla</i>	105	99	111	8	6	0.248
<i>Homo</i>	<i>Pongo</i>	105	100	111	20	5	0.027
<i>Homo</i>	<i>Papio</i>	105	105	111	19	0	0.837
<i>Pan</i>	<i>Gorilla</i>	113	99	47	8	14	0.004
<i>Pan</i>	<i>Pongo</i>	113	100	47	20	14	<.001
<i>Pan</i>	<i>Papio</i>	113	105	47	19	8	<.001
<i>Gorilla</i>	<i>Pongo</i>	99	100	8	20	1	0.91
<i>Gorilla</i>	<i>Papio</i>	99	105	8	19	6	0.24
<i>Pongo</i>	<i>Papio</i>	100	105	20	19	5	0.015

¹ Mean_A, mean of Genus A; N_A, sample size of Genus A; Mean_B, mean of Genus B; N_B, sample size of Genus B; | θ |, absolute value of difference between observed sample means; p, probability that a difference between the bootstrapped means equaled or exceeded | θ |. Numbers in bold indicate statistical significance at alpha = .01.

The capitata and trapezium articulations. The angle between these two surfaces is significantly different in eight of the ten pairwise comparisons between genus means (Table 5.10). This angle is significantly narrower in *Homo* (23°) and *Pan* (22°) than in the other genera, whereas both *Gorilla* (57°) and *Papio* (45°) have a significantly wider angle than does *Pongo* (37°).

TABLE 5.10 Pairwise comparisons of genus means for the angle between the capitata and trapezium joint surfaces¹

Genus A	Genus B	Mean _A	Mean _B	N _A	N _B	θ	p
<i>Homo</i>	<i>Pan</i>	23	22	111	47	2	0.104
<i>Homo</i>	<i>Gorilla</i>	23	57	111	8	34	<.001
<i>Homo</i>	<i>Pongo</i>	23	37	111	20	14	<.001
<i>Homo</i>	<i>Papio</i>	23	45	111	19	22	<.001
<i>Pan</i>	<i>Gorilla</i>	22	57	47	8	36	<.001
<i>Pan</i>	<i>Pongo</i>	22	37	47	20	16	<.001
<i>Pan</i>	<i>Papio</i>	22	45	47	19	24	<.001
<i>Gorilla</i>	<i>Pongo</i>	57	37	8	20	20	<.001
<i>Gorilla</i>	<i>Papio</i>	57	45	8	19	12	0.014
<i>Pongo</i>	<i>Papio</i>	37	45	20	19	8	<.001

¹ Mean_A, mean of Genus A; N_A, sample size of Genus A; Mean_B, mean of Genus B; N_B, sample size of Genus B; | θ |, absolute value of difference between observed sample means; p, probability that a difference between the bootstrapped means equaled or exceeded | θ |. Numbers in bold indicate statistical significance at alpha = .01.

Relative areas of the trapezoid

Lateral second metacarpal articulation. The relative area of the lateral second metacarpal joint surface is significantly different in seven of the ten pairwise comparisons between genus means (Table 5.11). This relative area is significantly larger in *Pan* (7.4%) than in all the other genera except *Homo* (6.7%). Both *Homo* and *Papio* (6.5%) also show significantly larger relative areas than does either *Gorilla* (5.7%) or *Pongo* (5.2%).

TABLE 5.11 Pairwise comparisons of genus means for relative area of the lateral 2nd metacarpal joint surface¹

Genus A	Genus B	Mean _A	Mean _B	N _A	N _B	θ	p
<i>Homo</i>	<i>Pan</i>	6.7	7.4	111	47	0.6	0.016
<i>Homo</i>	<i>Gorilla</i>	6.7	5.8	111	44	1.0	<.001
<i>Homo</i>	<i>Pongo</i>	6.7	5.2	111	20	1.5	<.001
<i>Homo</i>	<i>Papio</i>	6.7	6.5	111	19	0.2	0.27
<i>Pan</i>	<i>Gorilla</i>	7.4	5.8	47	44	1.6	<.001
<i>Pan</i>	<i>Pongo</i>	7.4	5.2	47	20	2.2	<.001
<i>Pan</i>	<i>Papio</i>	7.4	6.5	47	19	0.9	0.002
<i>Gorilla</i>	<i>Pongo</i>	5.8	5.2	44	20	0.6	0.172
<i>Gorilla</i>	<i>Papio</i>	5.8	6.5	44	19	0.7	0.011
<i>Pongo</i>	<i>Papio</i>	5.2	6.5	20	19	1.3	0.002

¹ Mean_A, mean of Genus A; N_A, sample size of Genus A; Mean_B, mean of Genus B; N_B, sample size of Genus B; | θ |, absolute value of difference between observed sample means; p, probability that a difference between the bootstrapped means equaled or exceeded | θ |. Numbers in bold indicate statistical significance at alpha = .01.

Medial second metacarpal articulation. The relative area of the medial second metacarpal joint surface is significantly different in seven of the ten pairwise comparisons between genus means (Table 5.12). This relative area is significantly larger in *Gorilla* (16.9%) than in all the other genera except *Pan* (16%), whereas *Homo* (13.5%) and *Papio* (13.9%) show significantly smaller relative areas than do either *Pan* or *Pongo* (15.8%).

TABLE 5.12 Pairwise comparisons of genus means for relative area of the medial 2nd metacarpal joint surface¹

Genus A	Genus B	Mean _A	Mean _B	N _A	N _B	θ	p
<i>Homo</i>	<i>Pan</i>	13.5	16.0	111	47	2.5	<.001
<i>Homo</i>	<i>Gorilla</i>	13.5	16.9	111	45	3.3	<.001
<i>Homo</i>	<i>Pongo</i>	13.5	15.8	111	20	2.3	<.001
<i>Homo</i>	<i>Papio</i>	13.5	13.9	111	19	0.3	0.313
<i>Pan</i>	<i>Gorilla</i>	16.0	16.9	47	45	0.8	0.013
<i>Pan</i>	<i>Pongo</i>	16.0	15.8	47	20	0.2	0.592
<i>Pan</i>	<i>Papio</i>	16.0	13.9	47	19	2.2	<.001
<i>Gorilla</i>	<i>Pongo</i>	16.9	15.8	45	20	1.1	0.004
<i>Gorilla</i>	<i>Papio</i>	16.9	13.9	45	19	3.0	<.001
<i>Pongo</i>	<i>Papio</i>	15.8	13.9	20	19	2.0	<.001

¹ Mean_A, mean of Genus A; N_A, sample size of Genus A; Mean_B, mean of Genus B; N_B, sample size of Genus B; | θ |, absolute value of difference between observed sample means; p, probability that a difference between the bootstrapped means equaled or exceeded | θ |. Numbers in bold indicate statistical significance at alpha = .01.

Scaphoid articulation. The relative area of the scaphoid joint surface is significantly different in seven of the ten pairwise comparisons between genus means (Table 5.13). This relative area is significantly smaller in *Homo* (8.3%) than in all the other genera, whereas *Papio* (16.3%) has a significantly larger relative area than the rest. Non-significant differences in mean relative area occur between *Pan* (14.3%), *Gorilla* (14.1%), and *Pongo* (13.2%).

TABLE 5.13 Pairwise comparisons of genus means for relative area of the scaphoid joint surface¹

Genus A	Genus B	Mean _A	Mean _B	N _A	N _B	θ	p
<i>Homo</i>	<i>Pan</i>	8.3	14.3	111	47	6.0	<.001
<i>Homo</i>	<i>Gorilla</i>	8.3	14.1	111	45	5.8	<.001
<i>Homo</i>	<i>Pongo</i>	8.3	13.2	111	20	4.9	<.001
<i>Homo</i>	<i>Papio</i>	8.3	16.3	111	19	8.1	<.001
<i>Pan</i>	<i>Gorilla</i>	14.3	14.1	47	45	0.2	0.483
<i>Pan</i>	<i>Pongo</i>	14.3	13.2	47	20	1.1	0.03
<i>Pan</i>	<i>Papio</i>	14.3	16.3	47	19	2.0	<.001
<i>Gorilla</i>	<i>Pongo</i>	14.1	13.2	45	20	0.9	0.13
<i>Gorilla</i>	<i>Papio</i>	14.1	16.3	45	19	2.3	<.001
<i>Pongo</i>	<i>Papio</i>	13.2	16.3	20	19	3.2	<.001

¹ Mean_A, mean of Genus A; N_A, sample size of Genus A; Mean_B, mean of Genus B; N_B, sample size of Genus B; | θ |, absolute value of difference between observed sample means; p, probability that a difference between the bootstrapped means equaled or exceeded | θ |. Numbers in bold indicate statistical significance at alpha = .01.

Trapezium articulation. The relative area of the trapezium joint surface is significantly different in five of the ten pairwise comparisons between genus means (Table 5.14).

This relative area is significantly smaller in *Gorilla* (10.6%) than in all other genera.

The remaining significant difference occurs between *Pan* (13.3%) and *Homo* (12.5%), with the former larger than the latter.

TABLE 5.14 Pairwise comparisons of genus means for relative area of the trapezium joint surface¹

Genus A	Genus B	Mean _A	Mean _B	N _A	N _B	θ	p
<i>Homo</i>	<i>Pan</i>	12.5	13.3	111	47	0.8	0.005
<i>Homo</i>	<i>Gorilla</i>	12.5	10.6	111	45	1.9	<.001
<i>Homo</i>	<i>Pongo</i>	12.5	12.6	111	20	0.1	0.837
<i>Homo</i>	<i>Papio</i>	12.5	13.1	111	19	0.6	0.207
<i>Pan</i>	<i>Gorilla</i>	13.3	10.6	47	45	2.7	<.001
<i>Pan</i>	<i>Pongo</i>	13.3	12.6	47	20	0.7	0.162
<i>Pan</i>	<i>Papio</i>	13.3	13.1	47	19	0.2	0.707
<i>Gorilla</i>	<i>Pongo</i>	10.6	12.6	45	20	2.0	<.001
<i>Gorilla</i>	<i>Papio</i>	10.6	13.1	45	19	2.5	<.001
<i>Pongo</i>	<i>Papio</i>	12.6	13.1	20	19	0.5	0.428

¹ Mean_A, mean of Genus A; N_A, sample size of Genus A; Mean_B, mean of Genus B; N_B, sample size of Genus B; | θ |, absolute value of difference between observed sample means; p, probability that a difference between the bootstrapped means equaled or exceeded | θ |. Numbers in bold indicate statistical significance at alpha = .01.

Capitate articulation. The relative area of the capitate joint surface is significantly different in eight of the ten pairwise comparisons between genus means (Table 5.15). This relative area is significantly larger in *Homo* (8%) than in all other genera (note that the mean for *Gorilla* represents the average relative capitate surface area when the articulation is present). *Gorilla* (2.2%) and *Papio* (2.4%) have significantly smaller relative areas than do *Pan* (5.2%) and *Pongo* (5.8%).

TABLE 5.15 Pairwise comparisons of genus means for relative area of the capitate joint surface¹

Genus A	Genus B	Mean _A	Mean _B	N _A	N _B	θ	p
<i>Homo</i>	<i>Pan</i>	8.0	5.2	111	47	2.8	<.001
<i>Homo</i>	<i>Gorilla</i>	8.0	2.2	111	8	5.8	<.001
<i>Homo</i>	<i>Pongo</i>	8.0	5.8	111	20	2.2	<.001
<i>Homo</i>	<i>Papio</i>	8.0	2.4	111	19	5.5	<.001
<i>Pan</i>	<i>Gorilla</i>	5.2	2.2	47	8	3.0	<.001
<i>Pan</i>	<i>Pongo</i>	5.2	5.8	47	20	0.6	0.013
<i>Pan</i>	<i>Papio</i>	5.2	2.4	47	19	2.8	<.001
<i>Gorilla</i>	<i>Pongo</i>	2.2	5.8	8	20	3.6	<.001
<i>Gorilla</i>	<i>Papio</i>	2.2	2.4	8	19	0.3	0.758
<i>Pongo</i>	<i>Papio</i>	5.8	2.4	20	19	3.3	<.001

¹ Mean_A, mean of Genus A; N_A, sample size of Genus A; Mean_B, mean of Genus B; N_B, sample size of Genus B; | θ |, absolute value of difference between observed sample means; p, probability that a difference between the bootstrapped means equaled or exceeded | θ |. Numbers in bold indicate statistical significance at alpha = .01.

Non-articular surface. The relative non-articular area of the trapezoid is significantly different in eight of the ten pairwise comparisons between genus means (Table 5.16). This relative area is significantly larger in *Gorilla* (52.4%) than in all the other genera except *Homo* (51%); *Homo* also has significantly more non-articular area than does *Pan* (43.9%), *Pongo* (47.5%), and *Papio* (47.8%). Although *Pongo* and *Papio* are not significantly different in terms of relative non-articular area, both have significantly more relative area than does *Pan*.

TABLE 5.16 Pairwise comparisons of genus means for relative area of the non-articular surface¹

Genus A	Genus B	Mean _A	Mean _B	N _A	N _B	θ	p
<i>Homo</i>	<i>Pan</i>	51.0	43.9	111	47	7.1	<.001
<i>Homo</i>	<i>Gorilla</i>	51.0	52.4	111	45	1.4	0.026
<i>Homo</i>	<i>Pongo</i>	51.0	47.5	111	20	3.5	<.001
<i>Homo</i>	<i>Papio</i>	51.0	47.8	111	19	3.2	0.002
<i>Pan</i>	<i>Gorilla</i>	43.9	52.4	47	45	8.6	<.001
<i>Pan</i>	<i>Pongo</i>	43.9	47.5	47	20	3.6	<.001
<i>Pan</i>	<i>Papio</i>	43.9	47.8	47	19	3.9	<.001
<i>Gorilla</i>	<i>Pongo</i>	52.4	47.5	45	20	5.0	<.001
<i>Gorilla</i>	<i>Papio</i>	52.4	47.8	45	19	4.6	<.001
<i>Pongo</i>	<i>Papio</i>	47.5	47.8	20	19	0.3	0.727

¹ Mean_A, mean of Genus A; N_A, sample size of Genus A; Mean_B, mean of Genus B; N_B, sample size of Genus B; | θ |, absolute value of difference between observed sample means; p, probability that a difference between the bootstrapped means equaled or exceeded | θ |. Numbers in bold indicate statistical significance at alpha = .01.

Multivariate analyses

In this section, the results of the canonical and discriminant function analyses using two combinations of trapezoid carpal and carpometacarpal joint and non-articular variables are presented. In Full Model I, eleven trapezoid variables are used as predictor variables; these include six angles between articular surfaces and five relative articular areas. This analysis does not incorporate any angles or areas that involve the capitate joint surface because of the typical absence of this surface in *Gorilla*. In Full Model II, *Gorilla* is excluded and fifteen trapezoid variables are used as predictor variables; the variables include all ten angles between joint surfaces and five of the six relative areas. Using all six relative areas results in a singular covariance matrix because all six sum to 1; this is an unacceptable violation for multivariate analyses. It should be noted, however, that the results are statistically identical no matter which five relative areas are selected because the sixth is always implied by the others.

Full Model I: Relative areas and angles (capitate variables excluded). The first canonical axis (CAN1) accounts for 76% of the variation, the second (CAN2) accounts for 14%, and the third (CAN3) 8%. Along CAN1, *Homo* is clustered on the left, while the remaining taxa cluster on the right (Fig. 5.2). The correlations with CAN1 indicate that the observed variation is a combination of the relative area of the scaphoid surface and the angle between the medial second metacarpal and scaphoid surfaces (Table 5.17). Along CAN2, *Papio* and *Homo* cluster centrally while *Gorilla* clusters more positively and *Pan* and *Pongo* more negatively (Fig. 5.3). The correlations with CAN2

indicate that this axis represents a comparison of the relative non-articular area with the relative area of the trapezium surfaces (Table 5.17).

Along CAN3, the hominines are more positively clustered whereas *Papio* is clustered more negatively (Fig. 5.3). The correlations with CAN3 indicate that this axis represents a comparison of all the angle and area variables involving the second metacarpal surfaces except for the angle between the lateral second metacarpal and scaphoid surfaces (Table 5.17).

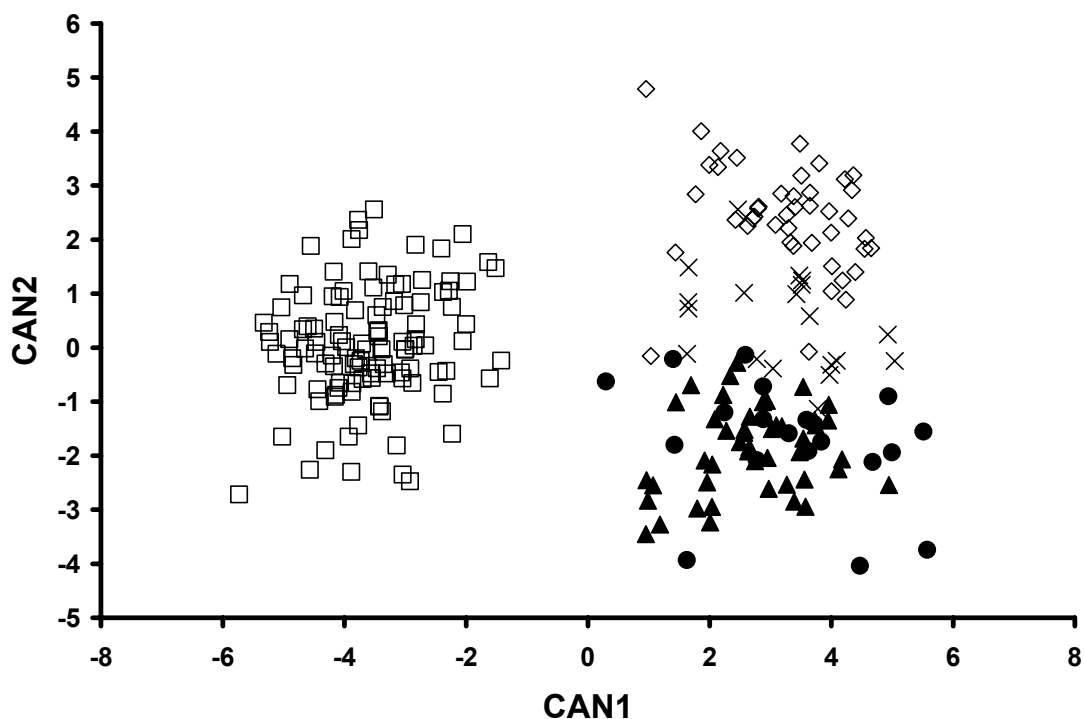


Fig. 5.2 Plot of the canonical variables (CAN1, CAN2) generated from analysis of relative areas and angles of the trapezoid articular surfaces (*Homo* = open squares, *Pan* = closed triangles, *Gorilla* = open diamonds, *Pongo* = closed circles, *Papio* = Xs).

TABLE 5.17 Correlations between each variable and canonical axis (bolded values indicate the variables that best explain the observed variation along each axis)

Variable		Pooled-within canonical structure			
Angle between		CAN1	CAN2	CAN3	CAN4
lateral 2nd metacarpal	medial 2nd metacarpal	0.00	0.09	0.13	-0.61
lateral 2nd metacarpal	scaphoid	0.18	-0.06	0.27	-0.07
lateral 2nd metacarpal	trapezium	0.08	-0.25	0.44	0.35
medial 2nd metacarpal	scaphoid	0.51	-0.22	-0.28	0.31
medial 2nd metacarpal	trapezium	0.14	-0.19	0.63	-0.46
scaphoid	trapezium	-0.12	0.22	0.04	-0.23
Relative surface area					
	nonarticular	-0.13	0.49	0.12	-0.38
	lateral 2nd metacarpal	-0.04	-0.14	-0.12	0.53
	medial 2nd metacarpal	0.22	0.08	0.35	0.30
	scaphoid	0.44	0.00	-0.28	0.21
	trapezium	-0.03	-0.37	-0.23	0.04

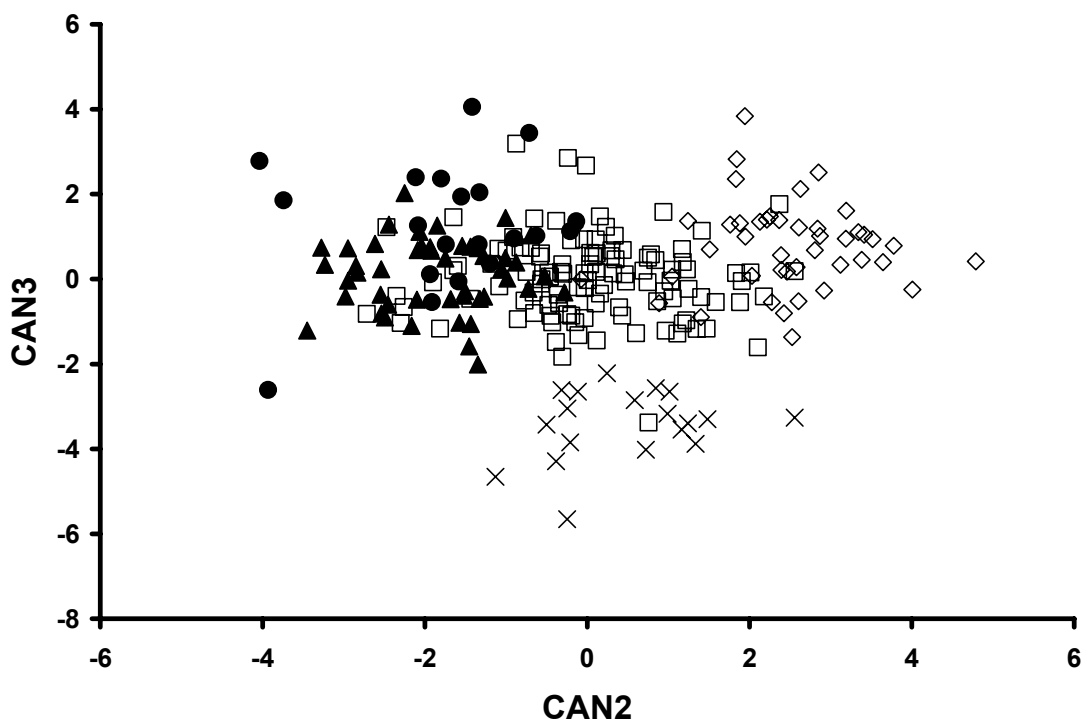


Fig. 5.3 Plot of the canonical variables (CAN2, CAN3) generated from analysis of relative areas and angles of the trapezoid articular surfaces (*Homo* = open squares, *Pan* = closed triangles, *Gorilla* = open diamonds, *Pongo* = closed circles, *Papio* = Xs).

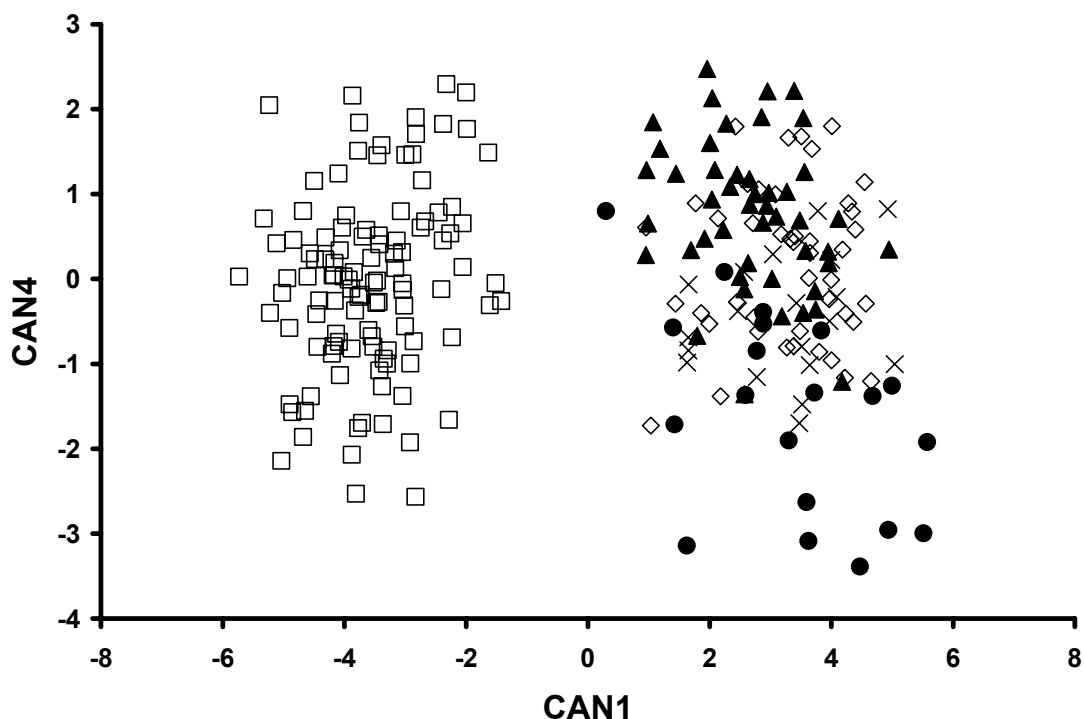


Fig. 5.4 Plot of the canonical variables (CAN1, CAN4) generated from analysis of relative areas and angles of the trapezoid articular surfaces (*Homo* = open squares, *Pan* = closed triangles, *Gorilla* = open diamonds, *Pongo* = closed circles, *Papio* = Xs).

Finally, *Pan* clusters more positively whereas *Pongo* clusters more negatively along CAN4 (Fig. 5.4). The correlations with CAN4 indicate that this axis represents a multi-variable comparison: the medial second metacarpal joint surface angles with the lateral second metacarpal and trapezium joint surfaces are compared with the angle between the lateral second metacarpal and trapezium joint surfaces, the angle between the medial second metacarpal and scaphoid joint surfaces, and the relative areas of both second metacarpal joint surfaces (Table 5.17).

Together, the four canonical variables result in distinct clusters for each genus (Figs. 2-4). The angle between the medial second metacarpal and scaphoid surfaces is almost

twice as narrow in *Homo* as in any of the non-human taxa (Table 5.4). In addition, *Homo* has the smallest relative scaphoid joint surface (Table 5.13). Together, these two variables drive *Homo* negatively along CAN1 whereas the other taxa are driven positively. *Gorilla* has the largest relative medial second metacarpal joint surface and non-articular area (Tables 5.12 and 5.16), as well as the smallest relative trapezium joint surface (Table 5.14). Together, these three variables drive positively along CAN1 and CAN2 generating the upper right cluster of *Gorilla* (Fig. 5.2). The *Papio* cluster results primarily from the two trapezium joint surface angles with the lateral and medial second metacarpal joint surfaces, both of which load negatively along CAN3 and are significantly narrower in baboons compared with the hominids (Tables 5.3 and 5.5, Fig. 5.3).

Although *Pan* and *Pongo* cluster together along the first three canonical axes (Figs. 5.2 and 5.3), along CAN4 these two genera cluster apart from one another (Fig. 5.4). The separation along this axis results primarily from *Pongo* having significantly larger medial second metacarpal joint surface angles with the lateral second metacarpal and trapezium joint surfaces than does *Pan* (Tables 5.1 and 5.5); both of these angles have a negative loading along CAN4 (Table 5.17).

TABLE 5.18 Cross-validated posterior probabilities of genus membership using the trapezoid carpal and carpometacarpal joint and non-articular relative surface area and angle measures

	<i>Homo</i>	<i>Pan</i>	<i>Gorilla</i>	<i>Pongo</i>	<i>Papio</i>
<i>Homo</i>	111	0	0	0	0
%	100.0	0.0	0.0	0.0	0.0
<i>Pan</i>	0	42	0	3	2
%	0.0	89.4	0.0	6.4	4.3
<i>Gorilla</i>	0	1	42	1	0
%	0.0	2.3	95.5	2.3	0.0
<i>Pongo</i>	0	3	0	16	1
%	0.0	15.0	0.0	80.0	5.0
<i>Papio</i>	0	0	0	0	19
%	0.0	0.0	0.0	0.0	100.0

The cross-validation procedure of the discriminant function analysis resulted in the correct classification of 111 *Homo* (100%), 42 *Pan* (89.4%), 42 *Gorilla* (95.5%), 16 *Pongo* (80%), and 19 *Papio* (100%; Table 5.18). Overall, the results indicate that the combined measures of the trapezoid clearly discriminate all of these genera from each other with significant accuracy.

Full Model II: Relative areas and angles (Gorilla excluded). The first canonical axis (CAN1) accounts for 75% of the variation, the second (CAN2) accounts for 18%, and the third (CAN3) 7%. Along CAN1, *Homo* clusters on the left, while the remaining taxa cluster on the right (Fig. 5.5). The correlations with CAN1 indicate that the observed variation is a combination of the angle between the medial second metacarpal and scaphoid joint surfaces and the relative scaphoid joint area (Table 5.19). Along CAN2, *Papio* clusters positively and *Pan* clusters more negatively, while *Homo* and *Pongo* are centrally clustered (Fig. 5.6). The correlations with CAN2 indicate that this axis represents three of the four angles involving the capitate surface in comparison

with the two trapezium joint surface angles with the second metacarpal joint surfaces (Table 5.19).

Along CAN3, *Pongo* clusters more positively while the remaining taxa are more negatively clustered (Fig. 5.6). The correlations with CAN3 indicate that this axis represents a multi-variable comparison but the strongest positive loading is associated with the angle between the medial second metacarpal and trapezium joint surfaces (Table 5.19).

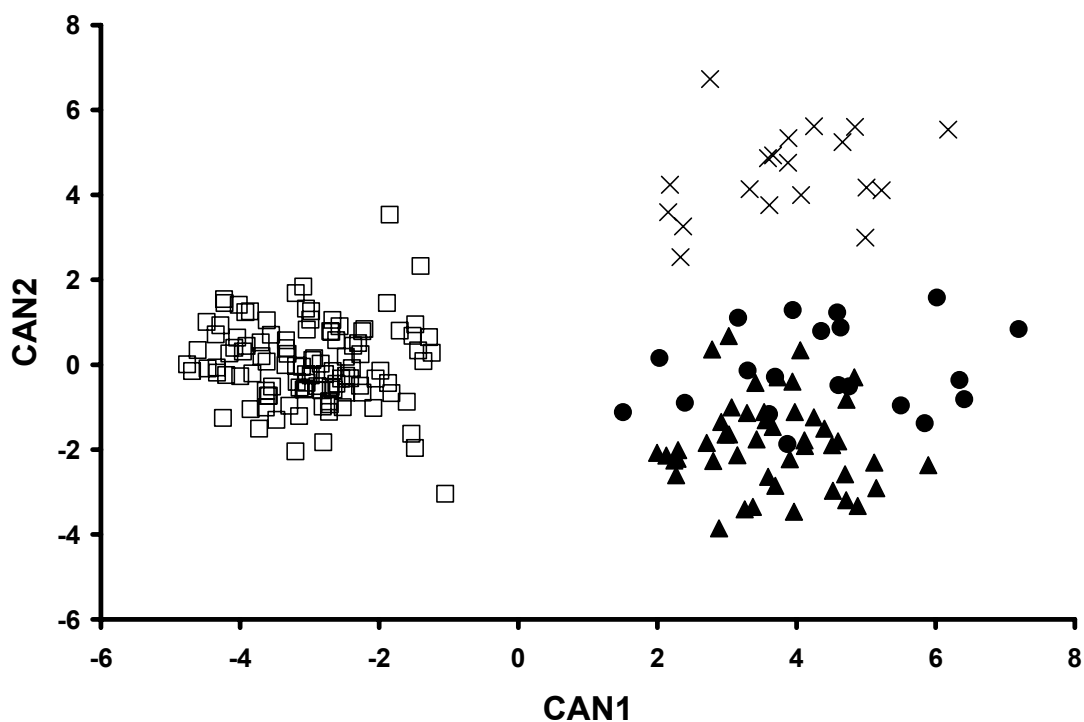


Fig. 5.5 Plot of the canonical variables (CAN1, CAN2) generated from analysis of relative areas and angles of the trapezoid articular surfaces (*Homo* = open squares, *Pan* = closed triangles, *Pongo* = closed circles, *Papio* = Xs).

The first two axes result in three distinct clusters: one each for *Homo* and *Papio*, and one for *Pongo* and *Pan* (Fig. 5.5), while the second two axes result in *Pongo* clustering away from the remaining taxa (Fig. 5.6). The variables that drive the separation between taxa in Figures 5.5 and 5.6 are essentially the same as those discussed above in Full Model I and are therefore not repeated here.

The cross-validation procedure of the discriminant function analysis resulted in the correct classification of 111 *Homo* (100%), 47 *Pan* (100%), 16 *Pongo* (80%), and 19 *Papio* (100%; Table 5.20). Overall, the results indicate that the combined relative measures of trapezoid articular surfaces clearly discriminate all of these genera from each other with significant accuracy.

TABLE 5.19 Correlations between each variable and canonical axis (bolded values indicate the variables that best explain the observed variation along each axis)

Variable		Pooled-within canonical structure		
Angle between		CAN1	CAN2	CAN3
lateral 2nd metacarpal	medial 2nd metacarpal	-0.02	0.07	0.40
lateral 2nd metacarpal	scaphoid	0.16	-0.14	0.19
lateral 2nd metacarpal	trapezium	0.10	-0.40	0.09
medial 2nd metacarpal	scaphoid	0.53	0.04	-0.34
medial 2nd metacarpal	trapezium	0.14	-0.32	0.62
scaphoid	trapezium	-0.15	0.09	0.13
capitate	lateral 2nd metacarpal	0.25	0.48	0.28
capitate	medial 2nd metacarpal	0.27	0.42	-0.08
capitate	scaphoid	0.05	-0.14	-0.37
capitate	trapezium	0.14	0.47	0.30
<u>Relative surface area</u>				
	nonarticular	-0.22	0.18	0.24
	lateral 2nd metacarpal	-0.01	-0.09	-0.35
	medial 2nd metacarpal	0.17	-0.21	0.03
	scaphoid	0.42	0.14	-0.30
	trapezium	0.05	-0.02	-0.12

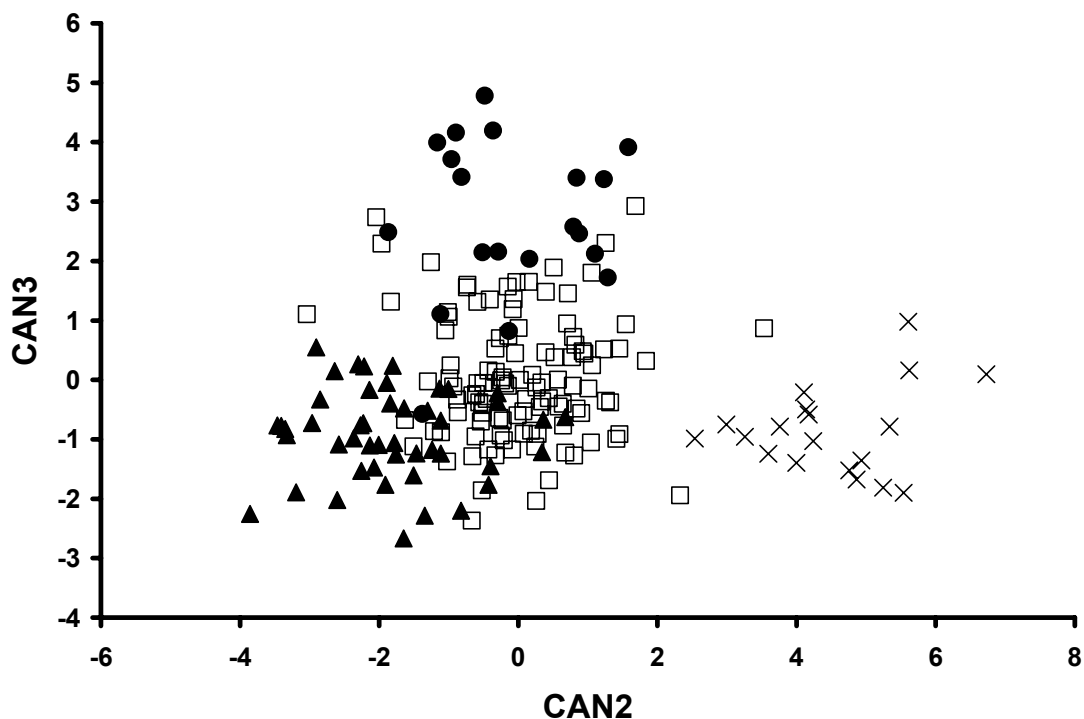


Fig. 5.6 Plot of the canonical variables (CAN2, CAN3) generated from analysis of relative areas and angles of the trapezoid articular surfaces (*Homo* = open squares, *Pan* = closed triangles, *Pongo* = closed circles, *Papio* = Xs).

TABLE 5.20 Cross-validated posterior probabilities of genus membership using the trapezoid carpal and carpometacarpal joint and non-articular relative surface area and angle measures

	<i>Homo</i>	<i>Pan</i>	<i>Pongo</i>	<i>Papio</i>
<i>Homo</i>	111	0	0	0
%	100.0	0.0	0.0	0.0
<i>Pan</i>	0	47	0	0
%	0.0	100.0	0.0	0.0
<i>Pongo</i>	0	3	16	1
%	0.0	15.0	80.0	5.0
<i>Papio</i>	0	0	0	19
%	0.0	0.0	0.0	100.0

Summary of shape characteristics

TABLE 5.21 Summary of mean trapezoid carpal joint and non-articular features (distinctive features in bold)

Variable		Genus				
Angle between		<i>Homo</i>	<i>Pan</i>	<i>Gorilla</i>	<i>Pongo</i>	<i>Papio</i>
lateral 2nd metacarpal	medial 2nd metacarpal	125	119	127	134	124
lateral 2nd metacarpal	scaphoid	24	37	38	43	28
lateral 2nd metacarpal	trapezium	117	128	120	126	106
medial 2nd metacarpal	scaphoid	38	69	61	63	72
medial 2nd metacarpal	trapezium	67	74	74	86	60
scaphoid	trapezium	86	72	83	78	78
capitate	lateral 2nd metacarpal	54	59	94*	80	91
capitate	medial 2nd metacarpal	108	119	141*	125	146
capitate	scaphoid	105	113	99*	100	105
capitate	trapezium	23	22	57*	37	45
<u>Relative surface area</u>						
	capitate	8.0	5.2	2.2*	5.8	2.4
	lateral 2nd metacarpal	6.7	7.4	5.7	5.2	6.5
	medial 2nd metacarpal	13.5	16.0	16.9	15.8	13.9
	scaphoid	8.3	14.3	14.1	13.2	16.3
	trapezium	12.5	13.3	10.6	12.6	13.1
	non-articular	51.0	43.9	52.4	47.5	47.8

* denotes the observed mean in *Gorilla* when a capitate articular surface is present

Papio. The probability of correctly classifying *Papio* based on features of the trapezoid carpal and carpometacarpal joints and non-articular area was 100% (Tables 5.18 and 5.20). The trapezoid features that best characterize *Papio* are the lateral second metacarpal-trapezium angle, the medial second metacarpal-trapezium angle, the capitate-lateral second metacarpal angle, the capitate-medial second metacarpal angle, the capitate-trapezium angle, and the relative areas of the medial second metacarpal and scaphoid surfaces (Table 5.21).

Many of the distinguishing features of the *Papio* trapezoid relate to a differently shaped palmar portion of the bone (see Fig. 5.1). For instance, in *Papio*, the palmar half of the trapezoid appears narrower and thinner in comparison to that in hominids.

Moreover, the palmar aspect of the medial second metacarpal surface does not tilt as far proximally as in the great apes. These trapezoid shape characteristics in *Papio* are evidenced by the significantly narrower angles between the trapezium and both second metacarpal joint surfaces (Tables 5.3, 5.5, and 5.21), as well as the significantly wider angles between the capitate and both second metacarpal joint surfaces and between the capitate and trapezium joint surfaces (Tables 5.7, 5.8, 5.10, and 5.21).

In terms of relative areas, the *Papio* trapezoid is distinguished by a relatively small medial second metacarpal joint surface combined with a relatively large scaphoid joint surface. However, it is when the second metacarpal and scaphoid areas are examined in combination that a further trapezoid characteristic of *Papio* is evident. For example, in the great apes and *Papio*, the scaphoid and total second metacarpal articulations take up approximately 35% of the entire surface area of the trapezoid. The ratio between the total second metacarpal and scaphoid areas within this 35%, however, is approximately 55:45 in *Papio*, whereas it is 60:40 in the great apes (Table 5.22).

TABLE 5.22 The ratio of total 2nd metacarpal to scaphoid relative areas

Relative surface area	<i>Homo</i>	<i>Pan</i>	<i>Gorilla</i>	<i>Pongo</i>	<i>Papio</i>
total 2nd metacarpal	20.2	23.4	22.5	21.0	20.3
scaphoid	8.3	14.3	14.1	13.2	16.3
ratio of above relative surface areas	71:29	62:38	62:38	61:39	55:45

Pongo. The probability of correctly classifying *Pongo* based on features of the trapezoid carpal and metacarpal joints and non-articular area was 80% (Tables 5.18 and 5.20); three *Pongo* specimens (15%) were misclassified as *Pan* and one (5%) as *Papio*. The trapezoid features that best characterize *Pongo* are the medial second metacarpal joint surface angles with the trapezium and with the lateral second metacarpal joint

surfaces, and the relative area of the lateral second metacarpal joint surface (Table 5.21).

The great apes show the most similarity relative to one another in the trapezoid variables measured. The *Pongo* trapezoid typically resembles the trapezoid in *Pan* (Figs. 5.2, 5.3, and 5.5). However, three features stand out that distinguish the *Pongo* trapezoid from that in the other taxa (see Fig. 5.1). First, the medial second metacarpal joint surface angles with the trapezium and lateral second metacarpal joint surfaces are significantly wider in *Pongo* (Tables 5.1 and 5.5). Second, the *Pongo* trapezoid is distinguished by a relatively small lateral second metacarpal surface (Table 5.11). Furthermore, the lateral second metacarpal surface in *Pongo* is often shifted palmarly, and corresponds with the laterally (i.e., palmar in the ‘true’ sense) expanded second metacarpal surface of the trapezium. These three features, in conjunction with the lack of distinctive morphology characteristic of the other genera, enable the correct classification of 80% of *Pongo* trapezoids in Full Models I and II.

***Gorilla*.** The probability of correctly classifying *Gorilla* based on features of the trapezoid carpal and metacarpal joints and non-articular area was 96% (Table 5.18); one *Gorilla* specimen (2%) was misclassified as *Pan* and one (2%) as *Pongo*. The trapezoid features that best characterize *Gorilla* are the typical lack of a dorso-medial articular facet for the capitate, the relative areas of the lateral second metacarpal, medial second metacarpal, and trapezium joint surfaces, and the relative non-articular area (Table 5.21).

The primary characteristic that makes the *Gorilla* trapezoid different from those in the other taxa is the lack of a dorso-medial articular facet for the capitate (see Fig. 5.1). Capitate facets occur occasionally in the trapezoid of *Gorilla* (Lewis, 1989; McHenry, 1983; this study), but overall, the severely reduced or absent joint is the common condition and is clearly derived from the primitive condition for primates. Moreover, this derived change is accompanied, on the opposite side of the bone, by reduced relative lateral second metacarpal and trapezium areas in comparison to the other hominids and *Papio* (Tables 5.11 and 5.14). Together, these reductions in articular surface area lead to the increased relative trapezoid nonarticular area (Table 5.16) in *Gorilla* despite the fact that this genus shows the largest relative medial second metacarpal area (Table 5.12).

Pan. The probabilities of correctly classifying *Pan* based on features of the trapezoid carpal and metacarpal joints and non-articular area were 89% and 100% (Tables 5.18 and 5.20); three *Pan* specimens (6%) were misclassified as *Pongo* and two (4%) as *Papio* (Table 5.18). The trapezoid features that best characterize *Pan* are the lateral second metacarpal joint surface angles with the medial second metacarpal and trapezium joint surfaces, the three angles between the scaphoid, trapezium, and capitate joint surfaces, the relative areas of the lateral second metacarpal and trapezium joint surfaces, and the relative non-articular area (Table 5.21).

Visually, the *Pan* trapezoid displays an overall resemblance to the *Papio* trapezoid (see Fig. 5.1). The variables quantified in the analyses presented here do not overtly reflect this visual similarity, mostly because some subtle morphological differences

produce marked changes in the relative areas and angles. Compared with the *Papio* trapezoid, the bone in *Pan* is thicker and broader palmarly and the medial second metacarpal joint surface slopes proximally toward the scaphoid joint surface. Also, the trapezium joint surface in *Pan* extends further distally whereas in *Papio* this distal portion of the articular surface is often absent, and is likely related to the lack of a trapezium-second metacarpal joint in many baboons. Together, these trapezoid differences clearly distinguish *Pan* from *Papio*, but *Pan* does not appear to show any features that distinguish it from the other hominid taxa. Rather, each other hominid taxon displays its own set of derived characteristics (e.g., lack of capitate facet in *Gorilla*, palmar expansion of the non-articular area in *Homo*, and reduced overall size in *Pongo*), and it is the lack of such features in *Pan* that clearly distinguishes it among the hominids.

***Homo*.** The probability of correctly classifying *Homo* based on features of the trapezoid carpal and metacarpal joints and non-articular area was 100% and no other genus was misclassified as *Homo* (Table 5.18 and 5.20). The trapezoid features that best characterize *Homo* are the scaphoid joint surface angles with the lateral and medial second metacarpal joint surfaces, the angle between the capitate and trapezium joint surfaces, the relative areas of the medial second metacarpal, scaphoid, and capitate joint surfaces, and the relative non-articular area (Table 5.21).

Overall, these distinct features contribute to the ‘boot-like’ shape of the *Homo* trapezoid. In *Homo*, both angles between the second metacarpal joint surfaces and the scaphoid joint surface are narrow in comparison with the non-human taxa (Tables 5.2

and 5.4). Therefore, the second metacarpal and scaphoid joint surfaces are considerably more parallel to one another in *Homo*. This morphology is partially explained by the expanse of nonarticular area that characterizes the palmar aspect of the *Homo* trapezoid. In *Homo*, the palmar portion of the trapezoid is expanded proximo-distally as well as radio-ulnarly. The proximo-distal expansion raises the palmar aspects of the second metacarpal joint surfaces such that they no longer slant proximally toward the palmar aspect of the scaphoid joint surface, resulting in more parallel articulations. Similarly, the radio-ulnar expansion results in the capitate and trapezium joint surfaces being more parallel to one another as well. The more parallel relationship of these two articular surfaces is even more striking when one considers that the capitate joint surface in *Homo* is more medio-palmarly-placed rather than dorso-medial as in non-human primates. For example, *Pan* also displays capitate and trapezium joint surfaces that are almost parallel; however, if the capitate articulation in *Pan* were more medio-palmarly-placed as in *Homo*, the capitate-trapezium angle would come closer to 90°.

The shape differences in the *Homo* trapezoid are further reflected by differences in relative areas. The *Homo* trapezoid is characterized by small relative medial second metacarpal and scaphoid joint areas (Tables 5.12 and 5.13), and by large relative capitate joint and nonarticular areas (Tables 5.15 and 5.16). The ratio between total second metacarpal and scaphoid relative joint areas (7:3) is also distinctive of the *Homo* trapezoid (Table 5.21).

The large relative nonarticular area of the trapezoid in *Homo* is directly related to the palmar expansion of the bone and the smaller relative medial second metacarpal and

scaphoid joint areas. In this sense, it is completely unlike the large relative nonarticular area in the *Gorilla* trapezoid. The large relative area of the more medio-palmarly-placed capitate joint surface further highlights the derived nature of the *Homo* trapezoid.

DISCUSSION

The previous three chapters examined features of the first carpometacarpal joint, the trapezium-second metacarpal joint, and the trapezium carpal joints and non-articular area. Thus far, the observed morphology in *Homo* in comparison to the non-human primate genera is consistent with the biomechanical predictions introduced in Chapter 2. The analytical results of this chapter inform on how the shape characteristics of the modern human and non-human primate trapezoid relate to the predicted compressive and shear stresses in a wrist better designed for forceful manipulative grasps involving the thumb in comparison to a wrist better designed for locomotor behaviors.

In non-human primates, the trapezoid is essentially shaped like a pyramidal wedge; the narrow tip of the pyramid is palmar and more proximal while the wide base is dorsal and extends further distally (Figs. 5.1 and 5.8). In contrast, the *Homo* trapezoid is shaped more like a ‘boot’—many human osteology textbooks describe the human trapezoid in this manner (e.g., Baker et al., 2005). The boot shape results from an expansion of the palmar half of the bone. This expansion occurs radio-ulnarly as well as proximo-distally such that the palmar nonarticular surface is more rectangular in shape rather than the pinched-tip wedge shape seen in non-human primates (Figs. 5.1, 5.7, and 5.8).

It is this palmar expansion of the trapezoid in *Homo* that results in a more efficient design for distributing radio-ulnarly directed joint reaction forces during manipulative behaviors involving strong contraction of the thumb musculature. For instance, the radio-ulnar expansion coupled with the relatively larger, more medio-palmarly-placed capitate joint surface, results in a more parallel angle between the capitate and trapezium joint surfaces (Fig. 5.7). The capitate is similarly derived in having an enlarged trapezoid joint surface that is situated more palmarly rather than more dorsally (Fick, 1904; Lewis, 1989; Tocheri et al., 2005). Together, these features in *Homo* provide more joint surface area that is oriented more orthogonal to the predicted direction of force being placed on these joints (Table 5.21). The larger surface areas widely distribute the compressive stress the joint is experiencing while the surface orientations reduce the levels of shear stress. In other words, as the base of the first metacarpal compresses into the trapezium, concomitant joint reaction forces occur at the trapezium-trapezoid and trapezoid-capitate joints; the derived trapezoid joint morphology in *Homo* is more efficiently designed to withstand the resulting stresses of these radio-ulnar joint reaction forces than is the primitive trapezoid joint morphology in non-human primates.

In addition, the palmar expansion of the trapezoid in *Homo* results in a more parallel angle between the second metacarpal and scaphoid joint surfaces (Fig. 5.7). This derived change occurs primarily because the medio-palmar portion of the medial second metacarpal joint surface has shifted distally. The resulting effect is that the ulnar side of the second metacarpal base is no longer buttressed against the disto-radial side of the

capitate, as it is in non-human primates (Fig. 5.7). This morphological change helps stabilize the capitate-trapezoid joint when the wrist is compressed radio-ulnarly because the capitate can no longer slide distally along the side of the second metacarpal base; as a result, however, the capitate-medial second metacarpal joint sacrifices the ability to stabilize the trapezoid-medial second metacarpal joint when the wrist is compressed proximo-distally (Figs. 5.7 and 5.8).

Alternatively, the primitive trapezoid joint morphology in non-human primates is more efficiently designed to withstand the resulting stresses of proximo-distally directed joint reaction forces during quadrupedal locomotor behaviors. For instance, the primitive condition has the radio-ulnarly stable capitate-second metacarpal joint discussed above (Fig. 5.7). When the wrist is close-packed during locomotor behaviors, the scaphoid-radius joint assumes a more parallel orientation with the trapezoid-medial second metacarpal joint because the latter joint tends to slant proximo-ulnarly toward the palmar aspect of the trapezoid-scaphoid joint (Figs. 5.1, 5.7, and 5.8). During locomotor behaviors, this orientation reduces shear stress at these joints while the larger relative area of the medial second metacarpal widely distributes the compressive stress component of the proximo-distal joint reaction forces. However, the trapezoid-scaphoid joint is caught in the middle of the relationship between the scaphoid-radius and the trapezoid-medial second metacarpal joints. Although the scaphoid joint area in non-human primates is large and takes up most, if not all of the proximal surface of the trapezoid, this joint surface is not oriented perpendicular to the predicted proximo-distal joint reaction forces (Fig. 5.7). Therefore, relatively large levels of shear stress are

likely experienced at this joint while the scaphoid-radius and the trapezoid-second metacarpal joints experience more compressive stress.

In non-hominoid primates, both the ulna and radius articulate with the proximal wrist. In these animals, the shear stress experienced at the trapezoid-scaphoid joint is likely less intense since the proximo-distal reaction forces are distributed fairly evenly across the ulnar-carpal and radio-carpal joints, although strong ligaments between the trapezoid and surrounding bones probably reduce shear stress as well. However, hominoid primates are derived in having lost the ulnar-carpal articulation (Lewis, 1989; Mivart, 1867) most likely as an adaptation to more cautious arboreal climbing or suspensory locomotor behaviors as it enables larger ranges of wrist mobility (Cartmill and Milton, 1977). The subsequent terrestrial knuckle-walking behavior in African apes directs the majority of force across the radio-carpal joint; hence, the trapezoid-scaphoid joints in these taxa likely experience the largest levels of shear stress. Since it is the centrale portion of the scaphoid that contributes the proximal surface of the trapezoid-scaphoid joint, it has been suggested that prenatal cartilaginous coalescence (or fusion) of the scaphoid and os centrale in African apes is probably related to accommodating the large shear levels at this joint during knuckle-walking behavior (Richmond et al., 2001); the information presented here in conjunction with visual inspection of Figure 5.7 reasonably supports such a suggestion.

In contrast, the scaphoid joint area of the human trapezoid is reduced such that it assumes a more restricted, rectangular shape rather than the larger, more triangular shape seen in non-human primates (Figs. 5.1 and 5.8). The medial second metacarpal

and scaphoid joint surfaces are also more parallel with one another, such that both are roughly perpendicular to the scaphoid-radius joint. Therefore, shear stress levels would be large at both the trapezoid-scaphoid and trapezoid-medial second metacarpal joints if the wrist underwent proximo-distal compression (not to mention the loss of radio-ulnar stability between the capitate and second metacarpal base). With no quadrupedal locomotor requirements, the reduction of the scaphoid articular surface on the trapezoid allows for the enlargement of the scaphoid joint surface on the trapezium in *Homo* (see Chapter 4). The trapezium and trapezoid share a continuous articulation with the scaphoid, and with such limited articular ‘real-estate’ available on the scaphoid, the joint surface on one of the distal carpals contracts as the other expands. Non-human primates show the primitive condition in which the trapezoid has the expanded joint surface whereas *Homo* shows the derived condition in which the trapezium has the expanded joint surface (Marzke et al., 1992).

Lewis (1989) qualitatively described many of these derived features of the *Homo* trapezoid and offered a functional interpretation. He suggested that “considerable compressive stresses may be transmitted from the first metacarpal base to the trapezium and thence across the expanded anterior part of the trapezoid to the capitate. The enlargement of the volar aspect of the trapezoid, readjusting the ‘set’ of the trapezium, and establishment of a new anterior diarthrosis with the capitate can then perhaps be interpreted as morphological markers of the human power grip” (Lewis, 1989: 114).

In total, the results of this chapter quantitatively confirm the morphological observations and interpretations of Lewis (1989). However, the results further suggest

that the derived features of the trapezoid in *Homo* are more than morphological markers of the human power grip. These derived trapezoid features provide a better proximo-distally stable design for withstanding the compressive and shear stresses associated with radio-ulnarly directed joint reaction forces, which arise from precision and power grips that involve strong contraction of the thumb musculature. Furthermore, these derived trapezoid features are strong candidates for evidence in Plio-Pleistocene hominins of morphological commitment to adaptive behaviors involving the use and manufacture of stone tools. However, such commitment comes at a price—the benefits for locomotor behavior provided by the primitive trapezoid condition in primates are lost (i.e., a better radio-ulnarly stable design for withstanding the compressive and shear stresses associated with proximo-distally directed joint reaction forces).

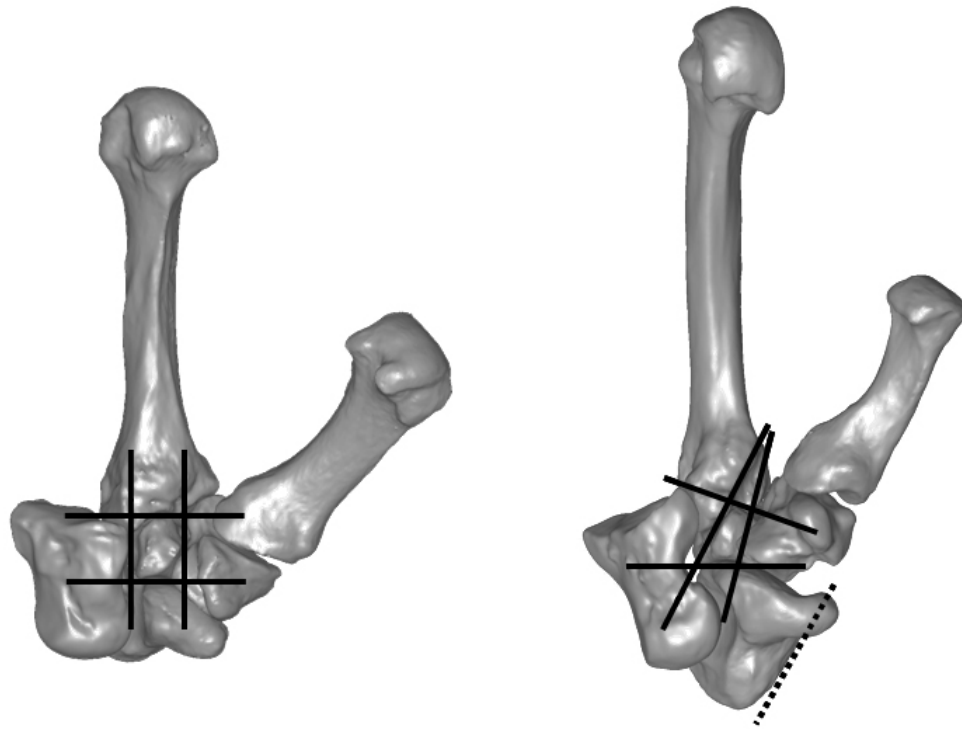


Fig. 5.7 Visual comparison of the differences between modern human and non-human primates in trapezoid morphology (*Homo*, shown at left; *Pan*, shown at right). In humans, the palmar portion of the trapezoid is expanded radio-ulnarly as well as proximo-distally such that the palmar nonarticular surface is more rectangular in shape rather than the pinched-tip wedge shape seen in non-human primates. Also, note the more parallel relationship in non-human primates between the radial articulation of the scaphoid (dotted-line) and the medial trapezoid-2nd metacarpal joint, as well as the radio-ulnar stability provided by the capitate-second metacarpal joint. Bones are from the right side.

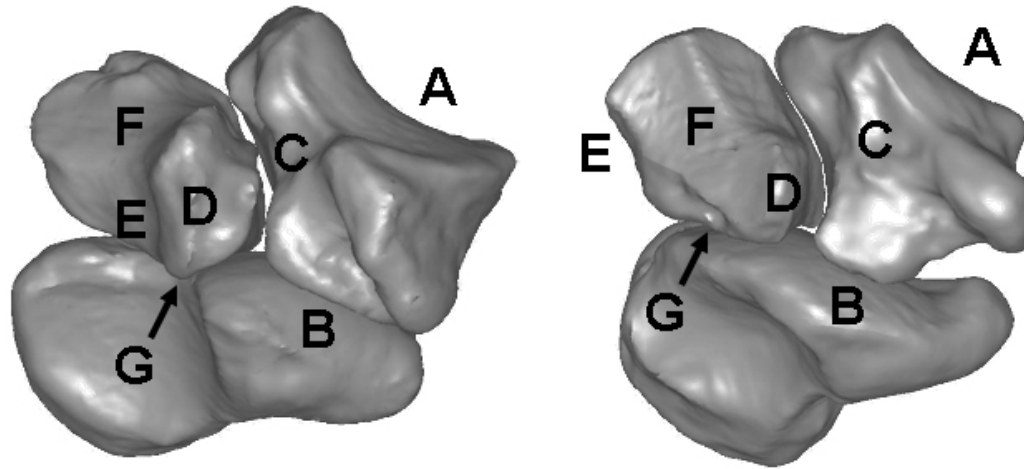


Fig. 5.8 Summary of differences in carpal joint morphology discussed in relation to the shape change of the trapezoid and the biomechanical predictions (*Homo*, shown at left; *Pan*, shown at right). The labeled features are derived in *Homo* relative to other primates; Key: **A**, larger 1st carpometacarpal joint; **B**, larger trapezium-scaphoid joint; **C**, narrower palmar trapezium non-articular area; **D**, broader palmar trapezoid non-articular area; **E**, larger, more medio-palmarly-placed trapezoid-capitate joint; **F**, medial 2nd carpometacarpal joint oriented more parallel to trapezoid-scaphoid joint; and **G**, smaller, rectangular shaped trapezoid-scaphoid joint. Bones are from the right side.

Chapter 6: The Scaphoid

RESULTS OF SHAPE ANALYSES

In this chapter, I present the results of the shape analyses performed on the carpal joints and non-articular area of the scaphoid. The variables measured include the angles between joint surfaces and the relative articular and non-articular areas of the scaphoid. As in the previous chapter, the name of the articulating bone is used to describe each joint surface. For example, the area on the scaphoid for articulation with the capitate is referred to as the capitate joint surface (see Fig. 6.3, top row). The trapezium and trapezoid joints are examined as a single joint surface because in the hominines these joints form a single, continuous surface (see Fig. 6.3, bottom row).

The scaphoid presents a challenge to the desired analysis because in both *Pongo* and *Papio*, this bone is comprised of two distinct, separate elements: the scaphoid proper and the centrale. Therefore, only two of the six possible joint surface angles are measurable using only the unfused scaphoid or the centrale portion of the bone: the angle between the lunate and radius joint surfaces (unfused scaphoid) and the angle between the capitate and trapezium-trapezoid joint surfaces (centrale). As such, only these two angles are used for comparisons involving all of the genera, but all six angles are used for comparisons among the hominines. Relative joint surface and non-articular areas in *Pongo* and *Papio* are calculated after adjusting the total scaphoid-centrale surface area by subtracting the reciprocal articular and non-articular areas that these two bones share. Therefore, all of the relative areas are used for comparisons among all five genera.

The results of the comparative shape analyses for each variable are presented separately, followed by multivariate analyses using two combinations of the variables (Full Model's I and II). Following the presentation of the statistical results, a summary of the scaphoid shape characteristics of each genus is given. Finally, the results are discussed in relation to the biomechanical predictions introduced in Chapter 2.

Angles of the scaphoid

The capitate and lunate articulations. The angle between these two surfaces is significantly different in two of the three pairwise comparisons between hominine genus means (Table 6.1). This angle is significantly narrower in *Homo* (157°) than in the African apes. No significant difference in this angle is observed between *Pan* (170°) and *Gorilla* (168°).

TABLE 6.1 Pairwise comparisons of genus means for the angle between the capitate and lunate joint surfaces¹

Genus A	Genus B	Mean _A	Mean _B	N _A	N _B	θ	p
<i>Homo</i>	<i>Pan</i>	157	170	116	47	13	<.001
<i>Homo</i>	<i>Gorilla</i>	157	168	116	48	11	<.001
<i>Pan</i>	<i>Gorilla</i>	170	168	47	48	2	0.147

¹ Mean_A, mean of Genus A; N_A, sample size of Genus A; Mean_B, mean of Genus B; N_B, sample size of Genus B; | θ |, absolute value of difference between observed sample means; p, probability that a difference between the bootstrapped means equaled or exceeded | θ |. Numbers in bold indicate statistical significance at $\alpha = .01$.

The capitate and radius articulations. The angle between these two surfaces is significantly different in one of the three pairwise comparisons between hominine genus means (Table 6.2). No significant differences in this angle are observed between *Homo* (32°) and *Pan* (33°), or between *Homo* and *Gorilla* (31°). However, the mean angle is significantly wider in *Pan* (33°) than in *Gorilla* (31°), even though the difference between these means is only 2°. This result occurs because the distributions of this angle for *Pan* and *Gorilla* are, in fact, different enough from one another for the means to appear significantly different, despite the fact that the distributions considerably overlap one another.

TABLE 6.2 Pairwise comparisons of genus means for the angle between the capitate and radius joint surfaces¹

Genus A	Genus B	Mean _A	Mean _B	N _A	N _B	θ	p
<i>Homo</i>	<i>Pan</i>	32	33	117	48	1	0.273
<i>Homo</i>	<i>Gorilla</i>	32	31	117	48	1	0.032
<i>Pan</i>	<i>Gorilla</i>	33	31	48	48	2	0.009

¹ Mean_A, mean of Genus A; N_A, sample size of Genus A; Mean_B, mean of Genus B; N_B, sample size of Genus B; | θ |, absolute value of difference between observed sample means; p, probability that a difference between the bootstrapped means equaled or exceeded | θ |. Numbers in bold indicate statistical significance at alpha = .01.

The capitate and trapezium-trapezoid articulations. The angle between these two surfaces is significantly different in eight of the ten pairwise comparisons between genus means (Table 6.3). This angle is significantly wider in *Homo* (82°) than in the other genera. *Pan* (67°) and *Gorilla* (70°) also have significantly wider angles than does either *Pongo* (56°) or *Papio* (58°). The angle is not significantly different between *Pan* and *Gorilla*, or between *Pongo* and *Papio*.

TABLE 6.3 Pairwise comparisons of genus means for the angle between the capitate and trapezium-trapezoid joint surfaces¹

Genus A	Genus B	Mean _A	Mean _B	N _A	N _B	θ	p
<i>Homo</i>	<i>Pan</i>	82	67	117	48	15	<.001
<i>Homo</i>	<i>Gorilla</i>	82	70	117	48	12	<.001
<i>Homo</i>	<i>Pongo</i>	82	56	117	19	26	<.001
<i>Homo</i>	<i>Papio</i>	82	58	117	22	24	<.001
<i>Pan</i>	<i>Gorilla</i>	67	70	48	48	2	0.065
<i>Pan</i>	<i>Pongo</i>	67	56	48	19	11	<.001
<i>Pan</i>	<i>Papio</i>	67	58	48	22	9	<.001
<i>Gorilla</i>	<i>Pongo</i>	70	56	48	19	14	<.001
<i>Gorilla</i>	<i>Papio</i>	70	58	48	22	12	<.001
<i>Pongo</i>	<i>Papio</i>	56	58	19	22	2	0.424

¹ Mean_A, mean of Genus A; N_A, sample size of Genus A; Mean_B, mean of Genus B; N_B, sample size of Genus B; | θ |, absolute value of difference between observed sample means; p, probability that a difference between the bootstrapped means equaled or exceeded | θ |. Numbers in bold indicate statistical significance at alpha = .01.

The lunate and radius articulations. The angle between these two surfaces is significantly different in nine of the ten pairwise comparisons between genus means (Table 6.4). Only between *Pan* (38°) and *Gorilla* (39°) is this angle not significantly different. A significantly wider angle is present in *Papio* (52°) compared with the other genera, whereas *Pongo* (30°) has a significantly narrower angle than do the rest. *Homo* (45°) also has a significantly wider angle than do either of the African apes.

TABLE 6.4 Pairwise comparisons of genus means for the angle between the lunate and radius joint surfaces¹

Genus A	Genus B	Mean _A	Mean _B	N _A	N _B	θ	p
<i>Homo</i>	<i>Pan</i>	45	38	116	47	7	<.001
<i>Homo</i>	<i>Gorilla</i>	45	39	116	48	6	<.001
<i>Homo</i>	<i>Pongo</i>	45	30	116	20	16	<.001
<i>Homo</i>	<i>Papio</i>	45	52	116	22	7	<.001
<i>Pan</i>	<i>Gorilla</i>	38	39	47	48	1	0.477
<i>Pan</i>	<i>Pongo</i>	38	30	47	20	8	<.001
<i>Pan</i>	<i>Papio</i>	38	52	47	22	14	<.001
<i>Gorilla</i>	<i>Pongo</i>	39	30	48	20	9	<.001
<i>Gorilla</i>	<i>Papio</i>	39	52	48	22	13	<.001
<i>Pongo</i>	<i>Papio</i>	30	52	20	22	22	<.001

¹ Mean_A, mean of Genus A; N_A, sample size of Genus A; Mean_B, mean of Genus B; N_B, sample size of Genus B; | θ |, absolute value of difference between observed sample means; p, probability that a difference between the bootstrapped means equaled or exceeded | θ |. Numbers in bold indicate statistical significance at alpha = .01.

The lunate and trapezium-trapezoid articulations. The angle between these two surfaces is not significantly different in any of the three pairwise comparisons between *Homo* (60°), *Pan* (62°), and *Gorilla* (60°; Table 6.5).

TABLE 6.5 Pairwise comparisons of genus means for the angle between the lunate and trapezium-trapezoid joint surfaces¹

Genus A	Genus B	Mean _A	Mean _B	N _A	N _B	θ	p
<i>Homo</i>	<i>Pan</i>	60	62	116	47	1	0.298
<i>Homo</i>	<i>Gorilla</i>	60	60	116	48	0	0.832
<i>Pan</i>	<i>Gorilla</i>	62	60	47	48	2	0.351

¹ Mean_A, mean of Genus A; N_A, sample size of Genus A; Mean_B, mean of Genus B; N_B, sample size of Genus B; | θ |, absolute value of difference between observed sample means; p, probability that a difference between the bootstrapped means equaled or exceeded | θ |. Numbers in bold indicate statistical significance at alpha = .01.

The radius and trapezium-trapezoid articulations. The angle between these two surfaces is significantly different in two of the three pairwise comparisons between genus means (Table 6.6). This angle is significantly narrower in *Homo* (79°) than in the African apes. No significant difference in this angle is observed between *Pan* (83°), and *Gorilla* (83°).

TABLE 6.6 Pairwise comparisons of genus means for the angle between the radius and trapezium-trapezoid joint surfaces¹

Genus A	Genus B	Mean _A	Mean _B	N _A	N _B	θ	p
<i>Homo</i>	<i>Pan</i>	79	83	117	48	4	<.001
<i>Homo</i>	<i>Gorilla</i>	79	83	117	48	5	<.001
<i>Pan</i>	<i>Gorilla</i>	83	83	48	48	0	0.81

¹ Mean_A, mean of Genus A; N_A, sample size of Genus A; Mean_B, mean of Genus B; N_B, sample size of Genus B; | θ |, absolute value of difference between observed sample means; p, probability that a difference between the bootstrapped means equaled or exceeded | θ |. Numbers in bold indicate statistical significance at alpha = .01.

Relative areas of the scaphoid

Capitate articulation. The relative area of the capitate joint surface is significantly different in eight of the ten pairwise comparisons between genus means (Table 6.7).

This relative area is significantly larger in *Homo* (15%) and *Pan* (14.8%) than in all the other genera, and in *Gorilla* (12.3%) it is also significantly larger than in either *Papio* (9.1%) or *Pongo* (10.2%).

TABLE 6.7 Pairwise comparisons of genus means for relative area of the capitate joint surface¹

Genus A	Genus B	Mean _A	Mean _B	N _A	N _B	θ	p
<i>Homo</i>	<i>Pan</i>	15.0	14.8	117	48	0.1	0.669
<i>Homo</i>	<i>Gorilla</i>	15.0	12.3	117	48	2.7	<.001
<i>Homo</i>	<i>Pongo</i>	15.0	10.2	117	19	4.8	<.001
<i>Homo</i>	<i>Papio</i>	15.0	9.1	117	22	5.8	<.001
<i>Pan</i>	<i>Gorilla</i>	14.8	12.3	48	48	2.5	<.001
<i>Pan</i>	<i>Pongo</i>	14.8	10.2	48	19	4.6	<.001
<i>Pan</i>	<i>Papio</i>	14.8	9.1	48	22	5.7	<.001
<i>Gorilla</i>	<i>Pongo</i>	12.3	10.2	48	19	2.1	<.001
<i>Gorilla</i>	<i>Papio</i>	12.3	9.1	48	22	3.2	<.001
<i>Pongo</i>	<i>Papio</i>	10.2	9.1	19	22	1.1	0.047

¹ Mean_A, mean of Genus A; N_A, sample size of Genus A; Mean_B, mean of Genus B; N_B, sample size of Genus B; | θ |, absolute value of difference between observed sample means; p, probability that a difference between the bootstrapped means equaled or exceeded | θ |. Numbers in bold indicate statistical significance at alpha = .01.

Lunate articulation. The relative area of the lunate joint surface is significantly different in seven of the ten pairwise comparisons between genus means (Table 6.8). This relative area is significantly larger in *Papio* (7.5%) than in the other genera, and *Pongo* (5.6%) also has a significantly larger relative area than do any of the hominines. No significant differences in this relative area occur between *Gorilla* (4%), *Pan* (3.9%), and *Homo* (3.6%).

TABLE 6.8 Pairwise comparisons of genus means for relative area of the lunate joint surface¹

Genus A	Genus B	Mean _A	Mean _B	N _A	N _B	θ	p
<i>Homo</i>	<i>Pan</i>	3.6	3.9	116	47	0.3	0.124
<i>Homo</i>	<i>Gorilla</i>	3.6	4.0	116	48	0.4	0.018
<i>Homo</i>	<i>Pongo</i>	3.6	5.6	116	19	2.0	<.001
<i>Homo</i>	<i>Papio</i>	3.6	7.5	116	22	3.9	<.001
<i>Pan</i>	<i>Gorilla</i>	3.9	4.0	47	48	0.2	0.444
<i>Pan</i>	<i>Pongo</i>	3.9	5.6	47	19	1.7	<.001
<i>Pan</i>	<i>Papio</i>	3.9	7.5	47	22	3.6	<.001
<i>Gorilla</i>	<i>Pongo</i>	4.0	5.6	48	19	1.5	<.001
<i>Gorilla</i>	<i>Papio</i>	4.0	7.5	48	22	3.4	<.001
<i>Pongo</i>	<i>Papio</i>	5.6	7.5	19	22	1.9	<.001

¹ Mean_A, mean of Genus A; N_A, sample size of Genus A; Mean_B, mean of Genus B; N_B, sample size of Genus B; | θ |, absolute value of difference between observed sample means; p, probability that a difference between the bootstrapped means equaled or exceeded | θ |. Numbers in bold indicate statistical significance at alpha = .01.

Radius articulation. The relative area of the radius joint surface is significantly different in six of the ten pairwise comparisons between genus means (Table 6.9). This relative area is significantly smaller in both *Gorilla* (21.4%) and *Pongo* (20.4%) compared with the other genera. No significant differences in this relative area occur between *Papio* (22.6%), *Pan* (22.7%), and *Homo* (22.8%).

TABLE 6.9 Pairwise comparisons of genus means for relative area of the radius joint surface¹

Genus A	Genus B	Mean _A	Mean _B	N _A	N _B	θ	p
<i>Homo</i>	<i>Pan</i>	22.8	22.7	117	48	0.2	0.67
<i>Homo</i>	<i>Gorilla</i>	22.8	21.4	117	48	1.4	<.001
<i>Homo</i>	<i>Pongo</i>	22.8	20.4	117	19	2.4	<.001
<i>Homo</i>	<i>Papio</i>	22.8	22.6	117	22	0.2	0.632
<i>Pan</i>	<i>Gorilla</i>	22.7	21.4	48	48	1.3	<.001
<i>Pan</i>	<i>Pongo</i>	22.7	20.4	48	19	2.3	0.001
<i>Pan</i>	<i>Papio</i>	22.7	22.6	48	22	0.1	0.889
<i>Gorilla</i>	<i>Pongo</i>	21.4	20.4	48	19	1.0	0.122
<i>Gorilla</i>	<i>Papio</i>	21.4	22.6	48	22	1.2	0.002
<i>Pongo</i>	<i>Papio</i>	20.4	22.6	19	22	2.2	0.002

¹ Mean_A, mean of Genus A; N_A, sample size of Genus A; Mean_B, mean of Genus B; N_B, sample size of Genus B; | θ |, absolute value of difference between observed sample means; p, probability that a difference between the bootstrapped means equaled or exceeded | θ |. Numbers in bold indicate statistical significance at alpha = .01.

Trapezium-Trapezoid articulation. The relative area of the trapezium-trapezoid joint surface is significantly different in nine of the ten pairwise comparisons between genus means (Table 6.10). The relative area is significantly larger in *Homo* (14.6%) than in all the other genera, while *Pan* (12.9%) also shows a significantly larger relative area than the other non-human taxa. In *Pongo* (10.4%), this relative area is significantly smaller than in both *Gorilla* (12.1%) and *Papio* (11.7%).

TABLE 6.10 Pairwise comparisons of genus means for relative area of the trapezium-trapezoid joint surface¹

Genus A	Genus B	Mean _A	Mean _B	N _A	N _B	θ	p
<i>Homo</i>	<i>Pan</i>	14.6	12.9	117	48	1.7	<.001
<i>Homo</i>	<i>Gorilla</i>	14.6	12.1	117	48	2.5	<.001
<i>Homo</i>	<i>Pongo</i>	14.6	10.4	117	19	4.2	<.001
<i>Homo</i>	<i>Papio</i>	14.6	11.7	117	22	2.9	<.001
<i>Pan</i>	<i>Gorilla</i>	12.9	12.1	48	48	0.8	0.005
<i>Pan</i>	<i>Pongo</i>	12.9	10.4	48	19	2.5	<.001
<i>Pan</i>	<i>Papio</i>	12.9	11.7	48	22	1.2	<.001
<i>Gorilla</i>	<i>Pongo</i>	12.1	10.4	48	19	1.7	0.001
<i>Gorilla</i>	<i>Papio</i>	12.1	11.7	48	22	0.4	0.255
<i>Pongo</i>	<i>Papio</i>	10.4	11.7	19	22	1.3	0.011

¹ Mean_A, mean of Genus A; N_A, sample size of Genus A; Mean_B, mean of Genus B; N_B, sample size of Genus B; | θ |, absolute value of difference between observed sample means; p, probability that a difference between the bootstrapped means equaled or exceeded | θ |. Numbers in bold indicate statistical significance at alpha = .01.

Non-articular surface. The relative non-articular area of the scaphoid is significantly different in nine of the ten pairwise comparisons between genus means (Table 6.11). This relative area is significantly smaller in *Homo* (44%) than in all the other genera, while *Pan* (45.8%) also shows a significantly smaller relative area than the other non-human taxa. In *Pongo* (53.4%), this relative area is significantly larger than in both *Gorilla* (50.2%) and *Papio* (49.1%).

TABLE 6.11 Pairwise comparisons of genus means for relative area of the non-articular surface¹

Genus A	Genus B	Mean _A	Mean _B	N _A	N _B	θ	p
<i>Homo</i>	<i>Pan</i>	44.0	45.8	117	48	1.8	0.003
<i>Homo</i>	<i>Gorilla</i>	44.0	50.2	117	48	6.2	<.001
<i>Homo</i>	<i>Pongo</i>	44.0	53.4	117	19	9.4	<.001
<i>Homo</i>	<i>Papio</i>	44.0	49.1	117	22	5.1	<.001
<i>Pan</i>	<i>Gorilla</i>	45.8	50.2	48	48	4.4	<.001
<i>Pan</i>	<i>Pongo</i>	45.8	53.4	48	19	7.7	<.001
<i>Pan</i>	<i>Papio</i>	45.8	49.1	48	22	3.3	<.001
<i>Gorilla</i>	<i>Pongo</i>	50.2	53.4	48	19	3.3	0.004
<i>Gorilla</i>	<i>Papio</i>	50.2	49.1	48	22	1.1	0.26
<i>Pongo</i>	<i>Papio</i>	53.4	49.1	19	22	4.4	<.001

¹ Mean_A, mean of Genus A; N_A, sample size of Genus A; Mean_B, mean of Genus B; N_B, sample size of Genus B; | θ |, absolute value of difference between observed sample means; p, probability that a difference between the bootstrapped means equaled or exceeded | θ |. Numbers in bold indicate statistical significance at alpha = .01.

Multivariate analyses

In this section, the results of the canonical and discriminant function analyses using two combinations of scaphoid carpal joint and non-articular variables are presented. In Full Model I, six scaphoid variables are used as predictor variables; these include two relative angles between articular surfaces and four relative articular areas. This analysis does not incorporate any angles that require coalescence of the scaphoid and centrale because of the typical unfused condition in *Pongo* and *Papio*. In Full Model II, *Pongo* and *Papio* are excluded and ten scaphoid variables are used as predictor variables; the variables include all six relative angles between joint surfaces, and four of the five relative areas (to avoid a singular covariance matrix). However, the results are statistically identical no matter which four relative areas are selected because the sixth is always implied by the others.

Full Model I: Six relative areas and angles (angles requiring scaphoid-centrale coalescence excluded). The first canonical axis (CAN1) accounts for 72% of the variation and the second (CAN2) accounts for 25%. Along CAN1, *Homo* clusters on the right whereas *Papio* clusters on the left. The great apes form a central cluster with the African apes more to the right and *Pongo* more to the left (Fig. 6.1). The correlations with CAN1 indicate that the observed variation represents the relative area of the lunate joint surface in comparison to the relative areas of the capitate and trapezium-trapezoid joint surfaces, as well as the angle between these two surfaces (Table 6.12). Along CAN2, *Papio* clusters more positively, the hominines cluster centrally, and *Pongo* clusters more negatively (Fig. 6.1). The correlations with CAN2

indicate that this axis represents a combination of the two angles, particularly the lunate-radius angle, as well as the relative trapezium-trapezoid joint surface area (Table 6.12).

Together, the first two axes result in four distinct clusters: one each for *Homo*, *Pongo*, and *Papio*, and one for African apes (Fig. 6.1). *Homo* has the largest angle between the capitate and trapezium-trapezoid joint surfaces, the largest relative capitate area, and the smallest relative lunate area (Tables 6.3, 6.7, and 6.8), all of which contribute to a more positive loading along CAN1. Alternatively, *Papio* and *Pongo* show the smallest angles between the capitate and trapezium-trapezoid joint surfaces, the smallest relative capitate areas, and the largest relative lunate areas, all of which contribute to a more negative loading along CAN1. *Papio* also has the largest angle between the lunate and radius joint surfaces (Table 6.4), which has a strong positive loading along CAN2.

The cross-validation procedure of the discriminant function analysis resulted in the correct classification of 103 *Homo* (88.8%), 36 *Pan* (76.6%), 35 *Gorilla* (72.9%), 15 *Pongo* (79%), and 22 *Papio* (100%; Table 6.13). The majority of misclassifications occur among the hominines (34/41). Overall, the results indicate that these six relative measures of scaphoid articular surfaces are effective in discriminating between *Homo*, *Papio*, and the great apes collectively.

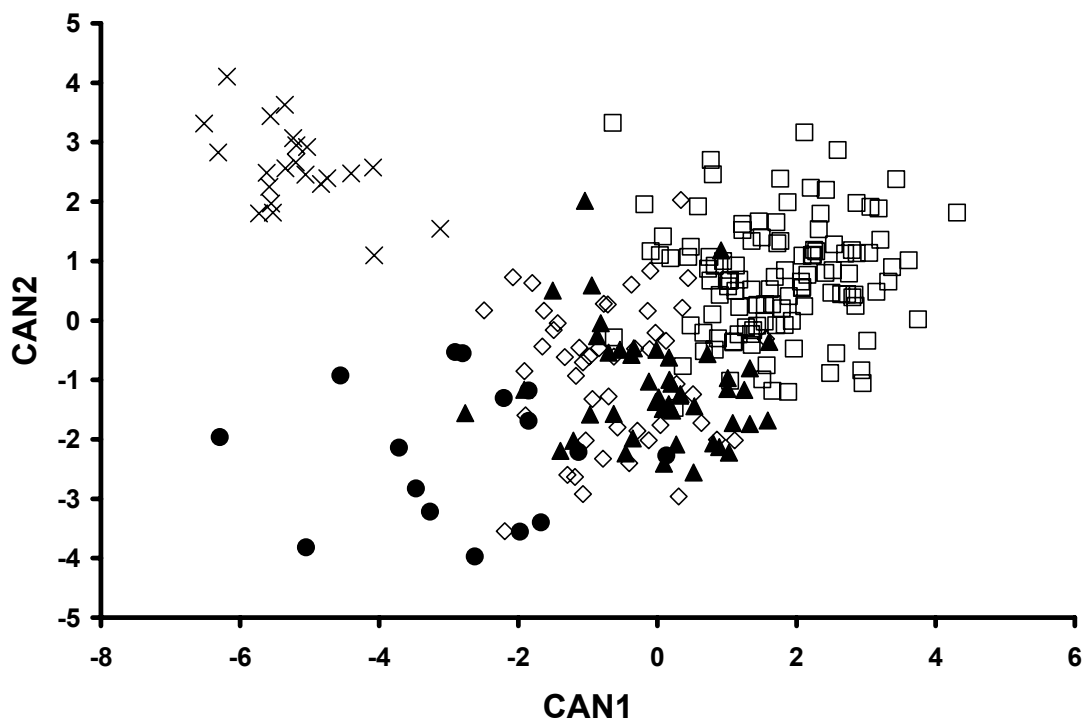


Fig. 6.1 Plot of the canonical variables (CAN1, CAN2) generated from analysis of six relative areas and angles of the scaphoid articular surfaces (*Homo* = open squares, *Pan* = closed triangles, *Gorilla* = open diamonds, *Pongo* = closed circles, *Papio* = Xs).

TABLE 6.12 Correlations between each variable and canonical axis (bolded values indicate the variables that best explain the observed variation along each axis)

Variable		Pooled-within canonical structure	
		CAN1	CAN2
Angle between			
capitate	trapezium-trapezoid	0.53	0.35
lunate	radius	0.05	0.68
<u>Relative surface area</u>			
	capitate	0.52	-0.01
	lunate	-0.42	0.22
	radius	0.08	0.18
	trapezium-trapezoid	0.34	0.32

TABLE 6.13 Cross-validated posterior probabilities of genus membership using six relative areas and angles of the scaphoid articular surfaces

	<i>Homo</i>	<i>Pan</i>	<i>Gorilla</i>	<i>Pongo</i>	<i>Papio</i>
<i>Homo</i>	103	8	5	0	0
%	88.8	6.9	4.3	0.0	0.0
<i>Pan</i>	2	36	7	2	0
%	4.3	76.6	14.9	4.3	0.0
<i>Gorilla</i>	4	8	35	1	0
%	8.3	16.7	72.9	2.1	0.0
<i>Pongo</i>	0	1	3	15	0
%	0.0	5.3	15.8	79.0	0.0
<i>Papio</i>	0	0	0	0	22
%	0.0	0.0	0.0	0.0	100.0

Full Model II: Ten relative areas and angles (Pongo and Papio excluded). The first canonical axis (CAN1) accounts for 87% of the variation and the second (CAN2) accounts for 13%. Along CAN1, *Homo* clusters on the right whereas the African apes cluster to the left (Fig. 6.2). The correlations with CAN1 indicate that the observed variation represents the angle between the capitate and lunate joint surfaces in comparison to the relative area of the trapezium-trapezoid joint surfaces, as well as the angles between the capitate and trapezium-trapezoid joint surfaces and between the lunate and radius joint surfaces (Table 6.14). Along CAN2, *Pan* clusters more positively, and *Gorilla* clusters more negatively, with *Homo* spread out in between (Fig. 6.2). The correlations with CAN2 indicate that this axis primarily represents the relative area of the capitate joint surface (Table 6.14).

Together, the first two axes result in three distinct clusters: one each for *Homo*, *Pan*, and *Gorilla* (Fig. 6.2). The results are essentially the same as presented in Full Model I,

except that the larger relative area of the capitate in *Pan* helps separate this taxon from *Gorilla* along CAN2.

The cross-validation procedure of the discriminant function analysis resulted in the correct classification of 107 *Homo* (92.2%), 35 *Pan* (74.5%), and 38 *Gorilla* (79.2%; Table 6.15). Overall, the results indicate that these ten measures of the scaphoid articular surfaces are effective in discriminating between *Pan*, *Gorilla*, and in particular, *Homo*.

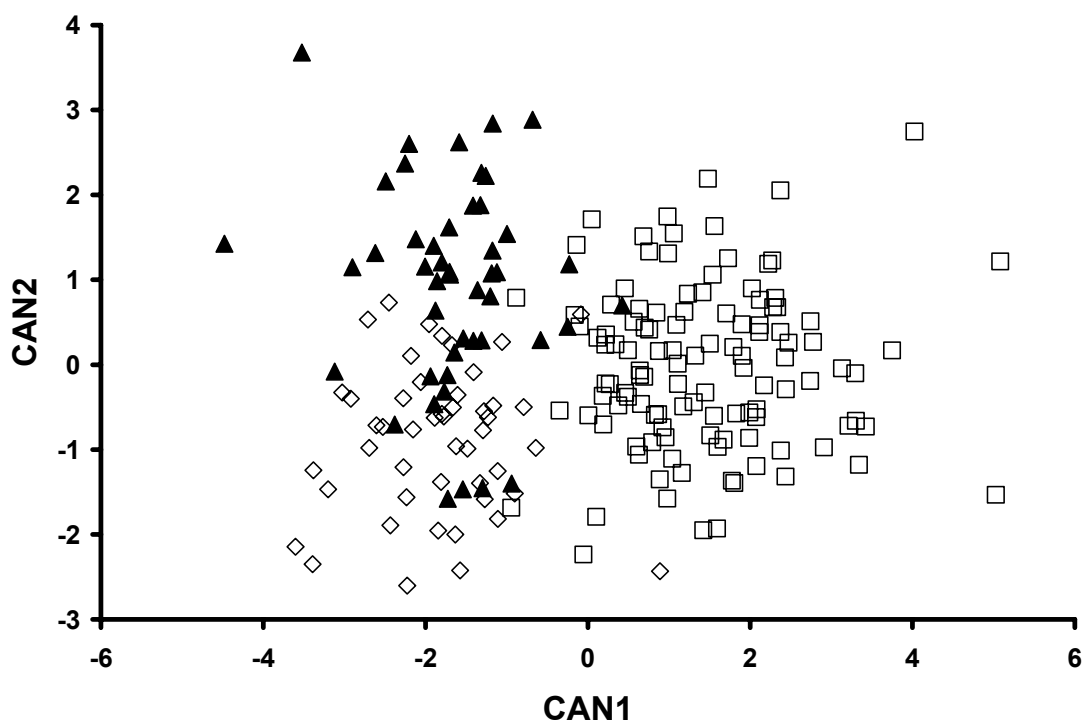


Fig. 6.2 Plot of the canonical variables (CAN1, CAN2) generated from analysis of ten relative areas and angles of the scaphoid articular surfaces (*Homo* = open squares, *Pan* = closed triangles, *Gorilla* = open diamonds, *Pongo* = closed circles, *Papio* = Xs).

TABLE 6.14 Correlations between each variable and canonical axis (bolded values indicate the variables that best explain the observed variation along each axis)

Variable		Pooled-within canonical structure	
Angle between		CAN1	CAN2
capitate	lunate	-0.50	0.18
capitate	radius	0.04	0.26
capitate	trapezium-trapezoid	0.56	-0.24
lunate	radius	0.34	-0.12
lunate	trapezium-trapezoid	-0.02	0.12
radius	trapezium-trapezoid	-0.24	0.03
<u>Relative surface area</u>			
	capitate	0.27	0.77
	lunate	-0.10	-0.07
	radius	0.11	0.30
	trapezium-trapezoid	0.39	0.21

TABLE 6.15 Cross-validated posterior probabilities of genus membership using ten relative areas and angles of the scaphoid articular surfaces

	<i>Homo</i>	<i>Pan</i>	<i>Gorilla</i>
<i>Homo</i>	107	5	4
%	92.2	4.3	3.5
<i>Pan</i>	2	35	10
%	4.3	74.5	21.3
<i>Gorilla</i>	2	8	38
%	4.2	16.7	79.2

Summary of shape characteristics

TABLE 6.16 Summary of mean scaphoid carpal joint and non-articular features (distinctive features shown in bold)

Variable		Genus				
Angle between		<i>Homo</i>	<i>Pan</i>	<i>Gorilla</i>	<i>Pongo</i>	<i>Papio</i>
capitate	lunate	157	170	168		
capitate	radius	32	33	31		
capitate	trapezium-trapezoid	82	67	70	56	58
lunate	radius	45	38	39	30	52
lunate	trapezium-trapezoid	60	62	60		
radius	trapezium-trapezoid	79	83	83		
<u>Relative surface area</u>						
	capitate	15.0	14.8	12.3	10.2	9.1
	lunate	3.6	3.9	4.0	5.6	7.5
	radius	22.8	22.7	21.4	20.4	22.6
	trapezium-trapezoid	14.6	12.9	12.1	10.4	11.7
	non-articular	44.0	45.8	50.2	53.4	49.1

Papio. The probability of correctly classifying *Papio* based on features of the scaphoid carpal joints and non-articular area was 100%, and no hominid specimens were misclassified as *Papio* (Table 6.13). The scaphoid features that best characterize *Papio* are the angle between the lunate and radius joint surfaces, the angle between the capitate and trapezium-trapezoid joint surfaces, and the relative areas of the capitate and lunate surfaces (Table 6.16).

In *Papio*, distinct articular facets for the lunate appear on both the scaphoid and the centrale. On the centrale, the facet is located dorso-medially, behind and underneath the capitate facet; on the scaphoid, the facet is located palmar-medially directly in front of the capitate facet and variably extending into the proximal area underneath the capitate facet. In contrast, the hominids only display a lunate facet in the proximal area beneath the capitate facet, which is expanded in the areas where *Papio* displays the majority of its surfaces for the lunate. This morphological difference is reflected by *Papio* showing

the largest relative lunate area and the smallest relative capitate area (Tables 6.7 and 6.8), as well as the largest angle between the lunate and radius joint surfaces (Table 6.4).

Pongo. The probability of correctly classifying *Pongo* based on features of the scaphoid carpal joints and non-articular area was 79% (Table 6.13); three *Pongo* specimens (16%) were misclassified as *Gorilla*, and one (5%) as *Pan*. The scaphoid features that best characterize *Pongo* are the angle between the lunate and radius joint surfaces, the angle between the capitate and trapezium-trapezoid joint surfaces, the relative areas of the radius and trapezium-trapezoid joint surfaces, and the relative area of non-articular surface (Table 6.16).

As was observed with the *Pongo* trapezium, the scaphoid in this taxon appears somewhat intermediate in the characteristics that distinguish *Papio* from the hominines. The relative areas of the capitate and lunate joint surfaces in *Pongo* fall between those observed in *Papio* and the hominines; however, the angle between the lunate and radius joint surfaces is definitely more hominine-like. Lastly, the relative areas of the radius and trapezium-trapezoid joint surfaces are the smallest of the genera examined.

Gorilla. The probabilities of correctly classifying *Gorilla* based on features of the scaphoid carpal joints and non-articular area were 73% and 79% (Tables 6.13 and 6.15). In Full Model I, eight *Gorilla* specimens (17%) were misclassified as *Pan*, four as *Homo* (8%), and one (2%) as *Pongo*. In Full Model II, eight *Gorilla* specimens (17%) were again misclassified as *Pan*, and two as *Homo* (4%).

In general, the *Gorilla* scaphoid shares its features with that of the other great apes; however, the *Gorilla* scaphoid is distinct in that all of the relative areas fall between the values observed in *Pan* and *Pongo*, yet all of the relative angles are more similar to those in *Pan* (Table 6.16).

Pan. The probabilities of correctly classifying *Pan* based on features of the scaphoid carpal joints and non-articular area were 77% and 75% (Tables 6.13 and 6.15). In Full Model I, seven *Pan* specimens (15%) were misclassified as *Gorilla*, and two each as *Homo* (4%) and *Pongo* (4%). In Full Model II, ten *Pan* specimens (21%) were again misclassified as *Gorilla*, and two as *Homo* (4%).

Overall, the *Pan* scaphoid shows a combination of features that it shares with either *Gorilla* or *Homo*. All of the relative areas in *Pan* are most similar to those of *Homo*, whereas all of the relative angles are more akin to *Gorilla* (Table 6.16). Together, it is this combination of features that makes the *Pan* scaphoid distinct.

Homo. The probabilities of correctly classifying *Homo* based on features of the scaphoid carpal and metacarpal joints and non-articular area were 89% and 92% (Tables 6.13 and 6.15). In Full Model I, eight *Homo* specimens (7%) were misclassified as *Pan*, and five as *Gorilla* (4%). In Full Model II, five *Homo* specimens (4%) were misclassified as *Pan*, and four as *Gorilla* (4%). The scaphoid features that best characterize *Homo* are the capitate joint surface angles with the lunate and trapezium-trapezoid joint surfaces, the angle between the radius and trapezium-trapezoid joint surfaces, the relative areas of the capitate, lunate, and trapezium-trapezoid joint surfaces, and the relative area of non-articular surface (Table 6.16).

Although the scaphoid in *Homo* generally appears more African ape-like than does either *Pongo* or *Papio*, there is no question that it displays several uniquely-derived characteristics. For instance, in *Homo* the relative area of the lunate joint surface is smallest. Moreover, the angle between the capitate and lunate joint surfaces is narrowest whereas the angle between the capitate and trapezium-trapezoid joint surfaces is widest. These angular changes reflect the reduced amount of bone present in *Homo* immediately distal to the capitate facet, where the trapezoid typically articulates. Recall that the proximal joint of the trapezoid is reduced in *Homo* and more rectangular in shape; the reduction of bone in the distal portion of the scaphoid corresponds with the reduction of the proximal joint of the trapezoid. However, also recall that the palmar aspect of the trapezoid has expanded radio-ulnarly, resulting in a reorientation of the trapezium relative to the other bones of the wrist. As discussed in previous chapters, the trapezium is effectively supinated and its articulation with the scaphoid expands further palmar-radially onto the scaphoid tubercle. Together, these changes make the *Homo* scaphoid quite distinct relative to other primates (Fig. 6.3).

DISCUSSION

The derived features of the scaphoid articular surfaces on the trapezium and trapezoid in modern humans were discussed in the previous chapters. In *Homo*, the scaphoid and first metacarpal articular surfaces of the trapezium are enlarged (reducing compressive stress) and oriented more parallel to one another (reducing shear stress). Similarly, the scaphoid articular surface of the trapezoid in *Homo* is smaller and more rectangular-shaped compared with the larger more triangular shape in other primates. The more

rectangular shape of the trapezoid places the trapezium-trapezoid and trapezoid-capitate joints more parallel to one another (reducing shear stress). Together these morphological features are a better design for accommodating joint reaction forces directed radio-ulnarly that result from strong contraction of the thumb musculature.

Several derived features on the modern human scaphoid strongly mimic the changes to the trapezium and trapezoid described above. In *Homo*, the reduction of bone along the distal border of the capitate joint surface corresponds with less surface area for the trapezoid joint surface—that is, change in trapezoid bone shape equates to change in scaphoid bone shape (Fig. 6.3, top and bottom rows; Fig. 6.4). However, the radio-ulnar expansion of the palmar aspect of the trapezoid reorients the trapezium and pushes it palmar-radially onto the scaphoid tubercle (Fig. 6.3, bottom row; Fig. 6.4). Similarly, the palmar-radial expansion of the trapezium-trapezoid joint corresponds with more surface area for the trapezium joint surface—that is, change in trapezium bone shape equates to change in scaphoid bone shape (Fig. 6.3, middle row; Fig. 6.4).

Since the primary relationships of these features to the biomechanical predictions of Chapter 2 were discussed in the previous chapters on trapezium and trapezoid morphology, I do not repeat them again here. However, there are a few additional points worth making. First, notice how the differences in the size, shape, and orientation of the capitate and trapezium-trapezoid joint surfaces impact this region of the wrist as a unit (Fig. 6.4). In *Homo*, the trapezium is more supinated and extends further palmarly and radially onto the scaphoid tubercle (Fig. 6.4A). These changes in the overall geometry of the carpus may influence general muscular function in this

region. Also, the opening up of the bony area distal to the scaphoid-capitate joint creates a novel relationship between the capitate joint surfaces on the trapezoid and scaphoid (Fig. 6.4B; Fig. 6.5). Together, the changes to the modern human trapezium, trapezoid, capitate, and scaphoid provide a better proximo-distally stabile design for withstanding the compressive and shear stresses associated with radio-ulnarly directed joint reaction forces, which arise from precision and power grips that involve strong contraction of the thumb musculature.

The derived changes seen in the scaphoid and trapezoid of *Homo* result in a combined joint surface for the capitate that is considerably larger and more palmarly-placed than that seen in other primates (Fig. 6.5). This enlarged combination of joint areas is better designed for distributing the compressive stress associated with radio-ulnarly directed joint reaction forces. Additionally, the configuration of the capitate-trapezoid and capitate-scaphoid joints appears reasonably flexible in distributing compressive stresses while minimizing shear regardless of whether the thumb is compressed into the trapezium in an abducted, adducted, flexed, extended, or neutral posture. In other words, a large proportion of the capitate-trapezoid and capitate-scaphoid joint surface area is always oriented approximately perpendicular to the applied force regardless of the exact position of the thumb (Fig. 6.6). The combination of derived features represents a complete reorganization of the radial carpal and carpometacarpal region of the wrist in comparison to the primitive primate condition. Such structural reorganization likely results in performance advantages for a wide variety of precision and power grips while the benefits for quadrupedal locomotor behaviors are sacrificed.

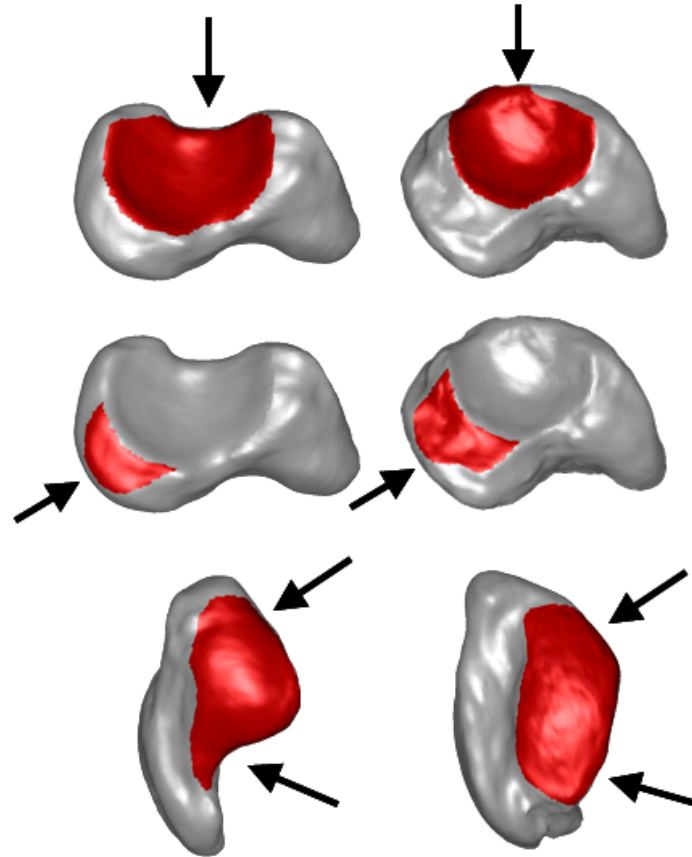


Fig. 6.3 Visual comparison of the different scaphoid joint morphology observed in *Homo* (at left) in comparison to other primates (*Pan* is shown at right). Key: top row, difference in distal portion of capitate joint; middle row, difference in relative area of lunate joint; bottom row, differences in shape and orientation of trapezium-trapezoid joint. Bones are from the right side.

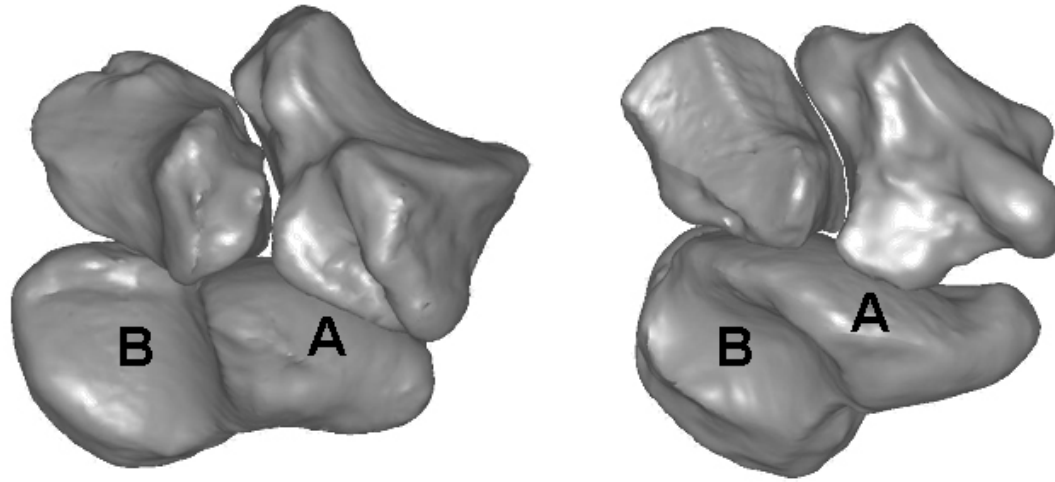


Fig. 6.4 Visual comparison of the differences between modern human and non-human primates in scaphoid morphology (*Homo*, shown at left; *Pan*, shown at right). The labeled features are derived in *Homo* relative to other primates; Key: **A**, larger scaphoid-trapezium joint; **B**, distally more open scaphoid-capitate joint. Bones are from the right side.

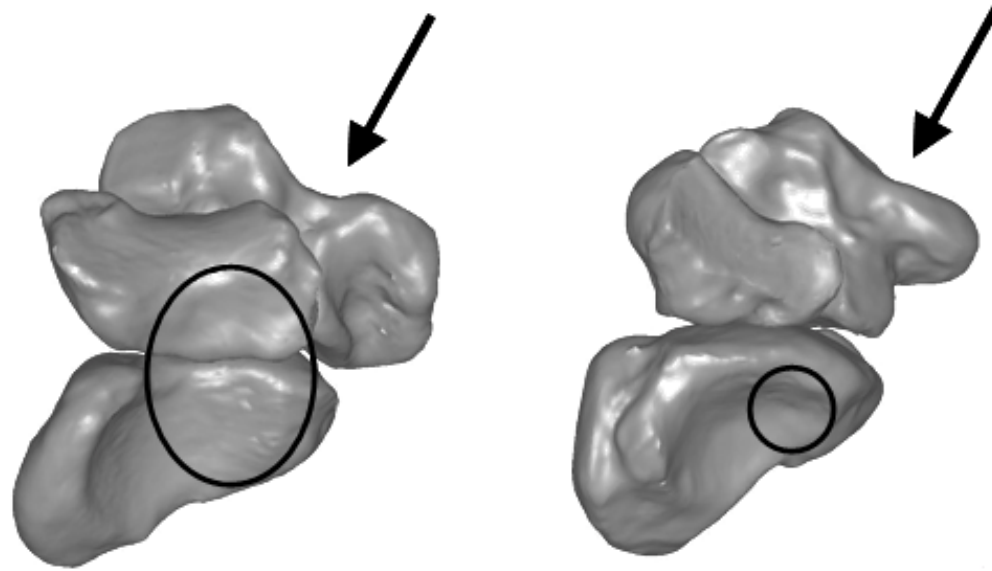


Fig. 6.5 Key differences, viewed medially, in scaphoid carpal joint morphology discussed in relation to the biomechanical predictions of Chapter 2 (*Homo*, shown at left; *Pan*, shown at right). The arrows denote the direction of applied net force at the first carpometacarpal joint during strong contraction of the thumb musculature. Note the larger ulnar joint area (circles) for the capitulum created by the combination of trapezoid and scaphoid joint surfaces in *Homo*.
Bones are from the right side.

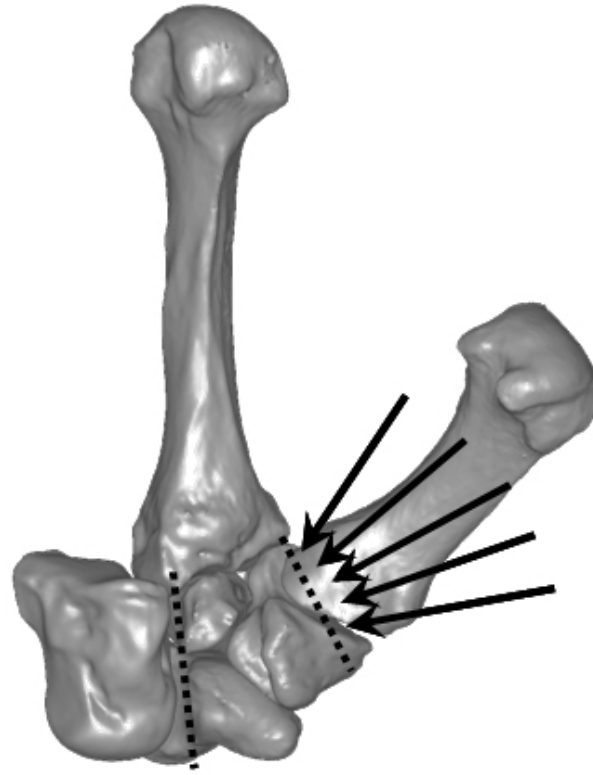


Fig. 6.6. The capitate-trapezoid and capitate-scapoid joints are oriented relative to the 1st carpometacarpal joint (dotted lines) such that shear stress is minimized regardless of the direction in which the thumb is compressed into the trapezium (arrows). Bones are from the right side.

Chapter 7: The Second Metacarpal Base

RESULTS OF SHAPE ANALYSES

In this section, I present the results of the shape analyses performed on the joints of the proximal end of the second metacarpal. Since all of the features examined in this chapter belong to the second metacarpal, the name of the articulating bone is used to describe each joint surface. For example, the area on the second metacarpal for articulation with the capitate is referred to as the capitate joint surface (Fig. 7.1). The trapezoid joint is divided into lateral and medial surfaces because in primates this joint is typically \wedge -shaped. The second metacarpal variables measured include the relative areas and angles of the carpometacarpal joints. The results of the comparative shape analyses for each variable are presented separately, followed by multivariate analysis of all the variables for each joint surface (Full Model). Following the presentation of the statistical results, a summary of the shape characteristics of each genus is given. Finally, the results are discussed in relation to the biomechanical predictions introduced in Chapter 2.

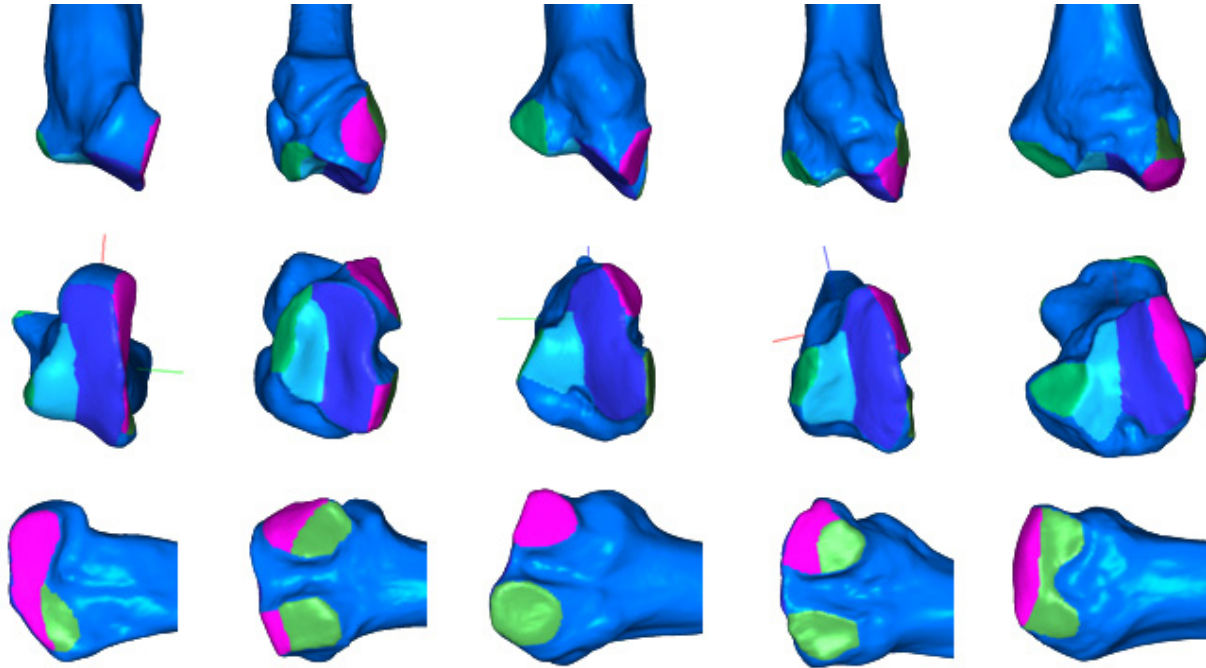


Fig. 7.1 Visual comparison of 2nd metacarpal base shape in five primate genera (*Papio*, far left; *Pongo*, 2nd from left; *Gorilla*, middle; *Pan*, 2nd from right; *Homo*, far right). Key: top row, palmar view; middle row, proximal view; bottom row, medial view; dark green, 3rd metacarpal joint; pink, capitate joint; dark blue, medial trapezoid joint; light blue, lateral trapezoid joint; light green, trapezium joint; medium blue, non-articular area. Bones are from the left side.

Angles of the second metacarpal base

The capitate and third metacarpal articulations. The angle between these two surfaces is significantly different in five of the ten pairwise comparisons between genus means (Table 7.1). This angle is significantly narrower in *Homo* (118°) than in the other genera, while in *Gorilla* (150°) it is significantly wider than in *Pan* (143°). No other significant differences in this angle are observed between *Pongo* (137°), *Papio* (146°), and the African apes.

TABLE 7.1 Pairwise comparisons of genus means for the angle between the capitate and 3rd metacarpal joint surfaces¹

Genus A	Genus B	Mean _A	Mean _B	N _A	N _B	θ	p
<i>Homo</i>	<i>Pan</i>	118	143	87	17	25	<.001
<i>Homo</i>	<i>Gorilla</i>	118	150	87	18	32	<.001
<i>Homo</i>	<i>Pongo</i>	118	137	87	12	19	0.001
<i>Homo</i>	<i>Papio</i>	118	146	87	21	28	<.001
<i>Pan</i>	<i>Gorilla</i>	143	150	17	18	7	0.002
<i>Pan</i>	<i>Pongo</i>	143	137	17	12	6	0.273
<i>Pan</i>	<i>Papio</i>	143	146	17	21	3	0.273
<i>Gorilla</i>	<i>Pongo</i>	150	137	18	12	13	0.015
<i>Gorilla</i>	<i>Papio</i>	150	146	18	21	4	0.18
<i>Pongo</i>	<i>Papio</i>	137	146	12	21	9	0.095

¹ Mean_A, mean of Genus A; N_A, sample size of Genus A; Mean_B, mean of Genus B; N_B, sample size of Genus B; | θ |, absolute value of difference between observed sample means; p, probability that a difference between the bootstrapped means equaled or exceeded | θ |. Numbers in bold indicate statistical significance at alpha = .01.

The capitate and medial trapezoid articulations. The angle between these two joint surfaces on the second metacarpal is significantly different in six of the ten pairwise comparisons between genus means (Table 7.2). This angle is significantly wider in *Homo* (112°) than in any of the other genera, whereas in *Pan* (67°) it is significantly narrower than in *Gorilla* (76°) and *Papio* (78°). No significant differences in this angle occur between *Pongo* (80°) and any of the non-*Homo* genera.

TABLE 7.2 Pairwise comparisons of genus means for the angle between the capitate and medial trapezoid surfaces¹

Genus A	Genus B	Mean _A	Mean _B	N _A	N _B	θ	p
<i>Homo</i>	<i>Pan</i>	112	67	87	17	45	<.001
<i>Homo</i>	<i>Gorilla</i>	112	76	87	18	37	<.001
<i>Homo</i>	<i>Pongo</i>	112	80	87	12	32	<.001
<i>Homo</i>	<i>Papio</i>	112	78	87	21	35	<.001
<i>Pan</i>	<i>Gorilla</i>	67	76	17	18	9	0.001
<i>Pan</i>	<i>Pongo</i>	67	80	17	12	13	0.023
<i>Pan</i>	<i>Papio</i>	67	78	17	21	11	<.001
<i>Gorilla</i>	<i>Pongo</i>	76	80	18	12	4	0.465
<i>Gorilla</i>	<i>Papio</i>	76	78	18	21	2	0.486
<i>Pongo</i>	<i>Papio</i>	80	78	12	21	2	0.704

¹ Mean_A, mean of Genus A; N_A, sample size of Genus A; Mean_B, mean of Genus B; N_B, sample size of Genus B; | θ |, absolute value of difference between observed sample means; p, probability that a difference between the bootstrapped means equaled or exceeded | θ |. Numbers in bold indicate statistical significance at alpha = .01.

The capitate and lateral trapezoid articulations. The angle between these two joint surfaces on the second metacarpal is significantly different in five of the ten pairwise comparisons between genus means (Table 7.3). This angle is significantly wider in *Homo* (158°) than in all the other genera, while *Papio* (116°) also shows a significantly wider angle than does *Gorilla* (108°). Neither *Pan* (112°) nor *Pongo* (102°) show any significant differences in this angle with the other non-*Homo* genera.

TABLE 7.3 Pairwise comparisons of genus means for the angle between the capitate and lateral trapezoid surfaces¹

Genus A	Genus B	Mean _A	Mean _B	N _A	N _B	θ	p
<i>Homo</i>	<i>Pan</i>	158	112	87	17	45	<.001
<i>Homo</i>	<i>Gorilla</i>	158	108	87	17	50	<.001
<i>Homo</i>	<i>Pongo</i>	158	102	87	12	56	<.001
<i>Homo</i>	<i>Papio</i>	158	116	87	21	41	<.001
<i>Pan</i>	<i>Gorilla</i>	112	108	17	17	5	0.114
<i>Pan</i>	<i>Pongo</i>	112	102	17	12	10	0.079
<i>Pan</i>	<i>Papio</i>	112	116	17	21	4	0.102
<i>Gorilla</i>	<i>Pongo</i>	108	102	17	12	6	0.343
<i>Gorilla</i>	<i>Papio</i>	108	116	17	21	9	0.001
<i>Pongo</i>	<i>Papio</i>	102	116	12	21	14	0.012

¹ Mean_A, mean of Genus A; N_A, sample size of Genus A; Mean_B, mean of Genus B; N_B, sample size of Genus B; | θ |, absolute value of difference between observed sample means; p, probability that a difference between the bootstrapped means equaled or exceeded | θ |. Numbers in bold indicate statistical significance at alpha = .01.

The capitate and trapezium articulations. The angle between these two joint surfaces on the second metacarpal is significantly different in nine of the ten pairwise comparisons between genus means (Table 7.4). Only between *Pan* (65°) and *Gorilla* (65°) is the difference between means non-significant. This angle is significantly wider in *Homo* (102°) than in the other genera, whereas in *Papio* (51°) it is significantly narrower. *Pongo* (83°) also shows a significantly wider angle than do the African apes.

TABLE 7.4 Pairwise comparisons of genus means for the angle between the capitate and trapezium joint surfaces¹

Genus A	Genus B	Mean _A	Mean _B	N _A	N _B	θ	p
<i>Homo</i>	<i>Pan</i>	102	65	85	17	37	<.001
<i>Homo</i>	<i>Gorilla</i>	102	65	85	17	37	<.001
<i>Homo</i>	<i>Pongo</i>	102	83	85	12	20	0.002
<i>Homo</i>	<i>Papio</i>	102	51	85	15	51	<.001
<i>Pan</i>	<i>Gorilla</i>	65	65	17	17	1	0.787
<i>Pan</i>	<i>Pongo</i>	65	83	17	12	18	0.007
<i>Pan</i>	<i>Papio</i>	65	51	17	15	14	<.001
<i>Gorilla</i>	<i>Pongo</i>	65	83	17	12	17	0.011
<i>Gorilla</i>	<i>Papio</i>	65	51	17	15	14	<.001
<i>Pongo</i>	<i>Papio</i>	83	51	12	15	32	<.001

¹ Mean_A, mean of Genus A; N_A, sample size of Genus A; Mean_B, mean of Genus B; N_B, sample size of Genus B; | θ |, absolute value of difference between observed sample means; p, probability that a difference between the bootstrapped means equaled or exceeded | θ |. Numbers in bold indicate statistical significance at alpha = .01.

The lateral trapezoid and trapezium articulations. The angle between these two joint surfaces on the second metacarpal is significantly different in six of the ten pairwise comparisons between genus means (Table 7.5). This angle is significantly wider in *Pongo* (115°) and *Homo* (114°) than in the other genera. No significant differences in this angle are observed between *Pan* (96°), *Gorilla* (100°), and *Papio* (100°).

TABLE 7.5 Pairwise comparisons of genus means for the angle between the lateral trapezoid and trapezium joint surfaces¹

Genus A	Genus B	Mean _A	Mean _B	N _A	N _B	θ	p
<i>Homo</i>	<i>Pan</i>	114	96	85	17	17	<.001
<i>Homo</i>	<i>Gorilla</i>	114	100	85	16	13	<.001
<i>Homo</i>	<i>Pongo</i>	114	115	85	12	1	0.744
<i>Homo</i>	<i>Papio</i>	114	100	85	15	14	<.001
<i>Pan</i>	<i>Gorilla</i>	96	100	17	16	4	0.299
<i>Pan</i>	<i>Pongo</i>	96	115	17	12	19	<.001
<i>Pan</i>	<i>Papio</i>	96	100	17	15	4	0.314
<i>Gorilla</i>	<i>Pongo</i>	100	115	16	12	15	0.002
<i>Gorilla</i>	<i>Papio</i>	100	100	16	15	1	0.893
<i>Pongo</i>	<i>Papio</i>	115	100	12	15	15	<.001

¹ Mean_A, mean of Genus A; N_A, sample size of Genus A; Mean_B, mean of Genus B; N_B, sample size of Genus B; | θ |, absolute value of difference between observed sample means; p, probability that a difference between the bootstrapped means equaled or exceeded | θ |. Numbers in bold indicate statistical significance at alpha = .01.

The lateral and medial trapezoid articulations. The angle between these two joint surfaces on the second metacarpal is significantly different in four of the ten pairwise comparisons between genus means (Table 7.6). The mean angle in both *Pan* (125°) and *Homo* (130°) is significantly narrower than in either *Gorilla* (142°) or *Papio* (137°). The angle in *Pongo* (136°) is not significantly different than in any of the other genera.

TABLE 7.6 Pairwise comparisons of genus means for the angle between the lateral and medial trapezoid joint surfaces¹

Genus A	Genus B	Mean _A	Mean _B	N _A	N _B	θ	p
<i>Homo</i>	<i>Pan</i>	130	125	87	17	5	0.033
<i>Homo</i>	<i>Gorilla</i>	130	142	87	17	12	<.001
<i>Homo</i>	<i>Pongo</i>	130	136	87	12	6	0.246
<i>Homo</i>	<i>Papio</i>	130	137	87	21	7	<.001
<i>Pan</i>	<i>Gorilla</i>	125	142	17	17	16	<.001
<i>Pan</i>	<i>Pongo</i>	125	136	17	12	11	0.053
<i>Pan</i>	<i>Papio</i>	125	137	17	21	11	<.001
<i>Gorilla</i>	<i>Pongo</i>	142	136	17	12	5	0.357
<i>Gorilla</i>	<i>Papio</i>	142	137	17	21	5	0.096
<i>Pongo</i>	<i>Papio</i>	136	137	12	21	0	0.929

¹ Mean_A, mean of Genus A; N_A, sample size of Genus A; Mean_B, mean of Genus B; N_B, sample size of Genus B; | θ |, absolute value of difference between observed sample means; p, probability that a difference between the bootstrapped means equaled or exceeded | θ |. Numbers in bold indicate statistical significance at alpha = .01.

The medial trapezoid and trapezium articulations. The angle between these two joint surfaces on the second metacarpal is significantly different in six of the ten pairwise comparisons between genus means (Table 7.7). This angle is significantly narrower in *Gorilla* (130°) than in the other genera, whereas *Pongo* (150°) shows a significantly wider angle than does either *Papio* (140°) or *Pan* (142°). The angle in *Homo* (145°) is not significantly different from that in any of the non-*Pongo* genera.

TABLE 7.7 Pairwise comparisons of genus means for the angle between the medial trapezoid and trapezium joint surfaces¹

Genus A	Genus B	Mean _A	Mean _B	N _A	N _B	θ	p
<i>Homo</i>	<i>Pan</i>	145	142	85	17	3	0.181
<i>Homo</i>	<i>Gorilla</i>	145	130	85	17	15	<.001
<i>Homo</i>	<i>Pongo</i>	145	150	85	12	4	0.047
<i>Homo</i>	<i>Papio</i>	145	140	85	15	5	0.025
<i>Pan</i>	<i>Gorilla</i>	142	130	17	17	12	<.001
<i>Pan</i>	<i>Pongo</i>	142	150	17	12	7	0.009
<i>Pan</i>	<i>Papio</i>	142	140	17	15	2	0.471
<i>Gorilla</i>	<i>Pongo</i>	130	150	17	12	20	<.001
<i>Gorilla</i>	<i>Papio</i>	130	140	17	15	10	0.003
<i>Pongo</i>	<i>Papio</i>	150	140	12	15	9	0.003

¹ Mean_A, mean of Genus A; N_A, sample size of Genus A; Mean_B, mean of Genus B; N_B, sample size of Genus B; | θ |, absolute value of difference between observed sample means; p, probability that a difference between the bootstrapped means equaled or exceeded | θ |. Numbers in bold indicate statistical significance at alpha = .01.

The third metacarpal and trapezium articulations. The angle between these two joint surfaces on the second metacarpal is significantly different in seven of the ten pairwise comparisons between genus means (Table 7.8). This angle is significantly wider in *Homo* (46°) and *Pongo* (46°) than in the other genera, whereas in *Papio* (26°) it is also significantly narrower than in *Gorilla* (38°). No significant differences in this angle occur between *Pan* (32°) and either *Gorilla* or *Papio*.

TABLE 7.8 Pairwise comparisons of genus means for the angle between the 3rd metacarpal and trapezium joint surfaces¹

Genus A	Genus B	Mean _A	Mean _B	N _A	N _B	θ	p
<i>Homo</i>	<i>Pan</i>	118	143	87	17	25	<.001
<i>Homo</i>	<i>Gorilla</i>	118	150	87	18	32	<.001
<i>Homo</i>	<i>Pongo</i>	118	137	87	12	19	0.001
<i>Homo</i>	<i>Papio</i>	118	146	87	21	28	<.001
<i>Pan</i>	<i>Gorilla</i>	143	150	17	18	7	0.002
<i>Pan</i>	<i>Pongo</i>	143	137	17	12	6	0.273
<i>Pan</i>	<i>Papio</i>	143	146	17	21	3	0.273
<i>Gorilla</i>	<i>Pongo</i>	150	137	18	12	13	0.015
<i>Gorilla</i>	<i>Papio</i>	150	146	18	21	4	0.18
<i>Pongo</i>	<i>Papio</i>	137	146	12	21	9	0.095

¹ Mean_A, mean of Genus A; N_A, sample size of Genus A; Mean_B, mean of Genus B; N_B, sample size of Genus B; | θ |, absolute value of difference between observed sample means; p, probability that a difference between the bootstrapped means equaled or exceeded | θ |. Numbers in bold indicate statistical significance at alpha = .01.

Relative areas of the second metacarpal base

Third metacarpal articulation. The relative area of this articular surface is significantly different in eight of the ten pairwise comparisons between genus means (Table 7.9). The mean relative area in *Homo* (23.9%) and *Pongo* (23.2%) is significantly larger than in the other genera, whereas *Papio* (15%) shows a significantly smaller area than does *Pan* (19.1%) or *Gorilla* (20.1%). No significant differences in this relative area occur between *Homo* and *Pongo*, or between *Pan* and *Gorilla*.

TABLE 7.9 Pairwise comparisons of genus means for relative area of the 3rd metacarpal joint surface¹

Genus A	Genus B	Mean _A	Mean _B	N _A	N _B	θ	p
<i>Homo</i>	<i>Pan</i>	23.9	19.1	87	17	4.8	<.001
<i>Homo</i>	<i>Gorilla</i>	23.9	20.1	87	18	3.8	<.001
<i>Homo</i>	<i>Pongo</i>	23.9	23.2	87	12	0.7	0.468
<i>Homo</i>	<i>Papio</i>	23.9	15.0	87	21	9.0	<.001
<i>Pan</i>	<i>Gorilla</i>	19.1	20.1	17	18	1.0	0.375
<i>Pan</i>	<i>Pongo</i>	19.1	23.2	17	12	4.1	0.002
<i>Pan</i>	<i>Papio</i>	19.1	15.0	17	21	4.1	0.001
<i>Gorilla</i>	<i>Pongo</i>	20.1	23.2	18	12	3.1	0.011
<i>Gorilla</i>	<i>Papio</i>	20.1	15.0	18	21	5.1	<.001
<i>Pongo</i>	<i>Papio</i>	23.2	15.0	12	21	8.2	<.001

¹ Mean_A, mean of Genus A; N_A, sample size of Genus A; Mean_B, mean of Genus B; N_B, sample size of Genus B; | θ |, absolute value of difference between observed sample means; p, probability that a difference between the bootstrapped means equaled or exceeded | θ |. Numbers in bold indicate statistical significance at alpha = .01.

Capitate articulation. The relative area of this articular surface is significantly different in eight of the ten pairwise comparisons between genus means (Table 7.10). The mean relative area in *Gorilla* (14.4%) and *Homo* (15.6%) is significantly smaller than in the other genera, whereas *Papio* (28.5%) also shows a significantly larger area than does *Pan* (20.1%) or *Pongo* (21.6%). No significant differences in this relative area occur between *Gorilla* and *Homo*, or between *Pan* and *Pongo*.

TABLE 7.10 Pairwise comparisons of genus means for relative area of the capitate joint surface¹

Genus A	Genus B	Mean _A	Mean _B	N _A	N _B	θ	p
<i>Homo</i>	<i>Pan</i>	15.6	20.1	87	17	4.5	<.001
<i>Homo</i>	<i>Gorilla</i>	15.6	14.4	87	18	1.2	0.21
<i>Homo</i>	<i>Pongo</i>	15.6	21.6	87	12	6.0	<.001
<i>Homo</i>	<i>Papio</i>	15.6	28.5	87	21	12.9	<.001
<i>Pan</i>	<i>Gorilla</i>	20.1	14.4	17	18	5.7	<.001
<i>Pan</i>	<i>Pongo</i>	20.1	21.6	17	12	1.5	0.305
<i>Pan</i>	<i>Papio</i>	20.1	28.5	17	21	8.3	<.001
<i>Gorilla</i>	<i>Pongo</i>	14.4	21.6	18	12	7.2	<.001
<i>Gorilla</i>	<i>Papio</i>	14.4	28.5	18	21	14.1	<.001
<i>Pongo</i>	<i>Papio</i>	21.6	28.5	12	21	6.9	<.001

¹ Mean_A, mean of Genus A; N_A, sample size of Genus A; Mean_B, mean of Genus B; N_B, sample size of Genus B; | θ |, absolute value of difference between observed sample means; p, probability that a difference between the bootstrapped means equaled or exceeded | θ |. Numbers in bold indicate statistical significance at alpha = .01.

Medial trapezoid articulation. The relative area of this articular surface is significantly different in nine of the ten pairwise comparisons between genus means (Table 7.11). Only between *Pan* (36.9%) and *Papio* (37.4%) is the difference between means non-significant. The mean relative area in *Pongo* (31.5%) is significantly smaller than in all other genera, whereas in *Gorilla* (43.6%) it is significantly larger than the rest. Both *Pan* and *Papio* also show significantly larger relative areas than does *Homo* (34.5%).

TABLE 7.11 Pairwise comparisons of genus means for relative area of the medial trapezoid joint surface¹

Genus A	Genus B	Mean _A	Mean _B	N _A	N _B	θ	p
<i>Homo</i>	<i>Pan</i>	34.5	36.9	87	17	2.4	0.001
<i>Homo</i>	<i>Gorilla</i>	34.5	43.6	87	18	9.1	<.001
<i>Homo</i>	<i>Pongo</i>	34.5	31.5	87	12	3.0	<.001
<i>Homo</i>	<i>Papio</i>	34.5	37.4	87	21	2.9	0.001
<i>Pan</i>	<i>Gorilla</i>	36.9	43.6	17	18	6.7	<.001
<i>Pan</i>	<i>Pongo</i>	36.9	31.5	17	12	5.4	<.001
<i>Pan</i>	<i>Papio</i>	36.9	37.4	17	21	0.5	0.57
<i>Gorilla</i>	<i>Pongo</i>	43.6	31.5	18	12	12.2	<.001
<i>Gorilla</i>	<i>Papio</i>	43.6	37.4	18	21	6.3	<.001
<i>Pongo</i>	<i>Papio</i>	31.5	37.4	12	21	5.9	<.001

¹ Mean_A, mean of Genus A; N_A, sample size of Genus A; Mean_B, mean of Genus B; N_B, sample size of Genus B; | θ |, absolute value of difference between observed sample means; p, probability that a difference between the bootstrapped means equaled or exceeded | θ |. Numbers in bold indicate statistical significance at alpha = .01.

Lateral trapezoid articulation. The relative area of this articular surface is significantly different in four of the ten pairwise comparisons between genus means (Table 7.12).

The mean relative area in *Pongo* (10.7%) is significantly smaller than in all other genera except *Gorilla* (14%). *Gorilla* also shows a significantly smaller area than does *Homo* (17.1%). No significant differences in this relative area occur between *Gorilla* and *Pan* (16%), between *Gorilla* and *Papio*, or between *Homo*, *Pan*, and *Papio* (16.7%).

TABLE 7.12 Pairwise comparisons of genus means for relative area of the lateral trapezoid joint surface¹

Genus A	Genus B	Mean _A	Mean _B	N _A	N _B	θ	p
<i>Homo</i>	<i>Pan</i>	17.1	16.0	87	17	1.1	0.091
<i>Homo</i>	<i>Gorilla</i>	17.1	14.0	87	17	3.1	0.004
<i>Homo</i>	<i>Pongo</i>	17.1	10.7	87	12	6.3	<.001
<i>Homo</i>	<i>Papio</i>	17.1	16.7	87	21	0.4	0.608
<i>Pan</i>	<i>Gorilla</i>	16.0	14.0	17	17	2.0	0.064
<i>Pan</i>	<i>Pongo</i>	16.0	10.7	17	12	5.2	<.001
<i>Pan</i>	<i>Papio</i>	16.0	16.7	17	21	0.7	0.446
<i>Gorilla</i>	<i>Pongo</i>	14.0	10.7	17	12	3.2	0.019
<i>Gorilla</i>	<i>Papio</i>	14.0	16.7	17	21	2.7	0.021
<i>Pongo</i>	<i>Papio</i>	10.7	16.7	12	21	5.9	<.001

¹ Mean_A, mean of Genus A; N_A, sample size of Genus A; Mean_B, mean of Genus B; N_B, sample size of Genus B; | θ |, absolute value of difference between observed sample means; p, probability that a difference between the bootstrapped means equaled or exceeded | θ |. Numbers in bold indicate statistical significance at alpha = .01.

Trapezium articulation. The relative area of this articular surface is significantly different in seven of the ten pairwise comparisons between genus means (Table 7.13). The mean relative area in *Pongo* (13%) is significantly larger than in all other genera, whereas *Papio* (3.5%) shows a significantly smaller area than do the rest. No significant differences in this relative area occur between *Homo* (9.1%), *Gorilla* (9.2%), and *Pan* (7.9%).

TABLE 7.13 Pairwise comparisons of genus means for relative area of the trapezium joint surface¹

Genus A	Genus B	Mean _A	Mean _B	N _A	N _B	θ	p
<i>Homo</i>	<i>Pan</i>	9.1	7.9	85	17	1.2	0.045
<i>Homo</i>	<i>Gorilla</i>	9.1	9.2	85	17	0.1	0.852
<i>Homo</i>	<i>Pongo</i>	9.1	13.0	85	12	3.9	<.001
<i>Homo</i>	<i>Papio</i>	9.1	3.5	85	15	5.5	<.001
<i>Pan</i>	<i>Gorilla</i>	7.9	9.2	17	17	1.3	0.063
<i>Pan</i>	<i>Pongo</i>	7.9	13.0	17	12	5.1	<.001
<i>Pan</i>	<i>Papio</i>	7.9	3.5	17	15	4.4	<.001
<i>Gorilla</i>	<i>Pongo</i>	9.2	13.0	17	12	3.8	<.001
<i>Gorilla</i>	<i>Papio</i>	9.2	3.5	17	15	5.6	<.001
<i>Pongo</i>	<i>Papio</i>	13.0	3.5	12	15	9.5	<.001

¹ Mean_A, mean of Genus A; N_A, sample size of Genus A; Mean_B, mean of Genus B; N_B, sample size of Genus B; | θ |, absolute value of difference between observed sample means; p, probability that a difference between the bootstrapped means equaled or exceeded | θ |. Numbers in bold indicate statistical significance at alpha = .01.

Multivariate analyses

In this section, the results of the canonical and discriminant function analyses using the joints of the second metacarpal base are presented. A total of twelve second metacarpal variables are used as predictor variables; these include eight angles between articular surfaces and four relative articular areas.

Full Model: Relative areas and angles. The first canonical axis (CAN1) accounts for 70% of the variation, the second (CAN2) accounts for 15%, and the third (CAN3) 12%. Along CAN1, *Homo* is clustered on the right, while the remaining taxa cluster on the left (Fig. 7.2). The correlations with CAN1 indicate that the separation along this axis is mostly accounted for by a comparison of the four angles involving the capitate joint surface (Table 7.14). Along CAN2, *Papio* clusters more negatively while *Pongo* clusters more positively, with the hominines spread out in between (Figs. 7.2 and 7.3). The correlations with CAN2 indicate that this axis represents the relative trapezium area along with the capitate-trapezium and third metacarpal-trapezium angles in comparison to the relative capitate area (Table 7.14). Along CAN3, *Gorilla* clusters more negatively while the remaining taxa cluster more positively (Fig. 7.3). The correlations with CAN3 indicate that this axis represents the relative medial trapezoid area in comparison with the trapezium-medial trapezoid angle and the relative capitate area (Table 7.14).

These three axes result in distinct clusters for each genus (Figs. 7.2 and 7.3). In *Homo*, the angle between the capitate and third metacarpal surfaces is significantly smaller than in any of the other taxa, while the remaining three capitate angles are

significantly larger in *Homo* (Tables 7.1-7.4). Together, these angles drive *Homo* positively along CAN1 whereas the rest are driven negatively. Compared with the hominids, the relative area of the capitate surface is largest in *Papio* while the relative area of the trapezium surface is smallest (Tables 7.10 and 7.13). Together, these two relative areas drive *Papio* negatively along CAN2 whereas the rest are driven positively. *Pongo*, in particular, loads the most positively along CAN2, and this is the result of this taxon having the largest relative area for the trapezium joint surfaces (Figs. 7.2 and 7.3).

Gorilla shows the smallest relative capitate area and the largest relative medial trapezoid area along with the smallest trapezium-medial trapezoid angle (Table 7.7, 7.10, and 7.11). Together, these three variables drive *Gorilla* negatively along CAN3, creating a cluster separate from that of *Pan* (Fig. 7.3).

The cross-validation procedure of the discriminant function analysis resulted in the correct classification of 84 *Homo* (99%), 13 *Pan* (77%), 16 *Gorilla* (100%), 9 *Pongo* (75%), and 15 *Papio* (100%; Table 7.15). Overall, the results indicate that the combined measures of the second metacarpal base joint surfaces are effective in discriminating all of these genera from each other, particularly *Homo*, *Gorilla*, and *Papio*.

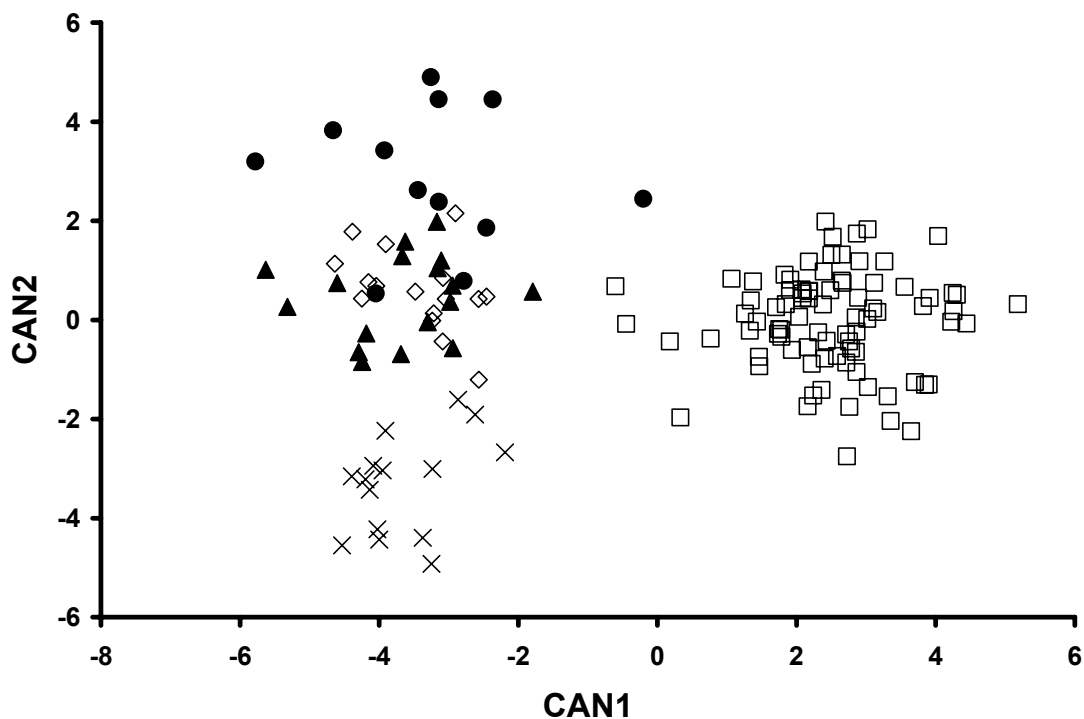


Fig. 7.2 Plot of the canonical variables (CAN1, CAN2) generated from analysis of the relative articular areas and angles of the 2nd metacarpal base (*Homo* = open squares, *Pan* = closed triangles, *Gorilla* = open diamonds, *Pongo* = closed circles, *Papio* = Xs).

TABLE 7.14 Correlations between each variable and canonical axis (bolded values indicate the variables that best explain the observed variation along each axis)

Variable		Pooled-within canonical structure		
		CAN1	CAN2	CAN3
Angle between				
capitate	3rd metacarpal	-0.38	-0.07	-0.17
capitate	lateral trapezoid	0.73	-0.23	-0.03
capitate	medial trapezoid	0.48	-0.03	0.05
capitate	trapezium	0.49	0.35	0.09
3rd metacarpal	trapezium	0.27	0.38	0.02
trapezium	lateral trapezoid	0.20	0.17	0.19
trapezium	medial trapezoid	0.12	0.11	0.46
lateral trapezoid	medial trapezoid	-0.09	-0.03	-0.13
Relative surface area				
capitate		-0.21	-0.30	0.51
trapezium		0.07	0.60	0.02
lateral trapezoid		0.11	-0.28	-0.10
medial trapezoid		-0.16	-0.19	-0.55

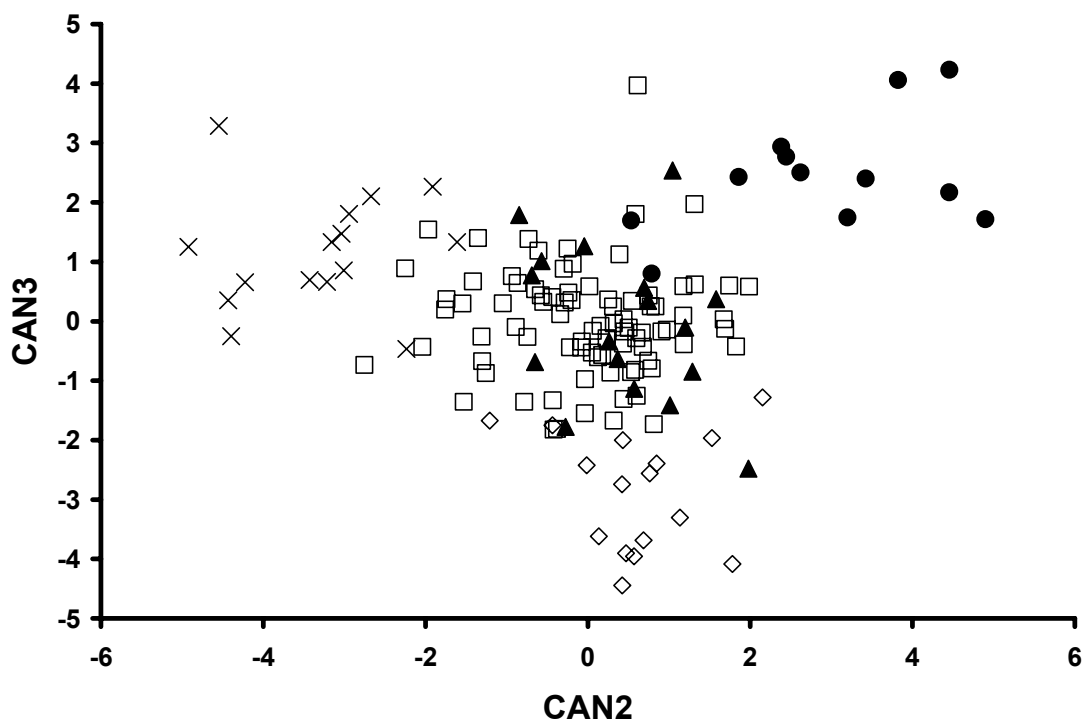


Fig. 7.3 Plot of the canonical variables (CAN2, CAN3) generated from analysis of the relative articular areas and angles of the 2nd metacarpal base (*Homo* = open squares, *Pan* = closed triangles, *Gorilla* = open diamonds, *Pongo* = closed circles, *Papio* = Xs).

TABLE 7.15 Cross-validated posterior probabilities of genus membership using the relative areas and angles of the articular surfaces of the 2nd metacarpal base

	<i>Homo</i>	<i>Pan</i>	<i>Gorilla</i>	<i>Pongo</i>	<i>Papio</i>
<i>Homo</i>	84	1	0	0	0
%	98.8	1.2	0.0	0.0	0.0
<i>Pan</i>	0	13	2	1	1
%	0.0	76.5	11.8	5.9	5.9
<i>Gorilla</i>	0	0	16	0	0
%	0.0	0.0	100.0	0.0	0.0
<i>Pongo</i>	1	1	1	9	0
%	8.3	8.3	8.3	75.0	0.0
<i>Papio</i>	0	0	0	0	15
%	0.0	0.0	0.0	0.0	100.0

Summary of shape characteristics

TABLE 7.16 Summary of mean 2nd metacarpal joint features (distinctive features in bold)

Variable		Genus				
Angle between		<i>Homo</i>	<i>Pan</i>	<i>Gorilla</i>	<i>Pongo</i>	<i>Papio</i>
capitate	3rd metacarpal	118	143	150	137	146
capitate	lateral trapezoid	158	112	108	102	116
capitate	medial trapezoid	112	67	76	80	78
capitate	trapezium	102	65	65	83	51
3rd metacarpal	trapezium	46	32	38	46	26
trapezium	lateral trapezoid	114	96	100	115	100
trapezium	medial trapezoid	145	142	130	150	140
lateral trapezoid	medial trapezoid	130	125	142	136	137
<u>Relative surface area</u>						
	capitate	15.6	20.1	14.4	21.6	28.5
	trapezium	9.1	7.9	9.2	13.0	3.5
	3rd metacarpal	23.9	19.1	20.1	23.2	15.0
	lateral trapezoid	17.1	16.0	14.0	10.7	16.7
	medial trapezoid	34.5	36.9	43.6	31.5	37.4

Papio. The probability of correctly classifying *Papio* based on features of the second metacarpal joints was 100% (Table 7.15). The joint surface features of the second metacarpal base that best characterize *Papio* are the capitate-trapezium angle, the third metacarpal-trapezium angle, and the relative areas of the capitate, trapezium, and third metacarpal joint surfaces (Table 7.16).

The trapezium and third metacarpal joint surfaces are typically relatively small in *Papio*, while the capitate joint surface is relatively large. All of these joint surfaces are oriented more in the sagittal plane, as evidenced by the angles with other joint surfaces. The mean third metacarpal-trapezium angle in *Papio* is 26°; this indicates the two surfaces are almost parallel with one another. The capitate joint surface is slightly offset from the third metacarpal surface (146°), resulting in a capitate-trapezium angle

that, although not completely parallel (51°), is narrower than that seen in the hominids (Table 7.16).

Pongo. The probability of correctly classifying *Pongo* based on features of the second metacarpal joints was 75% (Table 7.15); a single *Pongo* specimen (8%) was each misclassified as *Gorilla*, *Pan*, and *Homo*. The joint surface features of the second metacarpal base that best characterize *Pongo* are the capitate-lateral trapezoid angle, the third metacarpal-trapezium angle, the trapezium-lateral trapezoid angle, the trapezium-medial trapezoid angle, and the relative areas of the trapezium and lateral and medial trapezoid joint surfaces (Table 7.16).

The main distinguishing characteristics of the *Pongo* second metacarpal base relate to the morphological changes to the trapezium and lateral trapezoid joint surfaces. All four angles that appear somewhat distinct in *Pongo* involve either the trapezium or lateral trapezoid joint surfaces. The trapezium joint surface is large in *Pongo* and often extends palmarly across the entire lateral side of the second metacarpal base. This palmar expansion is reciprocated with the lateral trapezoid joint surface shifting to a more palmar position as well, resulting in a smaller relative area and subsequent changes to the angles between joint surfaces. The medial trapezoid relative area in *Pongo* also appears the smallest; however, this is more a reflection of the expanded trapezium area rather than a reduction of the medial trapezoid articulation itself.

Gorilla. The probability of correctly classifying *Gorilla* based on features of the second metacarpal joints was 100% (Table 7.15). The joint surface features of the second metacarpal base that best characterize *Gorilla* are the capitate-third metacarpal angle,

the trapezium-medial trapezoid angle, the lateral trapezoid-medial trapezoid angle, and the relative areas of the capitate and medial trapezoid joint surfaces (Table 7.16).

In *Gorilla*, the medial trapezoid joint area has expanded at the expense of the lateral trapezoid joint area; this results in changes in the relative angles involving the medial surface. *Gorilla* shows the widest angle between the lateral and medial trapezoid surfaces (146°) and the narrowest angle between the trapezium and medial trapezoid surfaces (130°). The relative capitate area is also small in *Gorilla*. The lateral side of the *Gorilla* second metacarpal shows two distinct facets, one palmar and one dorsal. Typically, the dorsal facet articulates solely with the third metacarpal whereas the palmar facet articulates solely with the capitate. Occasionally, the palmar facet also displays a small lip or facet for articulation with the third metacarpal as well. The typical condition in *Gorilla* is quite distinct from that in the other non-human taxa where either the palmar or dorsal facets (or both) articulate rather evenly with both the capitate and the third metacarpal.

Pan. The probability of correctly classifying *Pan* based on features of the second metacarpal joints was 77% (Table 7.15); two *Pan* specimens were misclassified as *Gorilla* (12%), and one each as *Pongo* (6%) and *Papio* (6%). The joint surface features of the second metacarpal base that best characterize *Pan* are the capitate-medial trapezoid angle, trapezium-lateral trapezoid angle, and the lateral trapezoid-medial trapezoid angle (Table 7.16).

Of the genera examined, the articular surfaces of the second metacarpal base are the least distinct in *Pan*. Although there are some distinguishing characteristics, most often

these are shared with at least one other taxon. That being said, the most distinctive feature of the second metacarpal base in *Pan* is its primary carpometacarpal joint. The \wedge -shaped joint surface is the most tightly notched, as evidenced by the narrowest angle between the lateral and medial trapezoid surfaces (125°). This angular difference of the trapezoid joint surfaces in *Pan* is further reflected by the resulting sharper angles between the capitate and medial trapezoid joint surfaces (67°) and between the trapezium and lateral trapezoid joint surfaces (96°).

Homo. The probability of correctly classifying *Homo* based on features of the second metacarpal joints was 99% (Table 7.15); a single *Homo* specimen was misclassified as *Pan* (1%). The joint surface features of the second metacarpal base that best characterize *Homo* are all four angles involving the capitate joint surface, the third metacarpal-trapezium angle, and the relative areas of the third metacarpal and lateral trapezoid joint surfaces (Table 7.16).

The main distinguishing characteristics of the *Homo* second metacarpal base relate to morphological changes to the trapezium and capitate joint surfaces. Both of these surfaces are oriented more proximally, as evidenced by all four angles involving the capitate surface (Table 7.16), as well as the wide angle between the trapezium and lateral trapezoid joint surfaces (114°).

The relative area of the capitate articulation in *Homo* has also reduced while the laterally-facing third metacarpal articular surface has expanded. These changes in articular areas are related to the presence of the third metacarpal styloid process, which accompanies a beveled dorso-distal surface of the capitate, and prevents the second

metacarpal base from articulating with the capitate dorsally (Marzke and Marzke, 1987).

DISCUSSION

The third biomechanical prediction of Chapter 2 stated that the carpal and carpometacarpal joints of modern humans should act to limit mobility proximo-distally, particularly when compressed radio-ulnarly (i.e., close-packed during forceful manipulative behaviors). In contrast, the carpal and carpometacarpal joints of non-human primates should act to limit mobility radio-ulnarly, particularly when compressed proximo-distally (i.e., close-packed during locomotor behaviors). These respective predictions are satisfied primarily through differences in the morphology of the second metacarpal base between modern human and non-human primates.

In modern humans, the trapezium-second metacarpal joint and the capitate-second metacarpal joint are both oriented more proximo-distally (Figs. 7.4 and 7.5). The orientation of these joints restricts movement or sliding of the trapezium and capitate in a distal direction. By stabilizing the trapezium, the mutually articulating surfaces of the trapezium-trapezoid joint maintain maximum surface area contact with one another. Similarly, by stabilizing the capitate, the mutually articulating surfaces of the trapezoid-capitate joint maintain maximum contact with one another. In contrast, the more radio-ulnar orientation of these joints in non-human primates prevents the second and third metacarpal bases from sliding or moving in a radio-ulnar direction; thus, minimizing the chance that either of these bases may sublux or slide during locomotion (Fig. 7.5).

In modern human and non-human primates, the flexor carpi radialis (FCR) and extensor carpi radialis (ECR—longus and brevis) muscles act in opposition to one another during wrist flexion and extension. The FCR tendon inserts primarily on the palmar portion of the second metacarpal base while the ECR longus tendon primarily inserts on the dorsal portion and the ECR brevis tendon primarily inserts on the dorsal portion of the third metacarpal base (Bowden and Bowden, 2005; Lewis, 1989; Olson, 1996). During wrist extension, the ECR muscles are recruited while the FCR acts as an antagonist helping to keep the radio-palmar region of the wrist stable.

In non-human primates, when the wrist is extended during locomotor behaviors the FCR stretches, producing a pull on the palmar base of the second metacarpal. This antagonistic action stabilizes the second metacarpal base and the trapezoid from moving too far distally with respect to the capitate and trapezium. This helps keep the base wedged in between the capitate and trapezium, reducing its mobility and preventing it from sliding radio-ulnarly (Fig. 7.5). Alternatively, in modern humans when the wrist is slightly extended during strong manipulative grasps (Napier, 1956), the antagonistic action of FCR on the second metacarpal base resists distal sliding of the capitate, trapezoid, and trapezium.

The styloid process of the third metacarpal base is also a derived feature in *Homo* and its development, function, and evolutionary history has been studied previously (Marzke and Marzke, 1987). The styloid process likely prevents subluxation of the third metacarpal base when large forces are proximally directed at the third metacarpal head via the third metacarpo-phalangeal joint (Marzke and Marzke, 1987). It is

possible that the third metacarpal styloid process in modern humans may also help stabilize the capitate (and possibly the second metacarpal base) from slipping dorsally while the second metacarpal base simultaneously stabilizes the palmar capitate-trapezoid-trapezium joints when the wrist is experiencing radio-ulnar compression during strong contraction of the thumb musculature (Figs. 7.5 and 7.6).

In summary, the basic primitive non-human primate pattern of carpal and carpometacarpal joint morphology in the radial wrist functions as follows: the capitate and trapezium stabilize the second metacarpal base from sliding radio-ulnarly such that the carpal and carpometacarpal mutual joint surfaces oriented perpendicular to proximo-distally directed joint reaction forces maintain maximum contact with one another. In contrast, the derived modern human pattern of carpal and carpometacarpal joint morphology in the radial wrist functions as follows: the second metacarpal base stabilizes the capitate and trapezium from sliding distally such that mutual joint surfaces oriented perpendicular to radio-ulnarly directed joint reaction forces maintain maximum contact with one another.

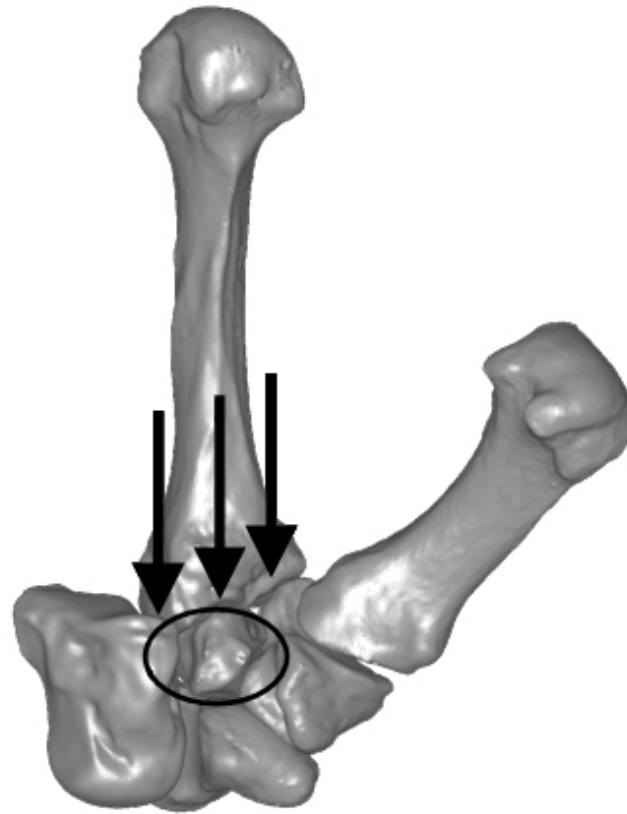


Fig. 7.4 In *Homo*, the 2nd metacarpal base acts to prevent the trapezium, trapezoid, and capitate from sliding distally with more proximo-distally oriented joints. This ensures that maximum joint surface area contact is maintained at the trapezium-trapezoid and capitate-trapezoid joints (circled portion). Bones are from the right side.

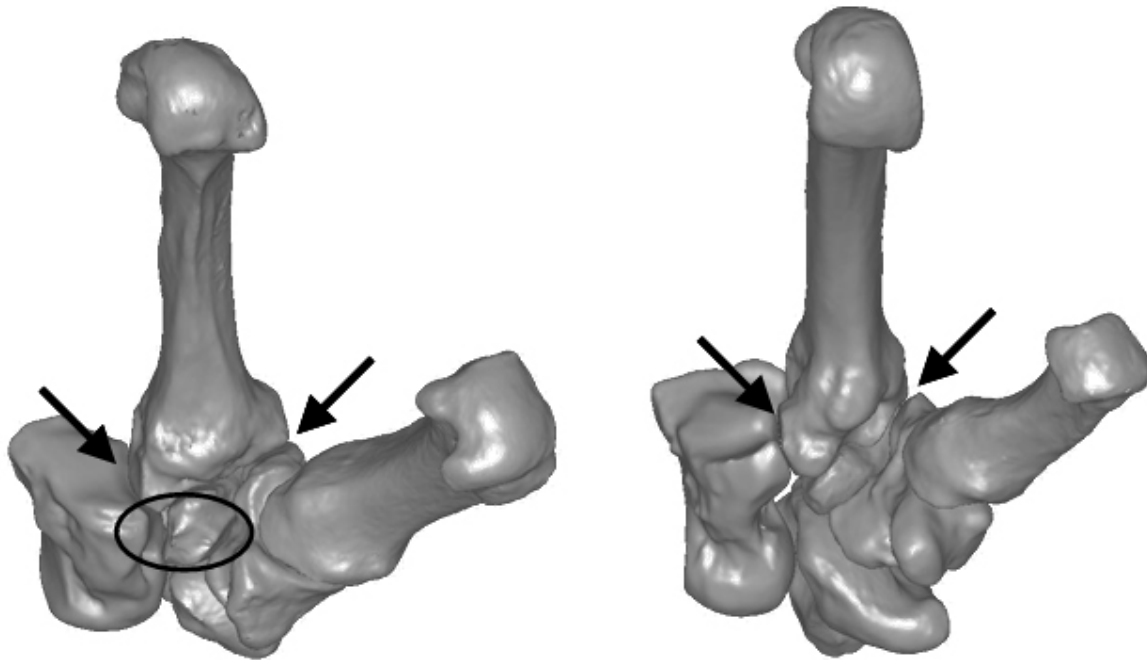


Fig. 7.5 Visual palmar comparison of the differences between modern human and non-human primates in 2nd carpometacarpal joint morphology (*Homo*, shown at left; *Pan*, shown at right). The arrows point to the more proximo-distally oriented joints in *Homo* versus the more radio-ulnarly oriented joints in the other genera. The derived features in *Homo* stabilize the inter-carpal joints of the trapezium, trapezoid, and capitate such that they maintain maximum contact with one another during radio-ulnar compression (circled area). Bones are from the right side.

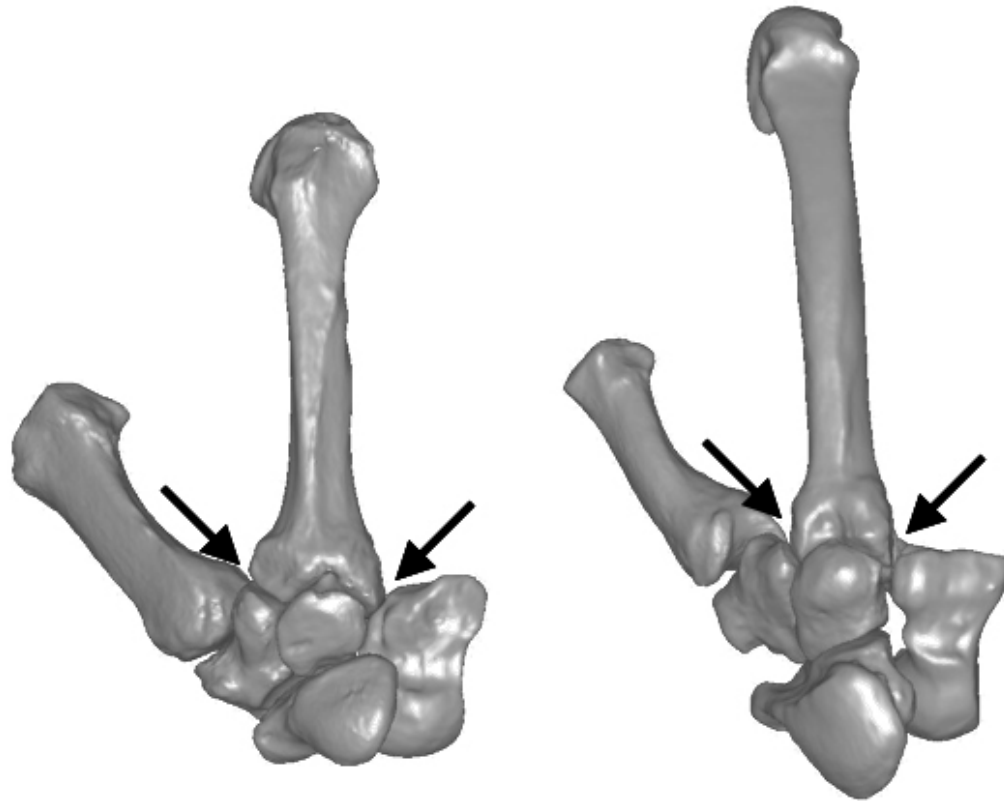


Fig. 7.6 Visual dorsal comparison of the differences between modern human and non-human primates in 2nd carpometacarpal joint morphology (*Homo*, shown at left; *Pan*, shown at right). The arrows point as in Figure 7.5. Bones are from the right side.

Chapter 8: Evolutionary History and Adaptive Significance

RESULTS OF SHAPE ANALYSES ON FOSSIL HOMININS

Among the five extant genera analyzed in the previous chapters, only modern *Homo sapiens* exhibits an entire complex of derived features that forms a radial carpal and carpometacarpal region that is more stable proximo-distally and more effective in distributing forces directed radially and ulnarly. This complex of derived morphology in modern *H. sapiens* is a more efficient design for distributing forces transversely across the wrist that arise from strong contraction of the thenar musculature during manipulative behaviors.

In this chapter, I investigate the evolutionary history and adaptive significance of this complex of derived features through an examination of the available hominin fossil evidence. The hominin fossil record presents several challenges to studying the evolution of the hominin hand. For instance, carpal and metacarpal remains of fossil hominin species are recovered considerably less often than craniodental remains (Ricklan, 1986a, b). Furthermore, when hand and wrist fossils are recovered, they are often isolated and fragmentary; thus, interpretations of the taxonomy and functional morphology are often tenuous at best (Marzke, 2005; Trinkaus and Long, 1990).

Despite these challenges, I performed quantitative 3D comparative analyses on available hominin fossil material. This material includes specimens of Upper Paleolithic *H. sapiens*, *Homo neanderthalensis*, *Homo habilis*, and *Australopithecus afarensis*, as well as the taxonomically tenuous first metacarpals SK84 and SKX5020. The multivariate analyses compare the fossil material only with modern *H. sapiens*, *Pan*, and *Gorilla* (unless otherwise noted) because of the known phylogenetic positions

of these taxa relative to other non-human primates (Eizirik et al., 2004; Kumar et al., 2005; Steiper and Young, 2006). The analytical results for each group of fossils are presented first in sequence from youngest fossil taxa to oldest, followed by five summary tables that include the individual measurements of each fossil specimen (see Tables 8.31-8.35). The presentation of the results is followed by a broad summary discussion regarding the evolutionary history and adaptive significance of the complex of derived morphology in hominins. This summary discussion includes data from additional fossil evidence that has been qualitatively described in the literature but was not part of the quantitative 3D comparative analyses of this research. Finally, the conclusions of this dissertation research are summarized and the implications for further research are discussed.

Upper Paleolithic *Homo sapiens* and *Homo neanderthalensis*

In the hominin fossil record, the hand and wrist are best represented for *H. neanderthalensis*. In fact, over 100 hand and wrist bones are preserved among the nine Neandertal specimens from Shanidar Cave in Iraq, including an almost complete left hand and wrist belonging to Shanidar 4 (Trinkaus, 1983). The Kebara 2 specimen also preserves both hands and wrists, each remarkably complete and well-preserved (Arensburg et al., 1985; Bar-Yosef et al., 1992).

A total of 28 carpal and metacarpal elements from undisputed Neandertal specimens along with seven elements from Upper Paleolithic *H. sapiens* are analyzed (see Chapter 9). Issues of fossil preservation preclude the ability to analyze the total complex of features in a single analysis. As such, the fossil comparative analysis is presented in

similar manner as was done for the extant analyses, through a series of canonical and discriminant function analyses. The analyses follow the biomechanical predictions introduced in Chapter 2, beginning with the first carpometacarpal joint where force is applied. Discussion of the results, however, is reserved until all analyses of the available fossil are presented.

The first carpometacarpal joint. A total of five complete first carpometacarpal joints, consisting of both articular surfaces, comprise the fossil sample. Upper Paleolithic *H. sapiens* is represented by Qafzeh 9, while *H. neanderthalensis* is represented by Kebara 2, Regourdou 1, La Ferrassie 1, and La Ferrassie 2.

Using a Full Model, the first carpometacarpal joints of these fossil hominins are compared to the extant hominine genera (Fig. 8.1). The variables utilized include the relative areas and curvedness measures of the mutually articulating surfaces. The fossils are used only as test classification cases. That is, the Full Model is based entirely on the three extant genera and is identical to that presented in Chapter 3, except in that *Pongo* and *Papio* are no longer included for comparison. The canonical scores of each fossil specimen are based on the particular measurements of each fossil joint.

The first canonical axis (CAN1) accounts for 85% of the variation while the second (CAN2) accounts for 15%. Along CAN1, modern *Homo* clusters more toward the right while the African apes cluster more toward the left (Fig. 8.1). All the fossils cluster clearly with modern *Homo*. The correlations with CAN1 (Table 8.1) indicate that this axis is a comparison of the absolute and RMS curvatures of both joint surfaces with the relative first metacarpal area of the trapezium and the Gaussian curvature of the

trapezium surface on the first metacarpal. The modern *Homo* cluster reflects a large relative first metacarpal area of the trapezium that is less curved than in the African apes; the four Neandertal joints and the joint of Qafzeh 9 all share these joint characteristics with modern *Homo* (Fig. 8.1).

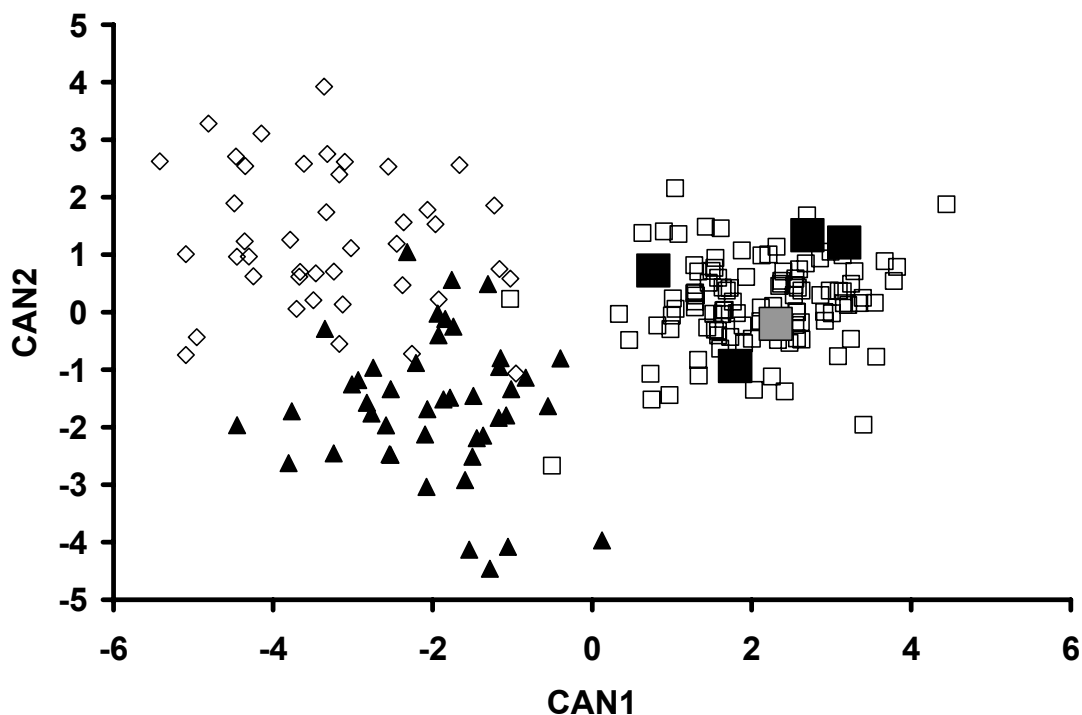


Fig. 8.1 Plot of the canonical variables (CAN1, CAN2) generated from analysis of the 1st carpometacarpal joint relative areas and curvedness measures (*Homo sapiens* = open squares, *Pan* = closed triangles, *Gorilla* = open diamonds, Qafzeh 9 = grey square, Neandertal = closed squares).

TABLE 8.1 Correlations between each variable and canonical axis (bolded values indicate the variables that best explain the observed variation along each axis)

Pooled-within canonical structure		
Variable	CAN1	CAN2
<u>Surface on Trapezium</u>		
RMS	-0.40	-0.16
Absolute	-0.35	-0.14
Gaussian	0.17	0.02
Mean	0.30	0.13
Relative Area	0.45	-0.09
<u>Surface on 1st Metacarpal</u>		
RMS	-0.64	0.13
Absolute	-0.67	0.27
Gaussian	0.51	-0.49
Mean	-0.05	0.48
Relative Area	-0.02	0.26

TABLE 8.2 Cross-validated posterior probabilities of genus membership using relative area and curvedness measures of the 1st carpometacarpal joint surfaces

	<i>Homo</i>	<i>Pan</i>	<i>Gorilla</i>
<i>Homo</i>	106	2	0
%	98.2	1.9	0.0
<i>Pan</i>	0	39	5
%	0.0	88.6	11.4
<i>Gorilla</i>	1	5	36
%	2.4	11.9	85.7

TABLE 8.3 Posterior probabilities of genus membership using relative area and curvedness measures of the of the 1st carpometacarpal joint surfaces

	Qafzeh 9	Kebara 2	La Ferrassie 1	La Ferrassie 2	Regourdou 1
<i>Homo</i> (%)	100.0	99.5	100.0	100.0	99.9
<i>Pan</i> (%)	0.0	0.0	0.0	0.0	0.0
<i>Gorilla</i> (%)	0.0	0.0	0.0	0.0	0.0

The cross-validation procedure of the discriminant analysis resulted in the correct classification of 106 *Homo* (98%), 39 *Pan* (89%), and 36 *Gorilla* (86%; Table 8.2).

Using the fossils as test classification cases results in all five specimens clearly classified as modern *Homo* (Table 8.3).

The trapezium carpal and carpometacarpal joints. A total of six reasonably complete trapezium bones comprise the fossil sample. Upper Paleolithic *H. sapiens* is represented by Qafzeh 9, while *H. neanderthalensis* is represented by Kebara 2, Regourdou 1, La Ferrassie 2, Shanidar 3 (see Fig. 8.15), and Shanidar 4.

A Full Model utilizing all relative areas and angles of the articular surfaces is used to compare these fossil hominins with the extant hominine genera (Fig. 8.2). The fossils are used only as test classification cases. The canonical scores of each fossil specimen are based on the particular measurements of each fossil trapezium.

The first canonical axis (CAN1) accounts for 83% of the variation while the second (CAN2) accounts for 17%. Along CAN1, modern *Homo* clusters more toward the right while the African apes cluster more toward the left (Fig. 8.2). All the fossils cluster with modern *Homo*, although Kebara 2 falls almost directly in the center of both axes in between the African ape and modern *Homo* clusters. The correlations with CAN1 indicate that this axis represents the angle between the first and second metacarpal joint surfaces and the relative areas of the first metacarpal and scaphoid joint surfaces, in comparison with the angles between the first metacarpal and scaphoid joint surfaces, the second metacarpal and scaphoid joint surfaces, and the second metacarpal and trapezoid joint surfaces (Table 8.4). The modern *Homo* cluster reflects the large relative joint areas and more parallel orientation of the first metacarpal and scaphoid articulations, and a more transversely-oriented second metacarpal joint surface; all six fossils share these characteristics of the trapezium with modern *Homo* (Fig. 8.2).

The cross-validation procedure of the discriminant analysis resulted in the correct classification of 110 *Homo* (98.2%), 42 *Pan* (89.4%), and 41 *Gorilla* (95.4%; Table 8.5). Using the fossils as test classification cases results in four of the six bones clearly classified as modern *Homo* (Table 8.6). Shanidar 4 shows a 19% probability of belonging to *Gorilla* while Kebara 2 shows an almost equal probability of belonging to *Homo*, *Pan*, or *Gorilla* (Table 8.6). Both of these specimens, however, display the major characteristics of the modern *Homo* trapezium and are within the observed range of modern *Homo* variation both metrically and visually (Fig. 8.2). In fact, if the curvedness measures of the first metacarpal articular surface are incorporated into the Full Model, all six of these fossils are classified as modern *Homo* with 98%-100% probability (data not shown).

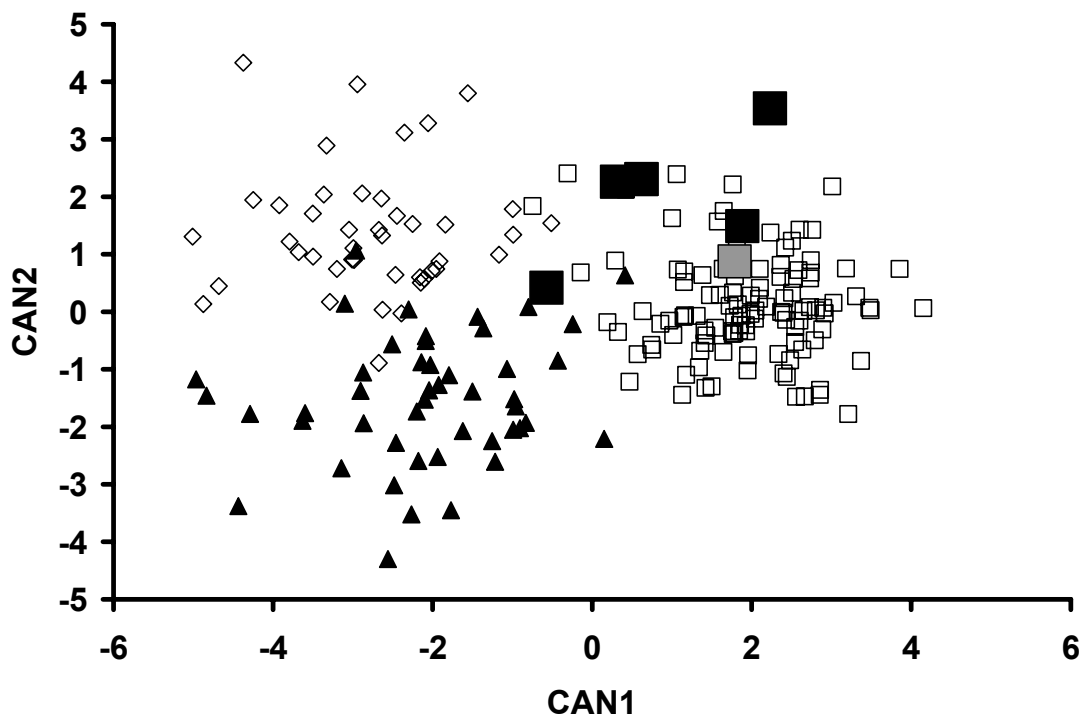


Fig. 8.2 Plot of the canonical variables (CAN1, CAN2) generated from analysis of relative areas and angles of the trapezium articular surfaces (*Homo sapiens* = open squares, *Pan* = closed triangles, *Gorilla* = open diamonds, Qafzeh 9 = grey square, Neandertal = closed squares).

TABLE 8.4 Correlations between each variable and canonical axis (**bolded values indicate the variables that best explain the observed variation along each axis**)

Variable		Pooled-within canonical structure	
Angle between		CAN1	CAN2
1st metacarpal	2nd metacarpal	0.59	0.34
1st metacarpal	scaphoid	-0.35	-0.14
1st metacarpal	trapezoid	0.23	0.41
2nd metacarpal	scaphoid	-0.47	0.03
2nd metacarpal	trapezoid	-0.46	0.09
scaphoid	trapezoid	0.04	0.03
<u>Relative surface area</u>			
	1st metacarpal	0.49	-0.17
	2nd metacarpal	0.01	0.09
	scaphoid	0.42	-0.11
	trapezoid	0.29	-0.62

TABLE 8.5 Cross-validated posterior probabilities of genus membership using relative areas and angles of the trapezium articular surfaces

	<i>Homo</i>	<i>Pan</i>	<i>Gorilla</i>
<i>Homo</i>	110	0	2
%	98.2	0.0	1.8
<i>Pan</i>	2	42	3
%	4.3	89.4	6.4
<i>Gorilla</i>	0	2	41
%	0.0	4.7	95.4

TABLE 8.6 Posterior probabilities of genus membership using relative areas and angles of the trapezium articular surfaces

	Qafzeh 9	Kebara 2	La Ferrassie 2	Regourdou 1	Shanidar 3	Shanidar 4
<i>Homo</i> (%)	100.0	28.0	100.0	94.4	100.0	81.0
<i>Pan</i> (%)	0.0	34.8	0.0	0.0	0.0	0.0
<i>Gorilla</i> (%)	0.0	37.2	0.0	5.5	0.0	18.9

The trapezoid carpal and carpometacarpal joints. A total of five reasonably complete trapezoid bones comprise the fossil sample. Upper Paleolithic *H. sapiens* is represented by Qafzeh 9 and Combe-Capelle 1, while *H. neanderthalensis* is represented by Kebara 2, La Ferrassie 1, and Amud 1 (see Fig. 8.16).

Using a Full Model, the trapezoid bones of these fossil hominins are compared to the extant hominine genera (Fig. 8.3). The variables utilized include the relative areas and angles of the articulating surfaces. The fossils are used only as test classification cases. The canonical scores of each fossil specimen are based on the particular measurements of each fossil trapezoid.

The first canonical axis (CAN1) accounts for 86% of the variation while the second (CAN2) accounts for 14%. Along CAN1, modern *Homo* clusters more toward the left while the African apes cluster more toward the right (Fig. 8.3). All the fossils cluster

clearly with modern *Homo*. The correlations with CAN1 indicate that this axis represents the relative area of the capitate joint surface compared with the angle between the medial second metacarpal and scaphoid joint surfaces and the relative area of the scaphoid joint surface (Table 8.7). The modern *Homo* cluster reflects the more parallel orientation of the medial second metacarpal and scaphoid joint surfaces and the smaller relative scaphoid joint surface; all five fossils share these characteristics of the trapezoid with modern *Homo* (Fig. 8.3).

The cross-validation procedure of the discriminant analysis resulted in the correct classification of 111 *Homo* (100%), 47 *Pan* (100%), and 5 *Gorilla* (71.4%; Table 8.8). Using the fossils as test classification cases results in all five bones classified as modern *Homo* (Table 8.9).

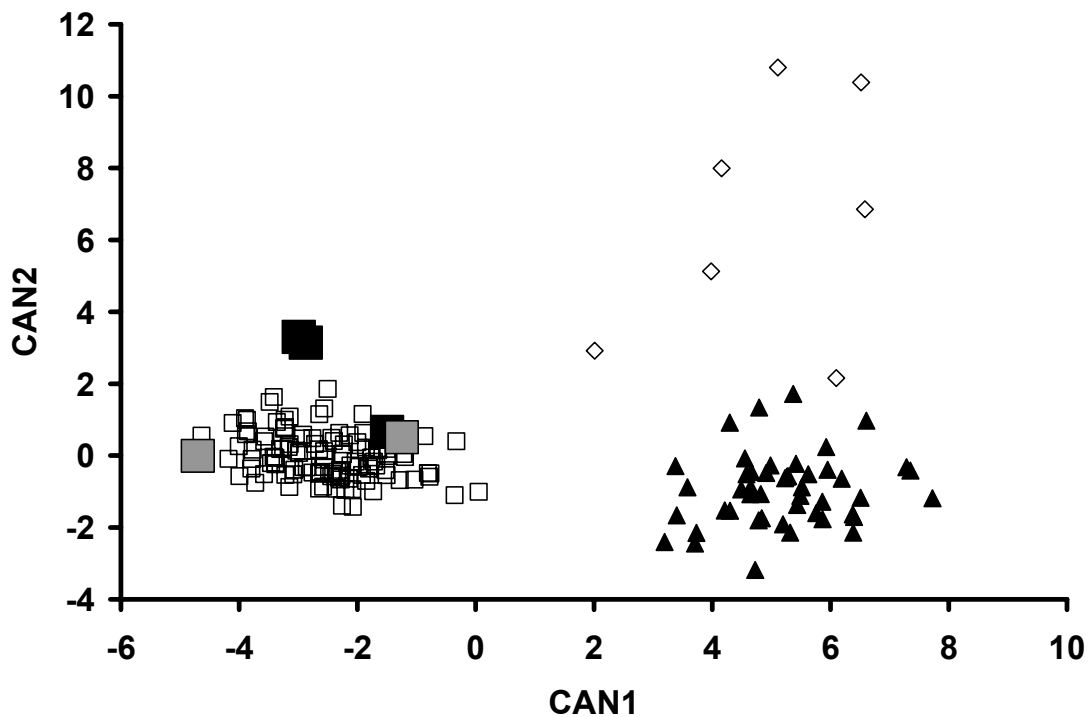


Fig. 8.3 Plot of the canonical variables (CAN1, CAN2) generated from analysis of relative areas and angles of the trapezoid articular surfaces (*Homo sapiens* = open squares, *Pan* = closed triangles, *Gorilla* = open diamonds, Upper Paleolithic *H. sapiens* = grey squares, Neandertal = closed squares).

TABLE 8.7 Correlations between each variable and canonical axis (bolded values indicate the variables that best explain the observed variation along each axis)

Variable		Pooled-within canonical structure	
		CAN1	CAN2
Angle between			
lateral 2nd metacarpal	medial 2nd metacarpal	-0.07	0.16
lateral 2nd metacarpal	scaphoid	0.15	0.07
lateral 2nd metacarpal	trapezium	0.15	-0.11
medial 2nd metacarpal	scaphoid	0.45	-0.09
medial 2nd metacarpal	trapezium	0.13	0.05
scaphoid	trapezium	-0.15	0.08
capitate	lateral 2nd metacarpal	0.10	0.41
capitate	medial 2nd metacarpal	0.15	0.25
capitate	scaphoid	0.09	-0.19
capitate	trapezium	0.04	0.57
Relative surface area			
	capitate	-0.21	-0.20
	lateral 2nd metacarpal	0.03	-0.13
	medial 2nd metacarpal	0.19	0.00
	scaphoid	0.35	-0.06
	trapezium	0.04	-0.23

TABLE 8.8. Cross-validated posterior probabilities of genus membership using relative areas and angles of the trapezoid articular surfaces

	<i>Homo</i>	<i>Pan</i>	<i>Gorilla</i>
<i>Homo</i>	111	0	0
%	100.0	0.0	0.0
<i>Pan</i>	0	47	0
%	0.0	100.0	0.0
<i>Gorilla</i>	0	2	5
%	0.0	28.6	71.4

TABLE 8.9 Posterior probabilities of genus membership using relative areas and angles of the trapezoid articular surfaces

	Qafzeh 9	Combe-Capelle 1	Kebara 2	La Ferrassie 1	Amud 1
<i>Homo</i> (%)	100.0	100.0	100.0	100.0	100.0
<i>Pan</i> (%)	0.0	0.0	0.0	0.0	0.0
<i>Gorilla</i> (%)	0.0	0.0	0.0	0.0	0.0

The scaphoid carpal and carpometacarpal joints. A total of nine reasonably complete scaphoid bones comprise the fossil sample. Upper Paleolithic *H. sapiens* is represented by Qafzeh 9 and Combe-Capelle 1, while *H. neanderthalensis* is represented by Kebara 2, La Ferrassie 1, Regourdou 1, Regourdou 2, Shanidar 3, Shanidar 4, and Shanidar 8 (see Fig. 8.17).

Using a Full Model, the scaphoid bones of these fossil hominins are compared to the extant hominine genera (Fig. 8.4). The variables utilized include selected relative areas and angles of the articulating surfaces; variables involving the lunate joint surface are excluded because this articulation is occasionally poorly-defined or absent in both the extant and fossil sample. As always, the fossils are used only as test classification cases. The canonical scores of each fossil specimen are based on the particular measurements of each fossil scaphoid.

The first canonical axis (CAN1) accounts for 89% of the variation while the second (CAN2) accounts for 11%. Along CAN1, modern *Homo* clusters more toward the right while the African apes cluster more toward the left (Fig. 8.4). All the fossils cluster clearly with modern *Homo*. The correlations with CAN1 indicate that the observed variation represents the relative area of non-articular surface in comparison with the angle between the capitate and trapezium-trapezoid joint surfaces and the relative areas of the trapezium-trapezoid and capitate articulations (Table 8.10). The modern *Homo* cluster reflects a larger angle between the capitate and trapezium-trapezoid joint surfaces, larger relative trapezium-trapezoid and capitate joint surfaces, and a smaller relative area of non-articular surface, all of which contribute to a more positive loading

along CAN1; all nine fossils share these characteristics of the scaphoid with modern *Homo* (Fig. 8.4).

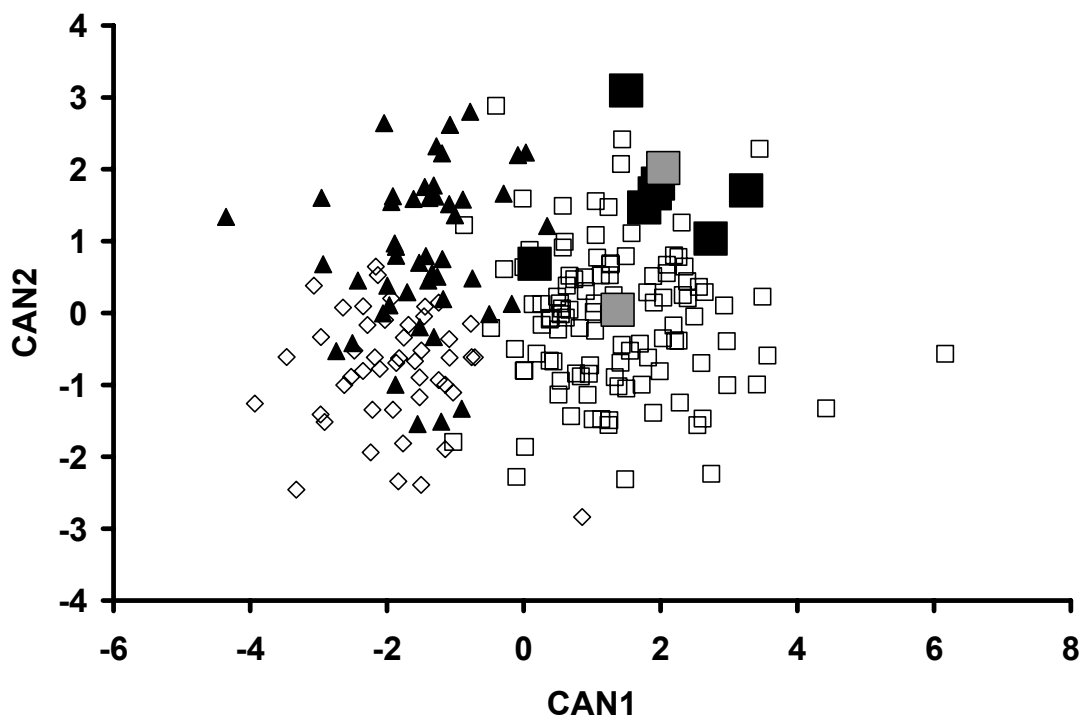


Fig. 8.4 Plot of the canonical variables (CAN1, CAN2) generated from analysis of relative areas and angles of the scaphoid articular surfaces (*Homo sapiens* = open squares, *Pan* = closed triangles, *Gorilla* = open diamonds, Upper Paleolithic *H. sapiens* = grey squares, Neandertal = closed squares).

TABLE 8.10 Correlations between each variable and canonical axis (bolded values indicate the variables that best explain the observed variation along each axis)

Variable		Pooled-within canonical structure	
		CAN1	CAN2
Angle between			
capitate	radius	0.04	0.32
capitate	trapezium-trapezoid	0.58	-0.34
radius	trapezium-trapezoid	-0.24	0.02
Relative surface area			
	capitate	0.29	0.84
	radius	0.13	0.32
	trapezium-trapezoid	0.41	0.19
	non-articular	-0.34	-0.59

TABLE 8.11 Cross-validated posterior probabilities of genus membership using relative areas and angles of the scaphoid articular surfaces

	<i>Homo</i>	<i>Pan</i>	<i>Gorilla</i>
<i>Homo</i>	106	7	4
%	90.6	6.0	3.4
<i>Pan</i>	2	36	10
%	4.2	75.0	20.8
<i>Gorilla</i>	2	9	37
%	4.2	18.8	77.1

TABLE 8.12 Posterior probabilities of genus membership using relative areas and angles of the scaphoid articular surfaces

	<i>Homo</i> (%)	<i>Pan</i> (%)	<i>Gorilla</i> (%)
Qafzeh 9	93.0	6.9	0.1
Combe-Capelle 1	99.8	0.2	0.0
Kebara 2	99.9	0.1	0.0
La Ferrassie 1	98.9	1.1	0.0
Regourdou 1	98.5	1.5	0.0
Regourdou 2	100.0	0.0	0.0
Shanidar 3	54.7	38.5	6.8
Shanidar 4	88.0	12.0	0.0
Shanidar 8	98.8	1.1	0.0

The cross-validation procedure of the discriminant analysis resulted in the correct classification of 106 *Homo* (90.6%), 36 *Pan* (75%), and 37 *Gorilla* (77.1%; Table 8.11). Using the fossils as test classification cases results in all nine bones classified as modern *Homo* (Table 8.12). The Shanidar 3 scaphoid falls near where the edges of the observed variation between modern *Homo* and the African apes overlap (Fig. 8.4), and this is reflected in its posterior probabilities of genus membership (Table 8.12). Along CAN1, specimens of modern *Homo* that fall closest to the African ape cluster tend to have a more distally-closed capitate joint surface, which results in a narrower angle between the capitate and trapezium-trapezoid joint surfaces; the Shanidar 3 scaphoid is similar in this respect.

The carpometacarpal joints of the second metacarpal base. A total of five reasonably complete bases of the second metacarpal comprise the fossil sample. *H. neanderthalensis* is represented by La Ferrassie 2, Regourdou 2, La Chappelle-aux-Saints 1, Shanidar 5, and Shanidar 6 (see Fig. 8.18).

Using a Full Model, the second metacarpal bases of these fossil hominins are compared to the extant hominine genera (Fig. 8.5). The variables utilized include the relative areas and angles of the articulating surfaces. Again, the fossils are used only as test classification cases. The canonical scores of each fossil specimen are based on the particular measurements of each fossil second metacarpal base.

The first canonical axis (CAN1) accounts for 88% of the variation while the second (CAN2) accounts for 12%. Along CAN1, modern *Homo* clusters more toward the right while the African apes cluster more toward the left (Fig. 8.5). All the fossils cluster clearly with modern *Homo*. The correlations with CAN1 indicate that the separation along this axis is mostly accounted for by a comparison of the four angles involving the capitate joint surface (Table 8.13). The modern *Homo* cluster reflects a smaller angle between the capitate and third metacarpal surfaces, and larger angles between the capitate joint surface and the trapezium, and lateral and medial trapezoid joint surfaces. Together, these four angles contribute to a more positive loading for modern *Homo* along CAN1; all five fossils share these characteristics of the second metacarpal base with modern *Homo* (Fig. 8.5).

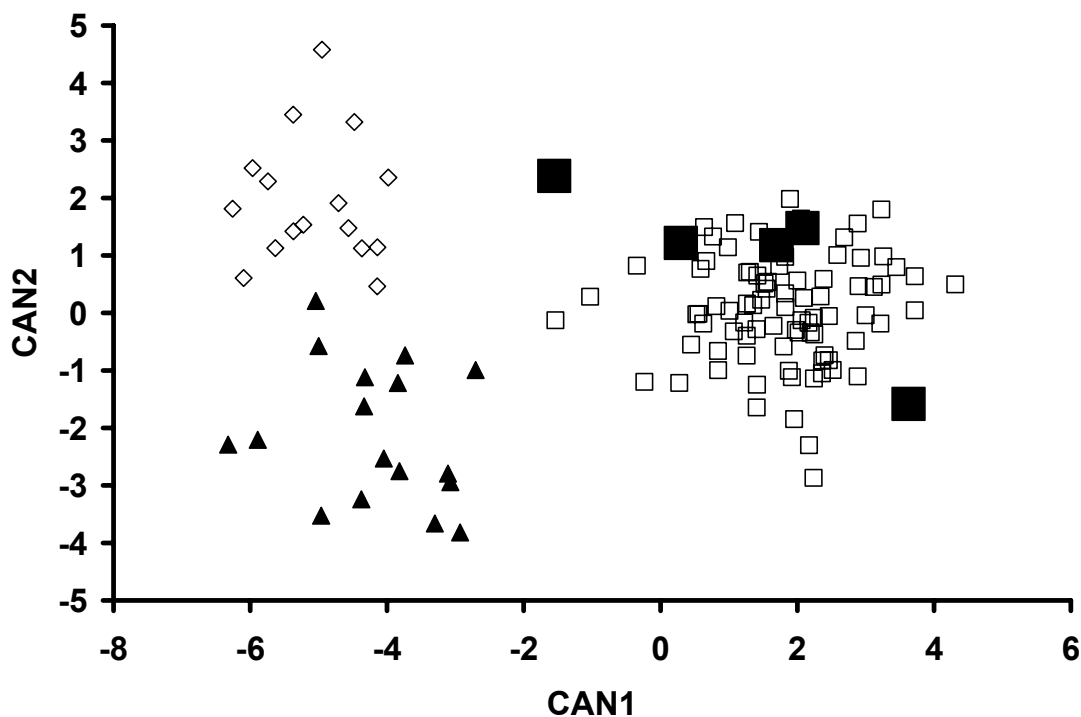


Fig. 8.5 Plot of the canonical variables (CAN1, CAN2) generated from analysis of relative areas and angles of the second carpometacarpal joint surfaces (*Homo sapiens* = open squares, *Pan* = closed triangles, *Gorilla* = open diamonds, Neandertal = closed squares).

TABLE 8.13 Correlations between each variable and canonical axis (bolded values indicate the variables that best explain the observed variation along each axis)

Variable		Pooled-within canonical structure	
		CAN1	CAN2
Angle between			
capitate	3rd metacarpal	-0.41	0.08
capitate	lateral trapezoid	0.74	0.07
capitate	medial trapezoid	0.51	0.29
lateral trapezoid	medial trapezoid	-0.08	0.51
3rd metacarpal	trapezium	0.23	0.23
capitate	trapezium	0.53	0.13
trapezium	lateral trapezoid	0.25	0.16
trapezium	medial trapezoid	0.21	-0.39
Relative surface area			
capitate		-0.05	-0.39
trapezium		0.03	0.14
lateral trapezoid		0.09	-0.08
medial trapezoid		-0.26	0.37

TABLE 8.14 Cross-validated posterior probabilities of genus membership using relative areas and angles of the second metacarpal base articular surfaces

	<i>Homo</i>	<i>Pan</i>	<i>Gorilla</i>
<i>Homo</i>	84	1	0
%	98.8	1.2	0.0
<i>Pan</i>	0	16	1
%	0.0	94.1	5.9
<i>Gorilla</i>	0	0	16
%	0.0	0.0	100.0

TABLE 8.15 Posterior probabilities of genus membership using relative areas and angles of the second metacarpal base articular surfaces

	<i>Homo</i> (%)	<i>Pan</i> (%)	<i>Gorilla</i> (%)
La Ferrassie 2	100.0	0.0	0.0
Regourdou 2	100.0	0.0	0.0
La Chappelle-aux-Saints 1	100.0	0.0	0.0
Shanidar 5	11.6	0.0	88.4
Shanidar 6	100.0	0.0	0.0

The cross-validation procedure of the discriminant analysis resulted in the correct classification of 84 *Homo* (98.8%), 16 *Pan* (94.1%), and 16 *Gorilla* (100%; Table 8.14). Using the fossils as test classification cases results in four of the five bones classified as modern *Homo* (Table 8.15). The discriminant function classifies the Shanidar 5 second metacarpal with an 88% probability of belonging to *Gorilla*. However, it is clear from the canonical analysis, particularly along CAN1 (Fig. 8.5), as well as visual inspection of the bone that it displays the essential characteristics of modern *Homo*.

***Homo habilis* (OH7)**

A trapezium (see Fig. 8.15), scaphoid (see Fig. 8.17), and badly damaged capitate and possible second metacarpal base from Olduvai Gorge make up part of the hand attributed to *H. habilis* (OH7). The OH7 fossils were recovered stratigraphically

between Tuff IB and Tuff IC and were the first hand bones recovered in association with Oldowan technology (Leakey et al., 1964). Radiometric age estimates for both Tuff IB and Tuff IC range between 1.76 and 1.86 Ma (Blumenschine et al., 2003; Walter et al., 1991). The OH7 hand fossils were at the center of the naming of *H. habilis* and are part of the type specimen of this taxon (Leakey et al., 1964). It should be emphasized that the OH 7 hand fossils could reasonably belong to *Paranthropus boisei* considering the OH 5 ('Zinjanthropus') cranium was recovered within a few hundred meters along with other postcranial remains loosely attributed to *P. boisei* (Day, 1976; Leakey, 1971; Leakey et al., 1964).

Only the trapezium and scaphoid of OH7 are preserved well enough to be included in this analysis (Susman and Creel, 1979; Susman and Stern, 1982; Trinkaus, 1989). The articular surfaces of the capitate and probable second metacarpal base are too poorly preserved to even facilitate any reasonable descriptive comparison.

The trapezium. This fossil displays a unique combination of features that make it extremely interesting yet raise serious issues for interpreting its morphology. Visually, the OH7 trapezium is quite distinct (see Fig. 8.15); it does not closely resemble any extant hominid trapezium in particular, although its overall form makes it easily recognizable as a trapezium belonging to some type of primate, possibly a hominid. Additional non-hominine primate genera are included for comparison to provide a broader framework for interpreting its distinctive morphology.

A Full Model using the relative angles, areas, and curvedness measures of the trapezium classifies the OH7 trapezium as *Homo* but close inspection of the model

reveals a combination of features in this fossil that are not seen among any of the genera analyzed here. The model uses extant *Homo*, *Pan*, *Gorilla*, *Pongo*, and *Papio* to create the classification rules while OH7, AL333-80, *Theropithecus*, and *Nasalis* are used as classification test cases.

The relative angles between the articular surfaces of the OH7 trapezium, particularly the angles involving the second metacarpal surface, mostly resemble African apes (Napier, 1962; Tocheri et al., 2003). Its first metacarpal-scaphoid angle (9°), however, is closer to the mean angle of *Homo* (10°) rather than of either *Pan* (19°) or *Gorilla* (18°). Its absolute and RMS curvatures (0.8 and 0.7 respectively) of the first metacarpal surface are lower than any of the other genus means, indicating it lies on the extreme of surface flatness variation (Trinkaus, 1989). In fact, this surface appears relatively flat dorso-palmarly (-0.5) as well as radio-ulnarly (0.3). This relative flatness in both directions makes it unlike the surfaces seen in hominids and more like those of cercopithecids.

With respect to the relative areas of OH7, these measures must be interpreted cautiously as several areas of nonarticular surface are either slightly damaged or missing. That being said, however, performing the multivariate analyses using differing estimates of its total surface area do not significantly alter the results presented. This is primarily because although the proportions of each relative area change slightly in value depending on the estimate of total surface area used, the correlations between the proportions do not. With these issues in mind, the relative area of the first metacarpal surface in OH7 is approximated at 21.1%, which falls within the ranges of values

observed in *Homo* and *Theropithecus*. The relative areas of the trapezoid and scaphoid surfaces are within the ranges seen in great apes whereas the relative second metacarpal area falls within the *Papio* range. However, part of the second metacarpal articular surface may be missing so this result in particular should be interpreted with caution.

In the Full Model (Fig. 8.6), OH7's more *Homo*-like first metacarpal-scaphoid angle, which has a strong negative loading along CAN1, acts to somewhat balance out the effect of two of its more African ape-like second metacarpal angles, which load strongly both positively (first metacarpal-second metacarpal) and negatively (second metacarpal-trapezoid). Finally, the first metacarpal relative area, which is proportionately large in OH7 and also has a strong positive loading on CAN1, drives the OH7 trapezium to the far right of this axis. The modern *Homo* specimens on the far right of CAN1 also tend to display relatively large first metacarpal surfaces and small first metacarpal-scaphoid angles compared to the modern *Homo* mean.

Along CAN2, the OH7 trapezium again falls on the edge of the *Homo* cluster but within the African ape clusters (Figs. 8.6 and 8.7). CAN2 separates the hominines from non-hominines because the relative angles between the first metacarpal, scaphoid, and trapezoid surfaces characterize a wider, rectangular trapezium form in hominines versus a longer, more triangular form in non-hominines. OH7 clearly displays a hominine-like condition. Along CAN3, OH7 clusters with *Papio* because of its small relative second metacarpal area (Figs. 8.7). Because a portion of this articular surface may be missing in this fossil, a Partial Model that excludes all of the second metacarpal measures is also examined.

Figures 8.8 and 8.9 highlight further the problematic issues for interpreting the morphology of the OH7 trapezium even when variables involving the second metacarpal surface are excluded (Full Model II). On both of the major canonical axes, it sits on the edge of observed variation. Although its relative angles suggest it is more like the hominines, as seen along CAN1, its relatively flat first metacarpal surface suggests it is more like cercopithecids (*Erythrocebus* is also included in this analysis because they typically lack a second metacarpal facet), as seen along CAN2. There is no simple solution to reconciling between these two extremes of morphological variation.

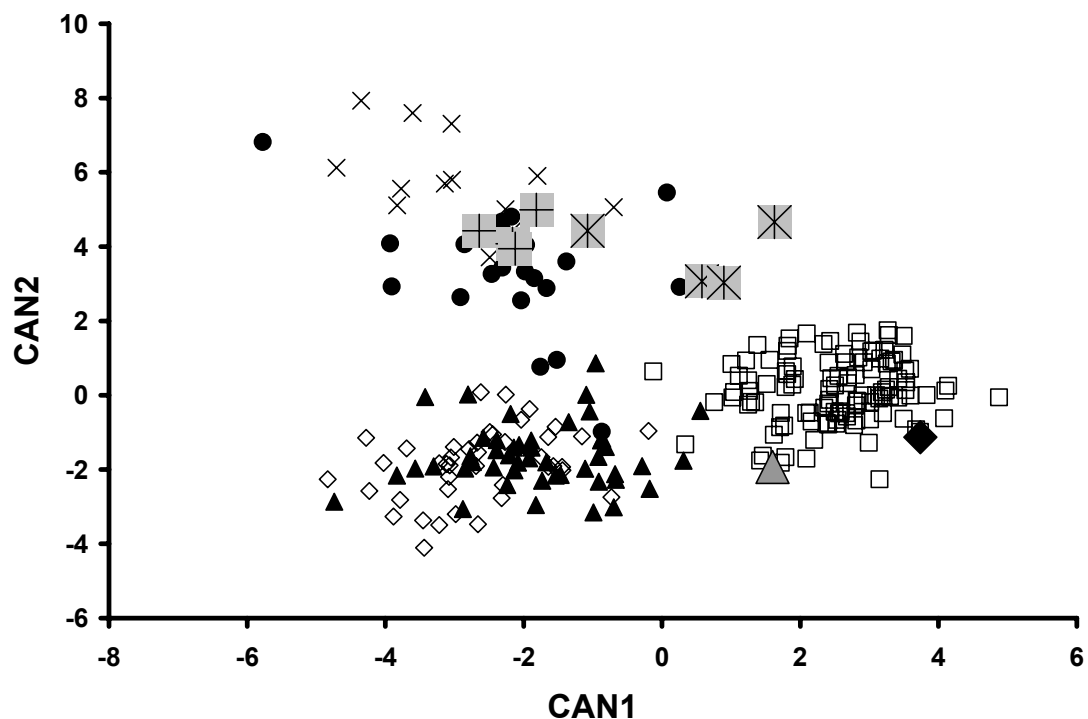


Fig. 8.6 Plot of the canonical variables (CAN1, CAN2) generated from analysis of trapezium relative areas, angles, and curvedness measures of the articular surfaces (*Homo* = open squares, *Pan* = closed triangles, *Gorilla* = open diamonds, *Pongo* = closed circles, *Papio* = Xs, *Theropithecus* = grey +s, *Nasalis* = grey stars, *A. afarensis* = grey triangle, *H. habilis* = closed diamond).

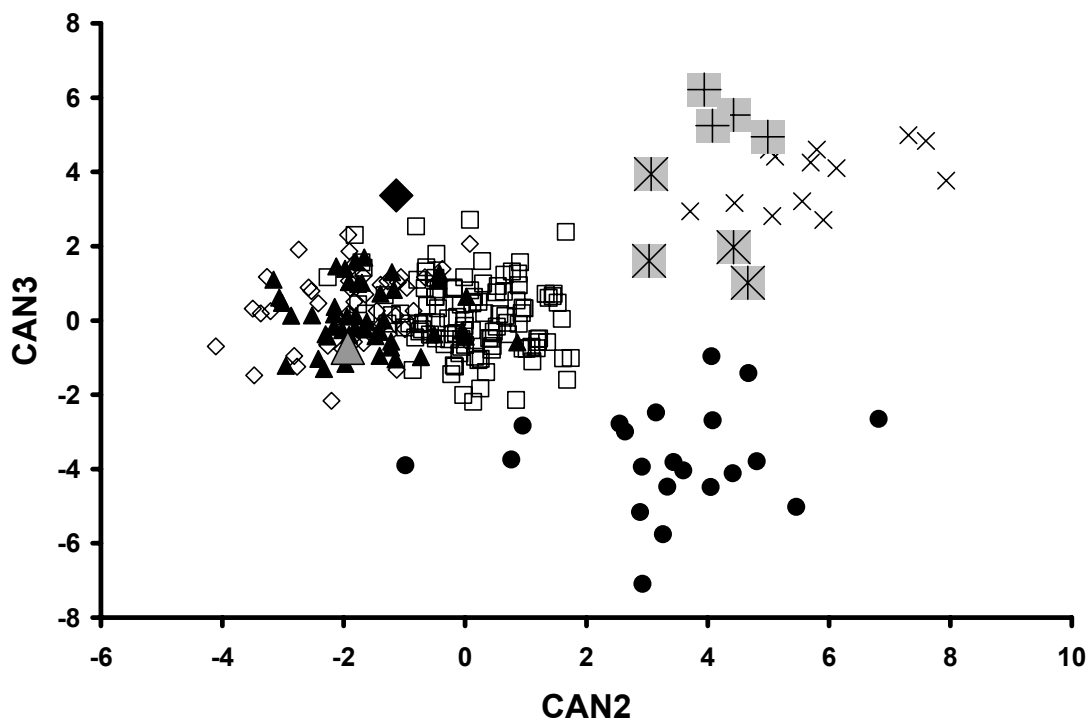


Fig. 8.7 Plot of the canonical variables (CAN2, CAN3) generated from analysis of trapezium relative areas, angles, and curvedness measures of the articular surfaces (*Homo* = open squares, *Pan* = closed triangles, *Gorilla* = open diamonds, *Pongo* = closed circles, *Papio* = Xs, *Theropithecus* = grey +s, *Nasalis* = grey stars, *A. afarensis* = grey triangle, *H. habilis* = closed diamond).

TABLE 8.16 Correlations between each variable and canonical axis (bolded values indicate the variables that best explain the observed variation along each axis)

<u>Variable</u>		<u>Pooled-within canonical structure</u>			
Angle between		CAN1	CAN2	CAN3	CAN4
first metacarpal	second metacarpal	0.43	0.23	0.05	0.32
first metacarpal	scaphoid	-0.46	0.47	-0.04	-0.13
first metacarpal	trapezoid	0.04	0.46	0.42	0.36
second metacarpal	scaphoid	-0.18	-0.54	0.22	0.02
second metacarpal	trapezoid	-0.40	-0.03	0.38	0.05
scaphoid	trapezoid	0.34	-0.80	-0.20	0.08
<u>Relative surface area</u>					
	first metacarpal	0.41	0.14	0.08	-0.17
	second metacarpal	-0.06	0.11	-0.68	0.13
	trapezoid	0.25	0.08	0.14	-0.63
	scaphoid-centrale	0.29	0.19	0.04	-0.10
<u>Relative surface curvature (mc1)</u>					
	RMS	-0.29	-0.34	-0.09	-0.05
	Absolute	-0.24	-0.35	-0.14	-0.04
	Gaussian	0.09	0.21	0.13	-0.01
	Mean	0.24	0.16	-0.07	0.04

TABLE 8.17 Cross-validated posterior probabilities of genus membership using the relative areas, angles, and curvedness measures of the trapezium articular surfaces

	<i>Homo</i>	<i>Pan</i>	<i>Gorilla</i>	<i>Pongo</i>	<i>Papio</i>
<i>Homo</i>	110	0	2	0	0
%	98.2	0.0	1.8	0.0	0.0
<i>Pan</i>	1	40	6	0	0
%	2.1	85.1	12.8	0.0	0.0
<i>Gorilla</i>	0	4	39	0	0
%	0.0	9.3	90.7	0.0	0.0
<i>Pongo</i>	0	0	1	20	0
%	0.0	0.0	4.8	95.2	0.0
<i>Papio</i>	0	0	0	0	13
%	0.0	0.0	0.0	0.0	100.0

TABLE 8.18 Posterior probabilities of genus membership using the relative areas, angles, and curvedness measures of the trapezium articular surfaces

	<i>Homo</i> (%)	<i>Pan</i> (%)	<i>Gorilla</i> (%)	<i>Pongo</i> (%)	<i>Papio</i> (%)
OH7	100.0	0.0	0.0	0.0	0.0
AL333-80	99.2	0.7	0.1	0.0	0.0
<i>Nasalis</i>	50.0	0.0	0.0	0.0	50.0
<i>Theropithecus</i>	0.0	0.0	0.0	0.0	100.0

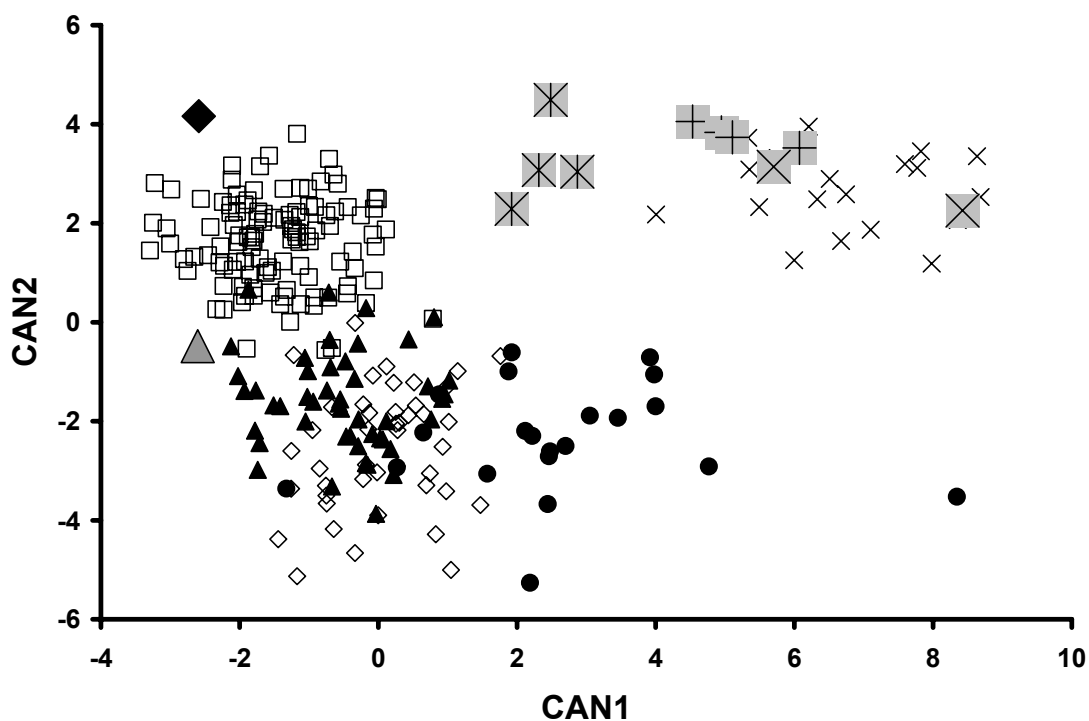


Fig. 8.8 Plot of the canonical variables (CAN1, CAN2) generated from analysis of trapezium relative areas, angles, and curvedness measures, excluding those involving the second metacarpal surface (*Homo* = open squares, *Pan* = closed triangles, *Gorilla* = open diamonds, *Pongo* = closed circles, *Papio* = Xs, *Theropithecus* = grey +s, *Erythrocebus* = grey Xs, *Nasalis* = grey stars, *A. afarensis* = grey triangle, *H. habilis* = closed diamond).

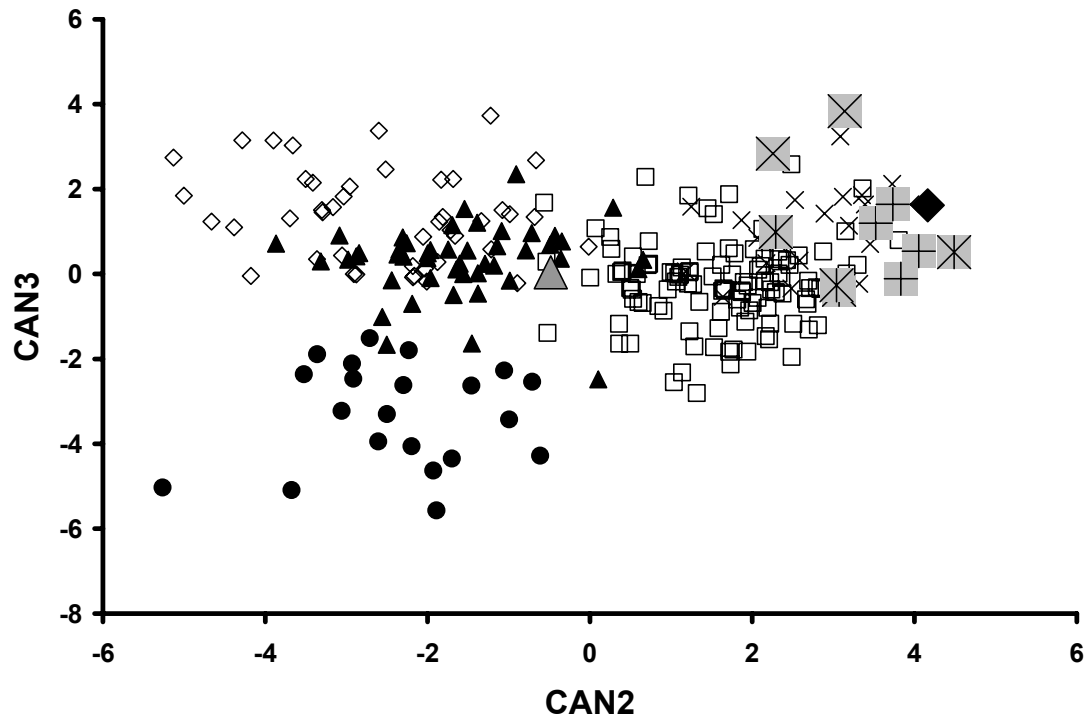


Fig. 8.9 Plot of the canonical variables (CAN2, CAN3) generated from analysis of trapezium relative areas, angles, and curvedness measures, excluding those involving the second metacarpal surface (*Homo* = open squares, *Pan* = closed triangles, *Gorilla* = open diamonds, *Pongo* = closed circles, *Papio* = Xs, *Theropithecus* = grey +s, *Erythrocebus* = grey Xs, *Nasalis* = grey stars, *A. afarensis* = grey triangle, *H. habilis* = black diamond).

The cross-validation procedure of the discriminant analysis resulted in the correct classification of 110 *Homo* (98.2%), 40 *Pan* (85.1%), 39 *Gorilla* (90.7%), 20 *Pongo* (95.2%), and 13 *Papio* (100%; Table 8.17). Using OH7 as a test classification case results in its classifying as *Homo* (100%) whereas *Nasalis* (n = 4) classifies on average either as *Homo* (50%) or *Papio* (50%); *Theropithecus* (n = 4) always classifies as *Papio* (100%; Table 8.18).

The scaphoid. This fossil displays less ambiguous morphology compared to its trapezium counterpart. It is clear that the centrale is completely coalesced to the

scaphoid (see Fig. 8.17), which is a derived character among the hominines. Overall, it appears similar to the scaphoid in the African apes (Susman and Creel, 1979; Susman and Stern, 1982). Considerable damage to the articular surfaces is present, making quantitative comparisons of its morphology somewhat challenging. However, three measures are reasonably estimated from the preserved morphology: the two angles between the capitate joint surface and the lunate and trapezium-trapezoid joint surfaces, and the relative area of the capitate joint surface. These three measures are used in a Partial Model to assess the morphological affinities of the OH7 scaphoid (Fig. 8.10).

The primary differences in scaphoid morphology that occur between the five extant genera relate to the relative area and orientation of the capitate facet. The first canonical axis (CAN1) accounts for 79% of the variation while the second (CAN2) accounts for 18%. Along CAN1, the modern hominines cluster more toward the right while the *Pongo* and, in particular, *Papio* cluster more toward the left (Fig. 8.10). The correlations with CAN1 indicate that the separation along this axis is mostly accounted for by a combination of the angle between the capitate and trapezium-trapezoid joint surfaces and the relative capitate area (Table 8.19). The hominine cluster reflects a wider angle between the capitate and trapezium-trapezoid surfaces, and a larger relative capitate joint area. The OH7 scaphoid clusters with the hominines along this axis mostly because it has a relatively large estimated capitate joint area.

Along CAN2, modern *Homo* and *Papio* cluster more negatively while the great apes cluster more positively (Fig. 8.10). The correlations with CAN2 indicate that the separation along this axis is mostly accounted for by a comparison of the angles

between the capitate joint surface and the lunate and trapezium-trapezoid joint surfaces (Table 8.19). Although *Papio* clusters negatively because both angles are narrower compared with the great apes (African apes in particular), the modern *Homo* cluster is the result of a narrower capitate-lunate angle and a wider angle between the capitate and trapezium-trapezoid joint surfaces, again in comparison to the great apes. The OH7 scaphoid clusters with the African apes (*Pan* in particular) along this axis because both angles are more similar to those observed in the non-*Homo* genera. Four Neandertal scaphoids are also shown for comparison, all of which clearly show the more derived condition observed in modern *Homo* (Fig. 8.10).

The narrow angle between the capitate and trapezium-trapezoid joint surfaces in the OH7 scaphoid has important interpretive consequences. The wider angle in modern *Homo* (and Neandertals) reflects the reduced amount of bone present immediately distal to the capitate facet, where the trapezoid typically articulates. Recall that the proximal joint surface of the trapezoid is reduced in *Homo* and more rectangular in shape; the reduction of bone in the distal portion of the scaphoid corresponds with the reduction of the proximal joint surface of the trapezoid.

The cross-validation procedure of the discriminant analysis resulted in the correct classification of 89 *Homo* (76.7%), 33 *Pan* (70.2%), 30 *Gorilla* (62.5%), 3 *Pongo* (37.5%), and 19 *Papio* (86.4%; Table 8.20). Using OH7 as a test classification case results in its classifying as *Pan* (92.3%) whereas premodern *Homo* specimens (4 Neandertals and Qafzeh 9) classify on average as *Homo* (93.6%; Table 8.21).

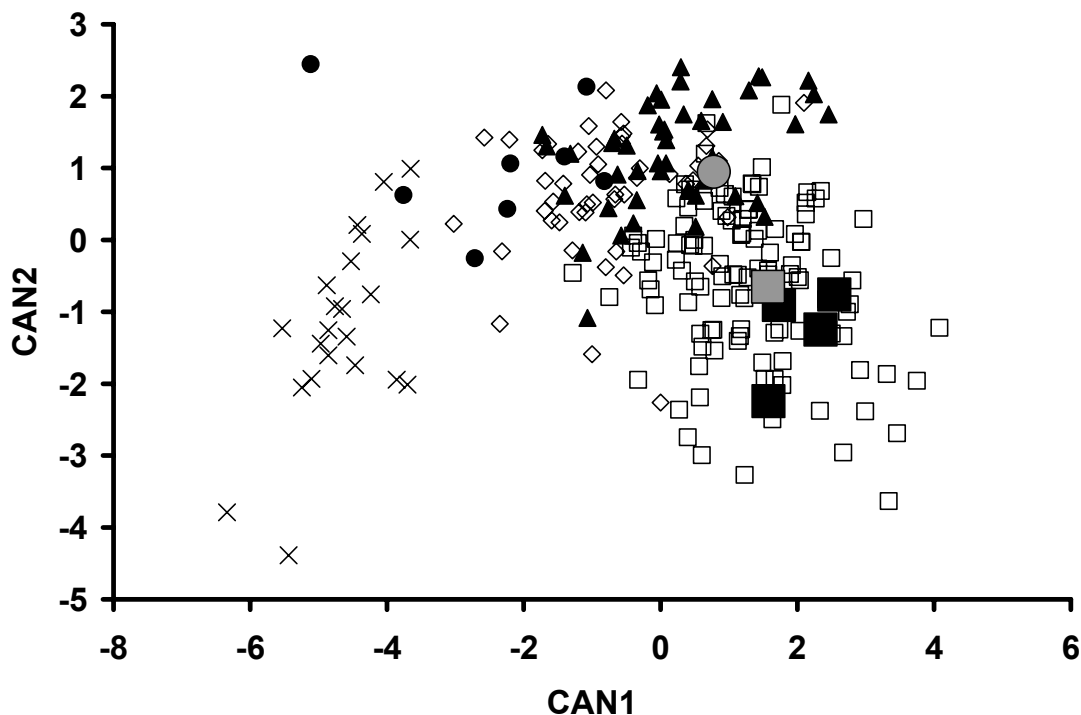


Fig. 8.10 Plot of the canonical variables (CAN1, CAN2) generated from analysis of three scaphoid joint surface measures (*Homo* = open squares, *Pan* = closed triangles, *Gorilla* = open diamonds, *Pongo* = closed circles, *Papio* = Xs, Qafzeh 9 = grey square, Neandertals = closed squares, *H. habilis* = grey circle).

TABLE 8.19 Correlations between each variable and canonical axis (bolded values indicate the variables that best explain the observed variation along each axis)

Variable		Pooled-within canonical structure	
		CAN1	CAN2
Angle between			
capitate	lunate	-0.03	0.96
capitate	trapezium-trapezoid	0.58	-0.62
Relative surface area			
	capitate	0.61	0.11

TABLE 8.20 Cross-validated posterior probabilities of genus membership using three relative areas and angles of the scaphoid articular surfaces

	<i>Homo</i>	<i>Pan</i>	<i>Gorilla</i>	<i>Pongo</i>	<i>Papio</i>
<i>Homo</i>	89	18	9	0	0
%	76.7	15.5	7.8	0.0	0.0
<i>Pan</i>	3	33	8	3	0
%	6.4	70.2	17.0	6.4	0.0
<i>Gorilla</i>	4	7	30	7	0
%	8.3	14.6	62.5	14.6	0.0
<i>Pongo</i>	0	2	2	3	1
%	0.0	25.0	25.0	37.5	12.5
<i>Papio</i>	0	0	0	3	19
%	0.0	0.0	0.0	13.6	86.4

TABLE 8.21 Posterior probabilities of genus membership using three relative areas and angles of the scaphoid articular surfaces

	<i>Homo</i> (%)	<i>Pan</i> (%)	<i>Gorilla</i> (%)	<i>Pongo</i> (%)	<i>Papio</i> (%)
OH7	6.8	92.3	0.7	0.0	0.0
premodern <i>Homo</i> (N=5)	93.6	6.1	0.3	0.0	0.0

Australopithecus afarensis

The hand and wrist bones of *A. afarensis* date to 3.2 million years ago (Walter, 1994), and predate the first appearance of Oldowan stone tools by approximately 600 thousand years (Semaw et al., 1997). Overall, the *A. afarensis* hand displays a combination of primitive and derived features in comparison to the great apes and later hominins (Bush et al., 1982; Johanson et al., 1982a, b; Marzke, 1983, 1997; McHenry, 1983; Susman, 1998; Tocheri et al., 2003). These fossils inform us as to the primitive condition of hand and wrist morphology for later appearing Plio-Pleistocene hominins. This analysis focuses on the trapezium (AL333-80), two first metacarpals (AL333-58 and AL333w-39), three second metacarpals (AL333-15, AL333-48, and AL333w-23), and two

capitates (AL333-40 and AL-288-1w) that are attributed to *A. afarensis* (Bush et al., 1982; Johanson et al., 1982a, b).

The first metacarpal. Two first metacarpals, AL333-58 and AL333w-39, comprise the *A. afarensis* sample. Using a Partial Model, these two first metacarpals are compared to the extant hominine genera. The variables utilized include the relative curvedness measures of the proximal articular surface of the first metacarpal. The fossils are used only as test classification cases. That is, the model is based entirely on the three extant genera and is identical to that presented in Chapter 3, except in that *Pongo* and *Papio* are no longer included for comparison.

The first canonical axis (CAN1) accounts for 93% of the variation while the second (CAN2) accounts for 7%. Along CAN1, modern *Homo* clusters more toward the left while the African apes cluster more toward the right (Fig. 8.11). One of the fossil bones clusters clearly with the African apes while the other falls where the respective distributions of *Homo* and the African apes overlap. The correlations with CAN1 indicate that this axis is a comparison of the absolute and RMS curvatures with the Gaussian curvature (Table 8.22). The modern *Homo* cluster reflects an articular area that is less curved than in the African apes; both *A. afarensis* articular surfaces show African ape-like curvedness (Fig. 8.11).

The cross-validation procedure of the discriminant analysis resulted in the correct classification of 112 *Homo* (92.6%), 32 *Pan* (69.6%), and 36 *Gorilla* (76.6%; Table 8.23). Using the fossils as test classification cases results in AL333-58 classified as *Pan*

(81.5%) and AL333w-39 classified as either *Pan* (56.2%) or *Homo* (43.2%; Table 8.24).

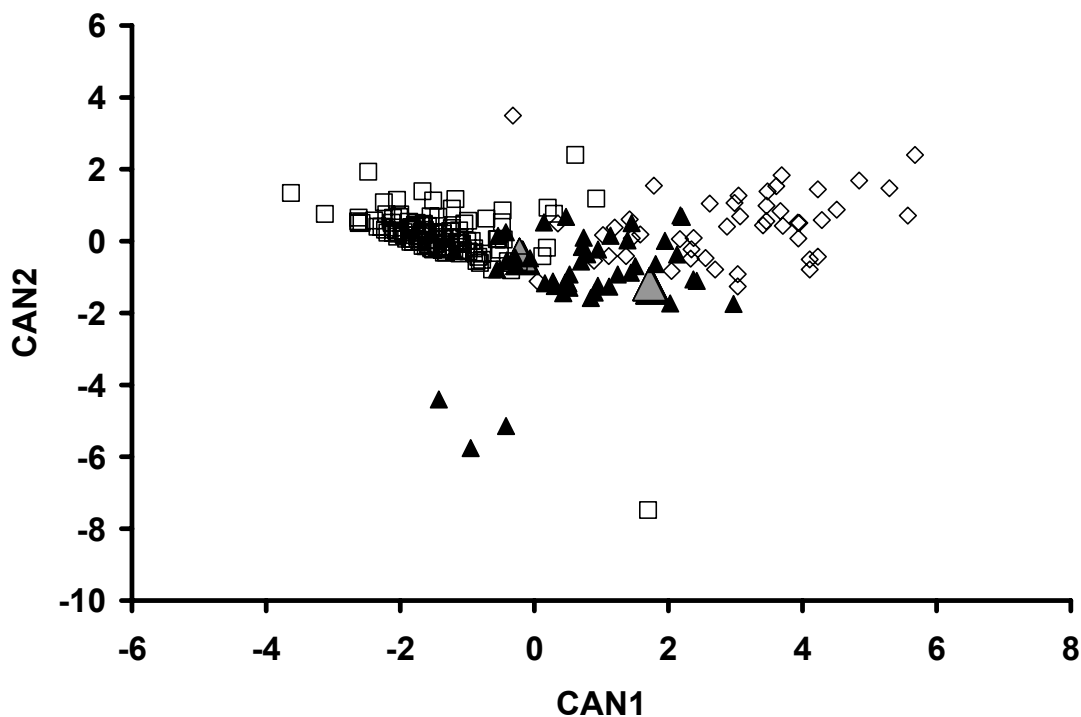


Fig. 8.11 Plot of the canonical variables (CAN1, CAN2) generated from analysis of relative curvedness of the proximal articular surface of the 1st metacarpal (*Homo sapiens* = open squares, *Pan* = closed triangles, *Gorilla* = open diamonds, *A. afarensis* = grey triangles).

TABLE 8.22 Correlations between each variable and canonical axis (bolded values indicate the variables that best explain the observed variation along each axis)

Variable	Pooled-within canonical structure	
	CAN1	CAN2
Curvedness		
RMS	0.85	-0.48
absolute	0.91	-0.24
Gaussian	-0.75	-0.37
mean	0.14	0.90

TABLE 8.23 Cross-validated posterior probabilities of genus membership using relative curvedness of the proximal 1st metacarpal articular surface

	<i>Homo</i>	<i>Pan</i>	<i>Gorilla</i>
<i>Homo</i>	112	7	2
%	92.6	5.8	1.7
<i>Pan</i>	6	32	8
%	13.0	69.6	17.4
<i>Gorilla</i>	1	10	36
%	2.1	21.3	76.6

TABLE 8.24 Posterior probabilities of genus membership using relative curvedness of the proximal 1st metacarpal articular surface

	<i>Homo</i> (%)	<i>Pan</i> (%)	<i>Gorilla</i> (%)
AL333-58	0.4	81.5	18.1
AL333w-39	43.2	56.2	0.6

The trapezium. Only one trapezium (AL333-80) is attributed to *A. afarensis* (see Fig. 8.15). A Full Model utilizing all relative areas and angles of the articular surfaces is used to compare this fossil hominin with the extant hominine genera. The fossil trapezium is used only as a test classification case.

The first canonical axis (CAN1) accounts for 83% of the variation while the second (CAN2) accounts for 17%. Along CAN1, modern *Homo* clusters more toward the right while the African apes cluster more toward the left (Fig. 8.12). AL333-80 clusters with modern *Homo*, although it falls on the edge that appears closest to the African ape clusters. The correlations with CAN1 indicate that this axis represents the angle between the first and second metacarpal joint surfaces and the relative areas of the first metacarpal and scaphoid joint surfaces, in comparison with the angles between the first metacarpal and scaphoid joint surfaces, the second metacarpal and scaphoid joint surfaces, and the second metacarpal and trapezoid joint surfaces (Table 8.25). The

modern *Homo* cluster reflects the large relative joint areas and more parallel orientation of the first metacarpal and scaphoid articulations, and a more transversely-oriented second metacarpal joint surface. AL333-80 resembles the trapezium of modern *Homo* in its orientation of the second metacarpal joint surface; however, its relative areas for the first metacarpal and scaphoid surfaces are more like those of *Pan* (Fig. 8.12).

Moreover, the palmar non-articular area between the first metacarpal and trapezoid facets is large like that in the African apes.

The cross-validation procedure of the discriminant analysis resulted in the correct classification of 110 *Homo* (98.2%), 42 *Pan* (89.4%), and 41 *Gorilla* (95.4%; Table 8.26). Using AL333-80 as a test classification case results in its classifying as modern *Homo* (99.8%; Table 8.27).

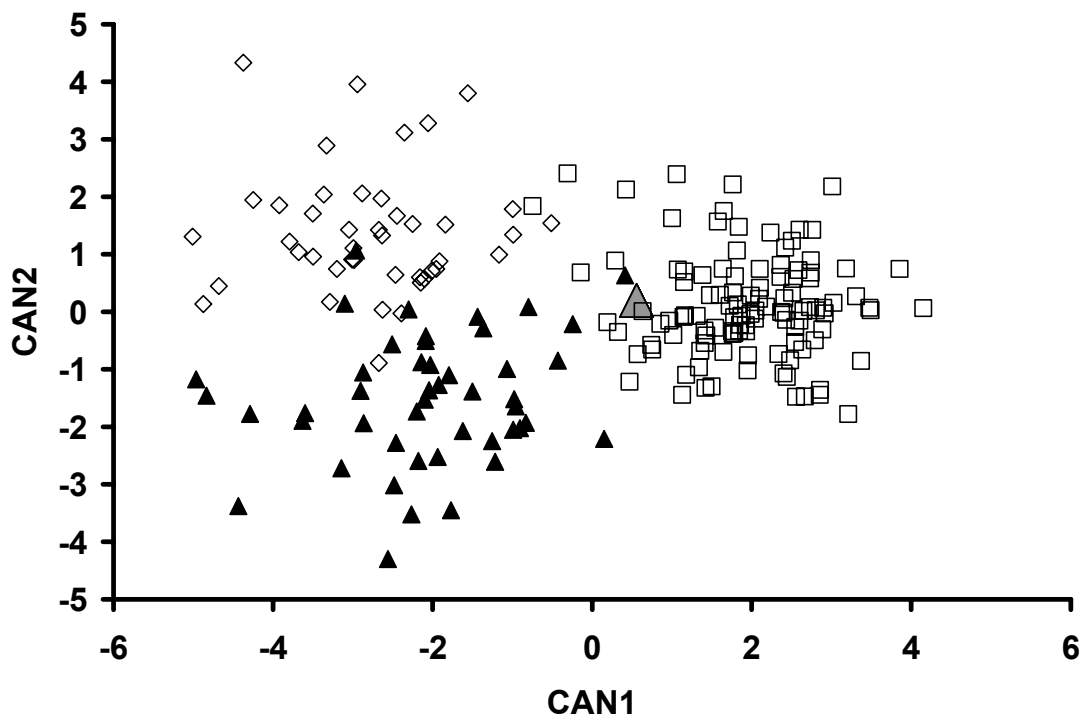


Fig. 8.12 Plot of the canonical variables (CAN1, CAN2) generated from analysis of relative areas and angles of the trapezium articular surfaces (*Homo sapiens* = open squares, *Pan* = closed triangles, *Gorilla* = open diamonds, *A. afarensis* = grey triangle).

TABLE 8.25 Correlations between each variable and canonical axis (bolded values indicate the variables that best explain the observed variation along each axis)

Variable		Pooled-within canonical structure	
		CAN1	CAN2
Angle between			
1st metacarpal	2nd metacarpal	0.59	0.34
1st metacarpal	scaphoid	-0.35	-0.14
1st metacarpal	trapezoid	0.23	0.41
2nd metacarpal	scaphoid	-0.47	0.03
2nd metacarpal	trapezoid	-0.46	0.09
scaphoid	trapezoid	0.04	0.03
Relative surface area			
	1st metacarpal	0.49	-0.17
	2nd metacarpal	0.01	0.09
	scaphoid	0.42	-0.11
	trapezoid	0.29	-0.62

TABLE 8.26 Cross-validated posterior probabilities of genus membership using relative areas and angles of the trapezium articular surfaces

	<i>Homo</i>	<i>Pan</i>	<i>Gorilla</i>
<i>Homo</i>	110	0	2
%	98.2	0.0	1.8
<i>Pan</i>	2	42	3
%	4.3	89.4	6.4
<i>Gorilla</i>	0	2	41
%	0.0	4.7	95.4

TABLE 8.27 Posterior probabilities of genus membership using relative areas and angles of the trapezium articular surfaces

	<i>Homo</i> (%)	<i>Pan</i> (%)	<i>Gorilla</i> (%)
AL333-80	99.8	0.2	0.0

The carpometacarpal joints of the second metacarpal base. A total of three reasonably complete bases of the second metacarpal, AL333-15, AL333-48, and AL333w-23, comprise the *A. afarensis* sample (see Fig. 8.18). Using a Full Model, the second metacarpal bases of these fossils are compared to the extant hominine genera. The variables utilized include the relative areas and angles of the articulating surfaces. As always, the fossils are used only as test classification cases. The canonical scores of each fossil specimen are based on the particular measurements of each fossil second metacarpal base.

The first canonical axis (CAN1) accounts for 88% of the variation while the second (CAN2) accounts for 12%. Along CAN1, modern *Homo* clusters more toward the right while the African apes cluster more toward the left (Fig. 8.13). The correlations with CAN1 indicate that the separation along this axis is mostly accounted for by a comparison of the four angles involving the capitate joint surface (Table 8.28). The modern *Homo* cluster reflects a smaller angle between the capitate and third metacarpal

surfaces, and larger angles between the capitate joint surface and the trapezium, and lateral and medial trapezoid joint surfaces. Together, these four angles contribute to a more positive loading for modern *Homo* along CAN1. The three *A. afarensis* fossil second metacarpal bases show characteristics of both modern *Homo* and *Pan* (Fig. 8.13). AL333-15 clusters with *Pan*, AL333w-23 with *Homo*, and AL333-48 falls directly between the clusters of *Homo* and *Pan* (Fig. 8.13).

The cross-validation procedure of the discriminant analysis resulted in the correct classification of 84 *Homo* (98.8%), 16 *Pan* (94.1%), and 16 *Gorilla* (100%; Table 8.29). Using the fossils as test classification cases results in two of the three bones classified as *Pan*, and one as modern *Homo* (Table 8.30).

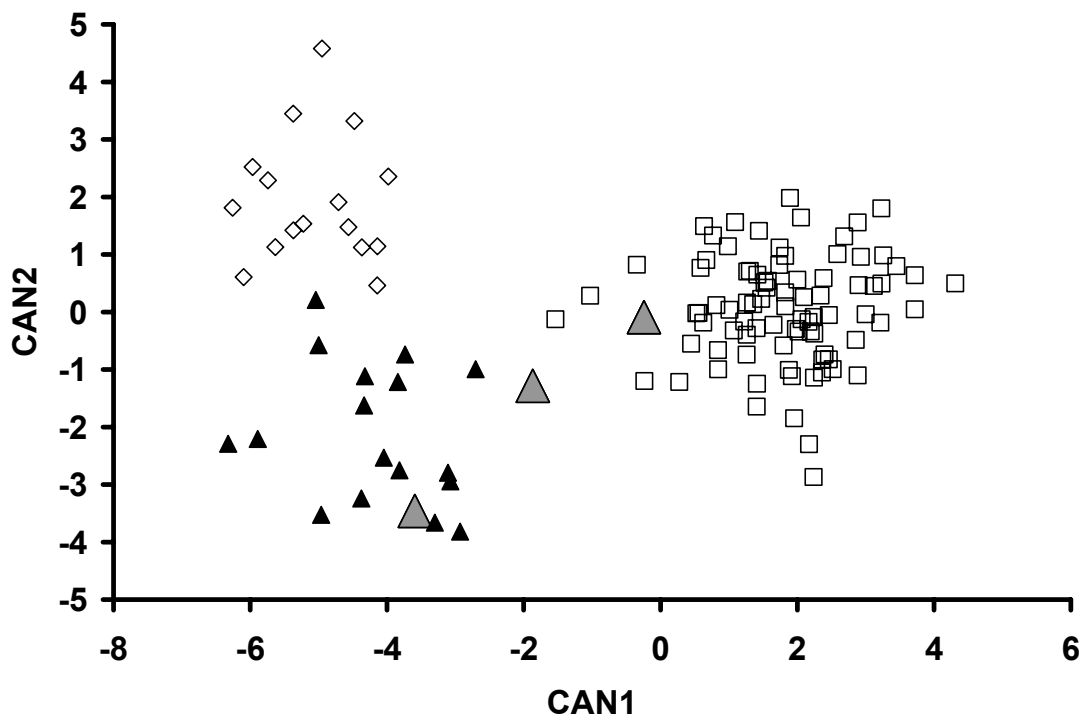


Fig. 8.13 Plot of the canonical variables (CAN1, CAN2) generated from analysis of relative areas and angles of the second carpometacarpal joint surfaces (*Homo sapiens* = open squares, *Pan* = closed triangles, *Gorilla* = open diamonds, *A. afarensis* = grey triangles).

TABLE 8.28 Correlations between each variable and canonical axis (bolded values indicate the variables that best explain the observed variation along each axis)

Variable		Pooled-within canonical structure	
Angle between		CAN1	CAN2
capitate	3rd metacarpal	-0.41	0.08
capitate	lateral trapezoid	0.74	0.07
capitate	medial trapezoid	0.51	0.29
lateral trapezoid	medial trapezoid	-0.08	0.51
3rd metacarpal	trapezium	0.23	0.23
capitate	trapezium	0.53	0.13
trapezium	lateral trapezoid	0.25	0.16
trapezium	medial trapezoid	0.21	-0.39
<u>Relative surface area</u>			
	capitate	-0.05	-0.39
	trapezium	0.03	0.14
	lateral trapezoid	0.09	-0.08
	medial trapezoid	-0.26	0.37

TABLE 8.29 Cross-validated posterior probabilities of genus membership using relative areas and angles of the second metacarpal base articular surfaces

	<i>Homo</i>	<i>Pan</i>	<i>Gorilla</i>
<i>Homo</i>	84	1	0
%	98.8	1.2	0.0
<i>Pan</i>	0	16	1
%	0.0	94.1	5.9
<i>Gorilla</i>	0	0	16
%	0.0	0.0	100.0

TABLE 8.30 Posterior probabilities of genus membership using relative areas and angles of the second metacarpal base articular surfaces

	<i>Homo</i> (%)	<i>Pan</i> (%)	<i>Gorilla</i> (%)
AL333-15	0.0	100.0	0.0
AL333-48	1.0	98.9	0.1
AL333w-23	100.0	0.0	0.0

Other hominin fossils

Two additional first metacarpal fossils from Swartkrans (SK84 and SKX5020) were also analyzed (Napier, 1959; Susman, 1988; Trinkaus and Long, 1990). A Partial Model is used to examine the morphological affinities of these fossils. This is the identical model that was used for the analysis of the *A. afarensis* first metacarpals and only the new canonical plot is displayed here (Fig. 8.14). For further details regarding the results of the model, please refer to Tables 8.22 and 8.23. The variables utilized include the relative curvedness measures of the proximal articular surface of the first metacarpal. The fossils are used only as test classification cases.

The taxonomic status of the two Swartkrans fossils has been the subject of debate as have interpretations regarding their tool-making capability (Hamrick and Inouye, 1995; Marzke, 1997; Ohman et al., 1995; Susman, 1988, 1991, 1994, 1998; Trinkaus and Long, 1990). An even more pressing issue is the lack of accurate dates for the Swartkrans material, and similarly for South African hominin fossil sites in general. In any event, from a strictly morphological perspective, the results here are similar to the original published descriptions of both of these pollical metacarpals: SK84 displays a morphological affinity to *Pan*, *Gorilla*, and *A. afarensis* (Napier, 1959; Rightmire, 1972) whereas SKX5020 displays a morphological affinity to *Homo* (Susman, 1988).

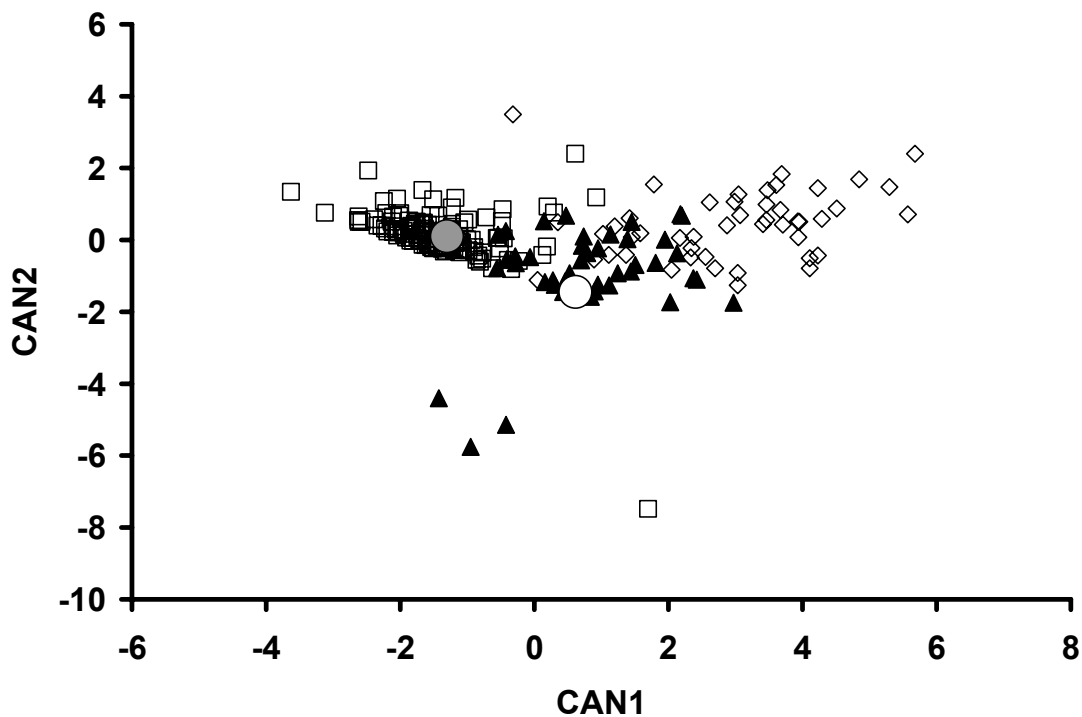


Fig. 8.14 Plot of the canonical variables (CAN1, CAN2) generated from analysis of relative curvedness of the proximal articular surface of the first metacarpal (*Homo sapiens* = open squares, *Pan* = closed triangles, *Gorilla* = open diamonds, SK84 = open circle, SKX5020 = grey circle).

TABLE 8.31 Summary of the trapezium surface curvedness measures of the 1st metacarpal in the fossil specimens

Variable	Qafzeh 9	Kebara 2	La Ferrassie 1	La Ferrassie 2	Regourdou 1	Amud 1	La Chapelle 1	SKX5020	SK84	AL333-58	AL333w-39
Dorsopalmar	0.17	-0.01	0.20	0.30	-0.07	0.18	-0.38	0.44	0.32	0.60	0.52
Radioulnar	-1.10	-1.08	-0.92	-1.07	-0.87	-0.91	-1.12	-0.83	-1.28	-1.34	-1.00
RMS	1.11	1.08	0.94	1.11	0.87	0.93	1.18	0.94	1.32	1.46	1.13
Absolute	1.27	1.09	1.12	1.37	0.94	1.09	1.49	1.28	1.60	1.94	1.52
Gaussian	-0.19	0.01	-0.19	-0.32	0.06	-0.16	0.42	-0.37	-0.41	-0.80	-0.52
Mean	-0.46	-0.55	-0.36	-0.38	-0.47	-0.36	-0.75	-0.19	-0.48	-0.37	-0.24

TABLE 8.32 Summary of the angles, relative areas, and curvedness measures of the trapezium in the fossil specimens

<u>Variable</u>		<u>Fossil Specimen</u>								
Angle between		Qafzeh 9	Kebara 2	La Ferrassie 1	La Ferrassie 2	Regourdou 1	Shanidar 3	Shanidar 4	OH7	AL333-80
1st metacarpal	2nd metacarpal	81	85		98	86	92	86	75	96
1st metacarpal	scaphoid	20	16	16	17	10	13	21	9	15
1st metacarpal	trapezoid	44	58		53	60	49	50	45	38
2nd metacarpal	scaphoid	80	79		66	85	75	74	106	85
2nd metacarpal	trapezoid	142	149		131	144	133	142	150	120
scaphoid	trapezoid	117	107		110	112	118	112	136	145
<u>Relative surface area</u>										
1st metacarpal		19.9	13.2	16.0	18.0	14.3	16.8	15.5	21.1	13.7
2nd metacarpal		1.9	2.0		3.9	2.5	2.2	1.5	1.6	2.9
scaphoid-centrale		8.5	6.8	6.8	7.6	6.4	7.3	4.4	6.6	7.1
trapezoid		7.0	8.6		5.1	5.9	7.1	6.7	7.1	9.5
non-articular		62.7	69.4	77.1	65.3	70.9	66.5	72.0	63.7	66.8
<u>Curvedness</u>										
Dorsopalmar		-1.00	-0.43	-0.54	-0.61	-0.52	-0.49	-0.32	-0.47	-0.92
Radioulnar		0.42	0.46	0.53	0.65	0.53	0.54	0.49	0.33	0.51
RMS		1.08	0.63	0.75	0.89	0.74	0.73	0.59	0.57	1.05
Absolute		1.41	0.89	1.07	1.26	1.04	1.02	0.82	0.80	1.43
Gaussian		-0.41	-0.20	-0.28	-0.39	-0.27	-0.26	-0.16	-0.16	-0.47
Mean		-0.29	0.02	0.00	0.02	0.00	0.03	0.09	-0.07	-0.20

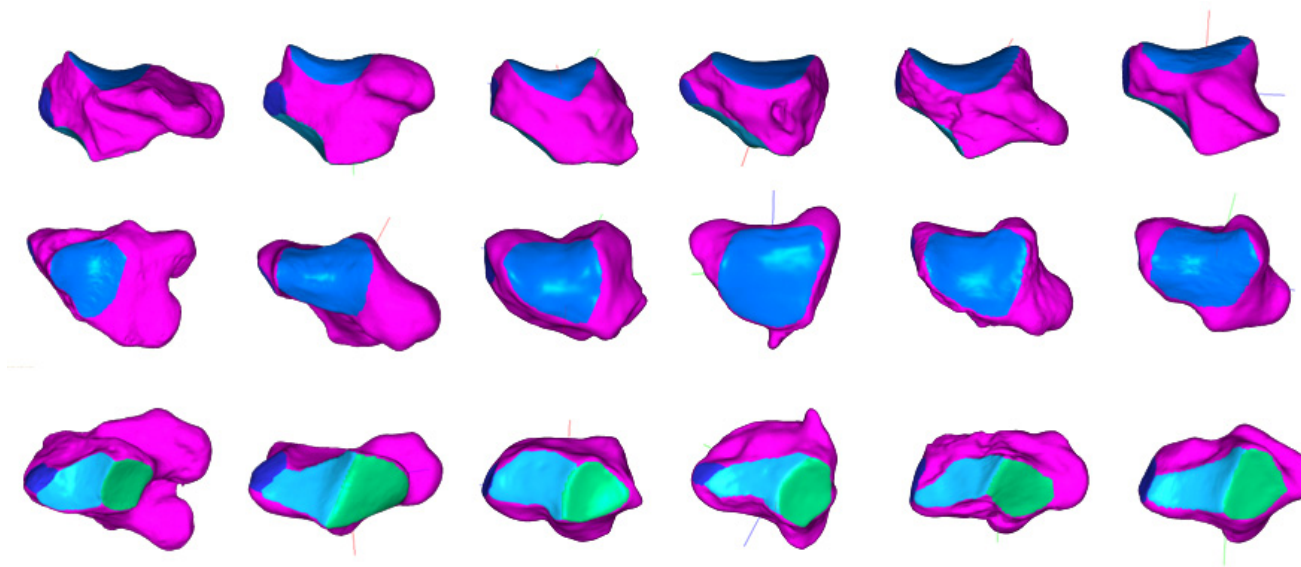


Fig. 8.15 Visual comparison of trapezium shape in extant hominines with fossil specimens (*Gorilla*, far left; *Pan*, 2nd from left; AL333-80, 3rd from left; OH7, 3rd from right; Shanidar 3, 2nd from right; modern *Homo sapiens*, far right). Key: top row, palmar view; middle row, distal view; bottom row, proximo-medial view; medium blue, 1st metacarpal joint; dark blue, 2nd metacarpal joint; light blue, trapezoid joint; light green, scaphoid joint; pink, non-articular area. Bones are from the right side.

TABLE 8.33 Summary of the angles and relative areas of the trapezoid in the fossil specimens

<u>Variable</u>		<u>Fossil Specimen</u>				
Angle between		Qafzeh 9	Combe-Capelle 1	Kebara 2	La Ferrassie 2	Amud 1
lateral 2nd metacarpal	medial 2nd metacarpal	128	123	153	136	142
lateral 2nd metacarpal	scaphoid	21	29	5	9	29
lateral 2nd metacarpal	trapezium	114	125	85	96	111
medial 2nd metacarpal	scaphoid	39	34	31	38	34
medial 2nd metacarpal	trapezium	65	74	59	59	76
scaphoid	trapezium	85	84	92	93	93
capitate	lateral 2nd metacarpal	53	66	82	84	72
capitate	medial 2nd metacarpal	104	123	109	128	110
capitate	scaphoid	111	86	103	90	94
capitate	trapezium	22	24	24	42	26
<u>Relative surface area</u>						
	capitate	7.1	7.5	7.6	4.0	3.2
	lateral 2nd metacarpal	9.1	2.8	9.4	4.2	6.3
	medial 2nd metacarpal	12.2	11.0	11.2	13.8	10.0
	scaphoid	11.2	5.6	13.7	12.3	6.1
	trapezium	12.3	12.3	13.6	10.7	5.8
	non-articular	48.1	60.8	44.5	55.1	68.5

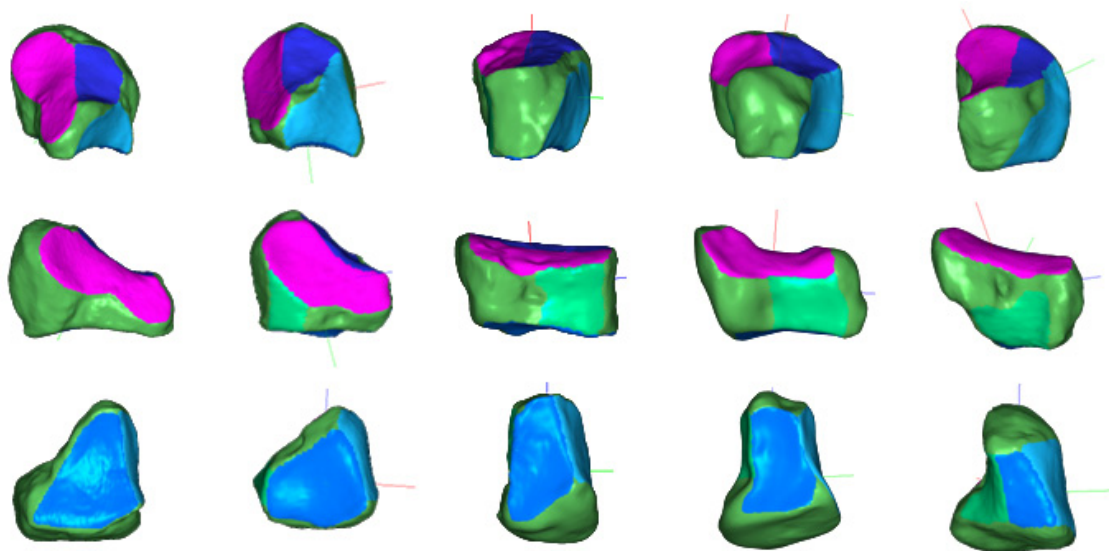


Fig. 8.16 Visual comparison of trapezoid shape in extant hominines with fossil specimens (*Gorilla*, far left; *Pan*, 2nd from left; Kebara 2, middle; Qafzeh 9, 2nd from right; modern *Homo sapiens*, far right). Key: top row, palmar view; middle row, medial view; bottom row, proximal view; pink, medial 2nd metacarpal joint; dark blue, lateral 2nd metacarpal joint; light blue, trapezium joint; medium blue, scaphoid joint; light green, capitate joint; dark green, non-articular area. Bones are from the right side (images of Kebara 2 and Qafzeh 9 are mirrored).

TABLE 8.34 Summary of the angles and relative areas of the scaphoid in the fossil specimens

<u>Variable</u>		<u>Fossil Specimen</u>									
Angle between		Qafzeh 9	Combe-Capelle 1	Kebara 2	La Ferrassie 1	Regourdou 1	Regourdou 2	Shanidar 3	Shanidar 4	Shanidar 8	OH7
capitate	lunate	151	146		153	147	150				161
capitate	radius	32	36	33	38	35	33	38	51	33	36
capitate	trapezium-trapezoid	73	93	81	83	80	77	73	66	78	58
lunate	radius	55	48		55	55	59				54
lunate	trapezium-trapezoid	44	66		57	47	49				40
radius	trapezium-trapezoid	84	67	76	74	83	82	82	71	80	87
<u>Relative surface area</u>											
	capitate	18.7	14.2	18.0	17.7	18.9	18.0	14.7	18.2	18.8	19.5
	lunate	2.6	2.3		2.7	2.3	2.2				5.0
	radius	24.5	26.5	23.7	21.5	22.6	23.2	26.1	19.3	23.7	15.8
	trapezium-trapezoid	16.4	14.8	17.9	12.2	15.7	15.2	14.4	15.2	15.4	10.4
	non-articular	37.9	42.2	40.5	45.8	40.4	41.4	44.8	47.3	42.1	49.3

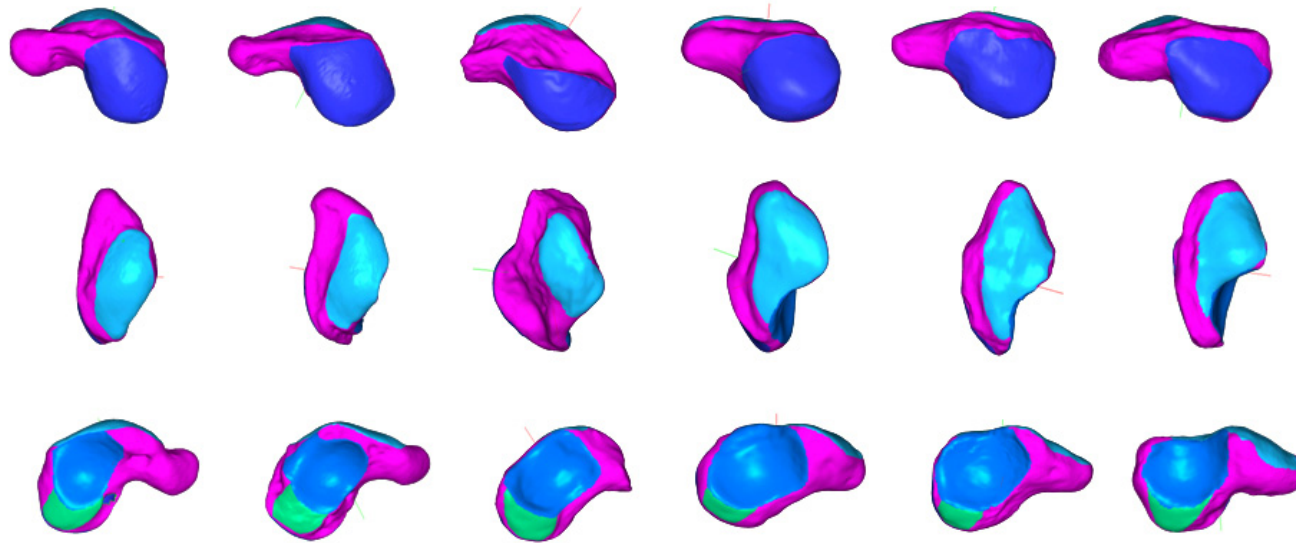


Fig. 8.17 Visual comparison of scaphoid shape in extant hominines with fossil specimens (*Gorilla*, far left; *Pan*, 2nd from left; OH7 (partial), 3rd from left; Regourdou 1, 3rd from right; Qafzeh 9, 2nd from right; modern *Homo sapiens*, far right). Key: top row, radial view; middle row, distal view; bottom row, ulnar view; medium blue, capitate joint; dark blue, radius joint; light blue, trapezium-trapezoid joint; light green, lunate joint; pink, non-articular area. Bones are from the right side (image of Regourdou 1 is mirrored).

TABLE 8.35 Summary of the angles and relative areas of the 2nd metacarpal base in the fossil specimens

<u>Variable</u>		<u>Fossil Specimen</u>							
Angle between		La Ferrassie 2	Regourdou 2	La Chapelle 1	Shanidar 5	Shanidar 6	AL333-15	AL333-48	AL333w-23
capitate	3rd metacarpal	134	122	96	151	109	152	163	139
capitate	lateral trapezoid	144	164	171	116	149	111	126	136
capitate	medial trapezoid	102	113	128	92	124	50	48	85
capitate	trapezium	112	99	112	73	125	52	70	84
3rd metacarpal	trapezium	67	57	40	47	58	36	53	44
trapezium	lateral trapezoid	133	107	120	123	110	106	99	116
trapezium	medial trapezoid	150	126	155	139	141	143	135	145
lateral trapezoid	medial trapezoid	136	129	134	155	132	118	102	129
<u>Relative surface area</u>									
capitate		8.7	14.9	15.6	17.1	9.0	25.7	22.5	25.7
trapezium		10.2	10.3	7.4	19.1	12.7	5.2	10.2	7.4
3rd metacarpal		31.8	31.2	20.7	17.7	30.2	21.4	16.9	12.2
lateral trapezoid		19.2	13.4	21.7	16.0	12.0	10.1	15.8	18.4
medial trapezoid		30.0	30.2	34.6	30.1	36.1	37.7	34.7	36.3

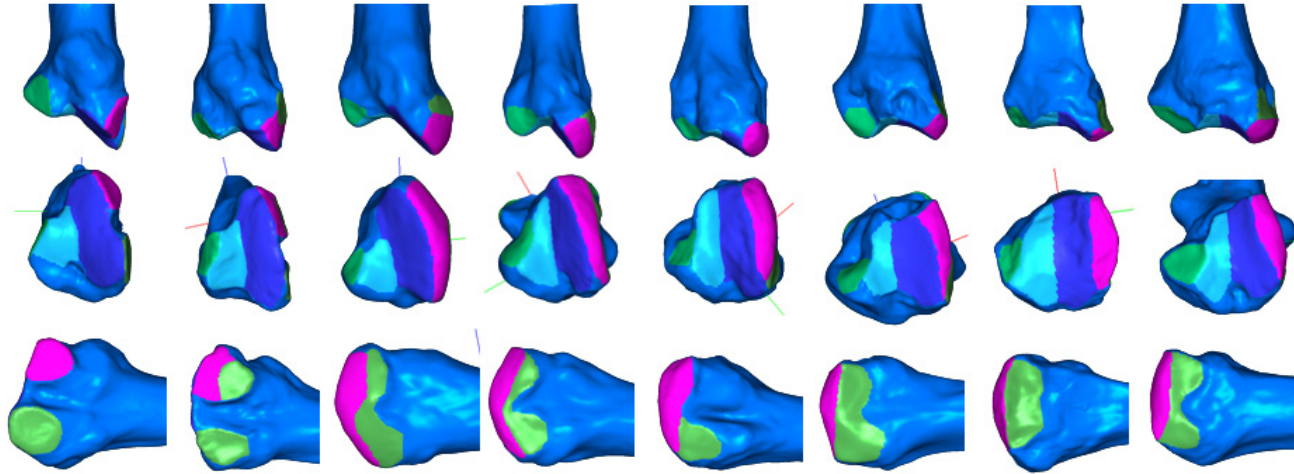


Fig. 8.18 Visual comparison of 2nd metacarpal base shape in extant hominines with fossil specimens (*Gorilla*, far left; *Pan*, 2nd from left; AL333-15, 3rd from left; AL333-48, 4th from left; AL333w-23, 4th from right; Regourdou 2, 3rd from right; La Chapelle-aux-Saints 1, 2nd from right; modern *Homo sapiens*, far right). Key: top row, palmar view; middle row, proximal view; bottom row, medial view; dark green, 3rd metacarpal joint; pink, capitate joint; dark blue, medial trapezoid joint; light blue, lateral trapezoid joint; light green, trapezium joint; medium blue, non-articular area. Bones are from the left side (images of AL333w-23, Regourdou 2, and La Chapelle-aux-Saints 1 are mirrored).

SUMMARY DISCUSSION

As I argued in the introductory chapter, this dissertation research tests a hypothesis of morphological adaptation to behavior using a combination of two historical definitions of adaptation. First, the adaptive characters must represent derived morphology that did not appear in the population until after the appearance of the adaptive behavior. Second, the derived morphology must have functional advantages for executing the adaptive behavior that the ancestral morphology does not.

Using both a derived trait definition of adaptation and a teleonomic definition of adaptation is typically too strict an approach for testing hypotheses of adaptation; however, the human fossil record is unique in that it includes direct evidence of behavior in the form of stone tool technology. It is the combination of evidence from behavioral and morphological sources that enables this otherwise strict approach to be undertaken.

Following Napier's influential studies of the evolution and functional morphology of the hand and wrist (e.g., 1955, 1956, 1959, 1960, 1961, 1962, 1965), significant contributions have been made by several researchers including Lewis (e.g., 1977, 1989), Marzke (e.g., 1971, 1992, 1997, 2005), McHenry (1983), Rose (e.g., 1977, 1988, 1992), Sarmiento (e.g., 1985, 1988), Susman (e.g., 1988, 1989, 1991, 1994, 1998), and Trinkaus (1983, 1989). The research presented in this dissertation is an extension of all of this important previous work as well as an attempt to synthesize the resulting knowledge of wrist structure and function into a common framework for interpreting

the evolutionary history and adaptive significance of the radial carpometacarpal and carpal region in hominins (Figs. 8.19 and 8.20).

The goal of this dissertation research is to answer the following basic question (the ‘riddle’ of the radial wrist): do hominins show morphological commitment in the radial carpometacarpal and carpal region of the hand to manipulative behaviors such that a) the ancestral morphology is sacrificed, and b) the derived morphology has performance advantages for the behavior (i.e., it is better than the primitive structure with respect to the novel behavior)? If so, when, in which hominins, and in which behavioral contexts did this event most likely occur?

Answering these three questions leads to the solution of the following riddle of the wrist: During the evolution of hominins, did an event occur in which a certain group of hominins underwent morphological specialization to manipulative behaviors related to the manufacture and use of tools, as evidenced by the presence of stone tool technology in the fossil record?

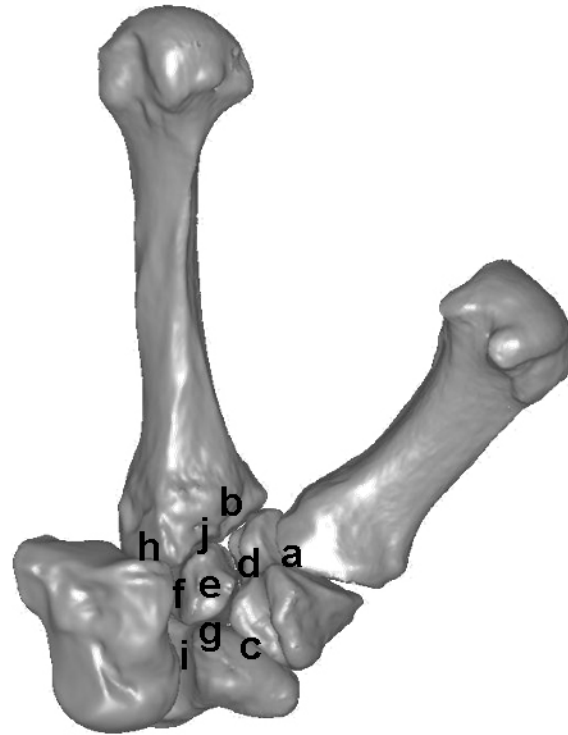


Fig. 8.19 Summary of key features of radial carpal and carpometacarpal joint morphology that are derived in *Homo sapiens* in comparison to non-human primates: **a**, larger 1st carpometacarpal joint; **b**, more proximo-distal orientation of trapezium-2nd metacarpal joint; **c**, larger trapezium-scaphoid joint that extends palmar-radially onto scaphoid tubercle; **d**, narrower palmar trapezium non-articular area; **e**, broader palmar trapezoid non-articular area; **f**, larger, more palmarly-placed trapezoid-capitate joint; **g**, smaller, rectangular shaped trapezoid-scaphoid joint; **h**, more proximo-distal orientation of capitate-2nd metacarpal joint; **i**, more distally-open capitate-scaphoid joint; **j**, medial 2nd carpometacarpal joint oriented more parallel to trapezoid-scaphoid joint. Bones are from the right side.

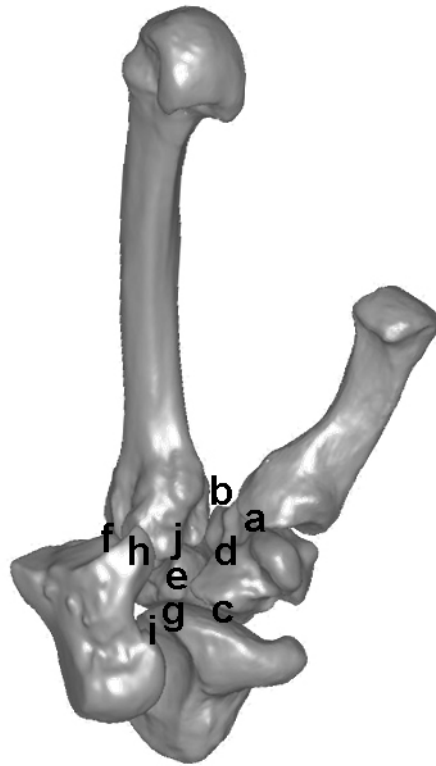


Fig. 8.20 Summary of key features of radial carpal and carpometacarpal joint morphology that are primitive in non-human primates (*Pan troglodytes* is shown): **a**, smaller 1st carpometacarpal joint; **b**, more radio-ulnar orientation of trapezium-2nd metacarpal joint; **c**, smaller trapezium-scapoid joint that extends palmarly in front of trapezoid; **d**, wider palmar trapezium non-articular area; **e**, narrower palmar trapezoid non-articular area; **f**, smaller, more dorsally-placed trapezoid-capitate joint; **g**, larger, triangular shaped trapezoid-scapoid joint; **h**, more radio-ulnar orientation of capitate-2nd metacarpal joint; **i**, more distally-closed capitate-scapoid joint; **j**, medial 2nd carpometacarpal joint oriented more parallel to scaphoid-radius joint. Bones are from the right side.

Evidence from extant catarrhines

The results of the comparative analyses of five extant genera indicate that the observed complex of morphological features in *Homo sapiens* is derived in relationship to the African apes and other primates (Figs. 8.19-8.21). Therefore, it is parsimonious to infer that this complex of derived features evolved sometime after the splitting of the *Pan-Homo* clade between four and eight million years ago (Eizerik et al., 2004; Kumar et al., 2005; Steiper and Young, 2006; Wood and Richmond, 2000).

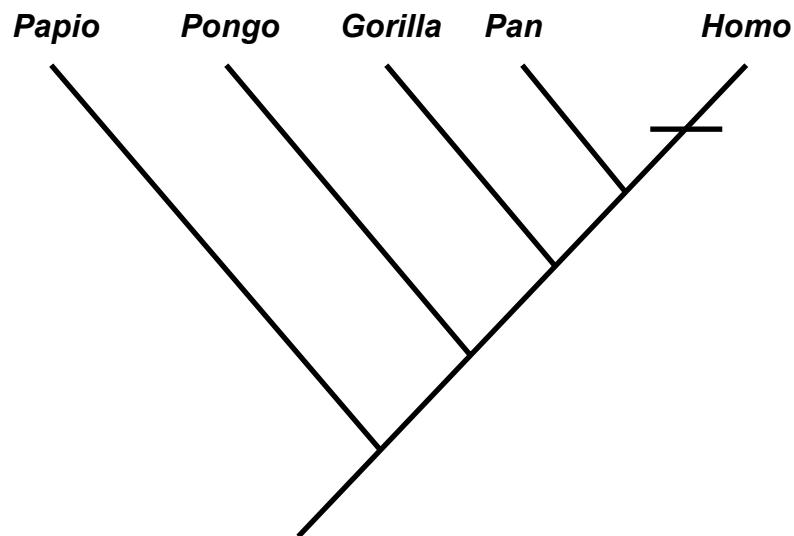


Fig. 8.21 Cladogram based on the comparative analyses presented in the previous chapters. Together, the evidence indicates that the complex of derived features observed in *H. sapiens* (horizontal line) evolved sometime after the *Pan-Homo* split.

Evidence from Upper Paleolithic *Homo sapiens* and Upper and Middle Paleolithic Neandertals

For the purposes of this analysis, whether Neandertals represent a distinct species of *Homo* or a distinct population of *Homo sapiens* is not a confounding issue. In either case, Neandertals and modern *Homo sapiens* share a most recent common ancestor

(MRCA), which genetic evidence is 95% confident existed between 468,000 and 1,015,000 years ago (Noonan et al., 2006). The presence or absence of the complex of derived features in Neandertals tests the likelihood that the complex was present or absent in the MRCA (Fig. 8.22). If the complex is present in Neandertals, then parsimony suggests that it was present in the MRCA; if it is absent in Neandertals, then parsimony suggests that the complex evolved sometime after modern *H. sapiens* diverged from the MRCA. Answering this question is a critical first step in determining the behavioral context in which this complex of features evolved. In other words, did the complex of derived features evolve in the behavioral context characteristic of modern *H. sapiens* as found at Upper Paleolithic sites? Or did it evolve much earlier in the evolution of hominins?

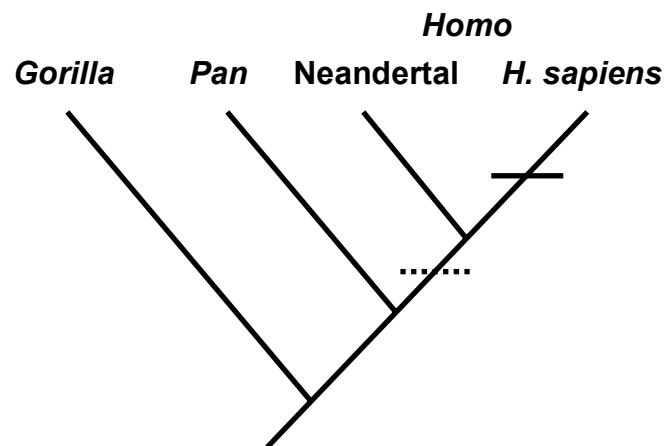


Fig. 8.22 The principle of parsimony suggests that the complex of derived features evolved either prior to the Neandertal-modern *H. sapiens* divergence (dotted line) or after (solid line) depending on whether the complex is present or absent in Neandertals.

All of the Upper Paleolithic *H. sapiens* and Upper and Middle Paleolithic Neandertal fossils examined exhibit the complex of morphological features as observed in modern

H. sapiens. Like modern *H. sapiens*, these fossil hominins show a) relatively large first carpometacarpal joint surfaces; b) more proximo-distal orientation of trapezium-second metacarpal joint; c) larger trapezium-scapoid joint that extends palmar-radially onto the scaphoid tubercle; d) narrower palmar trapezium non-articular area; e) broader palmar trapezoid non-articular area; f) larger, more medio-palmarly placed trapezoid-capitate joint; g) smaller, rectangular shaped trapezoid-scapoid joint; h) more proximo-distal orientation of capitate-second metacarpal joint; i) more distally-open capitate-scapoid joint; j) medial second carpometacarpal joint oriented more parallel to trapezoid-scapoid joint (Figs. 8.15-8.19).

In total, the evidence strongly suggests that the complex of derived morphological features was present in the MRCA of modern *H. sapiens* and Neandertals. Indeed, this result is corroborated by the morphological evidence of a left capitate (ATD6-24) from the Gran Dolina site at Sierra de Atapuerca (Lorenzo et al., 1999). This capitate, attributed to *H. antecessor*, was recovered from the Early Pleistocene level TD6, which dates to between 780 and 857 thousand years ago (Falgueres et al., 1999). Although the capitate was not part of the quantitative analyses in this dissertation, the radial side of this fossil bone exhibits morphology that corresponds with and therefore reflects the derived complex of features examined here, as follows. It is the trapezoid in *Homo* that is particularly derived in comparison to non-human primates, and each of the articulating bones shows morphological changes that correlate with the shape change of the trapezoid. In this sense, the trapezoid is the central unit of the complex of derived features and each articulating bone represents a supporting unit. On the ulnar side of

the trapezoid, the derived condition in *Homo* is an enlarged, more palmarly-placed facet for the capitate. The correlated change in the capitate is an enlarged, more palmarly-placed facet for the trapezoid. This distinctive feature of *Homo* has long been recognized (Fick, 1904; Lewis, 1989; McHenry, 1983), and Lewis (1989) even discussed its possible importance to the human power grip. A further change in *Homo* occurs on the base of the second metacarpal where the articulation for the capitate is more proximally oriented (Marzke, 1983; McHenry, 1983), particularly on the more palmar aspect. This supporting change helps stabilize the capitate during radio-ulnar compression of the wrist such that the more palmarly-positioned joint surfaces between the capitate and trapezoid maintain maximum contact with one another.

The ATD6-24 capitate clearly shows the derived condition for its trapezoid and second metacarpal joint surfaces. The angle between its second and third metacarpal joint surfaces is similar to that in modern humans while the trapezoid joint surface is enlarged and palmarly-placed (Lorenzo et al., 1999). Interestingly, Lorenzo et al. (1999) note that this capitate also displays a very small, dorsally-placed articulation for the trapezoid, which is the primitive condition in non-human primates. They conclude that “ATD6-24 is the most ancient fossil with a morphology of the trapezoid facet transitional between *Australopithecus* and later *Homo*” (Lorenzo et al., 1999: 509). However, the facet pattern is a relatively common variation seen in approximately 10% of the modern humans sampled in this study. Rather than being transitional, this facet pattern is correlated with changes relating to the neighboring scaphoid and trapezoid. In *Homo*, the joint surfaces for the scaphoid and trapezoid on the radial side of the capitate

are typically confluent. The confluence of these articular facets is correlated with a more distally-open capitate joint on the scaphoid. In approximately 10% of modern humans, however, the two facets on the capitate are variably separated. When this occurs, the capitate joint on the scaphoid is less distally-open, which results in the trapezium-trapezoid joint surface resembling the more primitive condition in the African apes—the joint area for the trapezoid is enlarged and there is ligament between the centrale portion of the scaphoid and the capitate (Lewis, 1989). Consequently, the trapezoid displays a relatively larger, more triangular joint surface for the scaphoid and also often displays a small, dorsally-placed facet for the capitate. However, this latter feature always occurs in addition to the derived enlarged, palmarly-placed facet.

Indeed, Lewis (1989) describes and illustrates a modern human capitate that retains the dorsal trapezoid joint surface. It is the same condition seen in the ATD6-24 capitate. Lewis (1989), however, did not recognize the connection between this feature and the separation of the scaphoid and palmar trapezoid facets on the capitate (although it is clearly evident in his illustration) and the correlated changes involving the scaphoid and trapezoid. As a group of correlated morphological features forming part of the derived condition in *Homo*, these represent one end of the range of variation that more closely resembles some of the features that characterize the primitive primate condition. These features underscore the developmental processes that result in correlated morphology among the carpal bones.

In total, the evidence from the Upper Paleolithic *H. sapiens* and Upper and Middle Paleolithic *H. neanderthalensis* samples, along with the evidence of the ATD6-64

capitate, suggests that the complex of derived morphological features in the radial carpal and carpometacarpal region of *Homo* evolved at least as early as 800 thousand years ago.

Evidence from *Australopithecus*

The presence or absence of the complex of derived features in *A. afarensis* tests whether the complex is primitive for later appearing hominins (Fig. 8.23). Answering this question is critical in determining the behavioral context in which this complex of features evolved. Presence of the complex in *A. afarensis* would suggest that these features evolved prior to the intensification of stone tool-related behaviors during the Oldowan (falsifying a hypothesis of adaptation to stone tool-related manipulative behaviors). Absence of the complex in *A. afarensis* would suggest that these features evolved later in the hominin lineage, increasing the likelihood that the complex is a morphological adaptation to the intensification of stone tool-related manipulative behaviors.

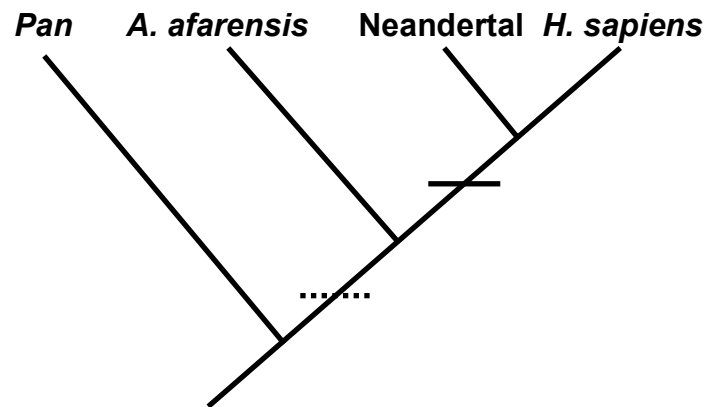


Fig. 8.23 The principle of parsimony suggests that complex of derived morphological features evolved either prior to the first appearance of intensified stone tool-related manipulative behaviors (dotted line) or after (solid line) depending on whether the complex is present or absent in *A. afarensis*.

A. afarensis does not exhibit the complex of derived morphological features associated with modern *H. sapiens*, Neandertals, or *H. antecessor*. However, this hominin species shows one of the derived features and possibly a second as well. The trapezium-second metacarpal joint is oriented proximo-distally (the derived condition) but the capitate-second metacarpal joint falls somewhat in between the radio-ulnar orientation seen in great apes (the primitive condition) and the derived orientation seen in *Homo* (Figs. 8.15, 8.18-8.20). The more oblique angle of this latter joint has been described by others (Bush et al., 1982; Marzke, 1983; McHenry, 1983).

The remaining eight features are all more like that seen in the African apes. In particular, the AL333-80 trapezium displays a wide palmar non-articular area between the first metacarpal and trapezoid facets and a relatively small scaphoid articular area. The capitates of *A. afarensis* show a more dorsally-placed facet for the trapezoid (Bush

et al., 1982; Johanson et al., 1982a, b; Marzke, 1983; McHenry, 1983) and the second metacarpal articular surfaces for the trapezoid are strongly \wedge -shaped (Fig. 8.18).

Together, the morphological evidence from the trapezium, capitate, and second metacarpal base suggests that the trapezoid of *A. afarensis* retains the basic shape that is primitive for hominids and other non-human primates (Fig. 8.20)!

Without the radio-ulnar expansion of the trapezoid palmarly, the trapezium is in a more pronated position relative to the rest of the wrist. Recall that in *H. sapiens* and Neandertals the trapezium is in a more supinated position. The second metacarpal joints with the trapezium and capitate in *A. afarensis* have been interpreted as facilitating slight pronation, or ‘give’, of the metacarpal base as in modern humans despite noted differences in structural details (Marzke, 1983), and similar conclusions have been reached in subsequent analyses (McHenry, 1983; Marzke, 1997; Tocheri et al., 2003). It is possible that the more oblique orientation of the capitate-second metacarpal joint observed in *A. afarensis* is compensating for the more pronated position of the trapezium, and thus still allows a degree of pronation. However, it should also be considered that, given the likely inferred primitive shape of the trapezoid, this region of the wrist in *A. afarensis* may have functioned quite differently than it does in modern humans. For example, in great apes the joint between the second metacarpal and trapezoid is deeply \wedge -shaped because the medial half of the joint runs obliquely from the disto-radial point where it meets the lateral half of the joint to its proximo-ulnar edge (Fig. 8.18). This morphology effectively stabilizes the second metacarpal base radio-ulnarly while the overall wedge-shape of the trapezoid places the

trapezium in a more palmar position relative to the trapezoid. The results here suggest a similar condition in *A. afarensis*, raising questions about how this joint complex, which displays a unique combination of human-like and ape-like features, may have functioned in this fossil taxon.

It is not known with certainty which, if any, of the *A. afarensis* fossils analyzed here belong to the same individual (Johanson et al., 1982b); however, for exploratory purposes, I assume that the three second metacarpal bases, two first metacarpal bases, and one trapezium represent six possible individuals. Using a Partial Model that includes the relative areas, angles, and curvedness measures of these three bones, the six composite *A. afarensis* individuals are examined (Fig. 8.24). The variables that drive the separation of the genera are the same as presented for each bone separately and are not repeated here. However, the overall picture is clear. The condition of *A. afarensis* is one that is derived in comparison to the African apes (because of the changes in orientation of the trapezium and capitate joints with the second metacarpal base), yet primitive in comparison to *Homo* (because of retention of the ancestral trapezoid shape). Therefore, it is reasonable to conclude that the full complex of derived morphological features characteristic of later species of *Homo*, had yet to evolve within the hominin lineage in East Africa at 3 Ma.

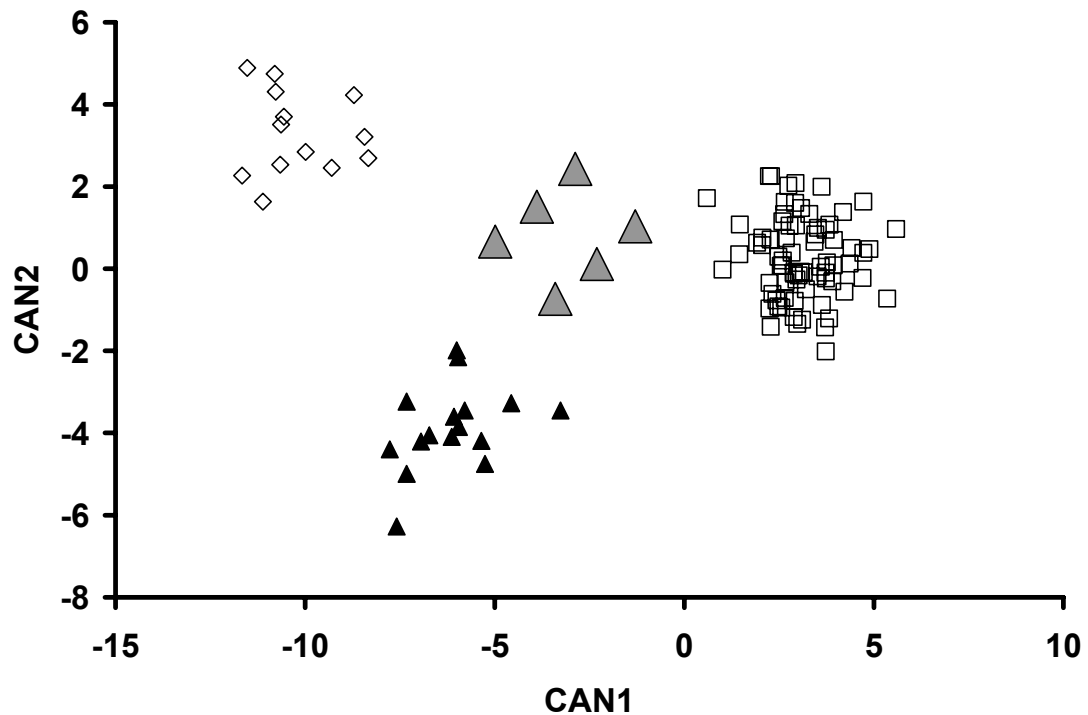


Fig. 8.24 Plot of the canonical variables (CAN1, CAN2) generated from analysis of relative areas, angles, and curvedness measures of the trapezium, 1st metacarpal, and 2nd metacarpal joint surfaces (*Homo sapiens* = open squares, *Pan* = closed triangles, *Gorilla* = open diamonds, *A. afarensis* = grey triangles).

There is also fossil evidence that suggests *A. africanus* exhibited an overall similar condition as seen and inferred here in *A. afarensis*. The *A. africanus* capitata (TM1526) is described as showing the same unique combination of characters as the *A. afarensis* capitates (McHenry, 1983). In particular, TM1526 displays a dorsally-placed trapezoid facet along with a ‘waisted’ neck (McHenry, 1983), both of which are shared, primitive characters that indicate that the trapezoid would also display the primitive shape. However, TM1526 also displays a disto-laterally facing articulation for the second metacarpal, which is the condition seen only in *A. afarensis* (McHenry, 1983)—recall

that the primitive condition is a laterally-facing articulation and the derived condition in *Homo* is a distally-facing articulation.

Although the first (STW418) and second (STW382) metacarpals have yet to be formally described, both show strong resemblances to their counterparts in *A. afarensis*. Digital photographs of the original specimens were kindly provided by David Green, a doctoral student at George Washington University. The first metacarpal base shows the highly curved saddle surface seen in *A. afarensis*, *Pan*, and *Gorilla*. The second metacarpal base shows the oblique orientation of the lateral half of the articulation for the trapezoid as seen in *A. afarensis*, *Pan*, and *Gorilla*, as well as the more proximal orientation of the trapezium articulation as seen in *A. afarensis*, *H. neanderthalensis*, and *H. sapiens*. And as expected, the second metacarpal base shows a proximo-medially facing articulation for the capitate—a condition shared only with *A. afarensis* that otherwise appears intermediate between the conditions seen in great apes and humans.

The combination of morphology observed in TM1526, STW418, and STW382, provides considerable information as to the articular positions and shapes of the trapezium and trapezoid in *A. africanus*. The first metacarpal surface of the trapezium likely resembles the surface seen in AL333-80 while the trapezoid likely retains the primitive shape observed in all great apes. The conclusion is similar as for *A. afarensis*: the full complex of derived features had yet to evolve within the South African hominin lineage between approximately 2 and 3 Ma (Clarke, 2002; Schwarcz et al., 1994).

Evidence from *Homo habilis*

Of all the fossils I have examined, the OH7 trapezium is by far the strangest. Its odd combination of features results in it occupying a morphospace that is difficult to interpret. Visually, it also has an overall characteristic that is all its own (Fig. 8.15). In other words, it does not quite look like any other trapezium in these analyses, including ones that plot close to it along any given canonical axis. However, it does bear a slight resemblance to the trapezium of *Nasalis larvatus*, a colobine monkey. It is of interest to note that two adult proximal phalanges that were originally part of the OH7 composite hand were recommended by Day (1976) to be excluded from any future reconstruction, in part because of clear morphological affinities to the modern black and white colobus monkey (*Colobus polykomos*). Perhaps a reappraisal of the taxonomic authenticity of the OH7 trapezium is in order as well, but that is not a goal of this research.

In total, however, the results are clear: the OH7 trapezium lacks the derived features characteristic of later species of *Homo*. A similar conclusion is reached regarding the OH7 scaphoid. With its overall African ape-like appearance, it is clear this fossil scaphoid also lacks the derived features characteristic of later species of *Homo* (Fig. 8.17). Therefore, it appears that by 1.8 Ma, despite 800,000 years of documented Oldowan stone tools, the complex of derived radial carpal and carpometacarpal morphological features had yet to evolve.

This result does not imply that the OH7 hand, or earlier hominin hands, did not possibly have other morphological adaptations for stone tool-related manipulative behaviors. I am well aware that the radial wrist is only a small portion of the complete

anatomical complex that makes up the hand as well as the entire upper limb—all of which are recruited in stone tool-related manipulative behaviors. The overall morphology of the thumb, and its relationship with the morphology of the fingers, may well show morphological adaptations to stone tool-related manipulative behaviors that occur prior to the evolution of the complex of derived radial carpal and carpometacarpal features (Susman, 1988, 1994, 1998). However, attempts to define derived features that appear at or around the same time as the earliest direct evidence of stone tool behavior risk the strong likelihood of identifying exaptations, rather than adaptations, resulting in incorrect inferences about the adaptive origins of such characters and the behavioral context in which they evolved (Marzke, 2005; Smith, 2000).

Evidence from Swartkrans

The two additional first metacarpal fossils analyzed offer only minimal information at best about the presence of the complex of derived features in these South African hominins. This is primarily due to the inability to infer the shape of the trapezoid from pollical joint morphology alone but the poor dating of the Swartkrans material also seriously undermines any specific evolutionary interpretation of these two metacarpals. That said, however, SK84 displays a morphological affinity to *Pan*, *Gorilla*, and *A. afarensis* (Napier, 1959; Rightmire, 1972) whereas SKX5020 shows modern human-like joint curvature.

Susman has argued that SKX5020 belongs to *Paranthropus robustus* and indicates that this hominin was adapted for precision grasping (Susman, 1988, 1991, 1994). The estimated date range of 1.8 to 1.5 Ma for Member 1 of Swartkrans is based on the

faunal composition of the member (Vrba, 1982) as the cave deposits are not suitable for reliable radiometric age estimates. Susman's probabilistic argument for assigning SKX5020, and other hand remains, to *P. robustus* given the presence of *Homo cf. erectus* fossils at Swartkrans is suspect (Trinkaus and Long, 1990). He incorrectly infers that because 95% of the craniodental fossils uncovered in Member 1 are attributed to *Paranthropus*, then "there is an overwhelming probability that any one specimen recovered from Member 1 samples *Paranthropus*" (Susman, 1988: 782). Without some *a priori* knowledge of why the hominin fossils are distributed as they are for the entire time interval the member spans (e.g., a known taphonomic bias), then no 'overwhelming probability' exists (Trinkaus and Long, 1990). For example, if a fair coin is flipped 100 times and it comes up heads 95 times (yes, it does happen), the probability that the next flip will be a head is 50%. Without a reasonable explanation for the bias that may cause the one-sided distribution of craniodental material in Member I, Susman's 'overwhelming probability' is nothing more than the gambler's fallacy applied to hominin postcrania (i.e., that the probability of an otherwise chance event is affected by previous outcomes) (Paulos, 1988). Moreover, even if a reasonable explanation for the bias is given (i.e., the coin is not fair), then the probability that any one postcranial element belongs to *Homo cf. erectus* is still at least 5%. Is it really necessary to rewrite a significant portion of what we think we know about hominin evolution when there is at least a 5% chance that the evidence used to support the revision is incorrect? It is also worth noting that Grine (1989) suggests that

approximately 92% of the craniodental material from Member I is *Paranthropus* and approximately 8% is *Homo*.

In any event, as I state clearly in the introductory chapter, I am more interested in morphological adaptation as evidence of commitment to an adaptive behavior rather than in capability of a particular behavior. In other words, I am less interested in determining which hominins made Oldowan tools using indirect functional assessments. I am comfortable with making a simple assumption based on evolutionary theory—organisms constantly diverge in their behavioral habits and nature is full of examples of organisms that behave in odd ways in which they are not morphologically adapted, and sometimes these behaviors are adaptive (Darwin, 1859)—therefore, I assume that all early hominin species living at around 2.5 Ma were likely capable of the manipulative behaviors necessary to make and use Oldowan tools.

Having made such an assumption, I ask the following research question: does the hominin hand display evidence of morphological specialization that evolved via natural selection within the context that stone tool-related manipulative behaviors were adaptive? In this dissertation, I have attempted to answer this question by focusing on the radial wrist for evidence of morphological commitment, or adaptation, to adaptive behaviors involving the manufacture, use, and transport of stone tools across varied paleohabitats and paleolandscapes.

Evidence from development

Some obvious questions relating to the acquisition of the complex of derived features surround the timing and sequence in which these features form during development.

Although this was not a specific component of this dissertation research, there is considerable evidence on humans available in the literature that helps address such questions (Čihák, 1972; Durand et al., 2006; Gray et al., 1957; Lewis, 1970, 1989; Mérida-Velasco et al., 1996; O’Rahilly et al., 1957; Senior, 1929; Tardif et al., 1998).

In humans, the primordial carpus is formed of skeletal blastema, a condensation of mesenchymal cells that migrate to the site of future osteogenesis of the wrist (Hall, 1988). This mesenchymal condensation appears around day 37 of embryonic development and begins to show signs of chondrification by day 48 (O’Rahilly et al., 1957; Senior, 1929; Streeter, 1948). As the carpus becomes chondrified over the next few days, interzones appear in the areas where the carpals will articulate with one another; this is followed by complete cavitation (i.e., separation of the chondrifying blastema into distinct carpal shapes), which occurs between the 9th and 11th weeks (Gray et al., 1957; O’Rahilly, 1949; O’Rahilly et al., 1957; O’Rahilly and Gardner, 1975; Scheuer and Black, 2000; Whillis, 1940).

At this early stage of development, three of the carpals have already originated “approximately in their definitive form and change neither their shape nor their location in the course of further development” (Čihák, 1972). These include the trapezium, the trapezoid, and the capitate (Čihák, 1972). During this same period, the condensed interzone between the scaphoid and centrale, which originate as separate elements, slowly begins to chondrify (Čihák, 1972). By the end of the 11th week, there is typically no remaining trace of this division between these two elements and the scaphoid has achieved its basic adult form (Čihák, 1972).

Carpal ligament formation follows a similar sequence as the carpals. The carpal ligaments are derived from mesenchyme and begin to show their distinguishing characteristics by the 9th week (Mérida-Velasco et al., 1996). By the end of the 14th week, organization of the carpal ligament complex is complete (Mérida-Velasco et al., 1996).

Although ossification of the chondrified carpals is not complete until adolescence, their distinctive shapes, articular and ligamentous configurations are set by these early developmental processes before the fetus enters its second trimester (Čihák, 1972; Durand et al., 2006; Gray et al., 1957; Mérida-Velasco et al., 1996; O’Rahilly et al., 1957; Scheuer and Black, 2000; Tardif et al., 1998). This fact is illustrated by the human embryo sections shown in Figures 8.25-8.27 (modified from Čihák [1972]).

In total, the developmental evidence indicates that the mechanisms for shape differentiation of the carpals occur early in ontogeny (Čihák, 1972; Gray et al., 1957; O’Rahilly, 1949; O’Rahilly et al., 1957; O’Rahilly and Gardner, 1975; Whillis, 1940). This evidence suggests that all of the derived radial carpal and carpometacarpal features of the complex that directly relate to the overall shape change of the trapezoid may represent a single change in the ontogenetic sequence. In other words, this evidence suggests that the majority of derived features that are so distinct in humans likely did not evolve through the slow accumulation of one feature after another; rather, that much of the complex likely evolved rapidly as a unit—the result of slight modifications to the underlying genetic information responsible for mesenchymal condensation and subsequent cavitation of the carpus.

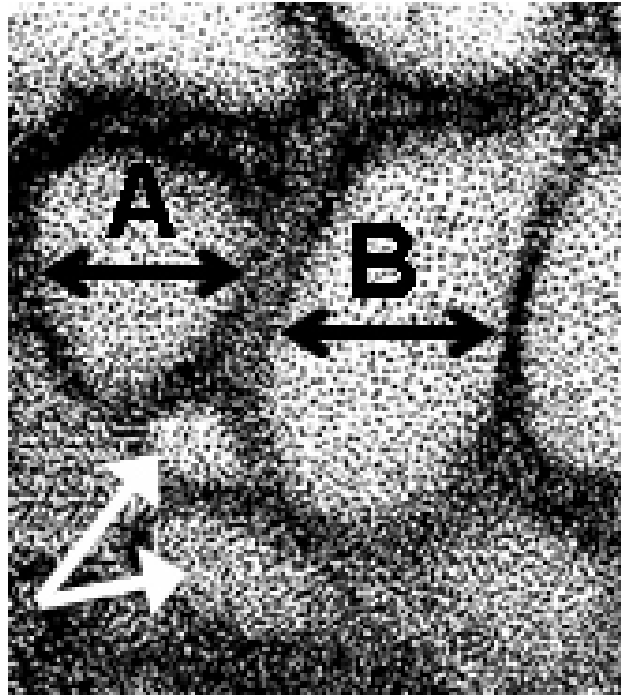


Fig. 8.25 A parallel section through the palm of the left wrist in a human embryo (crown-rump length, 16mm; approximately 45 days old). Note the radioulnar expansion of the trapezoid (**A**, black arrows) and the broadening of the capitate head (**B**, black arrows); the former corresponds to a more supinated trapezium and the latter corresponds to a distally-open scaphoid-capitate joint. The scaphoid is still separate from the centrale (white arrows) (adapted from Čihák, 1972).

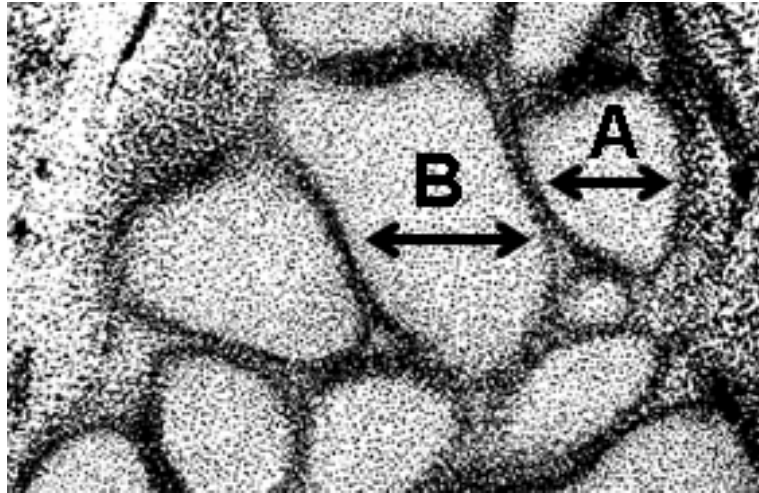


Fig. 8.26 A parallel section through the palm of the right wrist in a human embryo (crown-rump length, 25mm; approximately 54 days old). Note the radioulnar expansion of the trapezoid (**A**, black arrows) and the broadening of the capitate head (**B**, black arrows); the former corresponds to a more supinated trapezium and the latter corresponds to a distally-open scaphoid-capitate joint (adapted from Čihák, 1972).



Fig. 8.27 A transverse section through the distal carpal row in a human embryo (crown-rump length, 50mm; approximately 10-12 weeks old). Note the radioulnar expansion of the trapezoid (**A**), the palmar articulation (white circle) between the trapezoid and capitate (**B**), and the more supinated position of the trapezium (**C**) (adapted from Čihák, 1972).

CONCLUSIONS

The goal of this dissertation research was to answer the following basic question (the ‘riddle’ of the radial wrist): do hominins show morphological commitment in the radial carpometacarpal and carpal region of the hand to tool behaviors such that a) the ancestral morphology is sacrificed, and b) the derived morphology has performance advantages for the behavior (i.e., it is better than the primitive structure with respect to the novel behavior)? If so, when, in which hominins, and in which behavioral contexts did this event most likely occur?

The evidence presented in this dissertation indicates that the riddle of the radial wrist in hominids is solvable. The solution may be found in the trapezoid. There is evidence of a morphological commitment, which appears to have been achieved through a change in the shape of the trapezoid and the concomitant effects of this shape on the surrounding carpal and carpometacarpal joints. The radio-ulnar expansion of the palmar aspect of the trapezoid results in supination of the trapezium such that the distal carpals are more aligned with one another. The complex of derived features does not result in a hand capable of making and using tools, it makes an already capable hand better at making and using tools. Similarly, the complex of derived features does not make the hand incapable of being used to climb trees, knuckle-walk, or palm-walk, etc., but it reduces the hand’s effectiveness in such quadrupedal locomotor behaviors in comparison to the primitive complex of features in hominids.

It is important to consider ‘effectiveness’ in an evolutionary sense and not simply in an individual sense. Each individual of a population varies in both its behavioral and

morphological characteristics and the successes of particular themes of variation (e.g., the derived complex versus the primitive ancestral condition) are ultimately measured across generations, not within only one. In the game of hold'em poker, a pair of aces is roughly a four-to-one favorite before the flop over any other pair although the odds of being dealt any pair are the same (Sklansky, 1994). In any one hand, the lesser pairs are capable of beating the pair of aces but over the course of many hands, the pair of aces will win considerably more often (Sklansky, 1994). If evolutionary success were dependent on some form of quadrupedal locomotor behavior, the complex of derived features would most likely lose if it had to compete against some form of the primitive complex of features. Similarly, if evolutionary success were dependent on some form of manipulative behavior involving tools, the primitive complex of features would most likely lose if it had to compete against some form of the complex of derived features.

The shift to making, using, and transporting stone tools to procure food and other resources across paleohabitats and paleolandscapes was most likely a highly successful behavioral adaptation unique to hominins (Binford, 1985; Clark, 1971; Isaac, 1984; Panger et al., 2002; Potts, 1991; Schick, 1987; Toth, 1985, 1987; Toth and Schick, 1986; Wynn and McGrew, 1989). However, we must acknowledge that at least one hominin species became morphologically specialized further toward this behavior than did its close hominin relatives, who shared very similar behavioral adaptations and perhaps even some morphological adaptations as well (e.g., distal pollical phalanx morphology (Susman [1998]; but see Marzke et al. [1998], Marzke and Marzke [2000], or Smith [2000] for alternative interpretations to those of Susman [1998])).

The morphological specialization of the radial wrist is a hallmark of *H. sapiens*, *H. neanderthalensis*, and their most recent common ancestor. The evidence presented in this dissertation indicates that the distinct morphology of the complex is derived in comparison with extant hominids as well as *A. afarensis*, *A. africanus*, and *H. habilis*. Although attributing the OH7 trapezium to *H. habilis* may be questionable, attributing the OH7 scaphoid and other hand remains to this fossil taxon is reasonable. Given that OH7 is associated with direct evidence of stone tools, it is tentatively concluded that at 1.75 Ma, the complex of derived features had yet to evolve in hominins. However, the evidence is clear that by 800,000 years ago the complex of derived features had evolved within at least one hominin lineage represented by *H. antecessor* (Falgueres et al., 1999; Lorenzo et al., 1999).

In light of this evidence, it is worthwhile to revisit some of Napier's conclusions regarding the hand of *Homo habilis* (OH7) and the evolutionary history of the modern human hand:

“On the site, associated with the hand, were fragments of the skull, a lower jaw, an almost complete foot and a collar bone. In addition, and most significantly, there were stone-tools of a recognizable culture, the so-called Oldowan chopper tools, strongly indicating that *Homo habilis* was a tool-maker.

I have performed some experiments and they have convinced me that an advanced form of precision grip is not required to make or use such tools; they can in fact be made entirely by the use of a power grip. This conclusion led to the formulation of a hypothesis which is this: *that in the evolution of man stone tools are as good as the hands that made them*. It has always been assumed that by the time early man started to make stone tools his hand was indistinguishable functionally and structurally from the hand of modern man. I believe that this was not so; I believe that *Homo habilis* was making stone tools with a hand that had not yet evolved into a fully fledged *precision hand*. There is a popular view of human evolution which maintains that man's large brain and the functionally specialised hand were linked in a sort of self-perpetuating feedback system: the

more skilled the hands, the bigger the brain—the bigger the brain, the more skilled the hands—and so on. There is now evidence that the really progressive phase of brain enlargement followed a long time after the beginnings of power-tool making. *Homo habilis* was the possessor of a dawning intellect and an up-and-coming hand, but it was not until perhaps half a million years after his time that the brain started to enlarge rapidly; and this one might tentatively suggest was related to evolution of the full-fledged precision grip and the new cultural horizons that were thereby effectively opened. It is impossible, in the present state of our knowledge, to be certain when the true “precision hand” evolved; perhaps it was not until the Upper Paleolithic. It seems certain that at the time of the Aurignacian, the human hand was essentially modern because the stone tools of this period could probably not have been made—or used—without fully developed opposability of the thumb, the structural basis of a precision grip” (Napier, 1965:555-556; emphasis in original).

In many ways, the conclusions of this dissertation research are only slight modifications to the inferences Napier made over forty years ago. I would remove his references to the ‘true, fully-fledged, or advanced precision hand’ and replace them with references as to how precision and power grips are known to differ between hominid species (e.g., Marzke et al., 1992; Marzke, 1997)—all hominids are capable of both grips but some are more specialized, or committed, to performing them. I would agree that the hands of *H. habilis* and other Pliocene hominins were likely not as morphologically derived as in later species of *Homo*, and that at the time of the Aurignacian (approximately 40,000 years ago) the human hand was indistinguishable from its present form. However, the Upper Paleolithic does not signal the origin of the modern human hand as we know it. More likely, the origin occurs sometime between 1.75 and 0.8 Ma, as evidenced by *H. habilis* (OH7) on one end of this time scale, and *H. antecessor* (ATD6-24) and the MRCA of modern humans and Neandertals on the other.

The modified radial wrist is an acquisition that, in the context of stone tool-related manipulative behaviors representing a primary adaptive strategy, gives an advantage to one group of hominins over the other. Despite their shared behavioral adaptations, the complex of derived features may have led, either directly or indirectly, to the marginalization and eventual extinction of less morphologically specialized species of hominin (i.e., a cladogenetic explanation). At the very least, the derived complex of features replaced the primitive complex within the hominin species that eventually led to the modern human and Neandertal lineages (i.e., an anagenetic explanation). Meal after meal, day after day, generation after generation; the better adapted of two or more forms is more likely to outlast the less adapted form (Darwin, 1859).

Implications for further work

The results of this dissertation research have two important implications for further work. The first implication is that we need to determine the condition that was present in Asian *Homo erectus* and in African *Homo ergaster*. Both are likely candidates for having the complex of derived features but without fossil evidence to demonstrate this unequivocally, our understanding of the events surrounding the origin of this complex in Pleistocene hominins is limited. Moreover, such evidence is necessary to test whether the complex of derived features originated more within a context of Oldowan-like tool behaviors or more within a context of Acheulian-like tool behaviors.

The hand remains of LB1, the type specimen of *Homo floresiensis*, include a scaphoid, trapezoid, and capitate (William Jungers, personal communication), although no anatomical descriptions are yet published. The carpals of LB1 may provide indirect

evidence for the condition in Asian *H. erectus* if this newly discovered hominin does, in fact, represent a dwarfed descendant of *H. erectus*, as was initially suggested by its discoverers (Brown et al., 2004; Morwood et al., 2005). Presence of the primitive morphological features would support a hypothesis that the complex of derived features evolved sometime after the initial migrations of hominins out of Africa and increase the likelihood that its origin occurred within a context of Acheulian-tool behaviors.

Alternatively, presence of the derived features in *H. floresiensis* would support a hypothesis that the complex evolved prior to the initial hominin migrations out of Africa and increase the likelihood that its origin occurred within a context of Oldowan-tool behaviors.

The second implication of this research relates to the basic nature of the biomechanical predictions. These predictions are useful because they help demonstrate the correlated nature of the features that characterize later species of *Homo* within a morphological and functional context. However, further work is needed to refine these predictions such that more precise biomechanical hypotheses can be evaluated and tested empirically. Improving the explanatory power of the biomechanical predictions will facilitate the design of experiments to quantitatively compare the performance attributes of the differing morphological complexes of primitive and derived features, as they relate to locomotor and manipulative behaviors respectively.

Chapter 9: Materials and Methods

MATERIALS

In total, 1243 bones of the STT and adjacent carpometacarpal region were laser scanned, geometrically modeled, and analyzed (Tables 9.1 and 9.2). Together, these bones represent 303 individual specimens. Of these, 280 are from extant genera (1199 bones) and 23 are from extinct genera (44 bones). The 1199 extant bones include 252 first metacarpals, 255 trapezia, 242 trapezoids, 254 scaphoids, 41 centrales, and 155 second metacarpals (Table 9.1); the 45 fossil bones include 11 first metacarpals, 9 trapezia, 5 trapezoids, 11 scaphoids, and 8 second metacarpals (Table 9.2). In all fossil cases except Shanidar 3, casts of the original specimens were used.

TABLE 9.1 Sample breakdown by genus and bone for the extant taxa used in this study¹

Genus	N	Bone						TOTAL
		MC1	TPM	TZD	SCA	CEN	MC2	
<i>Homo</i>	124	121	113	111	117		87	549
<i>Pan</i>	51	46	47	47	48		17	205
<i>Gorilla</i>	51	47	44	45	48		18	202
<i>Pongo</i>	22	19	21	20	19	19	12	110
<i>Papio</i>	22	19	20	19	22	22	21	123
<i>Theropithecus</i>	4		4					4
<i>Erythrocebus</i>	2		2					2
<i>Nasalis</i>	4		4					4
TOTAL	280	252	255	242	254	41	155	1199

¹ N, total number of individual specimens; MC1, first metacarpal; TPM, trapezium; TZD, trapezoid; SCA, scaphoid; CEN, centrale; MC2, second metacarpal.

The sample includes specimens from the Smithsonian's National Museum of Natural History (n = 177), the Cleveland Museum of Natural History (n = 100), the Royal Ontario Museum (n = 2), the School of Human Evolution and Social Change at Arizona State University (ASU) (n = 4), the Institute of Human Origins at ASU (n = 6), and the Department of Anthropology at Washington University in St. Louis (n = 15).

TABLE 9.2 Sample breakdown of the fossil specimens used in this study¹

Specimen	Bone				
	MC1	TPM	TZD	SCA	MC2
<u><i>Australopithecus afarensis</i></u>					
AL333-15					X
AL333-48					X
AL333-58	X				
AL333-80		X			
AL333w-23					X
AL333w-39	X				
<u><i>Paranthropus robustus</i></u>					
SK84	X				
<u><i>Homo habilis</i></u>					
OH7		X		X	
<u><i>Homo sp.</i></u>					
SKX5020	X				
<u><i>Homo neanderthalensis</i></u>					
Kebara 2	X	X	X	X	
La Ferrassie 1	X	X	X	X	
La Ferrassie 2	X	X			X
Regourdou 1	X	X		X	
Regourdou 2				X	X
Amud 1	X		X		
La Chapelle-aux-Saints 1	X				X
Shanidar 3		X		X	
Shanidar 4		X		X	
Shanidar 6				X	X
Shanidar 5					X
Shanidar 8				X	
<u><i>Homo sapiens</i></u>					
Qafzeh 9	X	X	X	X	
Combe-Capelle 1			X	X	
TOTAL	11	9	5	11	8

¹ MC1, first metacarpal; TPM, trapezium; TZD, trapezoid; SCA, scaphoid; MC2, second metacarpal.

The analyses presented in this dissertation represent quantitative comparisons between five extant primate genera: *Homo*, *Pan*, *Gorilla*, *Pongo*, and *Papio* (Table 9.1).

These are followed by comparisons with fossil specimens (Table 9.2). Statistical analyses of sex differences within each genus, and of population differences within modern *Homo sapiens*, were investigated (data not shown). Overall, the within-genus variation appears continuously distributed and is small relative to the between-genus variation. Although many interesting within-genus differences occur, none are of a degree that would caution against pooling of the samples for the between-genus comparisons, which is the focus of the research presented here.

The genus *Homo* (n = 124) is represented by a world-wide sample of *H. sapiens* including individuals of recent African (n = 34), European (n = 30), Australian (n = 9), Asian (n = 26), and Native American (n = 25) descent. The genus *Pan* (n = 51) is represented by a sample of *P. troglodytes* while the genus *Gorilla* (n = 51) is represented by a combined sample of *G. gorilla* (n = 38) and *G. beringei* (n = 13). The genus *Pongo* (n = 22) is represented by a combined sample of *P. pygmaeus* (n = 21) and *P. abelii* (n = 1) while the genus *Papio* (n = 22) is represented by a combined sample of *P. anubis* (n = 13), *P. cynocephalus* (n = 3), *P. hamadryas* (n = 1), *P. ursinus* (n = 4), and *P. sp.* (n = 1).

The fossil specimens included for analysis represent a variety of taxa including: *Australopithecus afarensis* (AL333-15, -48, -58, -80, AL333w-23, -39), *Paranthropus robustus* (SK84), *Homo habilis* (OH7), *Homo sp.* (SKX5020), *Homo neanderthalensis* (Kebara 2, La Ferrassie 1 and 2, Regourdou 1 and 2, Amud 1, La Chapelle-aux-Saints 1, Shanidar 3, 4, 5, 6, and 8), and Upper Paleolithic *Homo sapiens* (Qafzeh 9, Combe-Capelle 1) (Arensburg et al., 1985; Bar-Yosef et al., 1992; Boule, 1908, 1911, 1912a, b,

1913; Endo and Kimura, 1970; Heim, 1974; Johanson et al., 1982a, b; Klaatsch and Hauser, 1909; Leakey et al., 1964; Napier, 1959, 1962; Piveteau, 1963, 1964, 1966; Susman, 1988; 1989; Trinkaus, 1982, 1983; Vandermeersch, 1981).

METHODS

Thee-dimensional data acquisition

All bones were scanned using the Cyberware Model 15 desktop laser digitizer (courtesy of the Partnership for Spatial Modeling (PRISM) at Arizona State University), resulting in a distinct 3D model of each bone. Each 3D model is a triangular mesh—a discrete representation of the actual bone consisting of a collection of points joined together by straight line-segments, or edges, which form triangles. The resulting surface of the triangular mesh is piecewise planar—that is, each triangle is a single plane. This surface forms the most basic geometric bone model, has the same topology as the actual bone, and interpolates the data points. An interpolating surface passes exactly through every point whereas an approximating surface is not guaranteed to pass through each point. Even though an interpolating surface may pass through each acquired point, the surface is still only an approximation of the actual bone since any points between the sampled points are not available. In this sense, the ability of the model to best represent the actual bone depends on the number and density distribution of the sampled points. On average, the 3D models used in this dissertation are high resolution triangular meshes consisting of more than 1,000 points per square centimeter.

This research involved quantitatively comparing joint surface properties; therefore, the mesh of each 3D bone model was digitally segmented into articular and non-

articular areas using Raindrop Geomagic Studio 8 (courtesy of PRISM). In most cases, individual articular areas were segmented by referring visually to the actual bone. After all of the articular and non-articular areas were segmented from each 3D model, three specialized algorithms were used to collect the desired data from the models and their segmented surfaces. These data consisted of relative surface areas (Tocheri et al., 2005), angles between joint surfaces (Tocheri et al., 2003), and measures of curvedness of the first carpometacarpal mutual joint surfaces (Tocheri et al., 2006; Tocheri and Femiani, in press).

Relative surface area

The absolute surface area of each triangle in the mesh was computed by taking the cross product of any two edges, or vectors, that span each triangle and dividing by two (Farin and Hansford, 1998, 2000); region surface areas were then computed by summing over all the triangles in each desired region. In order to compare the articular and nonarticular areas of the differently sized genera, shape ratios were calculated by dividing each area by the total surface area of the bone on which it is located. These shape ratios do not simply remove the effects of size; rather, they remove the effects of scale. In other words, these ratios represent scale-free shape variables and enable the examination of whether significant differences in shape exist between taxa (Jungers et al., 1995; Mosimann and James, 1979). Using total bone surface area as the denominator simplifies interpretation, since an area divided by an area results in a percentage; the result is the percentage (%) of total bone surface area that is represented by each specific joint surface or nonarticular region.

Angles between joint surfaces

The angles between joint surfaces were calculated by fitting a least-square plane to each segmented joint surface and computing the angle between the planes. The least-square plane was calculated as follows (Farin and Hansford, 2000; Hearn and Baker, 1986; Pulla, 2001; Tocheri et al., 2003):

Three non-collinear points define a plane given by the equation

$$Ax + By + Cz = D \quad (1),$$

where $[A \ B \ C]^T$ is the normal vector of the plane, and D is the distance of the origin to the plane. In other words, the plane is defined mathematically by its normal vector and its perpendicular distance (D) from the origin. The precise location of the origin is arbitrary and is defined by the coordinate system used. If there are $n + 1$ points $(x_i, y_i, z_i); 0 \leq i \leq n$, Eq. (1) is restated as

$$\frac{A}{D}x + \frac{B}{D}y + \frac{C}{D}z = 1 \quad (2).$$

This results in

$$\begin{bmatrix} 1 \\ 1 \\ \vdots \\ 1 \end{bmatrix} = \begin{bmatrix} x_0 & y_0 & z_0 \\ x_1 & y_1 & z_1 \\ \vdots & & \\ x_k & y_k & z_k \end{bmatrix} \begin{bmatrix} A/D \\ B/D \\ C/D \end{bmatrix} \quad (3).$$

For $k = 2$, an interpolating plane for the three points is calculated by directly solving the linear system. For $k > 2$, the resulting over-determined system is solved using a least squares approach.

Let

$$P = \begin{bmatrix} 1 \\ 1 \\ \vdots \\ 1 \end{bmatrix} \quad (4),$$

$$M = \begin{bmatrix} x_0 & y_0 & z_0 \\ x_1 & y_1 & z_1 \\ \vdots & & \\ x_k & y_k & z_k \end{bmatrix} \quad (5),$$

and

$$X = \begin{bmatrix} A/D \\ B/D \\ C/D \end{bmatrix} \quad (6).$$

Therefore, the system is represented as

$$P = MX \quad (7).$$

To solve this system, M is squared by multiplying both sides of Eq. (7) by the transpose of M, resulting in

$$M^T P = M^T M X \quad (8).$$

Gaussian elimination method is applied to solve Eq. (8). The solution of the system is the vector $[A/D \ B/D \ C/D]^T$, the inverse of the magnitude of which is the plane distance D.

A normal vector to each least-squares plane was projected into the modeled bone. The angles between the normal vectors were quantified and subtracted from 180° resulting in the angles between the least-square planes (Fig. 9.1).

The least-square plane is equivalent to the regression plane calculated using major axis regression rather than traditional least-squares regression. In major axis regression, error is assumed to occur in the x, y, and z directions. Therefore, the plane minimizes the sum of the orthogonal distances from each point on the surface to the plane. Since major axis regression shares essential characteristics with principal components analysis (PCA), the least-square plane is derivable using PCA. If PCA is performed on all the vertices of a given surface, the eigenvector associated with the smallest eigenvalue is also the normal vector of the least-square plane. The normal vectors of any two planes can be utilized to compute the angle between the planes. The angle is equal to 180° minus the inverse cosine (i.e., \arccos) of the dot product of the normal vectors. The angle between any two normal vectors and hence, their respective planes, is always measured such that the two vectors occur in the same plane. Thus, the orientation of the bone is completely independent of the angles being measured.

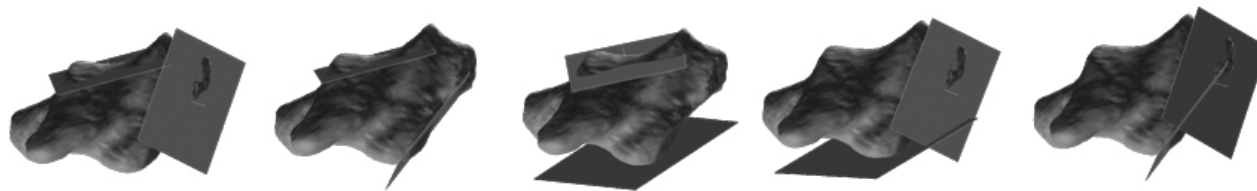


Fig. 9.1 Visual example of the process of fitting least-square planes to the articular areas of a left trapezium (*Gorilla* is shown).

Measures of curvedness

A quadric-based method was used to calculate 3D surface curvedness (Tocheri et al., 2006; Tocheri and Femiani, in press). This strategy involved fitting modeled quadric surfaces to the segmented joint surfaces; subsequent comparisons were performed on the modeled surfaces, rather than the segmented surfaces. A quadratic representation of the surface was motivated by the typical description of the first carpometacarpal mutual joint surfaces as having either one or two “curvatures”. The coefficients of a quadratic equation form a concise description of the salient qualities of shape and simultaneously establish a geometric correspondence between surfaces.

In 3D, a quadratic surface has the following equation:

$$z = ax^2 + by^2 + 2cxy + 2dx + 2ey + f \quad (9).$$

If the following rigid body transform is used,

$$\begin{bmatrix} \hat{x} \\ \hat{y} \\ \hat{z} \end{bmatrix} = R \begin{bmatrix} x - x_0 \\ y - y_0 \\ z - z_0 \end{bmatrix} \quad (10),$$

then

$$\hat{z} = A\hat{x}^2 + B\hat{y}^2 \quad (11),$$

and A and B summarize the shape of the surface.

Both the magnitudes and signs of A and B convey considerable information about the quadric surface (Fig. 9.2). If A and B have the same sign, then the surface is of an elliptical or parabolic form; the relative magnitudes of A and B describe the degree of curvature in each of the principal coordinates of the surface. Alternatively, if A and B are different in sign, then the surface is of an hyperbolic or saddle form and again, the

relative magnitudes of A and B describe the degree of curvature in each of the principal coordinates of the surface.

The A and B coefficients are analogous to the principle curvatures (k_{\max} and k_{\min}) of the fitted quadric surface. Therefore, A and B were used to calculate four different types of surface curvatures: Gaussian, mean, absolute, and root mean square (RMS) curvatures. The following conventional descriptions of these surface curvature measurements are derived from Farin (1995, 1996, 2002) and Farin and Hansford (1998, 2000).

Gaussian curvature. Gaussian curvature (k_{gaus}) equals the product of the principal curvatures:

$$k_{\text{gaus}} = k_{\min} * k_{\max} \quad (13).$$

The most important property of Gaussian curvature is its sign. Positive values indicate elliptical points, negative values indicate saddle points, and zero indicates a parabolic point. The magnitude, on the other hand, does not reveal information that can be used to differentiate between elliptical or saddle points, since multiple Gaussian curvature values can be derived from the products of any number of combinations of k_{\min} and k_{\max} . Another property of Gaussian curvature that is not useful relates to instances where k_{\min} or k_{\max} equal zero. In these instances, the product of the principal curvatures will also equal zero, implying that the surface has zero curvature or is flat. A cylindrical surface is a perfect example to illustrate the ‘intuitive’ drawbacks of Gaussian curvature in these instances. Any point on a cylinder results in a Gaussian

curvature equal to zero since k_{\min} always occurs in the direction in which the normal section is a straight line.

Mean curvature. Mean curvature (k_{mean}) equals the average of the principal curvatures:

$$k_{\text{mean}} = (k_{\min} + k_{\max}) / 2 \quad (14).$$

The most important property of mean curvature, which measures overall surface flatness, is how close it is to zero. Surfaces that are minimal have mean curvature zero at all points. A minimal surface has an area that is minimal with respect to its perimeter. Soap bubbles are minimal surfaces if no air or force is causing the surface to deviate from its perimeter.

Absolute curvature. Absolute curvature (k_{abs}) equals the sum of the absolute values of k_{\min} and k_{\max} :

$$k_{\text{abs}} = |k_{\min}| + |k_{\max}| \quad (15).$$

The most important property of absolute curvature is its magnitude. The further the value is away from zero, the more the surface is curved at that location.

RMS curvature. RMS curvature (k_{rms}) equals the square root of the mean of the squared values of k_{\min} and k_{\max} :

$$k_{\text{rms}} = \sqrt{(k_{\min}^2 + k_{\max}^2)} \quad (16).$$

RMS curvature has been used as a measure of surface flatness (Ateshian et al., 1992; Xu et al., 1998) because it minimizes the overall surface curvature by suppressing the value of the surface undulations.

Statistical analyses

Univariate analyses. For the trapezium (Chapter 4), trapezoid (Chapter 5), scaphoid (Chapter 6), and second metacarpal (Chapter 7), the variables analyzed include the angles between articular surfaces and the relative areas of articular and nonarticular surfaces. Various measures of curvedness are the focus of the analysis of the first carpometacarpal joint surfaces (Chapter 3).

The differences between the genus means of each measured variable are evaluated for statistical significance using the bootstrap (Efron and Tibshirani, 1993; Manly, 1997). The same procedure was used to test for differences between the means of males and females within each genus, and between the means of different populations of *Homo sapiens* (data not shown). Numbers appearing in parentheses indicate group means, which are also summarized along with the *p*-values of each pairwise comparison in the accompanying tables. The bootstrap is a distribution-free statistic ideally suited to examine differences between means of groups with varying sample sizes that are small relative to the population they represent (Efron and Tibshirani, 1993; Manly, 1997).

Exact *p*-values for the bootstrap test of significance were calculated as follows:

- 1) the original means of group A and group B were calculated as was the difference between group A and group B (the test statistic);
- 2) each group was sampled with replacement based on its actual sample size 999 times, and the mean of each bootstrapped sample was calculated;

- 3) the resulting 1000 means of each group were combined to form a single group of 2000 means (group AB), and the mean of group AB was calculated (hereafter referred to as the grand mean (GM));
- 4) a correction factor for each group was calculated by subtracting the mean of the 1000 means from the GM (i.e., the 1000 means of each bootstrapped sample were summed, divided by 1000, and subtracted from the GM);
- 5) the correction factor for each group was added to all 1000 means of its bootstrapped sample;
- 6) all 999 bootstrap means of group A were randomly paired with the 999 bootstrap means of group B and the difference between the means for each pairing was calculated (the correction factor ensured that the distribution of the differences between the means was centered on zero, rather than on the difference between the original means of group A and group B);
- 7) since there was no *a priori* reason for expecting any directionality in the differences between means, the absolute values of all the differences between means were calculated to perform a two-tailed test;
- 8) the number of times that the absolute difference between the bootstrapped means equaled or exceeded the difference between the

original means (the test statistic) was counted, and then divided by 1000;

- 9) the result was the exact p-value for the test of significance.

The bootstrap results ensure that statements about the means can be made with statistical confidence. For all comparisons, an alpha value of .01 was used to determine statistical significance.

Multivariate analyses. Discriminant and canonical analyses were used to evaluate the efficacy of different variable combinations in correctly classifying individual bones belonging to the extant genera. Both analyses are standard multivariate techniques that allow the simultaneous examination of multiple variables in multidimensional space. Discriminant analysis generates a linear combination of the variables for estimating the posterior probability of belonging to a genus given a combined set of data values. The posterior probability therefore represents the likelihood of correctly assigning an individual to its respective genus based on its 3D data values (i.e., shape). The cross-validation method was used to calculate the posterior probability of membership in each genus because it gives approximately unbiased estimates of the probabilities of misclassification (Johnson and Wichern, 2002). N-dimensional patterns in these data were also reduced to canonical variables. These canonical variables were interpreted using the pooled-within canonical structure, which represents the correlations between pairs of linear combinations of the variables for each genus and each canonical variable. Plotting these canonical variables enables the observed differences between genera to be examined and interpreted graphically (Johnson and Wichern, 2002).

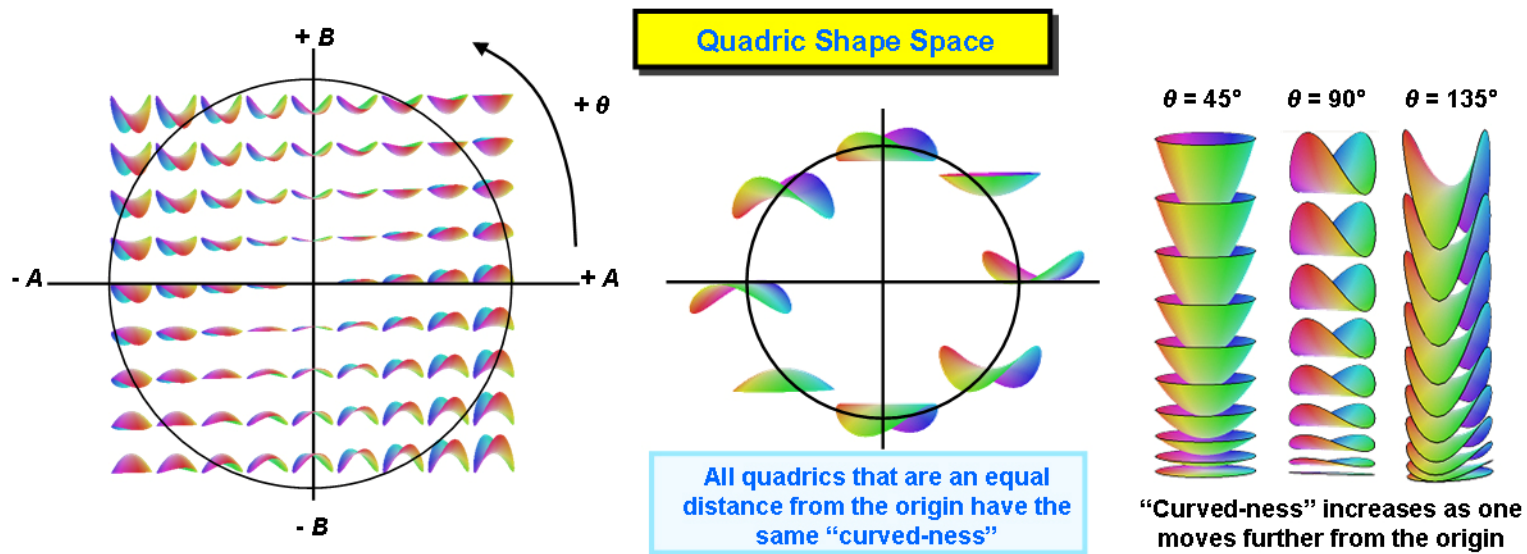


Fig. 9.2 Visual demonstration of the family of simple surfaces that exist within Quadric Shape Space (left). All quadric surfaces that are equidistant from the origin have the same amount of 'curved-ness' (middle), which increases as one moves further from the origin (right).

LITERATURE CITED

- Alba DM, Moya-Sola S, Kohler M. 2003. Morphological affinities of the *Australopithecus* hand on the basis of manual proportions and relative thumb length. *J Hum Evol* 44:225-254.
- Amundson R. 1996. Historical development of the concept of adaptation. In: Rose MR, Lauder, GV, editors. *Adaptation*. San Diego: Academic Press. p 11-53.
- Arensburg B, Bar-Yosef O, Chech M, Goldberg P, Laville H, Meignen L, Rak Y, Tchernov E, Tillier AM, Vandermeersch B. 1985. Une sépulture néanderthalien dans la grotto de Kebara (Israel). *C R Acad Sci Paris, Série II* 300:227-230.
- Ateshian GA, Rosenwasser MP, Mow VC. 1992. Curvature characteristics and congruence of the thumb carpometacarpal joint - differences between female and male joints. *J Biomech* 25:591-607.
- Baker BJ, Dupras TL, Tocheri MW. 2005. *The Osteology of Infants and Children*. College Station, TX: Texas A & M University.
- Bar-Yosef O, Vandermeersch B, Arensburg B, Belfer-Cohen A, Goldberg P, Laville H, Meignen L, Rak Y, Speth JD, Tchernov E, Tillier AM, Weiner S. 1992. The excavations in Kebara cave, Mt. Carmel. *Curr Anthropol* 33:497-450.
- Baum DA, Larson A. 1991. Adaptation reviewed: A phylogenetic methodology for studying character macroevolution. *Syst Zool* 40:1-18.
- Beard KC, Teaford MF, Walker A. 1986. New wrist bones of *Proconsul africanus* and *P. nyanzae* from Rusinga Island, Kenya. *Folia Primat* 47:97-118.
- Beck BB. 1980. *Animal Tool Behavior*. New York: Garland.
- Bettinger PC, Berger RA. 2001. Functional ligamentous anatomy of the trapezium and trapeziometacarpal joint (gross and arthroscopic). *Hand Clin* 17:151-168.
- Bettinger PC, Linscheid RL, Berger RA, Cooney WP, An KN. 1999. An anatomic study of the stabilizing ligaments of the trapezium and trapeziometacarpal joint. *J Hand Surg Am* 24A:786-798.
- Bettinger PC, Smutz P, Linscheid RL, Cooney WP, An KN. 2000. Material properties of the trapezium and trapeziometacarpal ligaments. *J Hand Surg Am* 25A:1085-1095.
- Binford LR. 1985. Human ancestors: Changing views of their behavior. *J Anthropol Arch* 4:292-327.

- Blumenschine RJ, Peters CR, Masao FT, Clarke RJ, Deino AL, Hay RL, Swisher CC, Stanistreet IG, Ashley GM, McHenry LJ, Sikes NE, van der Merwe NJ, Tactikos JC, Cushing AE, Deocampo DM, Njau JK, Ebert JJ. 2003. Late Pliocene *Homo* and hominid land use from Western Olduvai Gorge, Tanzania. *Science* 299:1217-1221.
- Bock WJ, von Wahlert G. 1965. Adaptation and the Form-Function Complex. *Evolution* 19:269-299.
- Bock WJ. 1981. The definition and recognition of biological adaptation. *American Zoologist* 20:217-227.
- Boule M. 1908. L'Homme fossile de la Chapelle-aux-Saints (Corrèze). *Anthropologie* 19:519-525.
- Boule M. 1911. L'Homme fossile de la Chapelle-aux-Saints. *Annales de Paléontologie* 6:111-172.
- Boule M. 1912a. L'Homme fossile de la Chapelle-aux-Saints. *Annales de Paléontologie* 7:21-56.
- Boule M. 1912b. L'Homme fossile de la Chapelle-aux-Saints. *Annales de Paléontologie* 7:85-192.
- Boule M. 1913. L'Homme fossile de la Chapelle-aux-Saints. *Annales de Paléontologie* 8:1-70.
- Bowden BS, Bowden JM. 2005. *An Illustrated Atlas of the Skeletal Muscles*. 2nd edition. Englewood, CO: Morton Publishing Company.
- Brand PW, Hollister A. 1999. *Clinical Mechanics of the Hand*. 3rd edition. St. Louis, MI: Mosby Year Book.
- Brandon R. 1990. *Adaptation and environment*. Princeton, NJ: Princeton University Press.
- Brandon RN. 1978. Adaptation and evolutionary theory. *Stud Hist Phil Sci* B205:453-474.
- Brooks DR, McLennan DH. 1991. *Phylogeny, ecology, and behavior: A research program in comparative biology*. Chicago: Univeristy of Chicago Press.
- Brooks DR, McLennan DH. 2002. *The nature of diversity: An evolutionary voyage of discovery*. Chicago: Univeristy of Chicago Press.

- Brown P, Sutikna T, Morwood MJ, Soejono RP, Jatmiko, Saptomo EW, Due RA. 2004. A new small-bodied hominin from the Late Pleistocene of Flores, Indonesia. *Nature* 431:1055-1061.
- Buford W, Hollister A, Myers L. 1990. Three dimensional computer simulation of thumb carpometacarpal kinematics. *J Clin Eng* 15:445-451.
- Burian RM. 1983. Adaptation. In: Grene M, editor. *Dimensions of Darwinism*. Cambridge: Cambridge University Press. p 287-314.
- Bush ME, Lovejoy CO, Johanson DC, Coppens Y. 1982. Hominid carpal, metacarpal, and phalangeal bones recovered from the Hadar Formation: 1974–1977 collections. *Am J Phys Anthropol* 57:651-677.
- Cartmill M. 2002a. Paleoanthropology: science or mythological charter. *J Anthropol Res* 58:183-201.
- Cartmill M. 2002b. Historical explanation and the concept of progress in primatology. *Evol Anthropol Suppl.* 1:12-15.
- Cartmill M, Milton K. 1977. The lorisform wrist joint and the evolution of "brachiating" adaptations in the Hominoidea. *Amer J Phys Anthropol* 47:249-272.
- Christel M, Fragaszy D. 2000. Manual function in *Cebus apella*. Digital mobility, preshaping, and endurance in repetitive grasping. *Int J Primatology* 21:697-719.
- Christel M. 1993. Grasping techniques and hand preferences in hominoidea. In: Preuschoft H, Chivers DJ, editors. *Hands of Primates*. New York: Springer, Wien. p 91-108.
- Christel MI, Kitzel S, Niemitz C. 1998. How precisely do bonobos (*Pan paniscus*) grasp small objects? *Int J Primatology* 19:165-194.
- Čihák R. 1972. Ontogenesis of the skeleton and intrinsic muscles of the human hand and foot. *Ergebnisse der Anatomie und Entwicklungsgeschichte* 46:1-194.
- Clark G. 1971. *World Prehistory: A New Outline*. Cambridge, UK: Cambridge University Press.
- Clarke RJ, Partridge TC. 2002. On the unrealistic 'Revised age estimates' for Sterkfontein. *S Afr J Sci* 98:415-419.

- Coates MI, Clack JA. 1990. Polydactyly in the earliest known tetrapod limbs. *Nature* 347:66-69.
- Coddington JA. 1988. Cladistic test of adaptational hypotheses. *Cladistics* 4:3-22.
- Coddington JA. 1990. Bridges between evolutionary pattern and process. *Cladistics* 6:379-386.
- Coddington JA. 1994. The roles of homology and convergence in studies of adaptation. In: Eggleton E, Vane-Wright RI, editors. *Phylogenetics and ecology*. London: Academic Press. p 53-78.
- Cooney WP, Chao EY. 1977. Biomechanical analysis of static forces in the thumb during hand function. *J Bone Joint Surg Am* 59:27-36.
- Darwin C. 1859. *On the Origin of Species by Means of Natural Selection, or the Preservation of Favoured Races in the Struggle for Life*. London: John Murray.
- Davis PR. 1964. Hominid fossils from Bed I, Olduvai Gorge Tanganyika: a tibia and fibula. *Nature* 201:967-968.
- Day M. 1976. Hominid postcranial material from Bed I, Olduvai Gorge. In: Isaac GL, McKown ER, editors. *Human Origins: Louis Leakey and the East African Evidence*. Menlo Park, CA: W.A. Benjamin, Inc. p 363-374.
- Day MH, Napier JR. 1964. Fossil foot bones. *Nature* 201:969-970.
- de Heinzelin J, Clark JD, White T, Hart W, Renne P, Woldegabriel G, Beyene Y, Vrba E. 1999. Environment and behavior of 2.5-million-year-old Bouri hominids. *Science* 284:625-629.
- Dobzhansky T. 1956. What is an adaptive trait? *American Naturalist* 90:337-347.
- Dobzhansky T. 1968. Adaptedness and fitness. In: Lewontin RC, editor. *Population biology and evolution*. New York: Syracuse University Press. p 109-121.
- Durand S, Delmas V, Ho Ba Tho M-C, Batchvarova Z, Uhl JF, Oberlin C. 2006. Morphometry by computerized three-dimensional reconstruction of the human carpal bones during embryogenesis. *Surg Radiol Anat* 28:355-358.
- Eaton RG, Littler JW. 1969. A study of the basal joint of the thumb: treatment of its disabilities by fusion. *J Bone Joint Surg* 51A:661-668.

- Efron B, Tibshirani RJ. 1993. An introduction to the bootstrap. Boca Raton, FL: CRC Press, LLC.
- Eizirik E, Murphy WJ, Springer MS, O'Brien SJ. 2004. Molecular phylogeny and dating of early primate divergences. In: Ross CF, Kay RF, editors. *Anthropoid Origins: New Visions*. New York: Kluwer Academic/Plenum Publishers. p 45-64.
- Endo B, Kimura T. 1970. Postcranial skeleton of the Amud Man. In: Suzuki H, Takai F, editors. *The Amud Man and his Cave Site*. Tokyo: Academic Press. p 231-406.
- Falgueres C, Bahain JJ, Yokoyama Y, Arsuaga JL, Bermudez de Castro JM, Carbonell E, Bischoff JL, Dolo JM. 1999. Earliest humans in Europe: the age of TD6 Gran Dolina, Atapuerca, Spain. *J Hum Evol* 37:343-352.
- Farin GE. 1995. *NURB curves and surfaces: From projective geometry to practical use*. Wellesley, MA: A K Peters, Ltd.
- Farin G. 1996. *Curves and surfaces for computer aided geometric design*. 4th edition. Boston: Academic Press.
- Farin G. 2002. A history of curves and surfaces in CAGD. In: Farin G, Hoschek J, Kim M-S, editors. *Handbook of computer aided geometric design*. Amsterdam: Elsevier. p 1-21.
- Farin GE, Hansford D. 1998. *The geometry toolbox: for graphics and modeling*. Natick, MA: A K Peters, Ltd.
- Farin GE, Hansford D. 2000. *The essentials of CAGD*. Natick, MA: A K Peters, Ltd.
- Felsenstein J. 1985. Phylogenies and the comparative method. *American Naturalist* 125:1-15.
- Fick R. 1904. *Handbuch der Anatomie und Mechanik der Gelenke, Erster Teil: Anatomie der Gelenke*. Jena: Gustav Fischer.
- Foley R. 1987a. Another unique species: patterns in human evolutionary perspective. London: Longham.
- Foley R. 1987b. Hominid species and stone-tool assemblages: how are they related? *Antiquity* 61:380-392.
- Foley R, Lahr MM. 2003. On stony ground: Lithic technology, human evolution, and the emergence of culture. *Evol Anthropol* 12:109-122.

- Galis F, van Alphen JJM, Metz JAJ. 2001a. Why five fingers? Evolutionary constraints on digit numbers. *Trends Ecol Evol* 16:637-646.
- Galis F, van Alphen JJM, Metz JAJ. 2001b. Why five fingers? Evolutionary constraints on digit numbers. *American Zoologist* 41:1448-1449.
- Gans C. 1988. Adaptation and the form-function relation. *American Zoologist* 28:681-697.
- Goodall J. 1964. Tool-using and aimed throwing in a community of free-living chimpanzees. *Nature* 201:1264-1266.
- Goodall J. 1986. *The Chimpanzees of Gombe: Patterns of Behavior*. Cambridge, MA: Belknap.
- Gould SJ, Lewontin RC. 1979. Spandrels of San-Marco and the Panglossian Paradigm - a Critique of the Adaptationist Program. *Proceedings of the Royal Society of London Series B-Biological Sciences* 205:581-598.
- Gould SJ, Vrba ES. 1982. Exaptation - a Missing Term in the Science of Form. *Paleobiology* 8:4-15.
- Gould SJ. 1993. *Eight little piggies: Reflections in natural history*. New York: W.W. Norton Company.
- Gray DJ, Gardner E, O'Rahilly R. 1957. The prenatal development of the skeleton and joints of the human hand. *Am J Anat* 101:169-223.
- Greene HW. 1986. Diet and arboreality in the emerald monitor, *Varanus prasinus*, with comments on the study of adaptation. *Fieldiana Zool New Ser* 31:1-12.
- Griffiths HE. 1943. Treatment of the injured workman. *Lancet* 244:729-733.
- Grine FE. 1989. New hominid fossils from the Swartkrans Formation (1979-1986 excavations): Craniodental specimens. *Am J Phys Anthropol* 79:409-449.
- Groves C. 2001. *Primate Taxonomy*. Washington: Smithsonian Institution Press.
- Guthrie EA. 1991. Variability of the primate trapezio-metacarpal articulation. MA Thesis, Arizona State University, Tempe, AZ.
- Haines RW. 1958. Arboreal or terrestrial ancestry of placental mammals. *Quart Rev*

- Biol 38:1-23.
- Hall BK. 1988. The embryonic development of bone. *American Science* 76:174-181.
- Hamrick MW, Inouye SE. 1995. Thumbs, tools and early humans. *Science* 268:587.
- Harris JWK, Williamson PG, Verniers J, Tappen MJ, Stewart K, Helgren D, De Heinzelin J, Boaz NT, Bellomo RV. 1987. Late Pliocene hominid occupation of the Senga 5A site, Zaire. *J Hum Evol* 16:701-728.
- Harvey PH, Pagel MD. 1991. *The comparative method in evolutionary biology*. Oxford: Oxford University Press.
- Harvey PH, Purvis A. 1991. Comparative methods for explaining adaptations. *Nature* 351:619-624.
- Hearn D, Baker MP. 1986. *Computer Graphics*. Upper Saddle River, NJ: Prentice-Hall, Inc.
- Heim J-L. 1974. Les hommes fossiles de La Ferrassie (Dordogne) et le problème de la définition des Néandertaliens Classiques. *L'Anthropologie* 78:81-112.
- Hinchliffe JR. 1989. Reconstructing the archetype: Innovation and conservatism in the evolution and development of the pentadactyl limb. In: Wake DB, Roth G, editors. *Complex organismal functions: Integration and evolution in vertebrates*. New York: John Wiley and Sons. p 171-189.
- Hollister A, Buford W, Myers L. 1992. Axes of rotation of the thumb carpometacarpal joint. *J Orthoped Res* 10:454-460.
- Isaac GL. 1984. The archaeology of human origins: Studies of the Lower Pleistocene in East Africa, 1971-1981. *Advances in World Archaeology* 3:1-87.
- Jacofsky MC. 2002. Variation in morphology and musculoskeletal stress marker expression of the first dorsal interosseous muscle in catarrhines. MA paper, Arizona State University.
- Johanson DC, Taieb M, Coppens Y. 1982b. Pliocene hominids from the Hadar Formation, Ethiopia (1973-1977): Stratigraphic, chronologic, and paleoenvironmental contexts, with notes on hominid morphology and systematics. *Am J Phys Anthropol* 57:373-402.
- Johanson DC, Lovejoy CO, Kimbel WH, White TD, Ward SC, Bush ME, Latimer BM,

- Coppens Y. 1982a. Morphology of the Pliocene partial hominid skeleton (A.L. 288-1) from the Hadar Formation, Ethiopia. *Am J Phys Anthropol* 57:403-451.
- Johnson RA, Wichern DW. 2002. Applied multivariate statistical analysis. 5th edition. Upper Saddle River, NJ: Prentice-Hall, Inc.
- Jolly CJ. 1970. The large African monkeys as an adaptive array. In: Napier JR, Napier P, editors. *Old World Monkeys*. New York: Academic Press. p 139-174.
- Jones S. 1999. *Darwin's Ghost: The Origin of Species Updated*. Canada: Doubleday Canada.
- Jordan C. 1982. Object manipulation and tool-use in captive pygmy chimpanzees (*Pan paniscus*). *J Hum Evol* 11:35-39.
- Jungers WL, Falsetti AB, Wall CE. 1995. Shape, relative size, and size-adjustments in morphometrics: Yearb Phys Anthropol 38:137-161.
- Kay RF, Cartmill M. 1977 Cranial morphology and adaptations of *Palaechthon nacimienti* and other Paromomyidae (Plesiadapoidea, ?Primates), with description of a new genus and species. *J Hum Evol* 6:19-53.
- Kimbel WH, Walter RC, Johanson DC, Reed KE, Aronson JL, Assefa Z, Marean CW, Eck GG, Bobe R, Hovers E, Rak Y, Vondra C, Yamane T, York D, Chen Y, Evenson NM, Smith PE. 1996. Late Pliocene *Homo* and Oldowan tools from the Hadar Formation (Kada Hadar Member), Ethiopia. *J Hum Evol* 38:549-561.
- Klaatsch H, Hauser O. 1909. *Homo Aurignacensis* Hauseri ein paläolithischer Skeletfund aus dem Aurignacien der Station Combe-Capelle bei Montferrand (Périgord). *Prähistorische Zeitschrift* 1:273-297.
- Kumar S, Filipski A, Swarna V, Walker A, Hedges SB. 2005. Placing confidence limits on the molecular age of the human-chimpanzee divergence. *Proc Nat Acad Sci* 102:18842-18847.
- Landsmeer JMF. 1962. Power grip and precision handling. *Ann Rheum Dis* 21:164-170.
- Larson A, Losos JB. 1996. Phylogenetic systematics of adaptation. In: Rose MR, Lauder GV, editors. *Adaptation*. San Diego: Academic Press. p 197-220.
- Lauder GV, Huey RB, Monson RK, Jensen RJ. 1995. Systematics and the Study of Organismal Form and Function - Advances in Systematics Are Defining New

- Directions for Functional-Morphology and Comparative Physiology. *Bioscience* 45:696-704.
- Lauder GV, Leroi AM, Rose MR. 1993. Adaptations and history. *Tree* 8:294-297.
- Lauder GV. 1981. Form and function: Structural analysis in evolutionary morphology. *Paleobiology* 7:430-442.
- Lauder GV. 1982. Historical Biology and the Problem of Design. *J Theor Biol* 97:57-67.
- Lauder GV. 1995. On the inference of function from structure. In: Thomason JJ, editor. *Functional morphology in vertebrate paleontology*. Cambridge: Cambridge University Press. p 1-18.
- Lauder GV. 1996. The argument from design. In: Rose MR, Lauder GV, editors. *Adaptation*. San Diego: Academic Press. p 55-91.
- Leakey LSB, Evernden JF, Curtis GH. 1961. Age of Bed I, Olduvai Gorge, Tanganyika. *Nature* 191:478-479.
- Leakey LSB, Tobias PV, Napier JR. 1964. A new species of the genus *Homo* from Olduvai Gorge. *Nature* 202:7-9.
- Leakey LSB. 1959. A new fossil skull from Olduvai. *Nature* 184:491-493.
- Leakey LSB. 1960. Recent discoveries at Olduvai Gorge. *Nature* 188:1050-1052.
- Leakey LSB. 1961. New finds at Olduvai Gorge. *Nature* 189:649-650.
- Leakey MD. 1971. Olduvai Gorge. Volume III. Excavations in Beds I and II, 1960-1963. Cambridge: The University Press.
- Leiberman DE, Devlin MJ, Pearson OM. 2001. Articular area responses to mechanical loading: effects of exercise, age, and skeletal location. *Am J Phys Anthropol* 116:266-277.
- Leroi AM, Rose MR, Lauder GV. 1994. What does the comparative method reveal about adaptation? *American Naturalist* 143:381-402.
- Lethmate J. 1982. Tool-using skills of orang-utans. *J Hum Evol* 11:49-64.
- Lewis OJ. 1970. The development of the human wrist joint during the fetal period. *Anat*

- Rec 166:499-516.
- Lewis OJ. 1977. Joint remodeling and the evolution of the human hand. *J Anat* 123:157-201.
- Lewis OJ. 1989. Functional morphology of the evolving hand and foot. Oxford: Clarendon Press.
- Lewontin RC. 1978. Adaptation. *Scientific American* 239:156-169.
- Lewontin RC. 1979. Sociobiology as an adaptationist program. *Behavioral Sciences* 24:5-14.
- Linscheid RL. 1982. The thumb axis joints: a biomechanical model. In: Strickland JW, Streichen JB, editors. *Difficult Problems in Hand Surgery*. St. Louis: CV Mosby. p 169-172.
- Lorenzo C, Arsuaga JL, Carretero JM. 1999. Hand and foot remains from the Gran Dolina Early Pleistocene site (Sierra de Atapuerca, Spain). *J Hum Evol* 37:501-522.
- Maddison WP, Maddison DR. 1992. *MacClade, Version 3*. Sunderland, MA: Sinauer Publishers.
- Manly BFJ. 1997. Randomization, bootstrap and Monte Carlo methods in biology. 2nd edition. Boca Raton, FL: CRC Press, LLC.
- Marzke MW, Marzke RF. 1987. The 3rd metacarpal styloid process in humans – origin and functions. *Am J Phys Anthropol* 73:415-431.
- Marzke MW, Marzke RF. 2000. Evolution of the human hand: approaches to acquiring, analysing and interpreting the anatomical evidence. *J Anat* 197:121-140.
- Marzke MW, Shackley MS. 1986. Hominid hand use in the in the Pliocene and Pleistocene: Evidence from experimental archaeology and comparative morphology. *J Hum Evol* 15:439-460.
- Marzke MW, Wullstein KL, Viegas SF. 1992. Evolution of the power (“squeeze”) grip and its morphological correlates in hominids. *Am J Phys Anthropol* 89:283-298.
- Marzke MW, Wullstein KL, Viegas SF. 1994. Variability at the carpometacarpal and midcarpal joints involving the fourth metacarpal, hamate, and lunate in catarrhini. *Am J Phys Anthropol* 93:229-240.

- Marzke MW, Wullstein KL. 1996. Chimpanzee and human grips: A new classification system with a focus on evolutionary morphology. *Int J Primatol* 17:117-139.
- Marzke MW. 1971. Origin of the human hand. *Am J Phys Anthropol* 34:61-84.
- Marzke MW. 1983. Joint function and grips of the *Australopithecus afarensis* hand, with special reference to the region of the capitate. *J Hum Evol* 12:197-211.
- Marzke MW. 1992. Evolutionary development of the human thumb. *Hand Clin* 8:1-8.
- Marzke MW. 1997. Precision grips, hand morphology, and tools. *Am J Phys Anthropol* 102:91-110.
- Marzke MW. 2005. Who made Stone Tools? In: Roux V, Blandine B, editors. *Stone knapping: the necessary conditions for a uniquely hominin behaviour*. Cambridge, UK: McDonald Institute for Archaeological Research. p 243-255.
- Marzke MW, Shrewsbury MM. 2006. The *Oreopithecus* thumb: Pitfalls in reconstructing muscle and ligament attachments from fossil bones. *J Hum Evol* 51:213-215.
- Matsuzawa T. 1994. Field experiments on use of stone tools in the wild. In: Wrangham RW, McGrew WC, de Waal FBM, Heltne PG, editors. *Chimpanzee Cultures*. Cambridge, MA: Harvard University Press. p 351-370.
- Mayr E. 1983. How to carry out the adaptationist program? *Am Nat* 121:324-334.
- Mayr E. 1988. *Toward a new philosophy of biology: Observations of an evolutionist*. Cambridge, MA: Harvard University Press.
- McBride ED. 1942. *Disability Evaluation*. 3rd edition. Philadelphia: JB Lippincott Company.
- McGrew WC. 1994. Tools compared: The material of culture. In: Wrangham RW, McGrew WC, de Waal FBM, Heltne PG, editors. *Chimpanzee Cultures*. Cambridge, MA: Harvard University Press. p 25-39.
- McHenry HM. 1983. The capitate of *Australopithecus afarensis* and *A. africanus*. *Am J Phys Anthropol* 62:187-198.
- Mérida-Velasco JA, Garcia-Garcia JD, Espín-Ferra J, Sánchez-Montesinos I. 1996. Development of the human wrist joint ligaments. *Anat Rec* 245:114-121.

- Mivart St GJ. 1867. On the appendicular skeleton of the primates. *Phil Trans Royal Soc Lond* 157:299-429.
- Morwood MJ, Brown P, Jatmiko, Sutikna T, Saptomo EW, Westaway KE, Due RA, Roberts RG, Maeda T, Wasisto S, Djubiantono T. 2005. Further evidence for small-bodied hominins from the Late Pleistocene of Flores, Indonesia. *Nature* 437:1012-1017.
- Mosimann JE, James FC. 1979. New statistical methods for allometry with application to Florida red-winged blackbirds. *Evol* 33:444-459.
- Moya-Sola S, Kohler M, Rook L. 1999. Evidence of hominid-like precision grip capability in the hand of the Miocene ape *Oreopithecus*. *Proc Nat Acad Sci* 96:313-317.
- Muller HJ. 1949. Natural selection and adaptation. *Proc Amer Phil Soc* 93:459-519.
- Munson R. 1971. Biological adaptation. *Phil Sci* 38:200-215.
- Napier JR, Davis PR. 1959. The fore-limb skeleton and associated remains of *Proconsul africanus*. *Fossil Mammals Africa* 16:1-69.
- Napier JR. 1955. The form and function of the carpometacarpal joint of the thumb. *J Anat* 89:362-369.
- Napier JR. 1956. The prehensile movements of the human hand. *J Bone Joint Surgery (British)* 38:902-913.
- Napier JR. 1959. Fossil metacarpals from Swartkrans. *Fossil Mammals of Africa* No. 17. London: British Museum of Natural History.
- Napier JR. 1960. Studies of the hands of living primates. *Proc Zool Soc Lond* 134:647-657.
- Napier JR. 1961. Prehensility and opposability in the hands of primates. *Symp Zool Soc Lond* 5:115-132.
- Napier JR. 1962. Fossil hand bones from Olduvai Gorge. *Nature* 196:409-411.
- Napier JR. 1965. Evolution of the human hand. *Proc Royal Institution of Great Britain* 40:544-557.

- Noonan JP, Coop G, Kudaravalli S, Smith D, Krause J, Alessi J, Chen F, Platt D, Pääbo S, Pritchard JK, Rubin EM. 2006. Sequencing and Analysis of Neanderthal Genomic DNA. *Science* 314:1113-1118.
- Ohman JC, Slanina M, Baker G, Mensforth RP. 1995. Thumbs, tools and early humans. *Science* 268:587-589.
- Olson TR. 1996. *A.D.A.M. Student Atlas of Anatomy*. Baltimore, MD: Williams & Wilkins.
- O’Rahilly R. 1949. Stereographic reconstruction of the carpus. *Anat Rec* 103:187-193.
- O’Rahilly R, Gardner E. 1975. The timing and sequence of events in the development of the limbs in the human embryo. *Anat Embryol* 148:1-23.
- O’Rahilly R, Gray DJ, Gardner E. 1957. Chondrification in the hands and feet of staged human embryos. *Contributions to Embryology* 36:183-192.
- Panger MA, Brooks AS, Richmond BG, Wood B. 2002. Older than the Oldowan? Rethinking the emergence of hominin tool use. *Evol Anthropol* 11:235-245.
- Paulos JA. 1988. *Innumeracy*. New York: Hill and Wang.
- Piveteau J. 1963. La grotte du Regourdou (Dordogne), Paléontologie humaine. *Annales de Paléontologie (Vertébrés)* 49:285-305.
- Piveteau J. 1964. La grotte du Regourdou (Dordogne), Paléontologie humaine. *Annales de Paléontologie (Vertébrés)* 50:155-194.
- Piveteau J. 1966. La grotte du Regourdou (Dordogne), Paléontologie humaine. *Annales de Paléontologie (Vertébrés)* 52:163-194.
- Plummer T, Bishop LC, Ditchfield P, Hicks J. 1999. Research in late Pliocene Oldowan sites at Kanjera South, Kenya. *J Hum Evol* 36:151-170.
- Potts R. 1991. Why the Oldowan? Plio-Pleistocene tool-making and the transport of resources. *J Anthropological Research* 47:153-176.
- Pulla S. 2001. Curvature based segmentation of 3-dimensional meshes. MS Thesis, Arizona State University, Tempe, AZ.

- Rafferty KL, Ruff CB. 1994. Articular structure and function in *Hylobates*, *Colobus*, and *Papio*. *Am J Phys Anthropol* 94:395-408.
- Reader J. 1981. *Missing Links*. Boston: Little, Brown and Company.
- Reed KE. 1997. Early hominid evolution and ecological change through the African Plio-Pleistocene. *J Hum Evol* 32:289-322.
- Reed KE. 2002. The use of paleocommunity and taphonomic studies in reconstructing primate behavior. In: Plavcan MJ, Kay R, van Schaik C, Jungers WL, editors. *Reconstructing Primate Behavior in the Fossil Record*. New York: Kluwer Academic/Plenum Press. p 217-259.
- Reeve HK, Sherman PW. 1993. Adaptation and the goals of evolutionary research. *Q Rev Biol* 68:1-32.
- Richmond BG, Begun DR, Strait DS. 2001. Origin of human bipedalism: The knuckle-walking hypothesis revisited. *Yearbk Phys Anthropol* 44:70-105.
- Richmond BG. 2006. Functional morphology of the midcarpal joint in knuckle-walkers and terrestrial quadrupeds. In: Ishida H, Tuttle R, Pickford M, Ogihara N, Nakatsukasa M, editors. *Human Origins and Environmental Backgrounds*. Springer. p 105-122.
- Ricklan DE. 1986a. The differential frequency of preservation of fossil hominid wrist and hand bones. *Hum Evol* 1:373-382.
- Ricklan DE. 1986b. The influence of mass, volume and density on the frequency of recovery of fossil hominid hand and wrist bones. *Hum Evol* 1:399-404.
- Rightmire GP. 1972. Multivariate analysis of an early hominid metacarpal from Swartkrans. *Science* 176:159-161.
- Robinson JT. 1960. The affinities of the new Olduvai australopithecine. *Nature* 186:456-457.
- Roche H, Delagnes A, Brugal JP, Feibel C, Kibunjia M, Mourrel V, Texier PJ. 1999. Early hominid stone tool production and technical skill 2.34 myr ago in West Turkana, Kenya. *Nature* 399:57-60.
- Rose MD. 1977. Positional behaviour of olive baboons (*Papio anubis*) and its relationship to maintenance and social activities. *Primates* 18:59-116.

- Rose MD. 1988. Function anatomy of the cheiridia. In: Schwartz JE, editor. *Orang-utan Biology*. New York: Oxford University Press. p 299-310.
- Rose MD. 1992. Kinematics of the trapezium-1st metacarpal joint in extant anthropoids and Miocene hominoids. *J Hum Evol* 22:255-266.
- Rose MR, Lauder GV. 1996. Post-spandrel adaptationism. In: Rose MR, Lauder GV, editors. *Adaptation*. San Diego: Academic Press. p 1-8.
- Ross CF, Lockwood CA, Fleagle JG, Jungers WL. 2002. Adaptation and behavior in the primate fossil record. In: Plavcan JM, Kay RF, Jungers WL, van Schaik CP, editors. *Reconstructing behavior in the primate fossil record*. New York: Kluwer Academic/Plenum Publishers. p 1-41.
- Ross CF. 1999. How to carry out functional morphology. *Evol Anthropol* 7:217-222.
- Rudwick MJS. 1964. The inference of function from structure in fossils. *Brit J Philos Sci* 15:27-40.
- Sarmiento EE. 1985. Functional differences in the skeleton of wild and captive orangutans and their adaptive significance. PhD dissertation, New York University.
- Sarmiento EE. 1988. Anatomy of the hominoid wrist joint—its evolutionary and functional implications. *Int J Primatol* 9:281-345.
- Scheuer L, Black S. 2000. *Developmental Juvenile Osteology*. London: Academic Press.
- Schick KD. 1987. Modeling the formation of Early Stone Age artifact concentrations. *J Hum Evol* 16:789-807.
- Schwarcz HP, Grün RG, Tobias PV. 1994. ESR dating studies of the australopithecine site of Sterkfontein, South Africa. *J Hum Evol* 26:175-181.
- Semaw S, Renne P, Harris JWK, Feibel CS, Bernor RL, Fesseha N, Mowbray K. 1997. 2.5-million-year-old stone tools from Gona, Ethiopia. *Nature* 385:333-336.
- Senior HD. 1929. The chondrification of the human hand and foot skeleton. *Anat Rec* 42:35.
- Shrewsbury MM, Sonek A. 1986. Precision holding in humans, non-human primates, and Plio-Pleistocene hominids. *Hum Evol* 1:233-242.

- Simpson GG. 1947. The problem of plan and purpose in nature. *Scientific Monthly* 64:481-495.
- Sklansky D. 1994. *The Theory of Poker*. Henderson, NV: Two Plus Two Publishing.
- Slocum DB, Pratt DR. 1946. Disability evaluation for the hand. *J Bone Joint Surg* 28:491-506.
- Smith SL. 2000. Shape variation of the human pollical distal phalanx and metacarpal. *Am J Phys Anthropol* 113:329-348.
- Sober E. 1984. *The Nature of Selection*. Cambridge, MA: MIT Press.
- Steiper ME, Young NM. 2006. Primate molecular divergence dates. *Mol Phylo Evol* 41:384-394.
- Stern JT. 1970. The meaning of "adaptation" and its relation to the phenomenon of natural selection. *Evol Biol* 4:39-66.
- Streeter GL. 1948. Description of age groups XV, XVI, XVII and XVIII being the third issue of a survey of the Carnegie collection. *Contributions to Embryology* 32:133-203.
- Sumita K, Kitahara-Frisch J, Norkiosh K. 1985. The acquisition of stone-tool use in captive chimpanzees. *Primates* 2:168-181.
- Susman RL, Creel N. 1979. Functional and morphological affinities of the subadult hand (OH 7) from Olduvai Gorge. *Am J Phys Anthropol* 51:311-331.
- Susman RL, Stern JT. 1982. Functional morphology of *Homo habilis*. *Science* 217:931-934.
- Susman RL. 1988. Hand of *Paranthropus robustus* from Member 1, Swartkrans: fossil evidence for tool behavior. *Science* 240:781-784.
- Susman RL. 1989. New hominid fossils from the Swartkrans formation (1979-1986 excavations): postcranial specimens. *Am J Phys Anthropol* 79:451-474.
- Susman RL. 1991. Who made the Oldowan tools? Fossil evidence for tool behavior in Plio-Pleistocene hominids. *J Anthropol Res* 47:129-149.
- Susman RL. 1994. Fossil evidence for early hominid tool use. *Science* 265:1570-1573.
- Susman RL. 1998. Hand function and tool behavior in early hominids. *J Hum Evol*

- 35:23-46.
- Susman RL. 2004. *Oreopithecus bambolii*: an unlikely case of hominidlike grip capability in a Miocene ape. *J Hum Evol* 46:105-117.
- Susman RL. 2005. *Oreopithecus*: still apelike after all these years. *J Hum Evol* 49:405-411.
- Swofford DL, Maddison WP. 1992. Parsimony, character-state reconstructions, and evolutionary inferences. In: Mayden RL, editor. *Systematics, historical ecology, and North American freshwater fishes*. Stanford: Stanford University Press. p 186-223.
- Tardif B, Duparc F, Muller JM, Freger P. 1998. Embryology of the human carpal bones (triangular cartilage, central carpal bone, morphogenesis of the scaphoid). *Chir Main* 17:266-276.
- Thewissen JGM, Bajpai S. 2001. Whale origins as a poster child for macroevolution. *Bioscience* 51:1037-1049.
- Tobias PV. 1964. The Olduvai Bed I Hominine with special reference to its cranial capacity. *Nature* 202:3-4.
- Tocheri MW, Femiani JC. In press. The “bare bones” of 3D: An introduction to 3D modeling concepts for the physical anthropologist. In: Hoppa RD, Nelson AJ, editors. *3D Imaging in Biological Anthropology and Bioarchaeology*. Cambridge, UK: Cambridge University Press.
- Tocheri MW, Femiani JC, Orr CM, Marzke MW. 2006. Quadric-based metrics for shape analysis of three-dimensional osteological surfaces. *Am J Phys Anthropol* 129:177-178.
- Tocheri MW, Marzke MW, Liu D, Bae M, Jones GP, Williams RC, Razdan A. 2003. Functional capabilities of modern and fossil hominid hands: Three-dimensional analysis of trapezia. *Am J Phys Anthropol* 122:101-112.
- Tocheri MW, Razdan A, Williams RC, Marzke MW. 2005. A 3D quantitative comparison of trapezium and trapezoid relative articular and nonarticular surface areas in modern humans and great apes. *J Hum Evol* 49:570-586.
- Toth N. 1985. The Oldowan reassessed: a close look at early stone artifacts. *J Arch Sci* 12:101-120.

- Toth N. 1987. Behavioral inferences from Early Stone Age artifact assemblages. *J Hum Evol* 16:763-787.
- Toth N, Schick KD. 1986. The first million years: the archaeology of protohuman culture. In: Schiffer MB, editor. *Advances in Archaeological Method and Theory*. Volume 9. Orlando: Academic Press. p 1-96.
- Toth N, Schick KD, Savage-Rumbaugh ES, Sevcik RA, Rumbaugh DM. 1993. Pan the tool-maker: Investigations into the stone tool-making and tool-using capabilities of a Bonobo (*Pan paniscus*). *J Arch Sci* 20:81-91.
- Trinkaus E, Long JC. 1990. Species attribution of the Swartkrans Member 1 first metacarpals: SK 84 and SKX 5020. *Am J Phys Anthropol* 83:419-424.
- Trinkaus E. 1982. The Shanidar 3 Neandertal. *Am J Phys Anthropol* 57:37-60.
- Trinkaus E. 1983. *The Shanidar Neandertals*. London: Academic Press.
- Trinkaus E. 1989. Olduvai Hominid 7 trapezoidal metacarpal 1 articular morphology: Contrasts with recent humans. *Am J Phys Anthropol* 80:411-416.
- Tuttle RH. 1967. Knuckle-walking and the evolution of hands. *Am J Phys Anthropol* 26:171-206.
- Tuttle RH. 1969. Quantitative and functional studies on the hands of the anthropoidea: I. The Hominoidea. *J Morphol* 128:309-363.
- Vandermeersch B. 1981. *Les Hommes Fossiles de Qafzeh (Israël)*. Paris: Éditions du CNRS.
- Vrba ES. 1982. Biostratigraphy and chronology, based particularly on Bovidae, of southern hominid-associated assemblages: Makapansgat, Sterkfontein, Taung, Kromdraai, Swartkrans; and also Elandsfontein (Saldanha), Broken Hill (now Kabwe) and Cave of Hearths. In: DeLumley F, DeLumley MA, editors. *L'Homo erectus et la place de l'homme de Tautavel parmi les hominidés fossils*. Prétirage du 1er Congrès International Paléontologie Humaine. Volume 2. Nice: Louis-Jean. p 707-752.
- Walter RC. 1994. Age of Lucy and the First Family: Single-crystal $^{40}\text{Ar}/^{39}\text{Ar}$ dating of the Denen Dora and lower Kada Hadar members of the Hadar Formation, Ethiopia. *Geology* 22:6-10.
- Walter RC, Manega PC, Hay RL, Drake RE, Curtis GH. 1991. Laser-fusion $^{40}\text{Ar}/^{39}\text{Ar}$ dating of Bed I, Olduvai Gorge, Tanzania. *Nature* 354:145-149.

- Washburn S. 1960. Tools and human evolution. *Scientific American* 203:3-15.
- West-Eberhard MJ. 1992. Adaptation: current usages. In: Keller EF, Lloyd ES, editors. *Keywords in Evolutionary Biology*. Cambridge, MA: Harvard University Press. p 13-18.
- Whillis J. 1940. The development of synovial joints. *J Anat* 74:277-283.
- Williams GC. 1966. *Adaptation and natural selection*. Princeton, NJ: Princeton University Press.
- Williams GC. 1992. *Natural Selection: Domains, Levels, and Challenges*. Oxford: Oxford University Press.
- Williams GC. 1997. *The pony fish's glow: And other clues to plan and purpose in nature*. New York: BasicBooks.
- Witmer LM. 1995. The extant phylogenetic bracket and the importance of reconstructing soft tissues in fossils. In: Thomason JJ, editor. *Functional morphology in vertebrate paleontology*. Cambridge: Cambridge University Press. p 19-33.
- Wood B, Richmond BG. 2000. Human evolution: taxonomy and paleobiology. *J Anat* 197:19-60.
- Wood Jones F. 1941. *The Principles of Anatomy as Seen in the Hand*. 2nd edition. London: Ballière, Tindall and Cox.
- Wright S. 1949. Adaptation and selection. In: Jepsen G, Mayr E, Simpson GG, editors. *Genetics, paleontology and evolution*. Princeton, NJ: Princeton University Press. p 365-389.
- Wright RV. 1972. Imitative learning of a flaked tool technology: the case of an orangutan. *Mankind* 8:296-306.
- Wynn TG, McGrew WC. 1989. An ape's view of the Oldowan. *Man* 24:383-398.
- Xu LF, Strauch RJ, Ateshian GA, Pawluk RJ, Mow VC, Rosenwasser MP. 1998. Topography of the osteoarthritic thumb carpometacarpal joint and its variations with regard to gender, age, site, and osteoarthritic stage. *J Hand Surg* 23A:454-464.